Identification and biosynthesis of bioactive triterpenes from *Calendula officinalis*

A thesis submitted to the University of East Anglia in partial fulfilment of the requirements for the degree of Doctor of Philosophy

Daria Golubova

February 2025

Abstract

Plants have been used in traditional medicine for centuries. In some cases, the therapeutic properties of medicinal plants have been attributed to specific metabolites, enabling their use as drugs in modern medicine. However, the exact molecule(s) responsible for the bioactivity of majority plant extracts remains unknown. Additionally, access to specific compounds is often hindered by their low abundance, presence in complex mixtures, or structural complexity, making chemical synthesis challenging. This thesis describes an investigation into the previously reported anti-inflammatory and wound-healing bioactivities of *Calendula officinalis* (pot marigold), a well-known medicinal plant. Previous studies suggested that the bioactivity of pot marigold floral extracts may be linked to an abundance of triterpene fatty acid esters (TFAEs). However, the literature has not definitively determined if molecules from this class are the most potent anti-inflammatory compounds present in the extracts. Further, little is known about the mechanism of action that underlines the bioactivity, or about the biosynthesis of these molecules. Thus, my research aimed to identify the key bioactive compound(s) in pot marigold extracts, investigate their mechanism of action, and to discover and characterise enzymes involved in their biosynthesis. This was achieved by integrating comparative metabolic profiling of Asteraceae species with bioactivity assays in model human cell lines, leading to the identification of faradiol and faradiol FAEs as key anti-inflammatory compounds in pot marigold extract. Following this, a combination of metabolomics, genomics, transcriptomics and transient expression in *Nicotiana benthamiana* enabled the identification and characterisation of the biosynthetic enzymes responsible for the production of these compounds. Finally, a method for gene silencing in pot marigold was developed, providing an additional tool for pathway characterisation. This work contributes to the discovery and sustainable production of plant-derived bioactive compounds, offering new opportunities for pharmaceutical applications.

Acknowledgements

Here, I would like to express my deepest gratitude to everyone who has supported me throughout this PhD journey.

First and foremost, I am incredibly grateful to the John Innes Foundation for funding this project - without their support, this incredible journey would not have been possible.

A special thanks to my supervisor, Prof. Nicola Patron, for her continued guidance, encouragement, and mentorship. Nicola, I have learned so much from you - how to be patient, resilient, and stay focused on what truly matters. Your support in navigating the experimental challenges of this project, as well as in writing this thesis, has been invaluable. I am also particularly grateful for your encouragement to attend conferences, engage in outreach, and explore research translation - these experiences have been among the highlights of my PhD.

I would also like to extend my sincere gratitude to my secondary supervisor, Prof. Maria O'Connell, for her continuous academic and personal support. Maria, you have always encouraged my curiosity and desire to try new things, and I deeply appreciate it. Thank you for making me feel welcome in your lab, especially during the final year of this journey.

My warm thanks go to the members of the Patron and O'Connell labs, past and present, for creating a supportive and collaborative research environment. I am especially grateful to Dr. Melissa Salmon and Dr. Connor Tansley for their constant help, advice, and much-needed moral support. Mel, thank you for patiently answering my endless questions, sharing your expertise in natural products, and training me in all plant-related techniques. Connor, I sincerely appreciate your encouragement in becoming an independent researcher, as well as your guidance in qPCR and cloning techniques. Additionally, I would like to thank Sam Witham for helping me integrate into the EI student community; Honghao Su for guidance and advice on structural modelling; Kalyani Kallam for baking delicious cookies, cupcakes, and biscuits to keep the PhD students going; Zhengao Di, Yaomin Cai, Tufan Oz, and Quentin Dudley for their advice on lab techniques, best practices, and constructive feedback during lab meetings. Sarah Guiziou for always offering a supportive and listening ear during moments of doubt and existential crises. At the Maria O'Connell lab, I would like to thank Emily Hobson for her invaluable assistance with biological assays and troubleshooting them.

Further, the work presented in this thesis would not have been possible without the metabolomics and NMR platforms at JIC. A special thanks to Dr. Lionel Hill and Dr. Paul Brett for their expertise and guidance in GC-MS and LC analysis, as well as to Sergey Nepogodiev for conducting NMR spectroscopy. Additionally, I am grateful to horticultural services for growing the plants.

Beyond the academic sphere, I am profoundly grateful for the love and support of my friends and family. Thank you to my parents, Alexey and Svetlana, thank you for your belief in me throughout my entire academic career; to my siblings, Maria, Victor, and Simon for your encouragement and for always bringing light into my life; to my wonderful friends Alina, Yana, Anna, Iliya, Yura, Roma, Becky, Basak, and Yash - thank you for listening, supporting, and lifting me up throughout the highs and lows of this project. Special thanks to my husband, Thomas, for moving to Norwich and standing by my side through the ups and downs of this journey. Your love, support, and patience - especially during the final stretch of writing - meant the world to me. Thank you for cooking delicious meals and taking on household responsibilities when I was buried in my thesis.

Further, I would like to say special thanks to the EI badminton club and the UEA/Norwich table tennis club for helping me maintain my well-being and bringing a sense of joy outside of research. I am also grateful to the ESB, for organising student socials and events that fostered connections and friendships. Lastly, I thank the whole Earlham Institute community, for making this PhD journey such an enjoyable experience among like-minded and passionate individuals.

Finally, I extend my gratitude to the Twinings company for their “Wind Down” herbal tea collection - your calming blends played an essential role in keeping me sane and positive throughout this project.

To all who have been part of this journey - thank you!

Table of contents

Table of Figures

Table of Tables

List of common abbreviations

ACT	Acyltransferase
BAY-11-7082	Small NF-κB inhibitor
BGC	Biosynthetic gene cluster
CHL-H	Magnesium chelatase subunit H
CYP	Cytochrome P450
DMAPP	Dimethylallyl diphosphate
DMEM	Dulbecco's modified eagle medium
DMSO	Dimethyl sulfoxide
EGF	Epidermal growth factor
ELISA	Enzyme-linked immunosorbent assay
ER	Endoplasmic reticulum
FAE	Fatty acid ester
FBS	Fetal bovine serum
FPP	Farnesyl diphosphate
GC-MS	Gas chromatography-mass spectrometry
GOI	Gene of interest
GPP	Geranyl diphosphate
HaCaT	Human-immortalised keratinocyte cell line
HL60	Promyeoloblast cell line
HMGR	3-hydroxy,3-methylglutaryl-CoA reductase
IC50	Inhibitory concentration
ID50	Inhibitory dose
IL-1β	Interleukin-1 beta
IL-6	Interleukin 6
IPP	Isopentenyl diphosphate
JAK	Janus kinase
LC-MS	Liquid chromatography–mass spectrometry
LPS	Lipopolysaccharide
MAPK	Mitogen-activated protein kinase
MeJA	Methyl jasmonate
MeOH	Methanol
MEP	2-C-methyl-D-erythritol 4-phosphate
MTS	3-(4,5-dimethylthiazol-2-yl)-5-(3-carboxymethoxyphenyl)-2-(4-sulfophenyl)-2H-tetrazolium
MVA	Mevalonic acid
NF-κB	Nuclear factor kappa B
NIST	National Institute of Standards and Technology
NMR	Nuclear magnetic resonance
NO	Nitric oxide
OSC	Oxidosqualene cyclase
PCR	Polymerase chain reaction

PDS	Phytoene desaturase
qRT-PCR	Real-time quantitative reverse transcription PCR
ROS	Reactive oxygen species
RPMI	Roswell Park Memorial Institute
Spp	Species
STAT	Signal transducer and the activator of the transcription
THP-1	Human monocytic cell line
TIC	Total ion chromatogram
TMS	Trimethylsilyl
TNF	Tumour necrosis factor
TNF-α	Tumour necrosis factor-α
TRV	Tobacco rattle virus
TXSS	ψ-taraxasterol synthase
VIGS	Virus-induced gene silencing
WT	Wild type

Chapter 1 – General Introduction

1.1 The Asteraceae (Aster) family

1.1.1 The evolution and diversity of Asteraceae

The Aster (Asteraceae) plant family is one of the largest and most successful families of flowering plants. They appeared on Earth more than 80 million years ago and are now found on all continents except Antarctica (Funk *et al.*, 2005) (Barreda *et al.*, 2015). Today, this large plant family consists of more than 23,600 species of herbs, shrubs, and trees. Notably, the highest abundance of species is found in South America, North America, and Asia with 6016 species (spp), 5404 spp and 4631 spp, respectively (Foster, 2016, Panero and Crozier, 2016). Recent phylogenetic research supports a South American origin of Asteraceae, after which, they spread through North America to Asia, Europe and Africa (Mandel *et al.*, 2019). This expansion also reached Antarctica before its thermal and biogeographical isolation, evidenced by the discovery of preserved Asteraceae pollen grains in 2015 (Barreda *et al.*, 2015).

In Europe, the most abundant Asteraceae subfamily is the Cichorioideae, which includes almost half (1126 spp) of all the Asteraceae species found in this region (Panero and Crozier, 2016). This subfamily includes a few common and well-known members such as *Lactuca sativa* (lettuce) and *Taraxacum officinale* (common dandelion). The second and the third most abundant subfamilies found in Europe are the Asteroideae with 649 spp and Carduoideae with 507 spp. These subfamilies include well-known plant species such as *Helianthus annuus* (common sunflower), *Artemisia dracunculus* (tarragon), *Dendranthema grandiflorum* (chrysanthemum) and pot marigold.

1.1.2 Asteraceae genetics

The incredible biodiversity of Asteraceae is thought to be related to the large number of whole-genome duplication events that took place in this lineage, resulting in species with high ploidy (Vitales *et al.*, 2019). Polyploids are termed autopolyploid or allopolyploid according to how they were formed. Autopolyploids occur when errors during meiosis lead to the formation of unreduced (2n) gametes rather than haploid (n) gametes (Van de Peer and Meyer, 2005). When two unreduced gametes fuse, the number of chromosomes in the offspring doubles compared to the parental species, leading to autopolyploidy. *Senecio*

doronicum (chamois ragwort) is an example of autopolyploidy in the Asteraceae, where an octoploid individual was formed by the fusion of tetraploids (Fernández *et al.*, 2022).

Polyploidy can also result from the hybridisation of two closely related species, which is called allopolyplodisation. If the new combined genome undergoes a chromosomal doubling, two identical sets of chromosomes are available to pair during meiosis, resulting in a fertile organism (Van de Peer and Meyer, 2005). Allopolyplodisation can occur between species with the same ploidy. For example, tetraploid *Tragopogon miscellus* (Moscow salsify) was formed from the hybridisation between diploid *Tragopogon dubius* (yellow salsify) and *Tragopogon pratensis* (meadow salsify) (Tate *et al.*, 2006). Alternatively, alloploids can be formed from closely related species with different ploidies. An example of this is *Calendula arvensis* (field marigold), which was formed by the hybridisation and subsequent chromosome doubling of the tetraploid *Calendula tripterocarpa* and the diploid *Calendula stellata* (Samatadze *et al.*, 2023). More recently, an analysis of 11 genomes from the species of 10 genera in Asteraceae revealed a so-called 'Asteraceae common hexaploidisation' (ACH) event predicted to have occurred 70.7–78.6 million years ago (Kong *et al.*, 2023).

These genome duplication events have led to high gene numbers across the Asteraceae family (Barker *et al.*, 2008). The additional genetic resources formed by polyploidisation events have been proposed to provide opportunities for the divergence of enzyme function and, consequently the emergence of new metabolites that help in adaptation to abiotic and biotic stresses (Van de Peer *et al.*, 2021). This thesis is focused on the elucidation of the biosynthesis of specific plant secondary metabolites in the tetraploid species, pot marigold. The ploidy of species in the *Calendula* genus, and the evolution of specialised metabolism through gene duplication are discussed in **sections 1.1.3.** and **1.4.2.**, respectively.

1.1.3 The *Calendula* genus

Within the Asteraceae family, the *Calendula* genus belongs to the Asteroideae subfamily, Asterodae supertribe and Calenduleae tribe of the Aster family. The Asteroideae subfamily is divided into three supertribes (Asterodae, Helianthodae and Senecionodae (**Figure 1.1**.). There are approximately 469 ssp of Asterodae, 125 spp of Senecionodae, and 55 ssp of Helianthodae supertribes in Europe (Panero and Crozier, 2016). The Asterodae supertribe includes four tribes: Anthemideae, Astereae, Calenduleae and Gnaphalieae. The *Calendula*

genus is within the Calenduleae tribe. This genus is native to Mediterranean countries and includes 15 species (**Table 1.1.**).

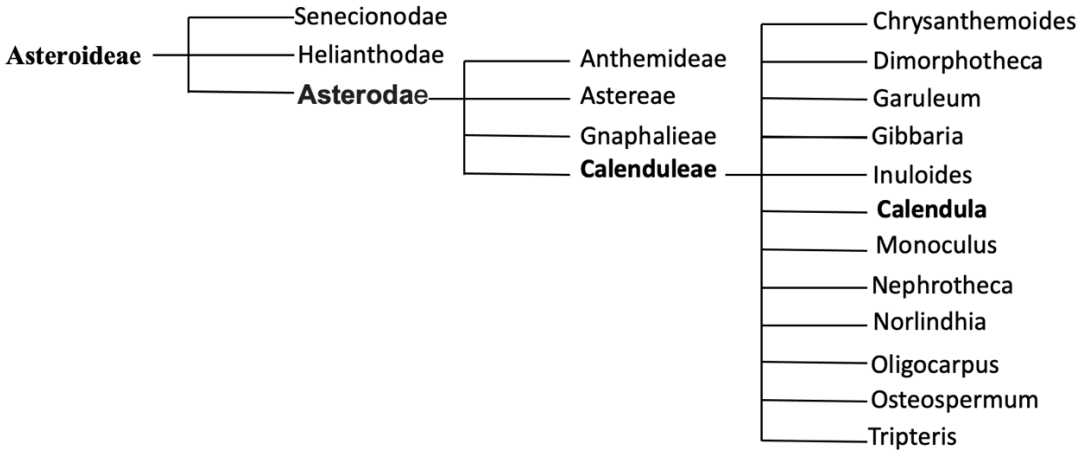

Figure 1.1 The position of the *Calendula* genus within the Asteroideae subfamily of the Asteraceae family.

Table 1.1 Binomial and common names, chromosome number (2n), genome size (1C) and ploidy levels of species in the *Calendula* genus.

Latin name	Common name	2n	1C (pg)	ploidy
Calendula alata		not reported	not reported	not reported
Calendula arvensis	field marigold	44	2.71	Hexaploid
Calendula denticulata		not reported	not reported	not reported
Calendula eckerleinii		18	not reported	Diploid
Calendula incana		32	1.67	Tetraploid
Calendula lanzae		18	not reported	Diploid
Calendula maritima	sea marigold	not reported	not reported	Tetraploid
Calendula maroccana		18	0.88	Diploid
Calendula meuselii		18	not reported	Diploid
Calendula officinalis	pot marigold	32	1.40	Tetraploid
Calendula palaestina		~85	not reported	Dodecaploid
Calendula persica		not reported	not reported	not reported
Calendula stellata		14	1.03	Diploid
Calendula suffruticosa		32	1.65	Tetraploid
Calendula tripterocarpa		30	1.74	Tetraploid

Some *Calendula* species are diploid, while others are polyploid (Plume, 2015) (**Table 1.1.**). A comprehensive study conducted in 2016 suggests multiple independent whole genome duplication events in the Calenduleae (Huang *et al.*, 2016). Moreover, at the level of

individual species, recent research showed a large variation in chromosome numbers (Rice *et al.*, 2015). Pot marigold, for example, is a tetraploid with 32 chromosomes, while field marigold has 44 chromosomes. *Calendula palaestina* and *Calendula pachysperma* have even larger genomes with about 85 chromosomes (Esmaeili *et al.*, 2020). This difference in the number of chromosomes within the genus is the result of frequent hybridisation, chromosome losses and dysploidy (Nora *et al.*, 2013). For example, it was suggested that *Calendula incana* (2n=32) arose from a cross between *Calendula stellata* (2n=14) and *Calendula meuselli* (2n=18), while *Calendula suffruticosa* (2n=32) is the product of a cross between *C. stellata* (2n=14) and *Calendula eckerleinii* (2n=18) (**Figure 1.2.**). Although the origin of pot marigold is unknown, it is believed to result from a cross between *C. stellata* (2n=14) and one of the species which have 2n=18 (*C. eckerleinii, C. meuselli, C. maroccana*) (Plume, 2015). Field marigold (2n = 44) is thought to be a product of a cross between *C. stellata* (2n=14) and *Calendula tripterocarpa* (2n = 30) (Nora *et al.*, 2013) (**Figure 1.2**.).

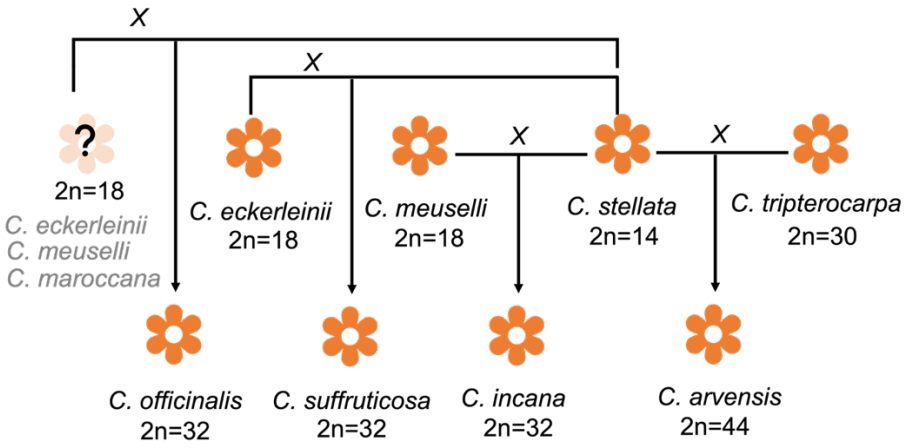

Figure 1.2 Proposed species origins in the *Calendula* genus. X = hybridization; Figure adapted from (Plume, 2015).

1.2 Asteraceae in medicine

Many plants in the Asteraceae family are of high economic and industrial value and have been naturalised and cultivated across the globe. The main application areas are medicine, food and beverages, and cosmetics with minor uses in fodder, dyes, and veterinary practice (Sherpa *et al.*, 2017). Below, I discuss the uses of Asteraceae species in medicine.

1.2.1 Asteraceae in traditional medicine

The history of Asteraceae in traditional medicine goes back thousands of years. For example, written references to the medicinal properties of *Matricaria chamomilla* (chamomile) dates to ancient Rome and Greece, where it was recorded as a medicinal plant by notable

philosophers such as Hippocrates and Galen (Zadeh *et al.*, 2014). Teas and liquid extracts of chamomile are still in use as traditional remedies. Named after Achilles, the Greek mythical hero, because of its wound-healing properties, *Achillea millefolium* (yarrow) was also used in traditional medicine in many countries. Infusions of yarrow flowers are employed in the treatment of inflammatory diseases, and the aerial parts have been used to treat phlegm conditions and as a diuretic agent (Geetha *et al.*, Villalva *et al.*, 2022). Another famous example is *Echinacea purpurea* (purple coneflower) (Samuel and Priyadarshoni, 2019). Infusions of this herb are still used in traditional remedies for the common cold, coughs and bronchitis (Linde *et al.*, 2006, Panero and Crozier, 2016). Additionally, *Arnica montana* (wolf's bane), has been widely used as a remedy for the treatment of several inflammatory conditions in pain management (Smith *et al.*, 2021). Moreover, the polysaccharide fractions of wolf's bane flowers were reported to have significant immunostimulant properties (Kriplani *et al.*, 2017).

This thesis explores the medicinal applications of plants from the *Calendula* genus, with a particular focus on pot marigold. This medicinal herb has been used in traditional medicine for its wound healing and anti-inflammatory activities for many centuries (Macht, 1955). Although pot marigold is native to Mediterranean countries, it is found in the wild across the UK (Stroh *et al.*, 2023), and is also cultivated in many European countries, including the United Kingdom, Asian and Middle Eastern countries (Jan and John, 2017, Sharma and Kumari, 2021). In Chinese herbal medicine, flower infusions of pot marigold are commonly used for treating skin disorders such as eczema, dermatitis, and small wounds (Jasoria *et al.*, 2024). In addition, its petals are often incorporated into various herbal formulas to treat digestive issues, including gastritis and peptic ulcers. In European traditional medicine, leaf and floral extracts of pot marigold have been used as analgesic and antiseptic agents to treat gastrointestinal disorders, eye problems, skin injuries, burns, and acne (Sapkota and Kunwar, 2024). Additionally, infusions made from flower heads are commonly used to treat insect bites, dermatitis, and sore throat (Dhingra *et al.*, 2022). Other solutions made from pot marigold flowers are also used as gargles, eye washes, and treatments for haemorrhoids, stomatitis, and conjunctivitis (Bokelmann, 2022, Verma *et al.*, 2018).

The *Calendula* genus includes other valuable medicinal plants such as field marigold. Field marigold extracts have been used to stimulate blood flow, as an diaphoretic and sedative, anti-inflammatory, anti-cancer and anti-pyretic agents in the folk medicine of such European countries as Italy and Spain (Arora *et al.*, 2013, Khouchlaa *et al.*, 2023, Muley *et al.*, 2009). It has also been used as a disinfectant, anti-spasmodic, as well as a healing agent for wounds

and burns. Further, some of the less-known members of the *Calendula* genus such as *C. persica* and *C. stellata* have also been used in medicine. For example, infusions of *C. persica* were used to treat kidney stones (Arora *et al.*, 2013)

1.2.2 Asteraceae in modern medicine

Unlike traditional medicine, modern medicine demands evidence from clinical trials that proves specific formulations outperform placebos. It also enforces standards for production, quality, and dosages. Natural products from a few plant species have passed these tests and are used as drugs in modern medicine. One of the most famous examples is artemisinin, for which the discovery was awarded the 2015 Nobel Prize (da Silva *et al.*, 2023). Artemisinin is an anti-malarial compound produced by the Asteraceae species, *Artemsia annua* (sweet wormwood), a herb with a long history of use in traditional Chinese medicine (Ikram and Simonsen, 2017, Septembre-Malaterre *et al.*, 2020).

Following the discovery of artemisinin, significant efforts were applied to increase its production due to high demand and inconsistent yields from field production (Qamar *et al.*, 2024b, Wani *et al.*, 2021). The complex chemical structure of artemisinin means that chemical synthesis is economically unfeasible. Therefore, synthetic biology and metabolic engineering approaches were used to identify the biosynthetic pathway and enable heterologous production in other organisms (Badshah *et al.*, 2018, Paddon and Keasling, 2014, Qamar *et al.*, 2024a). It was hoped that an alternative source of artemisinin might stabilise the supply and price of anti-malarial therapies for patients in the developing world. However, the economic sustainability of biological production has proved difficult (Bokelmann, 2022, Verma *et al.*, 2018).

The success of artemisinin in modern medicine was largely due to the ability to link the specific bioactive compound to the therapeutic effects of the plant extract. While many other Asteraceae plants have been reported to exhibit bioactivity, in most cases, the precise bioactive molecules remain unidentified. One of the most frequently reported biological properties of the Asteraceae plants is their strong anti-inflammatory activity (Rolnik and Olas, 2021). As discussed in the previous section, pot marigold is no exception and is valued for its anti-inflammatory and wound-healing activities, which will be investigated in this thesis. I, therefore, discuss inflammation and its current treatments in more detail in the next section.

1.3 Inflammation and its treatment

1.3.1 The inflammatory response

In mammals, inflammation is a vital biological process triggered by various factors, such as exposure to pathogens, toxins, or cell damage (Chen *et al.*, 2017). It is needed for the removal of harmful stimuli and to initiate the healing process. However, uncontrolled acute inflammation may become chronic, which is an underlying cause of non-communicable diseases such as stroke, cancer, and diabetes (Arulselvan *et al.*, 2016).

Although inflammatory responses depend on both the organism and the nature of the initial stimulus, they share a common mechanism (Chen *et al.*, 2017). First, pathogen- or danger-associated molecules (PAMs/DAMs) are recognised by the surface receptors of immune cells.

The types of receptors that are activated i on the nature of the stimuli:. Toll-like receptors (TLR) and interferon receptors (IFNR) respond to molecules associated with fungal, bacterial and viral infections. B-cell or T-cell receptors (TCR/BCR) recognise foreign antigens. Receptor tyrosine kinases (RTK) respond to polypeptide growth factors, cytokines and hormones. Tumour necrosis factor receptors (TNFRs) respond to inflammatory cytokines - soluble or membrane-bound tumour necrosis factor α (TNF-α). Cluster of differentiation 40 receptors (CD40) recognise CD40 transmembrane proteins, which are important for B and T cell activation; Receptor Activator of Nuclear Factor-kappa B (RANK) –recognises tumour necrosis factor ligand superfamily member 11 (RANKL), a master mediator of osteoclast differentiation, activity and survival (Chen *et al.*, 2017, Zhao *et al.*, 2021).

Depending on the cell type (e.g. monocytes, fibroblasts, neurons, keratinocytes), receptors activate different inflammatory signalling pathways. Among them are the nuclear factor kappa B (NF-κB) pathways (classical and non-classical), the mitogen-activated protein kinase (MAPK) pathways, the Janus kinase (JAK)/signal transducer and activator of transcription (STAT) pathway and the phosphatidylinositol 3kinase (PI3K)/protein kinase B (AKT) signalling pathway (Arulselvan *et al.*, 2016, Chen *et al.*, 2017, Zhao *et al.*, 2021) (**Figure 1.3.**). In each pathway, a cascade of biochemical reactions leads to the phosphorylation of transcription factors that bind to corresponding promoters or enhancer

sequences to drive the transcription of the genes associated with inflammatory mediators (Chen *et al.*, 2017, Criollo-Mendoza *et al.*, 2023, Megha *et al.*, 2021).

Of the transcription factors involved in the regulation of inflammatory responses, NF-κB is considered to be a master regulator, controlling the transcription of genes involved in inflammatory responses and cellular survival (Liu *et al.*, 2020). "NF-κB" refers to a family of transcription factorsthat comprises five members that form homo- and hetero-dimeric complexes, including NFκB1 (p50), NFκB2 (p52), RelA (p65), RelB, and c-Rel (Liu *et al.*, 2020). In this thesis, NF-κB is used to refer to the p65/p50 heterodimer, which participates in the classical NF-κB pathway (**Figure 1.3**.).

The classical NF-κB pathway is activated by lipopolysaccharide (LPS) or cytokines such as TNF-α or interleukin 1 (IL-1), which bind to either TLR, TCR/BCR, or TNFR receptors (Liu *et al.*, 2020) (**Figure 1.3.**). NF-κB is constitutively present in healthy cells, where it remains inactive in the cytosol controlled by an inhibitor of kappa-B (IκB) (**Figure 1.3.**). Upon activation of the NF-κB pathway, the β subunit of IKK is phosphorylated. IKK phosphorylates IκB, which resides in the cytosol bound to homo- or hetero-dimers of NF-κB, enabling it to be ubiquitinated and targeted for proteasomal degradation (Liu *et al.*, 2020). When release from the complex, NF-κB dimers translocate to the nucleus to activate the transcription of target genes (Trares *et al.*, 2022). A common p65/p50 heterodimer, for example, regulates the production of TNF-α and IL-6, while c-Rel/p65 regulates the production of interleukin IL-8. TNF-α is a pro-inflammatory cytokine known to play a key role in both innate and adaptive immunity by regulating cell proliferation, differentiation, migration, necrosis, apoptosis, and survival (Jang *et al.*, 2021). IL-6 has both pro- and anti-inflammatory properties depending on its concentrations and combinations with other cytokines (Borsini *et al.*, 2020). It is produced at the site of inflammation and plays a key role in the acute phase response by acting as a main stimulator of acute-phase protein synthesis (e.g. c-reactive protein, serum amyloid A, fibrinogen, alpha 1-antitrypsin) (Castell *et al.*, 1989, Gabay, 2006). IL-8 is known as a chemoattractant cytokine, which has a unique role in attracting neutrophils to the site of inflammation (Matsushima *et al.*, 2022).

In the non-classical NF-κB pathway (**Figure 1.3.**), activation of RANK/CD40 receptors leads to stabilisation of Nck Interacting Kinase (NIK), which is normally degraded in healthy cells (Sun, 2011, Sun, 2017). Increased levels of NIK promote IKKα phosphorylation which, in turn, phosphorylate RelB/p100. This induces partial proteasomal processing of p100, resulting in the release of RelB/p52 heterodimers that translocate to the nucleus to activate

the transcription of target genes, such as *C-X-C MOTIF CHEMOKINE LIGAND 12* and *13 (CXCL12* and *CXCL13)* (McDaniel *et al.*, 2016). *CXCL12* and *CXCL13* code for theed the chemokines CXCL12 and CXCL13, which are pro-inflammatory molecules that attract and activate immune cells at the site of inflammation. CXCL12 regulates the migration of leukocytes (Cambier *et al.*, 2023), while CXCL13 attracts B lymphocytes, T lymphocytes, and other immune cells (Hui *et al.*, 2024).

The MAPK pathway is an important signalling pathway in eukaryotes and has been described in mammals, plants and fungi (Bardwell, 2006) (**Figure 1.3.**). In mammals, receptors such as RTK, cytokines and growth factors activate a distinct set of downstream kinases (Zhang and Liu, 2002). In the first step, transforming growth factor-β (TGF-β)-activated kinase 1 (TAK1) and rapidly accelerated fibrosarcoma (RAF) kinases activate mitogen-activated protein kinase kinases, MKK and MEK, respectively. This results in the phosphorylation and activation of the MAPK extracellular signal-regulated kinase-1 (ERK1), c-Jun N-terminal kinase (JNK) and p38. In turn, they are responsible for the activation of the dimeric transcription factor activating protein-1 (AP-1) complex (Zhang and Liu, 2002), cellular myelocytomatosis oncogene transcription factor (c-Myc) and p65/p50 (via activation of IκB by TAK1). Members of AP-1 regulate the transcription of genes that are associated with many cellular processes ranging from cell survival, proliferation and differentiation to the immune cell apoptisis (Atsaves *et al.*, 2019). C-Myc is consisred to be a 'super-transcription factor' estimated to impact the expression of ~15% of all human genes and to influence essential processes such as proliferation, differentiation, the survival of normal cells, programmed cell death, and immune regulation (Dang *et al.*, 2006).

In the JAK/STAT inflammatory pathway (**Figure 1.3.**), interferons or cytokines (IL-6, IL-11, IL-12, IL-23, IFN-α/β/γ) bind to their corresponding receptors inducing receptor dimerisation of their subunits and the recruitment of JAK tyrosine kinases (Hu *et al.*, 2023). This results in the autophosphorylation and activation of JAKs, which, in turn, phosphorylate signal transducers and activators of transcription (STATs) (Hu *et al.*, 2021). Once activated, STAT proteins form homo- or hetero -dimers and translocate into the nucleus. In the nucleus, STAT dimers recognise and bind to specific gene regulatory DNA sequences and either induce or repress the transcription of genes associated with cell activation, proliferation, and differentiation. For example, STAT 3 regulates the expression of the anti-apoptotic factor B-cell lymphoma-extra arge (BclXL), c-Myc, which is necessary for cell division, and β-

Catenin transcriptional factor, which promotes cell-to-cell adhesion (Lu *et al.*, 2017). STAT4 drives the production of IFNγ, IL10 and Th1 cell differentiation (Lund *et al.*, 2004).

Finally, the PI3K signalling pathway begins with the binding of the corresponding ligand to RTK, cytokines or growth factor receptors (Fruman *et al.*, 2017). This results in the autophosphorylation orf tyrosine domains leading to the recruitment of PI3 kinase (p85 and p100 subunits) (Wankhede *et al.*, 2023). Activated PI3K phosphorylates and activates normally inactive protein kinase B (AKT). The phosphorylated AKT, in turn, activates various downstream substances, with the major downstream branch being activation of the mammalian target of rapamycin complex 1 (mTORC1), which affects S6 kinase-1 (S6K-1) and eukaryotic translation initiation factor 4E binding protein-1 (4EBP-1) (**Figure 1.3.**) (Sun *et al.*, 2020). S6K-1 and 4EBP-1 regulate cell cycle progression and the formation of new blood vessels. Phosphorylated AKT activates IKK through the phosphorylation of the IKKβ subunit leading to the activation of NF-κB downstream signalling (Wankhede *et al.*, 2023). As mentioned above, this drives the transcription of inflammation-related genes (IL-1β, IL-6, TNF-α, iNOS, and COX-2).

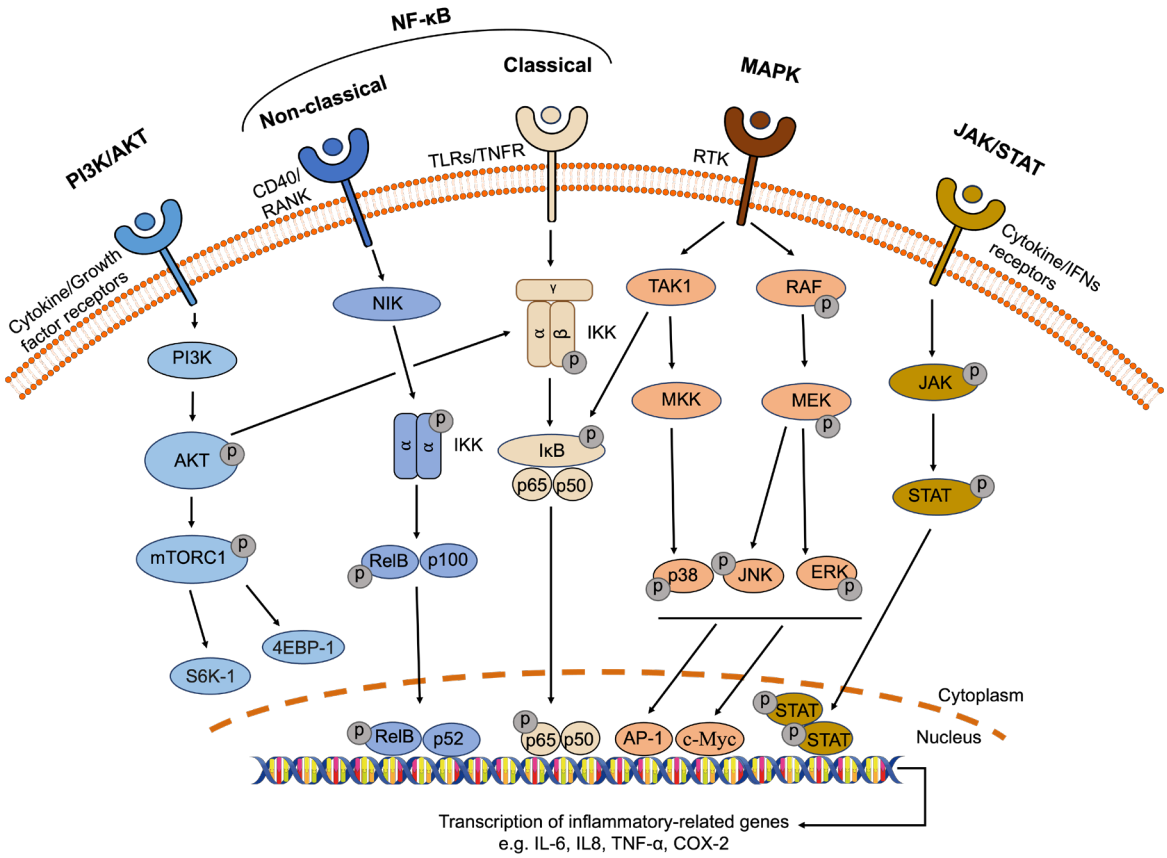

Figure 1.3 Examples of inflammatory responses. Inflammatory stimuli are recognised by the receptors displayed on the surface of immune cells (CD40 R = Cluster of differentiation 40 receptor; RANK = The receptor Activator of Nuclear Factor-kappa B; TLR = Toll-like receptors; TNFR = Tumour necrosis factor receptor; RTK = Receptor tyrosine kinases; IFNR = interferon receptors). This activates one or multiple signalling pathways (factor kappa b (NF-κB) pathways (classical and non-classical), the mitogen-activated protein kinase (MAPK), and the Janus kinase (JAK)/signal transducer and activator of transcription (STAT) pathway and the phosphatidylinositol 3-kinase (PI3K)/protein kinase B (AKT) signalling pathway). In the pathways, a chain of biochemical reactions involving protein kinases leads to the phosphorylation of the associated transcription factors. In the non-canonical NF-κB pathway, Nck Interacting Kinase (NIK) phosphorylates IkappaB kinase (IKK), which leads to the phosphorylation of RelB/p52 dimer. In the canonical NF-κB pathway, IKK phosphorylates IkappaB kinase (IkB), which leads to dissociation and formation of phosphorylated p65/p50 dimer. In MAPK, kinases like transforming growth factor-β (TGF-β)-activated kinase 1 (TAK1) and rapidly accelerated fibrosarcoma (RAF) kinases activate mitogen-activated protein kinase kinases - MKK and MEK, respectively. Members of MKK and MEK activate extracellular signal-regulated kinase-1 (ERK1), c-Jun N-terminal kinase (JNK) and p38 kinase. These phosphorylate and activate members of activating protein-1 (AP-1) transcription factors. In the JAK/STAT pathway, JAKs phosphorylate members of signal transducers and activators of transcription (STATs). In the PI3K/AKT pathway, activated PI3K phosphorylates and activates normally inactive protein kinase B (AKT). AKT in turn phosphorylates IKK, which phosphorylates IkB leading to dissociation and formation of phosphorylated p65/p50 transcription factor. In the nucleus, transcription factors bind to corresponding promoters to drive the production of pro-inflammatory mediators (cytokines, chemokines, oxygen and nitrogen reactive species (ROS/NOS)).

1.3.2 Anti-inflammatories

The primary categories of anti-inflammatory drugs include nonsteroidal anti-inflammatory drugs (NSAIDs), corticosteroids, biologicals, and disease-modifying anti-rheumatic drugs

(DMARDs) (Dinarello, 2010). NSAIDs such as ibuprofen, naproxen, and aspirin are the most commonly used anti-inflammatory agents. They inhibit the cyclooxygenase (COX) enzymes COX-1 and COX-2, which synthesise inflammatory mediators called prostaglandins and thromboxanes (Ferreira *et al.*, 2024). Corticosteroids, including prednisone, dexamethasone, and hydrocortisone modulate inflammation by suppressing multiple pro-inflammatory genes via glucocorticoid receptor-mediated inhibition of the NF-κB pathway (Barnes, 2006). In addition, a wide range of ''biologicals'' have been developed to treat inflammation in the past decade. These agents specifically target cytokines (TNF-α, IL-1β, IL-6, IL-17, IL-12, IL-23) or corresponding receptors (Dinarello, 2010). For example, TNF-α inhibitors, such as infliximab and adalimumab block the release of this pro-inflammatory cytokine via inhibition of the NF-κB pathway, reducing tissue damage and inflammation (Yu *et al.*, 2020). Other cytokine inhibitors include tocilizumab which downregulates the production of IL-6, and anakinra which inhibits IL-1 (Chandran *et al.*, 2021). Finally, DMARDs, including such compounds as methotrexate and sulfasalazine, are aimed at slowing down the progression of autoimmune inflammatory diseases by modulating immune cell activity and reducing cytokine production (Benjamin *et al.*, 2018).

One approach for discovering new anti-inflammatory agents is a bio-rational approach. This relies on deriving potential drugs from biological samples that are used either in traditional medicines or have ecological functions in microorganisms/plants (Jamtsho *et al.*, 2024). For instance, a potent anti-inflammatory diterpenoid, triptolide, was first isolated from *Tripterygium wilfordii* (thunder god vine), which is traditionally used in traditional Chinese medicine to treat inflammatory-related diseases (Bao *et al.*, 2024). This drug reduces inflammation by suppressing the activity of NF-κB p65 and has been shown to induce apoptosis in myeloma cancer cell lines and in malignant glioblastoma tumours (Li *et al.*, 2024a, YinJun *et al.*, 2005).

As noted above (**section 1.2.2.**) extracts of many Asteraceae species, including pot marigold, have shown anti-inflammatory activities. In many cases, these have been associated with plant secondary metabolites, which are discussed below.

1.4 Plant secondary metabolites

The bioactivity of medicinal plants is associated with the presence of natural products. In this section, I will describe the role, evolution, and diversity of plant secondary metabolites, which are also referred to as 'specialised' metabolites.

1.4.1 Role in plants

During their lifecycle, plants synthesise a great number of different compounds to accommodate their needs through development. Molecules that are found in all species, perform vital metabolic processes and are essential for survival are known as primary metabolites (Salam *et al.*, 2023). However, along with the primary metabolites, plants also synthesise a tremendous number of secondary metabolites, which use primary metabolites as precursors. They are also referred to as specialised metabolites because they are not essential for normal growth and development but play important roles in the interaction between plants and their specialised environments, contributing to the adaptation to ecological niches (Pagare *et al.*, 2015, Xu *et al.*, 2023b).

The majority of these molecules protect plants from biotic and abiotic factors. For example, many sesquiterpenes are toxic or unpalatable to herbivorous mammals (Pagare *et al.*, 2015). Other molecules such as 3,4′-di-O-methylellagic and ellagic acids or 3β-hydroxylanosta-9,24-dien-21-oic acid exhibit the ability to inhibit microbial growth (Mosa *et al.*, 2014). One mechanism of anti-microbial inhibition is the damage of negatively charged bacterial cell surfaces by positively charged metabolites (Spivak *et al.*, 2020).

It has also been shown that plants produce and accumulate toxic molecules in nectar to protect it from nectar robbers and inefficient pollinators (Barberis *et al.*, 2023). Further, secondary metabolites are important in responses to drought and heavy metals. These environmental stresses can induce oxidative stress, inducing the accumulation of toxic free radicals that result in protein, lipid, and DNA damage (Bartwal *et al.*, 2013). Flavonoids and polyphenols are natural free-radical scavengers that can reduce oxidative stress (Shomali *et al.*, 2022, Zagoskina *et al.*, 2023).

Defence is not the only function of secondary metabolites. Some are pigments or signalling compounds to attract pollinators. For instance, phenolic compounds including flavonoids and anthocyanins are responsible for flower colours (Kabera *et al.*, 2014) and small volatile

organic compounds are constituents of floral scents. The composition and emission rate of floral scents can attract different pollinators, for example, the bumblebee-pollinated purple monkeyflower and the hummingbird-pollinated scarlet monkeyflower (Byers *et al.*, 2014a).

Another function of secondary metabolites is to help plants to shape their microbiota (Huang *et al.*, 2019, Yang *et al.*, 2018). A recent study showed that the microbiome can be influenced by plant metabolites including coumarins, glucosinolates, benzoxazinoids, camalexin, and triterpenes (Borges *et al.*, 2015, Jacoby *et al.*, 2021, Su *et al.*, 2023, Yang *et al.*, 2016). Further, aldehydes, phenylpropanoids and some monoterpenes were shown to influence plant microbiomes through selective anti-microbial properties (Boachon *et al.*, 2019, Farré-Armengol *et al.*, 2016, Pang *et al.*, 2021, Schulz-Bohm *et al.*, 2018).

Plant hormones play a crucial role in the regulation of secondary metabolism, often dependent on the developmental stage or the environmental context (Kumari *et al.*, 2024). Although these signalling molecules are often involved in both developmental and stress responses, they are broadly classified into two groups: stress-related hormones and growth-related hormones. Compounds such as jasmonic, abscisic, salicylic acids, as well as ethylene are primarily associated with stress responses. These regulate the production of secondary metabolites during environmental stress conditions (Gasperini and Howe, 2024, Goossens *et al.*, 2016). On the other hand, auxin, gibberellic acid, cytokinins, brassinosteroids, and strigolactones are mainly involved in governing developmental processes.

1.4.2 The evolution of specialised metabolism

Natural selection and evolution have resulted in different plant species producing a distinct set of secondary metabolites suited for reproduction and survival in their environmental niches (Wink, 2003). To date, tens of thousands of plant secondary metabolites have been discovered (Dixon and Dickinson, 2024, Goossens *et al.*, 2003). Evidence of chemical defence can be found even in early land plants, which means that some enzymes evolved at least 450 million years ago (Waters, 2003). Plant species can evolve new enzymes but also lose enzymes used in the production of specialised metabolites. It has been observed that different plant lineages have independently evolved the ability to make compounds present in other plants, and sometimes evolve the ability to make different compounds with the same biological function (Ono and Murata, 2023).

There are two main principles by which plants evolve the ability to make an identical chemical: either the same substrate is converted to the same product by unrelated enzymes, or, alternatively, there are multiple substrates that can be converted to the same product through different reactions (Ono and Murata, 2023, Pichersky and Lewinsohn, 2011). An example of the former principal is the evolution of flavone apigenin that is produced in the Apiaceae family through the action of flavone synthase (FNS) which belongs to the oxoglutarate-dependent dioxygenase (OGD) family (Pucker and Iorizzo, 2023). However, in most other plant species, the oxidoreductase that catalyses the same reaction is a member of the cytochrome P450 family. An example of identical compounds that are synthesised from different substrates is the production of methyl anthranilate in *Vitis vinifera* (grape) and *Zea mays* (maize). In grapes, the substitution of the CoA group on anthranilate-CoA with methanol is facilitated by an enzyme from the BAHD acyl transferase family, while in maize, it involves the transfer of a methyl group from S-adenosyl-L-methionine to anthranilic acid, catalysed by an enzyme from the SABATH family (Köllner *et al.*, 2010, Wang *et al.*, 2018).

A classical example of different plant species using different compounds for the same physiological or ecological role is the use of pigments. For instance, anthocyanins are flavonoid pigments that give blue, purple, pink and red colours to the flowers, fruits, vegetables and berries of many plant species. However, plants that belong to the Caryophyllales order, except one family (Caryophyllaceae), lack anthocyanin pigments but, instead, produce betacyanins (Timoneda *et al.*, 2019).

Genetically, the formation of new biosynthetic pathways typically occurs through alterations in the regulatory and protein-coding sequences of genes or via gene duplication, followed by divergence and neofunctionalization (Kliebenstein and Osbourn, 2012). The latter is proposed to be the dominant mechanism because it allows the formation of novel biosynthetic pathways alongside the conservation of old pathways (Moghe and Last, 2015). Four main mechanisms of gene duplication have been described in plants: (1) local (tandem) duplication, (2) polyploidy, (3) chromosomal segment duplication and (4) single gene transposition-duplication (Freeling, 2009). In tandem duplication, an identical sequence is formed adjacent to the original gene. This type of gene duplication plays a particularly significant role in the evolution of BGCs (Liu *et al.*, 2020, Polturak and Osbourn, 2021). Such clusters are physically linked and comprised of co-expressed genes necessary for the biosynthesis of specific metabolites. Their products are known to be associated with biotic and abiotic stress responses (Polturak *et al.*, 2022).

As discussed in **section 1.1.2.**, polyploidisation is argued to drive the evolution of new traits by facilitating changes in genome size and enabling the development of novel functions, allowing organisms to adapt to new ecological niches (Barker *et al.*, 2008). Whole-genome duplications in polyploidy create gene redundancy, which provides the opportunity for homeologs to diverge and acquire new functions without compromising existing ones.

During meiosis, duplication of anything from a few genes to a whole chromosome can also occur. This can enable the divergence of genes within the segment (Freeling, 2009, Lallemand *et al.*, 2020). Finally, in single gene transposition-duplication, single genes relocate to a new chromosomal position and segregants contain duplicates (Freeling, 2009). This mechanism is also characteristic of highly dynamic regions of BGC which are enriched in transposable elements (Kliebenstein and Osbourn, 2012). Together, these genetic mechanisms increase the sizes of gene families, whereas deletions of genes or chromosome segments may decrease gene family size (Guo, 2013).

1.4.3 Diversity and biosynthesis of specialised metabolites

Plant secondary metabolites can be generally separated into four groups (a) Terpenoids (b) Phenolics (c) Sulphur containing compounds and (d) Nitrogen-containing compounds (Kabera *et al.*, 2014, Sawai and Saito, 2011).

Of these, terpenoids form the largest group. They are hydrophobic molecules with highly diverse structures (more than 29,000 known structures) synthesised via two distinct pathways – the mevalonic acid pathway (MVA) and the 2-C-methyl-D-erythritol 4-phosphate (MEP) pathway (Li *et al.*, 2023b). The MVA pathway is an essential metabolic pathway present in eukaryotes (animals, plants, protists and fungi), archaea and some bacteria (Borrelli and Trono, 2016) and plays an essential role in the production of triterpenoids, sterols and sesquiterpenoids from Acetyl-CoA molecules. The MEP pathway has been identified in eubacteria and in the plastids of algae and higher plants, which are derived from cyanobacteria. The MEP pathway is responsible for the formation of monoterpenoids, diterpenoids and tetraterpenoids via the metabolism of pyruvate and D-glyceraldehyde 3- phosphate (GAP) molecules (**Figure 1.4.**).

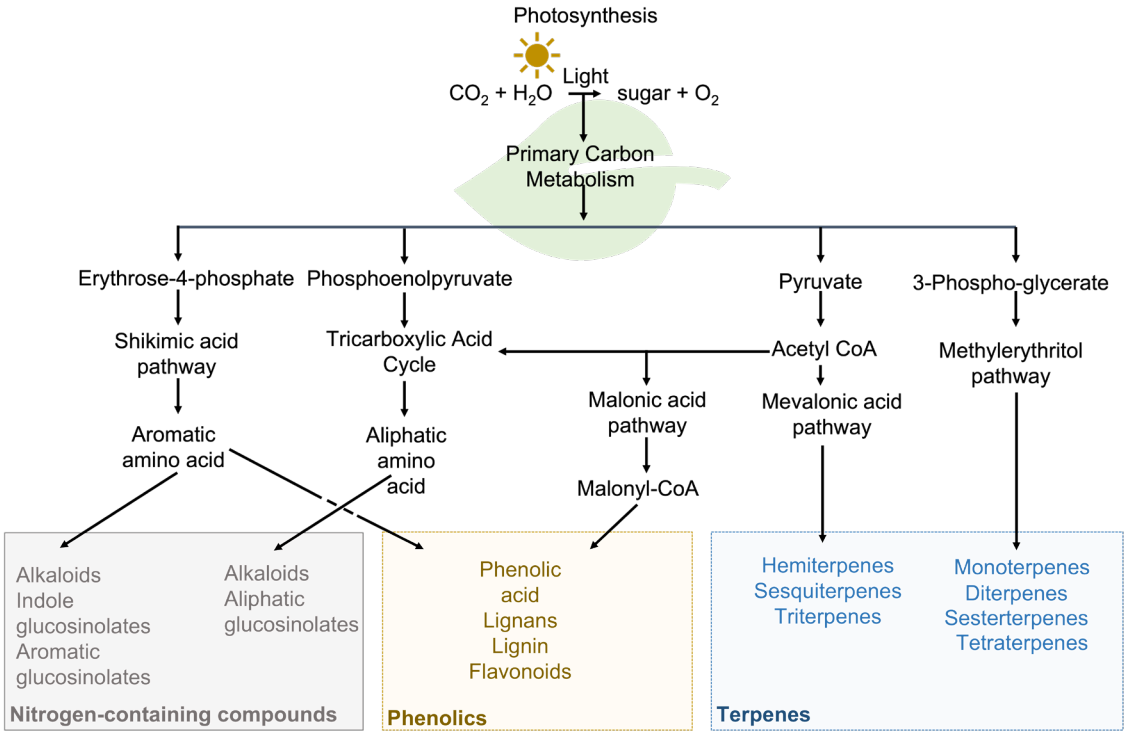

Figure 1.4 Schematic representation of the biosynthesis of the three main classes of plant secondary metabolites. Image adapted from (Borrelli and Trono, 2016).

1.4.4 Terpenes

Terpenes are further classified into five distinct groups: monoterpenes, sesquiterpenes, diterpenes, triterpenes and tetraterpenes (Jan *et al.*, 2021). All terpenes are made from five carbon molecules called isopentenyl diphosphate (IPP) and dimethylallyl diphosphate (DMAPP). In plants, monoterpenes (C10), diterpenes (C20), sesterterpenes (C25) and tetraterpenes (C40) are synthesised in plastids, however, hemiterpenes (C5), sesquiterpenes (C15) and triterpenes (C30) are produced in the cytosol and other subcellular compartments, such as the endoplasmic reticulum (Demurtas *et al.*, 2023, Vranová *et al.*, 2013). In the cytosol, IPP and DMAPP molecules are supplied from the MVA pathway and, in the plastid, from the methylerythritol phosphate (MEP) pathway (Kirby and Keasling, 2009) (**Figure 1.5.**).

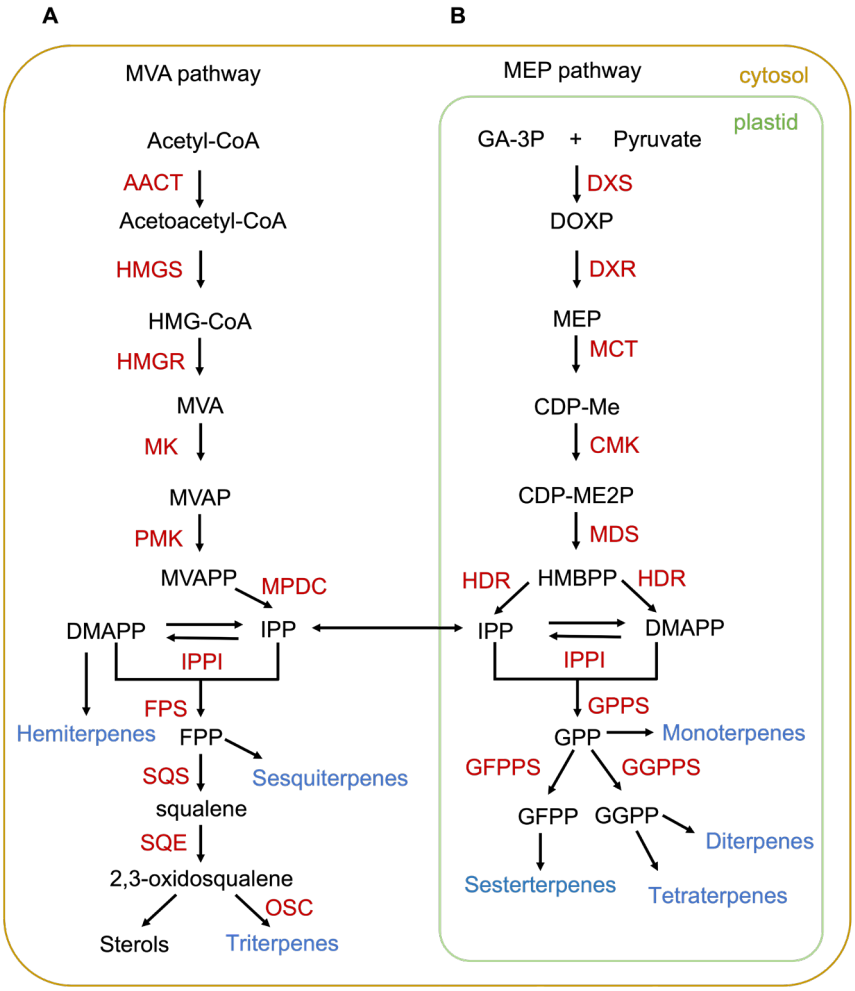

Figure 1.5 Terpene biosynthesis in plants. (A) The MVA pathway. Compound abbreviations: CoA = Coenzyme A; HMG = 3- hydroxy-3-methylglutaryl-CoA; MVA = mevalonate; MVAP = Mevalonate-5-phosphate; MVAPP = Mevalonate-5-diphosphate; FPP = farnesyl diphosphate; Enzymes abbreviations: AACT = Acetyl-CoA C-acetyltransferase; HMGS = HMG-CoA synthase; HMGR = HMG-CoA reductase; MK = MVA kinase; PMK = Phospho-MVA kinase; MPDC = Diphospho-MVA kinase; IPPI = IPP isomerase; FPS = FPP synthase; **(B) The MEP pathway.** Compound abbreviations: GA-3P = D-glyceraldehyde-3-phosphate; DXP = 1-deoxy-D-xylulose 5–phosphate; MEP = 2-C-Methyl-D-erythritol 4-phosphate; CDP-ME = 4- (Cytidine 5'-diphospho)-2-C-methyl-D-erythritol; CDP-ME2P = 2-Phospho-4-(cytidine 5'- diphospho)-2-C-methyl-D-erythritol; ME-2,4-cPP = 2-C-Methyl-D-erythritol , 2,4- cyclodiphosphate; HMBPP = 4-Hydroxy-3-methylbut-2-enyl-diphosphate; DMAPP = dimethylallyl diphosphate, GPP = geranyl diphosphate, GGPP = geranylgeranyl diphosphate. Enzymes abbreviations: DXS = DXP synthase; DXR = DXP reductoisomerase; MCT = MEP cytidylyltransferase; CMK = CDP-ME kinase; MDS = ME-2,4cPP synthase; HDS = HMBPP synthase; HDR = HMBPP reductase; GPPS = GPP synthase; GGPPS = GGPP synthase; SQS = Squalene synthase; SQE = Squalene epoxidase; OSC = Oxidosqualene cyclese. Made with ChemDraw (v. 22.2.0).

1.5 Triterpenoids

This thesis is focused on the biosynthesis of triterpenes, which are the largest group of terpenes with about 200 known scaffolds and more than 20,000 individual molecules (Thimmappa *et al.*, 2014). Many compounds that belong to this class of secondary metabolites have been associated with numerous bioactivities ranging from the reduction of

oxidative stress, and inhibition of cell proliferation to induction of cellular apoptosis (Rufino-Palomares *et al.*, 2015). In particular, however, many triterpenes, including those found in pot marigold, have been associated with the suppression of inflammation (Colombo *et al.*, 2015, Yadav *et al.*, 2010), which will be discussed in (**section 1.6.1.**). The biosynthesis of triterpenes is discussed below.

1.5.1 Triterpene biosynthesis

Triterpene biosynthesis occurs through the MVA pathway as follows: acetyl-CoA undergoes a set of conversion reactions to yield the universal triterpene precursor molecules - IPP and DMAPP (Kirby and Keasling, 2009). Acetyl-CoA thiolase condenses two acetyl-CoA molecules together to generate acetoacetyl-CoA. Then, HMG-CoA synthase adds a third molecule of acetyl-CoA to acetoacetyl-CoA producing 3-hydroxy-3-methylglutaryl-CoA (HMG-CoA). This molecule then undergoes nicotinamide adenine dinucleotide phosphate (NADPH)-dependent reduction by hydroxy-3-methylglutaryl-CoA reductase (HMGR), yielding mevalonic acid. Mevalonate is, in turn, converted to mevalonate-5-diphosphate through the successive addition of phosphate groups to mevalonate and mevalonate-5-phosphate by mevalonate kinase and phosphomevalonate kinase, respectively. At the final stage of IPP synthesis, mevalonate-5-diphosphate undergoes decarboxylation catalysed by diphospho-mevalonate decarboxylase producing IPP (**Figure 1.6.**). Once IPP molecules are formed, they can be reversibly converted to their isomer, DMAPP, by IPP-DMAPP isomerase (IDI) (Kirby and Keasling, 2009, Thimmappa *et al.*, 2014, Vranová *et al.*, 2013).

IPP and DMAPP, each consisting of 5-Carbon atoms, are combined to form a longer chain triterpene precursor, geranyl pyrophosphate (GPP). This reaction is catalysed by prenyltransferase geranyl pyrophosphate synthase. A second molecule of IPP is added to GPP forming 15-C farnesyl pyrophosphate (FPP). Then, two FPP molecules are fused together by squalene synthase to produce the 30-C squalene molecule. Finally, squalene undergoes oxidation by squalene epoxidase to form 2,3-oxidosqualene, the substrate for almost all triterpene scaffolds (Niżyński *et al.*, 2015) (**Figure 1.6.**).

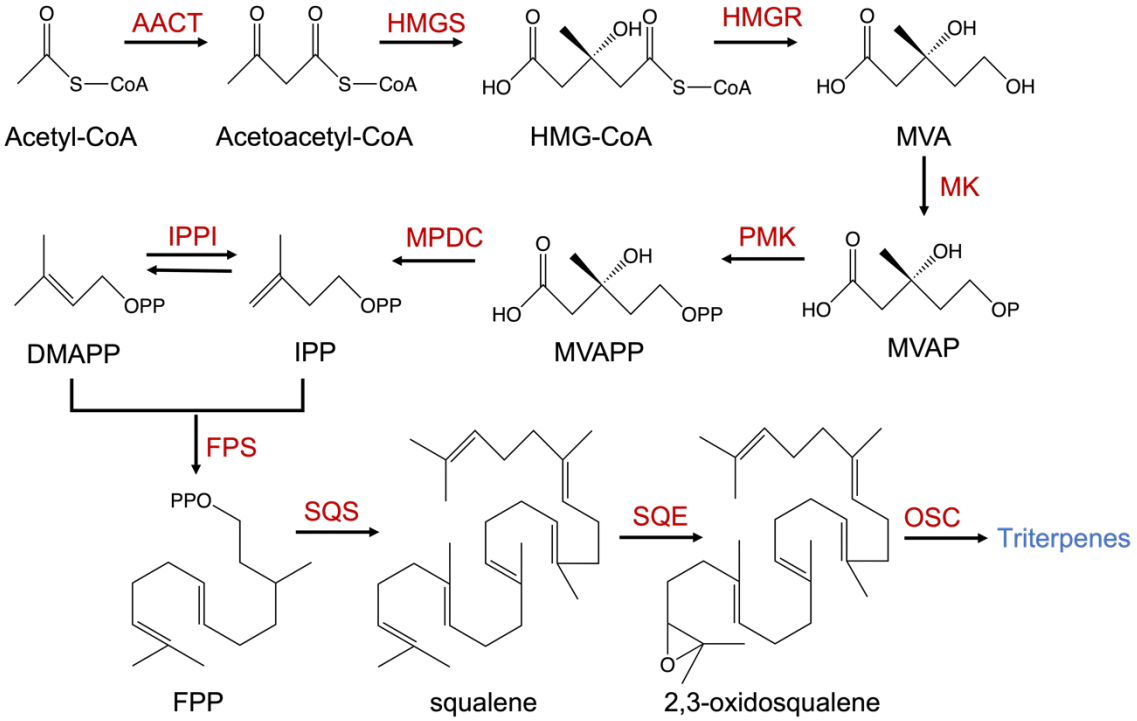

Figure 1.6 Triterpenes biosynthesis in plants. Compound abbreviations: CoA = Coenzyme A; HMG = 3- hydroxy-3-methylglutaryl-CoA; MVA = mevalonate; MVAP = Mevalonate-5-phosphate; MVAPP = Mevalonate-5-diphosphate; IPP = isopentenyl diphosphate, DMAPP = dimethylallyl diphosphate; FPP = farnesyl diphosphate. Enzymes abbreviations: AACT = Acetyl-CoA C-acetyltransferase; HMGS = HMG-CoA synthase; HMGR = HMG-CoA reductase; MK = MVA kinase; PMK = Phospho-MVA kinase; MPDC = Diphospho-MVA kinase; SQS = Squalene synthase; SQE = Squalene epoxidase; OSC = Oxidosqualene cycles. Made with ChemDraw (v. 22.2.0).

1.5.2 Oxidosqualene cyclases

The cyclisation of 2,3-oxidosqualene into triterpene scaffolds is a complex process performed by oxidosqualene cyclases (OSCs) and involves four main steps (Guo *et al.*, 2024, Thimmappa *et al.*, 2014). First, the OSC binds to the linear isoprenoid substrate (2,3-oxidosqualene) and folds it to either chair-boat-chair (CBC) or chair-chair-chair CCC confirmation. Most of the pentacyclic triterpene scaffolds (lupane, hopane, ursane, oleanane, taraxaterane, and friedelane) are formed from the CCC confirmation, while a few tetracyclic triterpene skeletons (lanostane, cycloartane, and cucurbitane) are also made from CBC confirmation of the same substrate - 2,3-oxidosqualene (Liang *et al.*, 2022, Zhang *et al.*, 2023a). The cyclisation reaction is initiated by the protonation of the terminal 2,3-oxidosqualene epoxide. Initiation is followed by cyclisation and carbocation rearrangement. In this process, the C20 dammarenyl cation moves to different carbons generating a wide range of scaffold intermediates (**Figure 1.7.**). The reaction ends either upon deprotonation, which leads to the formation of triterpene monol or through water capture, which leads to the formation of triterpene diols (Segura *et al.*, 2000).

To date, more than 100 plant OSCs from 56 plant species have been discovered and characterised (Golubova *et al.*, 2025). Individual plant species typically have multiple genes encoding different OSCs and can, therefore, generate a range of triterpene scaffolds. Moreover, some OSCs are multifunctional and can generate multiple scaffolds in different proportions. All this leads to the high diversity of triterpenes in individual species (Ghosh, 2016, Thimmappa *et al.*, 2014).

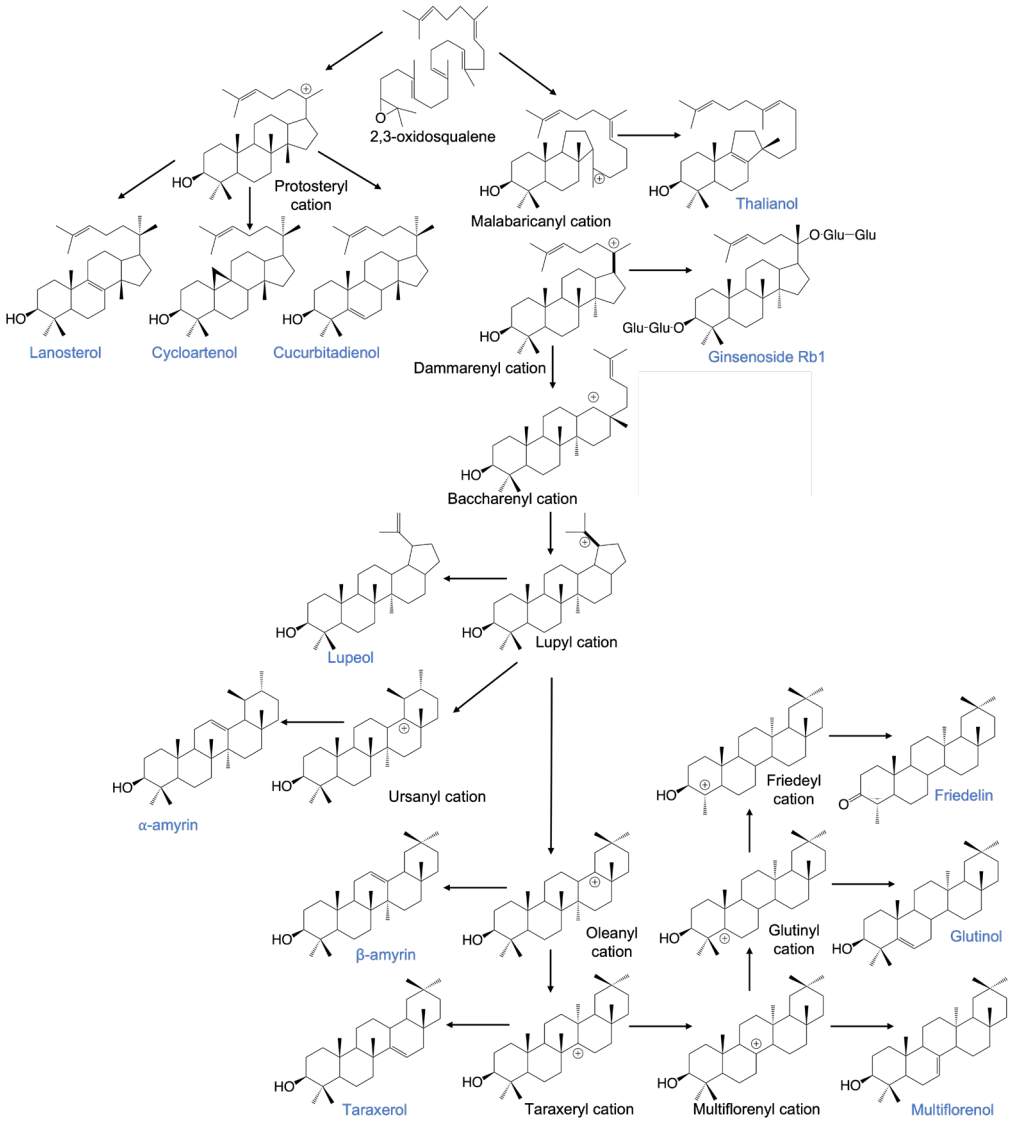

Figure 1.7 Oxidosqualene cyclisation into different triterpene scaffolds. Black text indicates positively charged intermediates, while blue text corresponds to final products. Figure is adapted from (Guo *et al.*, 2024) and made with ChemDraw (v. 22.2.0).

1.5.3 Structural diversification of triterpene scaffolds

1.5.3.1 Oxidation

Once the primary triterpene scaffolds are formed, they become substrates for decorating enzymes (Guo *et al.*, 2024). For example, cytochrome P450s (CYPs) introduce hydroxyl, ketone, aldehyde, carboxyl, or epoxy groups to one or more positions on the primary scaffold

(**Figure 1.8.**). Moreover, different CYPs can successively act on the same triterpene scaffold resulting in highly oxygenated triterpene derivatives (Ghosh, 2016).

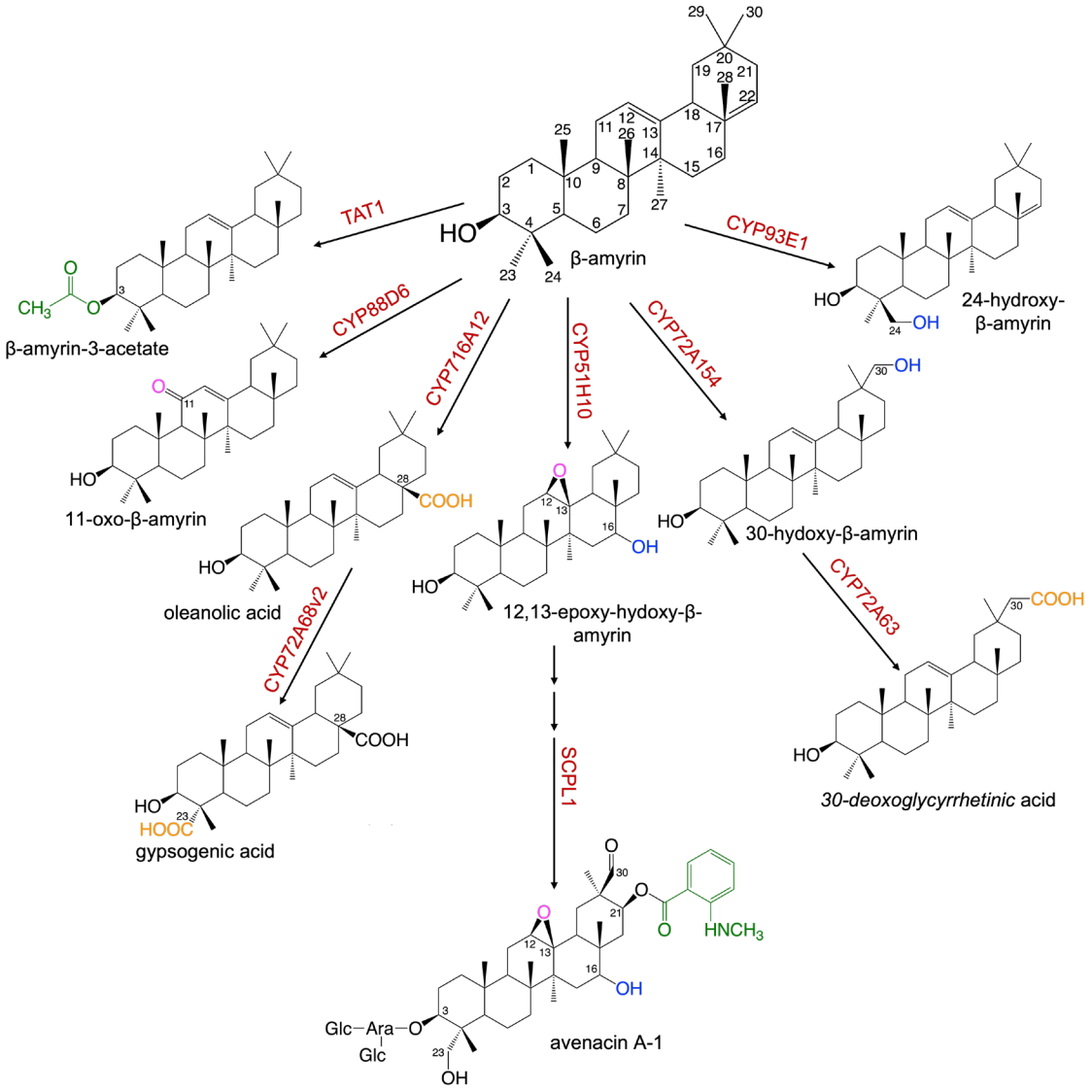

Figure 1.8 Examples of diversification of β-amyrin scaffold, by cytochrome p450s and acyltransferases. Enzymes abbreviations: TAT1 = C3 acetyl acyltransferase; CYP88D6 = 11-oxidase; CYP716A12 = C28 hydroxylase ; CYP72A68v2 = C23 oxidase; CYP51H10 = C12,13-epoxy-C16-oxidse ; SCPL1 = serine carboxypeptidase-like acyltransferase; CYP72A154 = C30 hydroxylase; CYP72 A63 = C30 oxidase; CYP3E1 = C24 hydroxylase. Made in ChemDraw (v. 22.2.0).

In the plant kingdom, CYPs play a key role in the evolution and diversification of secondary metabolites (Hamberger and Bak, 2013). The large number of these enzymes encoded in the plant genome, as well as their promiscuity, provides a base for the evolution of new specialised metabolites, which help them to interact with biotic factors and adapt to their environment (Hansen *et al.*, 2021). These enzymes have been classified into 13 distinct clans and 127 families based on their sequence homology (Ghosh, 2016). CYPs evolved to perform a wide range of functions including oxygenation to form alcohols, ketones, aldehydes, carboxylic acids, and epoxides, as well as rearrangement of carbon skeletons such as C–C bond cleavage, decarboxylation or desaturation (Hansen *et al.*, 2021, Minerdi *et al.*,

2023). Moreover, the diverse range of CYPs reactions further contributes to the expansion of the chemical diversity of secondary metabolites by providing substrates for further compound decoration by glycosylation and acylation (Ghosh, 2016, Rahimi *et al.*, 2019).

The largest eudicot family of CYPs involved in triterpenoid metabolism is CYP716. It has been suggested that this family evolved from the duplication of genes involved in brassinosteroid metabolism (Hansen *et al.*, 2021). This event resulted in new activities and contributed to the biosynthesis of triterpenoids with a defence function in land plants. The most common function that is performed by enzymes from this family is the oxidation of the C28 position of β-amyrin, α-amyrin and lupeol resulting in oleanolic acid, ursolic acid and betulinic acid production, respectively (Miettinen *et al.*, 2017a). Nevertheless, some CYP716s have been found to catalyse other triterpenoid oxidation reactions, namely C16α oxidation of β-amyrin, C22α oxidation of α-amyrin, C3 oxidation of β-amyrin, α-amyrin and lupeol, C12 oxidation of dammarenediol-II, C6 oxidation of protopanaxadiol (Ghosh, 2016, Han *et al.*, 2011, Miettinen *et al.*, 2017a).

CYPs are monooxygenases. They facilitate the transfer of an oxygen atom from molecular oxygen (O2) to their target substrates (Malhotra and Franke, 2022a). The essential element enabling this oxidative reaction is a heme prosthetic group, which activates molecular oxygen through the utilization of electrons supplied by an electron donor like NADPH. During this, a central Fe(III) ion is coordinated by both the heme porphyrin system and a cysteine thiolate ligand from the protein backbone (**Figure 1.9.**).

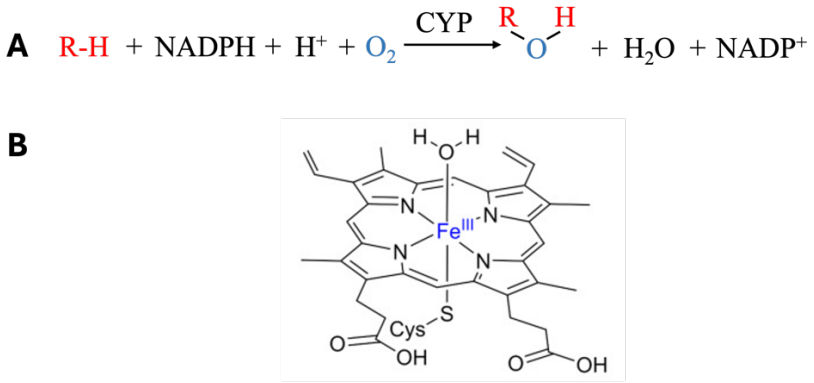

Figure 1.9 Mechanism of action of cytochrome P450 monooxygenases (CYPs). (A) The typical reaction of CYPs, resulting in hydroxylation of the substrate. **(B)** The heme prosthetic group, containing the reactive Fe^{III} ion. Figure adapted from (Malhotra and Franke, 2022a).

1.5.3.2 Glycosylation and Acylation

Many triterpenes are present in plant extracts in acylated or glycosylated forms. The addition of acyl or glycosyl group to the scaffold increases the overall polarity of the molecule and is

frequently associated with biological activities (Thimmappa *et al.*, 2014). Glycosylation and acylation most frequently occur at C3 and/or C28 positions, where sugar/s (e.g., glucose, galactose, arabinose) or acyl (acetyl, acetate, methyl, malonyl or fatty acid) are added to hydroxyl or carboxyl group to form acetates and esters, respectively (Liu *et al.*, 2020) (**Figure 1.8.**). However, apart from C3/C28, there are other positions, such as C4, C16, C20, C21 and C22, where the triterpene backbone can be glycosylated/acylated.

A 2019 examination of the public databases revealed close to 2000 putative glycosyltransferases (UGTs) in triterpene-producing plants (Rahimi *et al.*, 2019). Some of glycosylated triterpenes have been found to be bioactive, for example, triterpenoid saponins from *Xanthoceras sorbifolia* (yellow horn) have anti-tumor activity and one of the major oat root triterpene glucosides (avenacin A-1) has also been shown to have anti-microbial activity (Li *et al.*, 2021b).

Plant acyltransferases are a less-characterised class of decorating enzymes. Around 90 plant acyltransferases (ACTs) have been identified and characterised, including those that are involved in the biosynthesis of triterpenes (Xu *et al.*, 2023a). For example, the biosynthesis of avenacins, anti-microbial triterpene glycosides produced in the roots of *Avena sativa* (oat), requires acylation at the C21 position of des-acyl-avenacin A with either N-methyl anthranilate or benzoate by serine carboxypeptidase-like acyltransferase (AsSCPL1) (Mugford *et al.*, 2013) (**Figure 1.8.**). Two acetyl acyltransferases and one fatty acid acyltransferase were also found to act in thalianol biosynthesis, (Huang *et al.*, 2019). More recently, a triterpene acetyl acyltransferase from lettuce (LsTAT1), involved in the biosynthesis of pentacyclic triterpene acetates was characterised (Choi *et al.*, 2022). This study showed that LsTAT1 is a promiscuous enzyme that can produce taraxasterol, ψ-taraxasterol, β-amyrin and α-amyrin acetates.

Overall, the varied combinations of sugar, their chains and acyl groups result in the enormous diversity of triterpenes observed in plants.

1.5.3.3 Triterpene fatty acid esters (TFAEs)

The work in this thesis is focused on TFAEs, molecules that have been hypothesized to have valuable biological activities and are found in many species, including pot marigold (Colombo *et al.*, 2015, Xiao *et al.*, 2020, Yang *et al.*, 2017). Despite that TFAEs are widely distributed in nature, to date, only one triterpene fatty acid acyltransferase has been

functionally characterised (Huang *et al.*, 2016). An ACT found in *Arabidopsis thaliana* (Arabidopsis) was shown to catalyse the addition of different-length fatty acid groups (C12, C14 and C16) onto the C3 position of the triterpene scaffolds thalianol and arabidiol (**Figure 1.10.**).

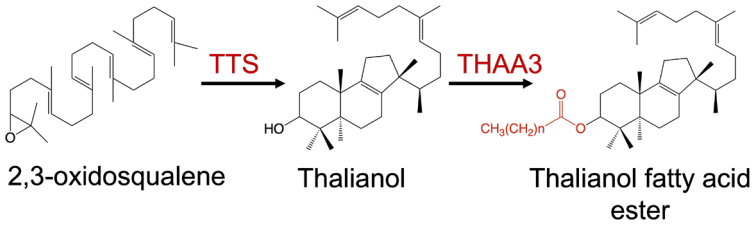

Figure 1.10 Thalianol FAEs biosynthesis. Enzymes abbreviations: TTS = thalianol synthase; THAA3 = thalianol fatty acid acyl transferase. Made with ChemDraw (v. 22.2.0).

1.6 Pharmaceutically valuable triterpenoids

Given the diversity of complex structures derived from triterpene scaffolds and the wide range of biological activities and physical properties associated with these structures, triterpenoids have attracted commercial interest as food supplements, cosmetics and pharmaceuticals (Balandrin, 1996, Miettinen *et al.*, 2017a). In particular, many triterpenes have been tested for pharmacological activities including anti-cancer, anti-microbial and anti-viral (Rufino-Palomares *et al.*, 2015). This thesis is focused on the anti-inflammatory activity of triterpenes, which I will discuss below in more detail.

1.6.1 Anti-inflammatory triterpenes

Over the years, a large body of literature has been accumulated with regard to anti-inflammatory triterpenes. For example, lupeol and its derivative, betulinic acid, obtained from *Hiptage benghalensis* (hiptage) were evaluated in LPS-stimulated RAW 264.7 macrophages (Hsu *et al.*, 2015). Both compounds displayed high anti-inflammatory potential inhibiting 80 and 57% of nitrogen oxide (NO) production at 10 μM and 25 μM. Both compounds increased IκB protein expression and decreased both p-p65 protein expression and the transcripts of NF-κB with 50% inhibitory concentration (IC50) values of 6.2 μM and 8.7 μM. Moreover, lupeol and its linoleate were tested *in vivo* and reduced inflammation in rat paws by 39% and 58%, respectively (Geetha and Varalakshmi, 2001). Similar activity has also been reported for three oleanane-type triterpenoids (Alnus-5(10)-en-3β-yl acetate, Oleanan-3-one and Alnus-5(10)-en-3β-ol) isolated from hiptage (Hsu *et*

al., 2015). These were shown to inhibit LPS-induced NO production in RAW 264.7 macrophages with an IC50 value of 9.6 μM, 14.3 μM and 15.3 μM, respectively.

Despite the generally low or moderate activity of the majority of ursane-type triterpenoids, α-amyrin acetate and 2β,3α,20β,23-tetrahydroxyurs-13(18)-en-28-oic-acid and javablumine A displayed significant activity on LPS-induced NO production in RAW 264.7 with IC50 values of 15.5 μM, 9.4 μM and 17.4 μM respectively (Chen *et al.*, 2020a, Ji *et al.*, 2020, Romero-Estrada *et al.*, 2016). Moreover, taraxasterol, another ursane-type triterpenoid abundant in many species including *Inula japonica* (elecampane root) and common dandelion, has also been tested in several *in vivo* anti-inflammatory assays, which suggested anti-inflammatory potential through inhibition of pro-inflammatory cytokines and NO release (Jiao *et al.*, 2022). Another study showed that taraxasterol has a concentration-dependent effect on the secretion of IL-6 and TNF-α in human colorectal adenocarcinoma (HT-29) cells (Che and Zhang, 2019). Lastly, taraxerol, isolated from the leaves of *Abroma augusta* (devil's cotton) showed a protective effect against induced acute inflammation by inhibiting pro-inflammatory cytokines (IL 1β, IL 6, IL 12 and TNF α) through the inhibition of NF-κB signalling (Khanra *et al.*, 2017).

Finally, a range of triterpene saponins with remarkable structural diversity have been shown to have strong anti-inflammatory activities. For example, species that belong to the genus *Panax* accumulate high amounts of different saponins, including ocotillol, ginsenoside Rb1 and Rg1 all shown to have anti-inflammatory potential (Gao *et al.*, 2020, Wang *et al.*, 2020). Further, the roots of liquorice have been shown to contain several anti-inflammatory triterpene glucosides. In particular, glycyrrhizin and glycyrrhizic acid can inhibit neutrophilic inflammation of the airways, regulating the expression of inflammatory cytokines and blocking the interleukin-17 (IL-17) / STAT3 pathway in animal models (Kim *et al.*, 2020, Tian *et al.*, 2020).

1.6.2 Structure-Activity Relationships

A few promising reports of triterpene bioactivity have underlined the importance of understanding the relationships between triterpene structure and the strengths of their bioactivity. For example, in a study in 2019, α-amyrin and ursolic acid were evaluated for their anti-inflammatory activity effects on phorbol ester 12-O-tetradecanoylphorbol-13-acetate (TPA) induced oedema in mice (Figueroa-Suárez *et al.*, 2019). The results of the study suggested that oleanane-type triterpenoids are far more active than those with ursane

skeleton. Based on the structure-activity relationship, the authors suggested that the presence of a keto group at C3 and carboxyl groups at C17 at the oleanane backbone, as well as an increase in the number of oxygenated functional groups in other positions, enhances the anti-inflammatory effect. In the study, it was also suggested that a double bond between C18 and C19 at the D-ring can further enhance the anti-inflammatory activity of the compounds such as moronic acids which displayed higher potential than oleanolic acid (Figueroa-Suárez *et al.*, 2019).

Similarly, the structure-activity relationship of pentacyclic triterpenoids was investigated for inhibition of four enzymes involved in the inflammatory process (5-LOX, 15-LOX-2, COX-1, and COX-2) (Vo *et al.*, 2019). This study determined that the types and configurations of polar moieties at positions C2, C3, C11, C24, and C30 are important for the inhibition of 5-LOX/COX enzymes.

Finally, another study investigated the possibility of developing more effective anti-inflammatory agents by chemically synthesising arylidene C2 derivatives of oleanolic acid (Hassan Mir *et al.*, 2021). Four out of 15 screened compounds showed stronger anti-inflammatory activity than oleanolic acid through the inhibition of TNF-α, IL-6 and NO release. The most potent compounds were found to be 3-oxo-2-(4-chlorobenzylidenyl)-olean-12-En-28-oic acid and 3-oxo-2-(4-nitrobenzylidenyl)-olean-12-en-28-oic acid, which included a benzylidenyl functional group, suggesting its importance for the anti-inflammatory potential of C2 oleanolic acid derivatives.

1.7 The discovery and engineering of biosynthetic pathways

The genetic basis of most plant metabolites has yet to be uncovered. As demonstrated for artemisinin as well as for plant compounds used in food such as vanillin, knowledge of biosynthetic pathways can provide options for biological synthesis in heterologous hosts (Cravens *et al.*, 2019). In this section, I discuss methods for elucidating biosynthetic pathways and the subsequent use of identified enzymes in pathway reconstruction in heterologous organisms.

1.7.1 Traditional approaches to the discovery of biosynthetic enzymes

Before genome and transcriptome sequencing technologies were widely available, researchers utilised classical biochemical approaches for enzyme identification. Many plant

enzymes have been identified by purification from crude extracts using chromatography and subsequent amino acid sequencing using N-terminal sequencing or mass spectrometry (O'Connor, 2009). For example, strictosidine synthase, which is involved in vinblastine biosynthesis, was among the earliest enzymes characterised from this biosynthetic pathway. It was identified by isolation from the soluble protein extract of *Catharanthus roseus* (Madagascar periwinkle) cell suspension cultures and subsequently purified by fractionation and column chromatography (Treimer and Zenk, 1979).

Enzymes from the same class often have high sequence similarity (Todd *et al.*, 2002). Primers which are complementary to these conserved regions were designed and used to amplify genes with corresponding sequences by polymerase chain reaction (PCR). This strategy was used to identify numerous CYPs, UGTs and ACTs. One example is a 2a-O-benzoyltransferase that catalyses the acylation step in the taxol biosynthetic pathway, in *Taxus cuspidate* (Japanese yew) (Walker and Croteau, 2000).

Further, one of the most common methods was forward genetics approach or expression cloning. Libraries of cDNA sequences were transformed and heterologously expressed in bacteria or fungi, which were then cultured on media containing enzyme substrates. Cultures that accumulated the desired product could be analysed to link sequence to function (O'Connor, 2009, Ren *et al.*, 2020, Scherlach and Hertweck, 2021). This method was used to identify, 20-oxidase, an enzyme involved in gibberellin biosynthesis which was discovered by screening a cDNA library from *Cucurbita maxima* (giant pumpkin) with a polyclonal antibody for 20-oxidase. Plaques that hybridized with the antibody catalysed the expected enzymatic reaction (Lange *et al.*, 1994).

Another approach was the subtraction of cDNA libraries. In this approach, cDNA libraries were prepared from RNA extracted from different tissues. The substruction of one from another provides a distinct set of genes unique to a given tissue. Combining this approach with the metabolic profile of the tissues can also enhance the search (O'Connor, 2009, Scherlach and Hertweck, 2021). This method was successfully used to identify genes preferentially expressed in *Citrus medica* (citrus) in response to pathogen infection (González-Candelas *et al.*, 2010).

Other plant biosynthetic enzymes have been discovered using degenerate primers following the hypothesis that enzymes belonging to the same class often have conserved regions in nucleotide and amino acid sequences. This method has been successfully applied to the

identification of CYPs, UGTs, and ACTs (O'Connor, 2009, Scherlach and Hertweck, 2021), including the identification of taxane 2α-O-benzoyltransferase, which catalyses the acylation step in the taxol biosynthesis in Japanese yew (Walker and Croteau, 2000).

1.7.2 Pathway discovery in the era of multi-omics

The availability of metabolomics, transcriptomics, genomics and proteomics technologies has enhanced the ability to identify the genetic basis of plant-derived compound production (Singh *et al.*, 2022b, Swamidatta and Lichman, 2024). This is evidenced by an increasing body of work reporting the discoveries of biosynthetic pathways for various plant secondary metabolites. For example, genes of interest can now be identified by combining comparative gene expression data with metabolomics data across different tissues. This enables gene expression levels to be correlated with metabolite abundance, allowing the selection of candidate genes.

For example, Lau and Sattely used transcriptome mining in *Podophyllum hexandrum* (Himalayan may apple) to identify biosynthetic genes of the chemotherapeutic etoposide and podophyllotoxin, which were later validated by targeted metabolomics (Lau and Sattely, 2015). A second example is the discovery of a metabolic network of triterpene biosynthetic genes, expressed in the roots of Arabidopsis, that give rise to more than 50 previously unknown root metabolites (Huang *et al.*, 2019). Further, integrated transcriptomics and metabolomics were also used to elucidate strychnine biosynthesis in seeds of *Strychnos nux-vomica* (strychnine tree) (Hong *et al.*, 2022).

More recently, single-cell multi-omics was employed for the identification of the monoterpene indole alkaloid (MIA) biosynthetic pathway in Madagascar periwinkle (Li *et al.*, 2023a). This approach identified reductase and secologanin transporter genes and revealed cell-type-specific partitioning of the MIA biosynthetic pathway. Other recent studies have used spatial transcriptomics and metabolomics to investigate the distribution of taxols and their gene expression profiles within the leaf in *Taxus mairei* (Maire's yew) (Yu *et al.*, 2023, Zhan *et al.*, 2023). This research found that the upstream genes of paclitaxel biosynthesis are expressed in the leaf mesophyll cells, whereas the downstream genes are expressed in the bundle sheath and vein cells.

Whole genome assembly technologies have further complemented biosynthetic pathway discovery as some secondary metabolite genes were found to cluster in the plant genome

(Field and Osbourn, 2008, O'Connor, 2009). In this case, if one gene in a pathway has been identified, other genes may be found in the genetic neighbourhood (O'Connor, 2009, Ren *et al.*, 2020, Scherlach and Hertweck, 2021). This approach has been used to identify and characterise the structures of small biosynthetic gene clusters (BGC) such as that associated with the production of thalianol, (Field and Osbourn, 2008), and larger BGCs such as the 12-gene avenacin biosynthetic pathway (Li *et al.*, 2021b).

To analyse available genomes, new computational tools are also emerging. For example, plantiSMASH (Kautsar *et al.*, 2017) is a plant-focussed version of the antiSMASH bioinformatic pipeline that enables the identification of clustered biosynthetic pathways. PlantiSMASH has already facilitated the discovery of an array of ten physically clustered genes, responsible for steroidal glycoalkaloids biosynthesis in *Solanum lycopersicum* (tomato) and *Solanum tuberosum* (potato) (Itkin *et al.*, 2013) and genes for thalianin synthesis in Arabidopsis (Huang *et al.*, 2019).

1.7.3 Characterisation of candidate genes

Heterologous expression of biosynthetic pathway genes in the model hosts such as *Escherichia coli*, *Saccharomyces cerevisiae* (brewer's yeast) and *N. benthamiana* are the most widely used strategies for gene characterisation (Zhang *et al.*, 2019). If the enzyme substrate is available in the heterologous organism, the expected product can be directly extracted and detected using physicochemical methods of analysis (discussed in the later **section 1.7.8.**). Alternatively, the recombinant enzyme can be purified, usually with the aid of a genetically encoded purification tag, and incubated with its substrate *in vitro* to yield the final product (Yesilirmak and Sayers, 2009). For example, to elucidate the gossypol biosynthetic pathway, four CYPs were overexpressed in *E. coli* and brewer's yeast, then purified and incubated with substrates before analysis by gas chromatography-mass spectrometry (GC-MS) (Tian *et al.*, 2018).

The advantages of *N. benthamiana* for the characterisation of plant enzymes include the presence of plant mRNA and protein processing machinery, the availability of all plant sub-cellular compartmentalisation, and the presence of many necessary metabolic precursors and co-enzymes (Yang *et al.*, 2020). In addition, over the past few decades, many new genetic manipulation tools have been developed for plant metabolic engineering (Mipeshwaree Devi *et al.*, 2023). Expression in *N. benthamiana* is facilitated by the use of *Agrobacterium tumefaciens* mediated transient gene expression or 'agroinfiltration' (Zhang *et al.*, 2020). In

this method, plant leaves are infiltrated with an agrobacterium cell culture carrying genes of interest on binary plasmid vectors (**Figure 1.11A.**). *N. benthamiana* plants of a particular ecotype, now known as 'LAB' are particularly amenable to *Agrobacterium*-mediated infiltration due to a disruptive insertion in its *RNA-DEPENDENT RNA POLYMERASE (RDR1)* gene, weakening its immunity (Bally *et al.*, 2015). The ability to simultaneously co-infiltrate multiple *Agrobacterium* strains carrying different candidate genes has allowed the elucidation of increasingly complex biosynthetic pathways of different terpenoids, alkaloids and polyphenolic compounds (Golubova *et al.*, 2024) (**Figure 1.11B.**).

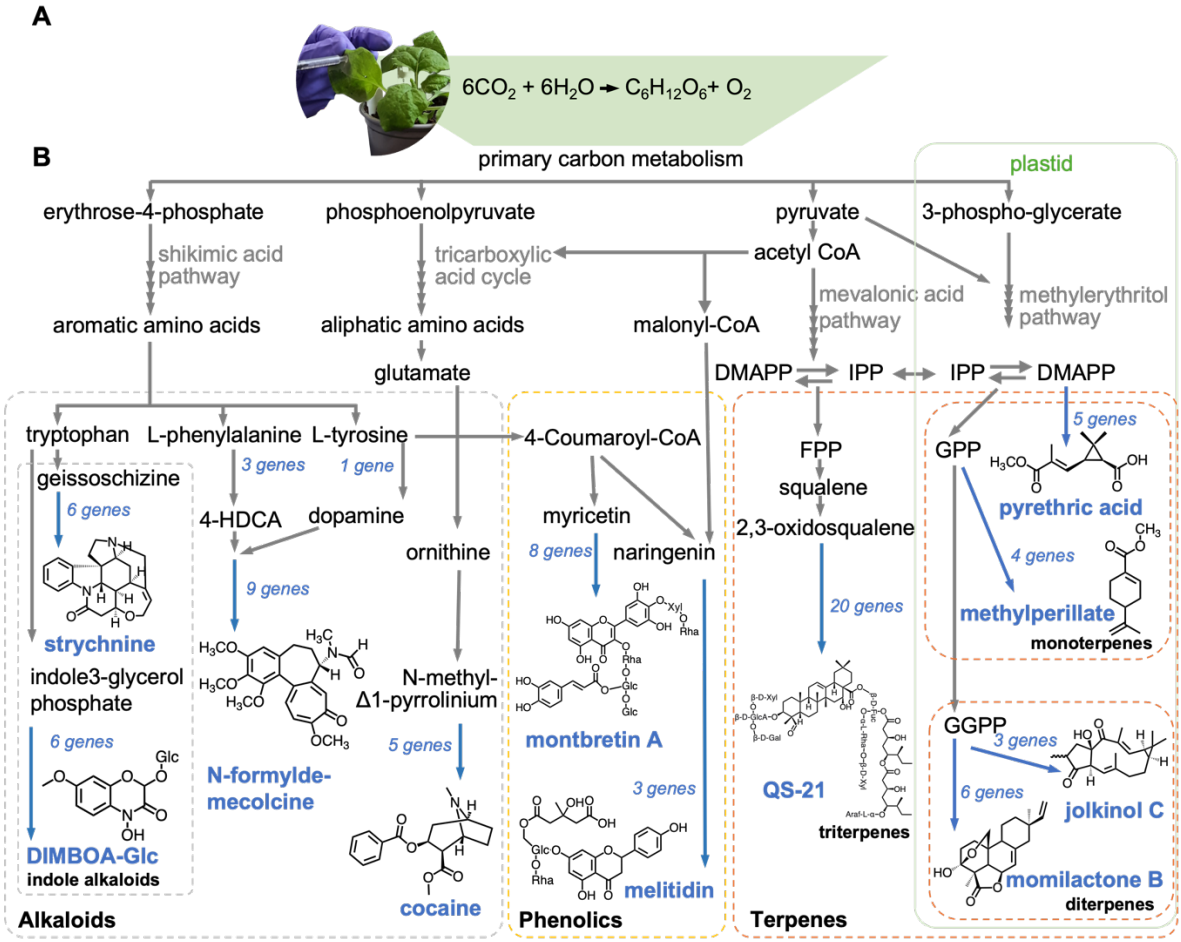

Figure 1.11 Examples of plant biosynthetic pathways reconstructed in *Nicotiana benthamiana*. **(A)** The infiltration of *Agrobacterium* strains carrying pathway genes into leaf tissues enables the conversion of endogenous metabolites, themselves derived from the products of photosynthesis, to target compounds. **(B)** Examples of multigene heterologous pathways reconstructed in *N. benthamiana.* Black/grey text indicates endogenous metabolites/pathways; blue text indicates heterologous pathways and products. Gene abbreviations: *C4H* = cinnamate 4-hydroxylase; *DAHPS* = 3-deoxy-D-arabinoheptulosonate 7-phosphate synthase; *DXR* = 1-deoxy-d-xylulose5-phosphate reductase; *DXS* = 1-deoxy-D-xylulose-5-phosphate synthase; *GGPPS* = geranylgeranyl pyrophosphate synthase; *GPPS* = geranyl pyrophosphate synthase; *HMGR* = 3-hydroxy-3-methylglutaryl reductase; *HMGS* = 3-hydroxy-3-methylglutaryl-coenzyme A synthase; *IDI* = isopentenyl diphosphate isomerase; *MPO* = N-methyl putrescine oxidase; *MYB4* = R2R3-subfamily transcription factor; *ODC* = ornithine decarboxylase; *PMT* = putrescine N-methyltransferase; *PAL* = phenylalanine ammonia lyase; *tyrA* = prephenate dehydrogenase; *TYDC/DDC* = L-tyrosine/L-DOPA decarboxylase; *DXS* = deoxyxylulose 5-phosphate synthase. Figure adapted from (Golubova *et al.*, 2024).

1.7.4 Endogenous characterisation of biosynthetic genes

Heterologous expression of biosynthetic pathway genes does not unequivocally prove the function of the genes in the native plant species. Thus, gene silencing or mutation technologies are also used to confirm gene function. One of these methods is RNA Interference (RNAi) Induced Gene Silencing. In this method, the introduction of short pieces of small interfering RNA (siRNA) into the cytosol initiates the targeted degradation of complementary mRNAs (Younis *et al.*, 2014, Zhang *et al.*, 2023b). Generation of stable RNAi lines through the introduction of DNA constructs encoding hairpin RNA, which are processed into siRNA by the host, leads to a heritable silencing (Younis *et al.*, 2014).

Stable RNAi has been used to silence genes encoding terpene synthases, CYPs, ACTs and transporters in order to link genes to their function in specialised metabolism. For instance, RNAi-mediated knockdown of Arabidopsis *STERYL ACYL CARRIER PROTEIN FATTY ACID DESATURASE (SACPD)* reduced oleic acid and increased stearic acid levels, indicating that this gene is responsible for fatty-acid desaturase activity (Jiang *et al.*, 2009). Further, this technique was used to explore pollinator preferences between humblebee-pollinated *Mimulus lewisii* (purple monkeyflower) and hummingbird-pollinated *Mimulus cardinalis* (scarlet monkeyflower) (Byers *et al.*, 2014b). In this study, RNAi-mediated silencing of *OCIMENE SYNTHASE* in transgenic purple monkeyflower led to a 6% decrease in visitation, suggesting that this locus likely contributes to differences in pollinator visitation, and promotes reproductive isolation between the two species.

Alternative methods include the use of gene-editing technologies such as clustered regularly interspaced short palindromic repeats (CRISPR)/Cas9. For instance, CRISPR approaches were used to introduce loss-of-function mutations into *PHYTOENE SYNTHASE 1* (*PSY1*) and *CrtR-b2* to investigate their role in carotenoid biosynthesis (D'Ambrosio *et al.*, 2018). The main limitation of gene-editing methods is that it typically requires the regeneration of stable lines via tissue culture, which is time-consuming, labour-intensive and can be difficult to develop for new species (Zhang *et al.*, 2021). Further, should the ultimate goal be field-growth, the introduction of mutations using gene-editing has an advantage over transgenic RNAi approaches as any introduced transgene used in their production can be segregated away. Transgene-free gene edited plants are subject to less regulations in many global jurisdictions compared to transgenic plants, which are classified as genetically modified (GM) (Papadopoulou *et al.*, 2020, Rozas *et al.*, 2022).

Another method which is commonly used to assess gene function *in vivo* is virus-induced gene silencing (VIGS). In this method, a viral vector that encodes the production of double-stranded RNA for the target gene is delivered to the plant. This triggers RNA-mediated gene silencing and a reduction in the target transcript, typically assayed by quantitative reverse-transcription PCR (qRT-PCR) (Rotenberg *et al.*, 2006). This method is also discussed in more detail in Chapter 5. VIGS is a transient technique that has been used to study the secondary metabolism of many plants, including *Ocimum basilicum* (sweet basil), tomato and Madagascar periwinkle, allowing the identification of genes involved in terpenoid, phytosterol and alkaloid biosynthesis, respectively (Liscombe and O'Connor, 2011, Misra *et al.*, 2017, Sonawane *et al.*, 2017). The disadvantage of this technique is that the silencing is not heritable and, as the plants contain GM bacteria, can only be grown within contained laboratories.

1.7.5 Approaches to the structure-function analysis of proteins

Characterisation, structure-function analysis and engineering can be used to identify and improve the performance of key enzymes for the construction of efficient and sustainable biosynthetic pathways (Zhou *et al.*, 2022). X-ray structures of more than 200,000 enzymes have been deposited into the RCSB data centre for the global Protein Data Bank (PDB) which accelerates the elucidation and characterisation of new biosynthetic pathways. Despite being the best tool for studying protein structure, X-ray crystallography has several limitations that can prevent the generation of a highly resolved structure. Among them are the large, milligram scale, quantities of pure protein required for the analysis, the difficulty to crystalise certain types of enzymes such as those that are membrane-bound, and the difficulty in obtaining the right condition for crystals to produce the desired diffraction (Acharya and Lloyd, 2005).

A second common method for resolving the structure and kinetics of specific proteins is nuclear magnetic resonance (NMR) spectroscopy. Sequences of more than 300 plant proteins have been determined using NMR (Kaas and Craik, 2013). However, this method also requires a large amount of pure sample (Teng, 2005), and is suitable for relatively small proteins with a molecular mass of less than 40 kDa (Kaas and Craik, 2013).

Cryo-electron microscopy (Cryo-EM) has also been applied for protein structure determination. In the last few years, the structure of plant proteins involved in photosynthesis (Opatíková *et al.*, 2023) and the respiratory system (Klusch *et al.*, 2023, Maldonado *et al.*,

2023), have been determined using Cryo-EM. However, this method requires expensive equipment, a high level of expertise, and extremely pure protein for analysis (Nwanochie and Uversky, 2019).

Due to the limitations of the methods above, computational methods have become widely used to infer structures of protein sequences. One commonly employed approach is homology modelling, which predicts the three-dimensional structure of a target protein based on the similarity to one or more well-characterised protein templates. Over the years, numerous software packages have been developed to facilitate homology modelling, including trRosetta, Phyre, Swiss-Model, Yasara, and others (Edmunds and McGuffin, 2021). A recent advancement in this area is the application of deep learning methods for sequence-based protein structure predictions (Jänes and Beltrao, 2024). AlphaFold, for example, utilises machine learning algorithms to predict a protein's 3D structure using only its primary amino acid sequence (Jumper *et al.*, 2021). AlphaFold has made its predictions widely accessible by providing open access to a database containing over a million protein structure models in addition to offering tools for predicting the structures of new proteins. An example of the successful utilisation of this tool for plant secondary metabolism elucidation is the recent discovery of non-squalene-dependent triterpene biosynthetic enzymes (Tao *et al.*, 2022).

1.7.6 Methods for identifying plant secondary metabolites

The accurate identification of enzyme products is critical for biosynthetic pathway discovery (Prosser *et al.*, 2014). For this purpose, various spectrometric methods, such as ultraviolet spectrometry (UV) or mass spectrometry (MS), can be used to identify unknown compounds (Zhang *et al.*, 2010). The underlying concept of mass spectrometry is the different trajectories of moving ions with different masses/charges (Ahamad *et al.*, 2022). For GC-MS, once a molecule is pushed into the mass spectrometer, it is ionised using either electron (EI) or chemical ionisation (CI) methods (Rao *et al.*, 2023). In the EI ionisation method, high-energy electrons bombard compounds that are present in the gaseous phase, break up the molecules leaving positively charged ions after the removal of electrons (Medhe, 2018). The CI technique is considered to be a soft ionisation technique, where reagent gases such as methane, isobutene or ammonia collide with the target compounds. During this collision, a proton is transferred from the reagent ion gas to the target compounds and their fragments, leaving positively charged ions (Medhe, 2018). Then, depending on the ion mass, parental compounds ions and their breakdown products are separated and detected, creating a unique

mass spectrum for each compound. Compared to EI, CI uses comparatively less energy, which leads to less fragmentation and a simpler spectra (Warren, 2013). CI therefore became the predominant method for the identification of large, less volatile and thermally unstable secondary metabolites (Stobiecki, 2000).

In LC-MS, the two most common methods of ionisation are electrospray ionisation (ESI) and atmospheric pressure chemical ionisation (APCI) (Kumar and Vijayan, 2014). In ESI, a strong electric field is applied to a liquid passing through a capillary tube. This produces charged droplets, which are then evaporated, resulting in the release of ions from the droplets (Ho *et al.*, 2003). This method is often used for large polar metabolites. While in APCI, liquid samples are turned into a fine aerosol using nitrogen gas and vaporised at high temperature (Gates, 2021). Similarly to CI, a proton is transferred from ionised reagent gas to the target compounds in the gas phase. This method has become commonly used for thermally stable medium-sized compounds such as steroids (Ma and Kim, 1997) and triterpenoids (Liu *et al.*, 2019b, Rhourri-Frih *et al.*, 2009).

The main advantage of this method is that it is possible to identify hundreds of compounds in one mixture, making it suitable for plant metabolic profiling and target compound detection (Salem *et al.*, 2020). This method, coupled with The National Institute of Standards and Technology (NIST) database that contains mass spectra for over 33,000 compounds allowed the detection and characterization of hundreds of plant metabolites, including triterpenes (Fang, 2024). For instance, eight polyhydroxy triterpenoid acids from *Eucalyptus globulus* (Tasmanian blue gum) were identified and quantified in one sample by comparing their GC-retention time and mass spectra with standards (Lourenço *et al.*, 2021).

Despite being the most common method for identifying plant enzyme products, mass spectrometry has several limitations for identifying new molecules. This is because of a lack of spectral data for compounds that are difficult to ionize or that are low in abundance in biological samples (Collins *et al.*, 2021). Thus, for the identification of such compounds, a more demanding but, at the same time, more accurate approach is frequently employed: NMR (Alves *et al.*, 2000). In this method, the material can be analysed by observing and measuring the interaction of nuclear spins when placed in a powerful magnetic field. Using this method, all the intermediates and final compounds in the biosynthesis of QS-21 and QS-7 saponins produced by the soap bark tree were identified and confirmed (Reed *et al.*, 2023). Although NMR is a very powerful physio-chemical method of analysis, it requires a high quantity of extremely pure products (Alves *et al.*, 2000).

1.7.7 Engineering triterpene production

At present, the predominant way of obtaining plant natural products for use in medicine and industry is by extraction from the native species. However, this process is not always sustainable and can be limited by long growth cycles, low concentrations of target molecules, and the presence of similar chemicals that complicate purification (Yang *et al.*, 2020). At the same time, the complex structures and stereochemistry of many plant natural products, including triterpenes, significantly reduce the efficiency and affordability of chemical synthesis. As well as being expensive, chemical synthesis often uses hazardous catalysts and reagents, which may be hard to recycle and may become environmental hazards (Kharissova *et al.*, 2019).

With advancements made in the fields of synthetic biology and metabolic engineering, heterologous biosynthesis of plant natural products within microbes and or other plant species is becoming a popular option (Yang *et al.*, 2020). Here I discuss advances in the production of triterpenes in heterologous hosts.

1.7.7.1 Engineering triterpene production in microbes

Although bacteria lack a native MVA pathway, triterpenes have been successfully produced in this organism. For example, *E. coli* has been used to produce α- and β-amyrin (Wang *et al.*, 2021c). In this study, the strategy of engineering fusion proteins, significantly increasing the yield of unmodified and hydroxylated triterpenes by fusing OCSs and CYPs, was used. Another is the production of ambrein in *E. coli* (Ke *et al.*, 2018). In this study, a gene encoding squalene synthase (ScERG9) was introduced into the *E. coli* genome and tetraprenyl-β-curcumene cyclase (BmeTC) was co-expressed with ScERG9 producing ambrein.

Unlike bacteria, fungi have a native MVA pathway, which makes it easier to increase the yield through overexpression of key MVA and triterpene synthesising enzymes (IPP, DMAPP, FPP or OSC and CYP) (Bureau *et al.*, 2023). Yeast has been used to produce β-amyrin, α-amyrin, lupeol, and their derivatives at the mg per litre scale (Arendt *et al.*, 2017, Dale *et al.*, 2020, Guo *et al.*, 2020, Hansen *et al.*, 2020, Liu *et al.*, 2024b, Sun *et al.*, 2024b). The main challenge associated with heterologous triterpene production in fungi is the toxicity of heterologous compounds, e.g., triterpene saponins to the host organism (Johnston

et al., 2023), and the requirement for extensive host genome engineering (Bureau *et al.*, 2023).

Terpene production in microbial hosts benefits from fast growth and low cost. In addition, the existence of well-developed genetic manipulation tools facilitates the metabolic engineering of species like *E. coli* and brewer's yeast. Further, their use in industrial-scale biomanufacturing facilities has been well established. However, production typically requires the provision of sugar feedstocks, which are usually obtained from plants themselves (Wendisch *et al.*, 2016). The production of plants such as sugarcane in areas that previously were rainforests for the provision of sugar feedstocks may have negative environmental consequences (El Chami *et al.*, 2020).

1.7.7.2 *N. benthamiana* as a host for triterpene production

Photosynthetic organisms, including plants, provide an attractive alternative for triterpene production (Arendt *et al.*, 2016). As discussed in **section 1.7.3.**, there are several advantages to expressing plant genes in plants, including *N. benthamiana*. These include enzyme functionality, availability of plant compartments, and the presence of metabolic precursors and enzyme cofactors.

Transient expression in *N. benthamiana* has been demonstrated for many triterpenes, enabling production within just a few days (Reed *et al.*, 2017b). To date, the main strategy to increase triterpene yields has been overexpression of a truncated version of the 3-hydroxy-3-methyl-glutaryl-coenzyme A reductase HMGR enzyme (Lee *et al.*, 2019) (**Figure 1.8.**). Truncation of this enzyme results in a feedback-insensitive protein and therefore enhances flux through the MVA pathway where HMGR is a key rate-limiting enzyme. Further increases in the yields of triterpenes have been achieved using a translational fusion of FPPS and HMGR (Reed *et al.*, 2017b).

Using these strategies, several studies have demonstrated the possibility of triterpene production at mg scale quantities (Reed and Osbourn, 2018, Reed *et al.*, 2017b, Stephenson *et al.*, 2018). For example, in a study conducted in 2017, combinatorial expression of different diversifying enzymes, CYPs, GTs and ACTs, yielded novel β-amyrin derivatives ranging from 0.12 to 3.87 mg per gram of dry *N. benthamiana* leaf powder (Reed *et al.*, 2017a). This approach can be further expanded to the large-scale assembly and screening of combinatorial libraries for new molecule discovery and production.

Plants employ a gene-silencing mechanism to limit viral infections. Constitutive overexpression of heterologous genes can also trigger gene silencing. To allow the high-level expression of foreign genes, a suppressor of silencing can be co-expressed. An example of this is the tombusviral protein, p19. P19 binds to small interfering RNAs (siRNAs) and micro-interfering RNAs (miRNAs) improving infection and increasing expression levels (Lakatos *et al.*, 2004) (Garabagi *et al.*, 2012b). Improved yield of oleanolic acid was achieved using a plasmid vector encoding a p19 expression cassette (Romsuk *et al.*, 2022).

N. benthamiana has been demonstrated as a host with potential for the scalable biomanufacturing of recombinant proteins, including mammalian antibodies and viral antigens (Goulet *et al.*, 2019, Klimyuk *et al.*, 2012, Lomonossoff and D'Aoust, 2016). However, transient expression requires facilities equipped with artificial lighting and temperature control (heating or cooling), feedstocks for culturing *A. tumefaciens* strains, and specialised infrastructure for moving plants or infiltration processes (Chen *et al.*, 2013). Thus, to date, it remains uncertain if *N. benthamiana* will be an economically viable production platform for natural products.

1.7.8 Isolation from heterologous hosts

After accumulation in heterologous hosts, triterpenes can be extracted and purified using standard biochemical approaches. For both microorganisms and plants, this follows a similar scheme: cell lysis and metabolite extraction using nonpolar solvents such as ethyl acetate or hexane (Hossain and Ismail, 2013). Extraction is then followed by purification and separation. In many cases, this is a very complex task, especially the separation of complex but structurally similar compounds. In these cases, fractions enriched in the class of compounds may be separated instead of individual compounds (Zhang *et al.*, 2018).
There are a few approaches developed for the isolation of triterpenes, mainly preparative-scale high-performance liquid chromatography HPLC (Oleszek and Stochmal, 2010) and gas chromatography (GC) (Neves *et al.*, 2020). The choice of method is normally dependent on the size, polarity and hydrophilicity of the target molecules.

1.8 PhD thesis overview

Plants have been used in traditional medicine for hundreds of years. In some cases, the therapeutic properties of medicinal plants have been attributed to specific metabolites, enabling their use as drugs in modern medicine. However, the exact molecule(s) responsible for the bioactivity of majority plant extracts remains unknown. Further, access to specific compounds is often complicated by low abundance, occurrence in complex mixtures, or by structural complexity, which can complicate chemical synthesis. In this thesis, I attempt to address these challenges for pot marigold, a medicinal plant known for its anti-inflammatory activity. Floral extracts from this plant are enriched in triterpene FAEs. However, the literature has not definitively assigned molecules from this class as the most potent anti-inflammatory compounds in the extract. Further, it is unclear which anti-inflammatory pathways they target. Thus, this work is focused on the identification of anti-inflammatory compounds in pot marigold extract, followed by the identification of the biosynthetic pathways for these compounds.

This is done by combining comparative metabolic profiling of Asteraceae species with bioactivity assays in model human cell lines to identify faradiol and faradiol FAEs as anti-inflammatory compounds in pot marigold extract (Chapter 3). Building on these findings, metabolomics, genomics, and transcriptomics are combined with rapid transient expression in *N. benthamiana* to identify and characterise the biosynthetic enzymes involved in the biosynthesis of these compounds (Chapter 4). Finally, a method for gene silencing in pot marigold was developed (Chapter 5). Overall, this work demonstrates how integrated studies of bioactivity and biosynthesis can unlock the therapeutic potential of medicinal plants and provide strategies for the production of bioactive triterpenes for pharmaceutical applications.

Chapter 2 – General Methods

2.1 Cell lines and maintenance

2.1.1 Cell lines and reagents

The human monocytic leukaemia cell line THP-1 (ECACC 88081201) derived from the peripheral blood of a 1-year-old male with acute monocytic leukaemia was obtained from the European Collection of Cell Cultures (ECACC, Health Protection Agency, Salisbury, UK). The human promyelocytic leukaemia cell line, HL-60, derived from peripheral blood leukocytes obtained by leukapheresis of a 36-year-old Caucasian female with acute promyelocytic leukaemia, was also obtained from ECACC. The immortalized human keratinocyte cell line, HaCaT, was obtained from CLS Cell Lines Service GmbH (Eppelheim, Germany). Dimethyl sulfoxide (DMSO), LPS from *E. coli* (O55:B5), and BAY 11-7082 were obtained from Sigma-Aldrich (Poole, UK). T25 and T75 culture flasks, 96-well, 24-well and 48-well cell culture plates, and falcon tubes (15 mL and 50 mL) were purchased from Thermo Fisher Scientific (Loughborough, UK).

2.1.2 Cell culture

THP-1 and HL-60 cells were cultured in complete media consisting of Roswell Park Memorial Institute (RPMI) 1640 media with 10% heat-inactivated foetal calf serum (FCS), L-glutamine (2 mM) and antibiotics (penicillin (100 U/mL); streptomycin (100 µg/mL) (all GIBCO, x, UK). HaCaT cells were cultured in Dulbecco's Modified Eagle Medium (DMEM) media with 10 % heat-inactivated FCS, L-glutamine (2 mM) and antibiotics (penicillin (100 U/mL); streptomycin (100 µg/mL)). All cell cultures were incubated at 37 °C in a humidified atmosphere with 5% CO_2. THP-1 and HL-60 were passaged every 3.5 days to maintain the desired cell density of between $3x10^5$ cells/mL and $9x10^5$ cells/mL. HaCaT cells were grown until 90% confluency, washed with Dulbecco's Phosphate-Buffered Saline (DPBS), detached using TryplE Express (GIBCO) and diluted 1:5 in fresh DMEM media.

Cell density was measured using a Neubauer haemocytometer. A 50 µL solution of 0.4 % trypan blue (Sigma) was mixed with the cells in an equal ratio and added to the haemocytometer for counting under a light microscope according to the manufacturer’s

instructions. Cells were then adjusted to a final density of $3x10^5$ cells/mL or $1x10^6$ cells/mL on the day of the assay by dilution in complete media.

2.2 Plant lines and maintenance

2.2.1 Sources of seeds

Asteraceae seeds were obtained from botanic gardens or UK seed vendors. Details are provided in **Table 2.1.**

Table 2.1 Sources of seeds. CS=Chiltern Seeds (Battle Barns, Wallingford, UK); CUBG=Cambridge University Botanic Garden (Brookside, Cambridge, UK); KMSB=Millennium Seed Bank, Royal Botanic Gardens at Kew (Wakehurst, Haywards Heath, UK); NC=Naturescape (Langar, Nottingham, UK); RP=Rareplants (Bjørn Malkmus-Hussein, Tenerife, Spain).

Species	**Common name**	**Seed origin**	**Serial number**	**Location of collection**	**Year of collection**
Achillea millefolium	yarrow	KMSB	601669	UK	2010
Bellis perennis	common daisy	NC	2624		
Calendula arvensis	field marigold	KMSB	32133	Cyprus	1972
Calendula officinalis	pot marigold	CS	1507		
Calendula suffruticosa algrabiensis		KMSB	22420	Portugal	1972
Calendula suffruticosa tomentosa		KMSB	29809	Morocco	1972
Chondrilla juncea	rush skeleton weed	CUBG	19670154		
Eupatorium cannabinum	hemp agrimony	KMSB	70672	UK	1988
Helianthus annuus	common sunflower	CS	672G		
Hypochaeris radicata	common cat's ear	NC	2553		
Inula ensifolia	sword-leaved inula	KMSB	776284	Austria	2013
Matricaria chamomilla	chamomile	KMSB	59341	UK	1985
Pentanema britannica	British yellowhead	RP	8391		
Pilosella officinarum	mouse-ear hawkweed	KMSB	666109	UK	2012
Silybum marianum	milk thistle	CS	1175E		

All seeds were stored at 4 °C.

2.2.2 Growth of Asteraceae species

Seeds of pot marigold, field marigold, *Calendula suffruticossa algarbiensis, Calendula suffruticossa tomentosa, Calendula suffruticossa fulgida*, *Pilosella officinarum* (mouse-ear hawkweed), yarrow, chamomilla, *Eupatorium cannabinum* (hemp agrimony), common sunflower, *Silybum marianum* (milk thistle), *Inula ensifolia* (sword-leaved inula), *Pentanema britannica* (British yellowhead), *Bellis perennis* (English daisy), *Hypochaeris radicata* (cat's ear) and *Chondrilla juncea* (rush skeleton weed) (**Table 2.1.**)were sown in Levington F2 starter (**Table 2.2.**) at a depth equal to seed size. After 7-10 days, seedlings were transplanted to 11 cm pots in John Innes Cereal Mix (**Table 2.2.**) All plants were grown in summer glasshouse conditions with natural day length and temperature.

2.2.3 Growth of *N. benthamiana*

N. benthamiana plants were grown at 25 °C/ 22 °C day/night with a 16/8-hour day/night cycle, 80 % humidity and ~200 µmol/m2/s light intensity. Seeds were sown in Levington F2 starter (**Table 2.2.**) for 2 weeks before transfer of seedlings to individual cells (Levington F2). Plants were grown for an additional 3-4 weeks before use in agroinfiltration experiments (see **methods 2.6.8.**).

Table 2.2 Composition of soil mixes used for plant cultivation.

Soil mix	Composition
Levington F2 starter	100% Peat
John Innes Cereal Mix	65% Peat
	25% Loam
	10% Grit
	3 Kg/m^3 Dolomitic limestone
	1.3 Kg/m^3 PG mix
	3 Kg/m^3 Osmocote Exact

2.3 Metabolite extraction and purification of triterpenes

2.3.1 Metabolite extraction

Metabolites were extracted from plant tissues that had been freeze-dried for 2-3 days (Lyotrap, VWR, UK). For Asteraceae, 50 mg of freeze-dried tissue was used; for *N.*

benthamiana, five 1 cm diameter disks. Freeze-dried tissue samples were powdered with 3 mm tungsten carbide beads (Qiagen, Hilden, Germany) using a Tissue Lyser (Qiagen, Hilden, Germany) (1 min, 25 1/s). The tungsten beads were decanted, and 500 µL of ethyl acetate was added to each tube (Sigma Aldrich, Burlington, MA, USA). Samples were vortexed and incubated in a thermomixer (Eppendorf) at 40 °C at 700 rpm for 2 h. Samples were left at room temperature for 2-3 days to maximise metabolite extraction.

2.3.2 Derivatisation and GC-MS analysis

To allow for better separation and to improve detectability, extracts were derivatised prior to GC-MS analysis. For derivatisation, ethyl acetate extracts were centrifuged at 15,000 rpm for 5 min to pellet plant material. 50 µL of the clarified extract was transferred into a new 2 mL tube and ethyl acetate was evaporated under N_2 flow. Samples were derivatised using 100 µL N-Methyl-N-(trimethylsilyl)trifluoroacetamide (MSTFA) reagent (Sigma-Aldrich), followed by vortexing and incubation at 37 °C for 30 min. Samples were transferred to 2 mL amber GC-MS vials (Thermo Scientific) with micro inserts and spring (100 µL) GC-MS for analysis.

GC-MS analysis was performed using an Agilent 7890B GC (Agilent; Sata Clara, CA, USA) fitted with a Zebron ZB5-HT Inferno column (35 m x 250 µm x 0.1 µm) with 5% phenyl 95% dimethyl-polysiloxane stationary phase (Phenomenex; Washington D.C, USA). Injections of 2 µL were performed in pulsed splitless mode (10 psi pulse pressure) with the inlet temperature set to 325 °C. The flow rate was set at 1 mL/min. The GC oven temperature program was 150 °C and held for 30 seconds with a subsequent increase to 360 °C (20 °C/min) and held at 360 °C for an additional 12.5 min (total run time 27 min). The GC oven was coupled to an Agilent 5977B Mass Selective detector set to scan mode from 60-800 mass units (solvent delay 3 min).

Data analysis was carried out using MassHunter workstation software (v B.08.00; Agilent). Compounds were identified by either (i) the comparison of mass spectra and retention time with standards bought from commercial suppliers (**Table 2.3.**), (ii) the comparison of mass spectra with compounds recorded in the NIST database, (iii) or using internal mass spectra database of TFAEs.

Table 2.3 Triterpene standards purchased from commercial suppliers.

Triterpene monols		
Taraxasterol	PHL84272-10MG	Merck
Lupeol	18692-10MG	Merck
Betulin	92648-50MG	Merck
Triterpene diols and acids		
Faradiol	PHL82536-10MG	Merck
Arnidiol	HY-N4165-1MG	MedChem Express
Betulinic acid	91466-10MG	Merck
Oleanolic acid	42515-10MG	Merck

2.3.3 Fractionation of pot marigold extracts

Fractionation of pot marigold flower extracts was done using an adaptation of a previously described method (Reznicek and Zitterl-Eglseer, 2003). Liquid chromatography of methanol extract from pot marigold flowers was performed using an ACQUITY UPLC BEH C18 2.1 mm X 50 mm column (Waters Corp.; Milford, MA, USA) on a single quadrupole LC-MS/MS (Nexera UHPLC from Shimadzu; Kypto, Japan). The flow rate was set to 0.6 mL/min and the column temperature was kept constant at 40 °C for 28 min. Eluent A (50% methanol) was applied for 2.5 min followed by a gradient of 85% to 100% methanol for 20 min, followed by eluent B (100% methanol) for 2.5 min. Seven sequential fractions of 1.8 mL were collected and dried down, yielding (234 µg, 253 µg, 213 µg, 325 µg, 244 µg, 593 µg, and 237 µg of dried material, respectively.

2.3.4 Purification of triterpenes

Faradiol palmitate was purified form pot marigold floral tissue as described in 2.3.3 except that eluent A (90% methanol) was applied for 2.5 min, followed by a gradient of 90% to 97.5% methanol for 20 min, followed by eluent B (97.5% methanol) for 5.5 min. Fractions were analysed by GC-MS to identify a fraction containing a single peak with the mass and spectra for faradiol palmitate (15-16 min). This fraction was collected and dried, yielding 1.2 mg of compound.

2.3.5 Nuclear magnetic resonance (NMR)

The structure of faradiol palmitate was confirmed by 1D and 2D NMR analysis. For this, spectra were recorded in 3 mm tubes using $CDCl_3$ as a solvent at 298 K on a Bruker Neo 600 MHz spectrometer (Billerica, MA, USA) equipped with a 5 mm TCI CryoProbe. 1D 1H, 13C NMR, 2D 1H-1H-COSY, 1H-13C-HSQCed and 1H-13C-HMBC experiments were performed using standard pulse sequences from the Bruker Topsin 4 library. Data were processed using Topspin 4.1.4 and MestReNova 15.0.1 software, and spectra were calibrated to an internal TMS reference.

2.4 Bioassays

2.4.1 Preparation of extracts and pure compounds

Metabolites were extracted from plant tissues as detailed in 2.3.1. Extracts were centrifuged at 15,000 rpm for 5 min to pellet plant material. The supernatants were decanted to new pre-weighed 1.5 mL microcentrifuge tubes and left open in the fume hood until dry. Tubes were re-weighed, and the mass of extract was quantified. Pellets were diluted in sterile DMSO to prepare stock solutions of 100 mg/mL and 50 mg/mL. Pure compounds were weighed and diluted in sterile DMSO to prepare stock solutions of 10 mM and 5 mM. Stock solutions were vortexed vigorously and heated at 42 °C for 10 min to ensure solubility prior to dilution into working solutions.

2.4.2 3-(4,5-dimethylthiazol-2-yl)-5-(3-carboxymethoxyphenyl)-2-(4-sulfophenyl)-2H-tetrazolium (MTS) assay

MTS assays were performed in 96-well plates under sterile conditions. THP-1 or HL-60 cells were seeded into a 96-well plate at a density of $1x10^6$ cells/mL. HaCaT cells were seeded into a 96-well plate at a density of $3.5x10^5$ cells/mL incubated overnight at 37°C; 5% CO_2 to allow the formation of monolayer. The outermost wells were filled with 250 µL of water to maintain humidity and minimise media evaporation. The appropriate wells were left untreated or treated with vehicle control (DMSO; Sigma-Aldrich Poole, UK) and the compounds of interest for 24 h at 37 °C; 5% CO_2, as described in (Steel *et al.*, 2018). After the addition of the plant extracts, fractions or triterpenes, cells were incubated for 24 h at 37°C; 5% CO_2. Following this, 10 µL MTS (CellTiter 96 Aqueous One Solution Reagent, Promega, Southampton, UK) was added to all wells (excluding the outermost wells). Cells were returned to the incubator for 3 h at 37 °C; 5% CO_2. Finally, absorbance at 492 nm was

measured using the POLARstar Optima microplate reader (BMG Labtech, Aylesbury, UK) and the averaged 'media-only' reading was subtracted from all wells. Data analysis was performed using GraphPad Prism software (v. 10.3.1) (Dotmatics, Boston, MA, USA).

2.4.3 Enzyme-Linked Immunosorbent Assays (ELISA)

THP-1 cells were seeded into a 24-well plate at $1x10^6$ cells/well and treated with triterpenes or plant extracts at non-cytotoxic concentrations. DMSO was used as a vehicle control, and IκB-α inhibitor (E)-3-(4-Methylphenylsulfonyl)-2-propenenitrile (BAY 11-7082; 10 μM, Sigma-Aldrich) was used as a positive control. Cells were incubated at 37 °C; 5% CO_2 for 30 min prior to treatment with 10 ng/mL *E. coli* LPS (O55:B5) from Sigma Aldrich for 3 hrs to stimulate TNF-α secretion or 1 μg/ml LPS for 24 h to stimulate IL-6 secretion. Non-toxic concentrations of extracts, fractions, and pure compounds were determined using MTS assay prior ELISA. 3 hours or 24 hours after LPS stimulation, the supernatants were collected and stored at -80 °C until required. TNF-α or IL-6 concentrations were determined using OptEIA human TNF-α ELISA set (BD Biosciences, Berkshire, UK) and human IL-6 ELISA set (Bio-Techne, Abingdon, UK) according to the manufacturer's instructions. In summary, a 96-well plate was coated with anti-human TNF-α antibody or anti-human IL-6 antibody overnight at 4 °C or room temperature, respectively. The plate was washed with 0.05% Tween-20 in DPBS and incubated at room temperature with assay diluent for 1 h. Following this, the plate was washed again, and standards (in a serial dilution) or supernatant samples (at a 1:2 dilution with assay diluent for IL-6 and 1:3 dilution for TNF-α) were added to the wells and incubated at room temperature for 2 h. The plate was washed again, and the TNF-α or IL-6 detection antibody was added to the plate (1 h for TNF-α or 2 h for IL-6). The plate was washed a final time before substrate reagent (BD Biosciences) was added to the wells and incubated in the dark for 5-10 min. Following this, 1M H_2SO_4 was added to the wells. TNF-α/IL-6 concentrations were then determined by measuring absorbance at 450 nm corrected for absorbance at 570 nm using a POLARstar Optima microplate reader.

2.4.4 Western Blots

THP-1 cells were seeded into a 24-well plate at 1 x 10^6 cells/mL and treated with triterpenes at a non-cytotoxic concentration (20 μM). DMSO was used as a vehicle control and BAY 11-7082 (10 μM) as a positive control. Cells were incubated at 37 °C; 5% CO_2 for 30 min prior to treatment 1 μg/ml LPS. Plates were then incubated at 37 °C; 5% CO_2 for 2 h before the cells were washed with DPBS and lysed with 1:1 tris-glycine SDS lysis buffer/DPBS

then boiled and sonicated. The protein content of each sample was quantified using Nanodrop and the ND-1000 Spectrophotometer (Thermo Fisher Scientific, Loughborough, UK). Electrophoresis was then performed on the samples as per the manufacturer's instructions using the NuPAGE electrophoresis system kit (Invitrogen, Thermo Fisher Scientific, Loughborough, UK) in the XCell SureLock Mini-Cell with NuPAGE MOPS SDS Running Buffer. In summary, the samples and molecular weight marker (Invitrogen) were loaded onto a NuPAGE 4-12% bis-tris gel (Invitrogen) and electrophoresed at 150 V until the samples had passed through the stacking gel, and then at 200 V. The proteins on the gel were transferred from the gel to a pre-equilibrated PVDF membrane in NuPAGE Transfer Buffer at 33 V using an Invitrogen™ XCell II™ Blot Module (Invitrogen). The membrane was blocked with 5% dried skimmed milk in TBST (blocking buffer) overnight before adding the primary antibody in which the membrane was incubated for 1.5 h. Primary antibodies against STAT3), phospho-STAT3 (Tyr705), NF-κB p65, phospho-NF-κB p65 (Ser536) and β-tubulin were purchased from Cell Signalling Technology (London, UK) (**Table 2.4.**). The membrane was rinsed in TBST, washed three times in blocking buffer, and then three times in TBST, each wash lasting 5 min. Following this, a secondary antibody conjugated with horseradish peroxidase (HRP) (Cell Signalling Technology at a 1:1000 dilution in blocking buffer was added to the membrane for 40 min (**Table 2.4.**). The membrane was then washed as previously described and blotted dry with blotting paper before ECL HRP chemiluminescent substrate reagent (Invitrogen) was added for 1 min, then blotted. Chemiluminescence was measured using an Image Quant LAS 4000 (GE HealthCare, Chalfont St Giles, UK).

Table 2.4 Antibodies used in the study.

Antibody	Serial number	Stock concentration (µg/ml)	Dilution	Concentration in assay (ng/ml)
STAT3	12640	23	1:1000	23
pSTAT3	9145	100	1:1000	100
NF-κB p65	8242	208	1:500	416
p-NF-κB p65	3033	57	1:750	277.3
β-Tubulin	2128	6	1:1000	6
HRP	7074	77	1:1000	77

2.4.5 Densitometry

To assess the changes in protein expression observed by western blot analysis, a semiquantitative method, densitometry, was used to quantify the protein band density of

each immunoblotting image. The bands on each individual gel image were measured using gel analysis software in Fiji Just Image J (v2.14.0) (Wayne Rasband National Institute of Health, USA). The band density of proteins was normalised to the β-tubulin, and then the ratio of phospho/non-phospho protein expressions was calculated using Excel.

2.4.6 Scratch assays

Wound healing/migration assays were performed using ibidi 4-well cell culture inserts (Thistle Scientific, Glasgow, UK) according to the manufacturer's instructions (**Figure 2.1.**). HaCaT cells were seeded into four-well cell culture inserts inside six-well plates at 3.5 x 10^5 cells/mL and incubated overnight at 37 °C; 5% CO_2. Cell culture inserts were removed using sterile tweezers, generating a cross-shaped wound. Any cellular debris was removed by washing the wells with warm DPBS. Cells were treated with 5 µg/mL mitomycin C for 2 h (Cat# M5353; Merck, Gillingham, UK) to inhibit proliferation. After that, cells were washed with warm DPBS and fresh serum-free DMEM media was added. DMSO (vehicle control), human epithelial growth factor (25 ng/ml) (Cat# AF-100-15-500UG; Thermo Fisher Scientific) (as positive control), and the pure compounds were added to wells and incubated for 24 h at 37 °C; 5% CO_2. Images were taken under the EVOS XL Core digital transmitted-light inverted imaging system and analysed using Fiji v 2.16.0. Wound closure was calculated using Excel.

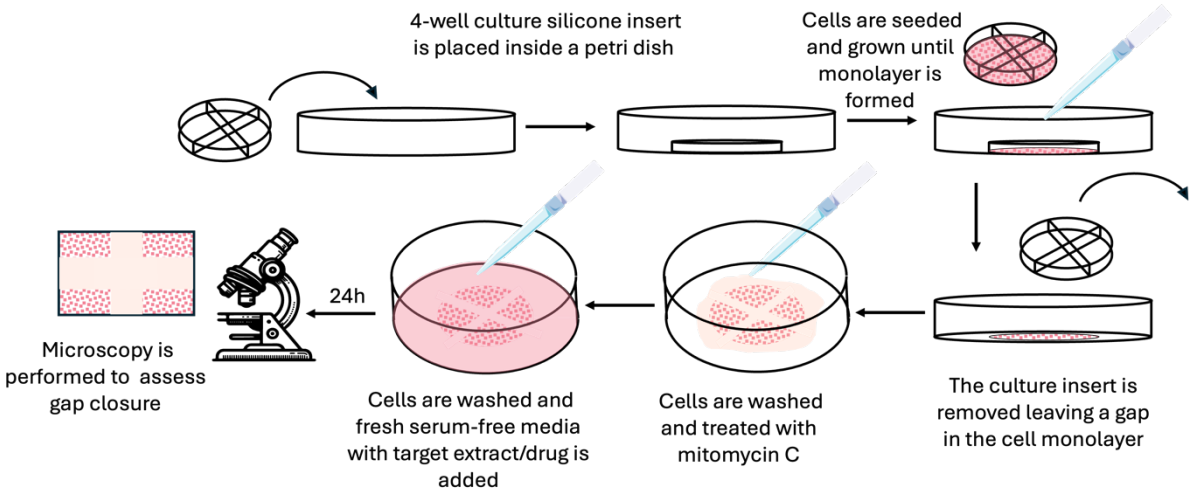

Figure 2.1 Graphical illustration of wound healing assays using ibidi culture inserts. The 4-well silicone insert with defined cell-free gaps is placed inside the petri dish. Cells are seeded and incubated overnight to form a monolayer. The silicone insert is removed, generating a cross-shaped wound (500 µm vertical/horizontal gap and 1000 µm diagonal gain in the cross-section). The media is removed and cells are rinsed and treated with mitomycin C to stop proliferation. Cells are rinsed, and fresh serum-free media with the target extracts or drug is added. Cells are left for 24 h, allowing them to migrate and close the wound. A microscope is used to observe the migration of cells into the gaps and closure of the wound. Figure adapted from (Suh *et al.*, 2022).

2.5 Bioinformatics methods

2.5.1 Phylogenetics

Prior to the start of this project, the genome of the pot marigold was sequenced and assembled as were the transcriptomes of pot marigold and field marigold by EI's core bioinformatics group. Candidate *CYTOCHROME P450* (*CYP*) and *ACYLTRANSFERASE (ACT)* genes were identified by searching the pot marigold genome using the protein sequences of CYP716A111 (APG38190.1) and THAA3 (ASAT1; At3g51970.1) as queries in tBLASTn (rational is described in **section 4.1.**). Cut-off values (4.52e-76 (CYPs) and 1e-60 (ACTs)) were defined to include at least five functional gene products (defined by the presence in transcriptome datasets and the absence of stop codons). The field marigold transcriptome datasets were similarly searched alongside the genomes of *Artemisia annua* (sweet wormwood) (txid:35608), lettuce (txid:4236), *Cichorium endive* (endive) (txid:114280), *Taraxacum kok-saghyz* (Russian dandelion) (txid:333970), common sunflower (txid:4232), *Chrysanthemum seticuspe* (txid:1111766) and *Cynara cardunculus* (cardoon) (txid:4265).

Protein sequences of identified candidate CYPs were aligned with 177 previously characterised terpenoid/sterol modifying P450s protein sequences (Ghosh, 2017a, Malhotra and Franke, 2022b, Miettinen *et al.*, 2018, Miettinen *et al.*, 2017b, Wang *et al.*, 2021b) using MUSCLE V3.8.425 (Edgar, 2004). Protein sequences of ACTs were aligned with 47 previously characterised acyltransferase protein sequences (D'Auria, 2006) using MUSCLE V3.8.425 (Edgar, 2004). Sites with gaps were trimmed using ClipKIT with smartgap mode (v2.1.3) (Steenwyk *et al.*, 2020). Maximum likelihood phylogenetic trees were inferred using IQ-TREE (Trifinopoulos *et al.*, 2016). For analysis of ACTs, a JTT matrix-based model allowing for invariable sites plus a discrete Gamma model and 1000 bootstraps (ACT model: JTT+F+I+G4). For analysis of CYPs, an LG model with empirical amino acid frequencies plus a discrete Gamma model and 1000 bootstraps (CYP model: LG+F+I+G4). Models were selected by ModelFinder (Kalyaanamoorthy *et al.*, 2017). Trees were then visualised in iTOL (available at https://itol.embl.de).

2.5.2 Differential gene expression analysis

Differential gene expression analyses of pot marigold and of field marigold transcripts and genes were performed by EI's core bioinformatics group using DESeq2 (http://www.bioconductor.org/packages/release/bioc/htmL/DESeq2.htmL). Samples were

compared pairwise as follows (baseline/control): (1) Disc/Leaf, (2) Disc/Ray, and (3) Leaf/Ray. Transcripts/genes that had only a single count across all samples or no count at all were removed. For quality control, the expression counts were normalised via regularised logarithm transformation (Love *et al.*, 2014).

I received the resulting comma-separated tables (.csv) of differentially expressed genes/transcripts, which were used to assess the expression levels of individual transcripts (average of the normalised count values (BaseMean) divided by the size factors and taken over all samples) and the expression patterns of candidate genes (log2 fold changes). Genes with adjusted (using the Benjamini-Hochberg adjustment) p-value > 0.1 (indicating weak support of fold change) were removed from the analysis.

2.5.3 Synteny analysis

Synteny between biosynthetic genes was analysed using Geneious Prime (2021.1.1). The locations of all biosynthetic genes (*CoTXSS* and *CoOSC17*, *CYP716A392* and *CYP716A393*, *CoACT1* and *CoACT2*) were annotated on the pseudo-chromosomes from the pot marigold genome assembly and pseudo-chromosome pairs were aligned using the "whole genome alignment" option and progressive Mauve algorithm (Darling *et al.*, 2004).

2.5.4 Molecular modelling

Structural models of CYP716A392 and CYP716A393 were constructed using Phyre2 (Kelley *et al.*, 2015), and the best-ranked models of each were used for docking (parameters taken into account were: sequence identity and resolution of the crystal structure). A 3D structure of ψ-taraxasterol was obtained from PubChem (ID: 5270605). CYP716A392 and CYP716A393 models were aligned with the CYP90B1 crystal structure in complex with cholesterol (PDB ID: 6A15) using the align function of PyMOL (v 3.0.5) and ψ-taraxasterol was manually docked to the active sites based on the location of cholesterol in 6A15. Energy minimisation was performed using the YASARA (25.1.13) force field (Land and Humble, 2018b). Structures were visualised in PyMOL (v 3.0.5) (Schrödinger, Inc., New York, NY, USA).

2.6 Molecular cloning and heterologous expression

2.6.1 Assembly of expression constructs

Candidate pot marigold *CYP* and *ACT* genes were chemically synthesised (Twist Bioscience, South San Francisco, CA, USA) removing any native BpiI, BsaI, BsmBI and SapI recognition sites by introducing synonymous mutations. Coding sequences were flanked with inverted BsaI sites resulting in standardised Level 0 DNA parts in the plant common syntax (Patron *et al.*, 2015). These Level 0 parts were assembled with (i) a Level 1 acceptor (pICH47732; Addgene #48000 or pICH47742; Addgene #48001), (ii) a CaMV35s promoter and omega sequence from tobacco mosaic virus (TMV) (pICH51277; Addgene #50268), and (iii) a CaMV 35s terminator (pICH41414; Addgene #50337) in one-step Type-IIS (Golden Gate) digestion-ligation reactions as previously described (Cai *et al.*, 2020). The following reaction mix was used:

Component	**Volume**	**Stock concentration**
Water	4.85 µL	-
NEB T4 DNA Ligase Buffer	1 µL	10 x
BSA	1 µL	(2 mg/mL)
NEB T4 DNA Ligase	0.5 µL	(400 U/µL)
BsaI (10 U/µL)	0.5 µL	(10 U/µL)
Acceptor*	0.5 µL	66 ng/µL
Promoter**	0.28 µL	66 ng/µL
CDS	0.46 µL	100 ng/µL
STOP codon***	0.42 µL	66 ng/µL
Terminator****	0.49 µL	66 ng/µL
Total Reaction Volume	10 µL	

* Level 1 acceptors = pICH47732 or pICH47742 **Level 0 promoter parts = pICH51277, *** Level 0 stop codon part = pEPQD0CM0030 **** Level 0 terminator part = pUAP41414 (See **Supplementary Table S2.1.** for details of plasmids).

Reactions were cycled as follows:

Step	**Temperature**	**Duration**	**Cycles**
Initial digestion	37 °C	20 seconds	x1
Digestion	37 °C	3 min	x26
Ligation	16 °C	4 min	
Final digestion	50 °C	5 min	x1
Inactivation	80 °C	5 min	x1
Hold	4 °C	infinite	x1

2.6.2 Assembly of VIGS constructs

To assembly constructs for VIGS, 300 bp fragments of target genes were amplified from existing clones or from cDNA introducing BsaI sites that, when digested, generated four-bp overhangs complementary to the vector plasmid (pTRV2:GG_SP/CM Addgene #105349). Fragments were inserted into this vector using the Golden Gate digestion-ligation reaction previously described **(**Cai *et al.*, 2020**)**.

The following reaction mix was used:

Component	**Volume**	**Stock concentration**
NEB T4 DNA Ligase Buffer	2 µL	10 x
BSA	1 µL	(2 mg/mL)
NEB T4 DNA Ligase	1 µL	(400 U/µL)
BsaI (10 U/µL)	1 µL	(10 U/µL)
Acceptor*	2.26 µL	66 ng/µL
GOI fragment *	0.84 µL	10 ng/µL
Water	11.9 µL	-
Total Reaction Volume	20 µL	

* Level 1 acceptor = ppTRV2:GG_SP/CM ** VIGS fragment = TATG_**PDS**_GCTT, GCTT_**TXSS**_GGTG, GCTT_**CAS**_GGTG, GCTT_**GFP**_GGTG, GCTT_**GFP**_TAGT or TATG_**FT**_GCTT.

Reactions were cycled as follows:

Step	**Temperature**	**Duration**	**Cycles**
Initial digestion	37 °C	20 seconds	x1
Digestion	37 °C	3 min	x26
Ligation	16 °C	4 min	
Final digestion	50 °C	5 min	x1
Inactivation	80 °C	5 min	x1
Hold	4 °C	infinite	x1

2.6.3 Site-directed mutagenesis

Site-directed mutagenesis of coding sequences was performed on Level 1 expression constructs using the previously reported single-site mutagenesis protocol described in (Liu and Naismith, 2008) (**Figure 2.2.**). Overlapping primers were designed according to the protocol listed in **Supplementary Table S2.2.** Reactions were amplified using the conditions described below and the resulting DNA pool (mutant and template) was treated with *Dpn*I to digest the methylated template DNA. A list of all plasmids used and created in this study is provided in **Supplementary Table S2.1.**

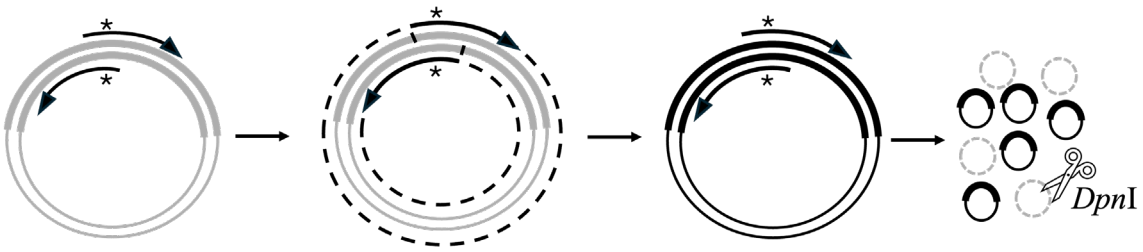

Figure 2.2 Schematic of mutagenesis. Primers were designed to introduce mutations. The long, non-overlapping regions of the primers bridge between 'nicks' (short black bars). Grey circles represent the template plasmid; black dashed lines represent newly synthesised DNA; black circles represent amplicons. Stars indicate the location of the mutation. Figure adapted from (Liu and Naismith, 2008).

The following PCR reaction mix was used:

Component	Volume	Stock concentration
Water	15.8 µL	-
HF buffer	5 µL	5 x
Primer mix	1 µL	10 µM
dNTPs	1 µL	10 mM
DMSO	1 µL	
Template DNA	1 µL	10 ng/µL
Phusion polymerase	0.2 µL	
Total Reaction Volume	25 µL	

Reactions were cycled as follows:

Step	Temperature	Duration	Cycles
Initial denaturation	98 °C	3 min	x1
Denaturation	98 °C	30 sec	x25
Annealing	50 °C	1 min	
Extension	68 °C	7 min	
Final extension	68 °C	10 min	x1
Hold	4 °C	infinite	x1

2.6.4 Transformation of *E. coli*

Assembly and mutagenesis reactions were transformed into high-efficiency DH5α *E. coli* cells (**Table 2.5.**). For transformation, cells were removed from -70 °C and thawed on ice. 0.75 µL of Golden Gate assembly reaction or ~200 ng plasmid DNA was added to 5 µL of NEB 5-α high-efficiency cells in pre-chilled tubes. These were incubated on ice for 30 min, then transferred to 42 °C for 45 seconds (Lab Armor bead bath; 74220-706). Reactions were returned to the ice for 2 min and 45 µL of pre-warmed (37 °C) super optimal broth with catabolite repression (SOC) media was added before incubation with shaking (200 rpm) for 1 h at 37 °C. A 20 µL aliquot was spread onto LB agar plates with appropriate antibiotics (**Table 2.6.**), 1 mM IPTG and 20 mg/mL of X-Gal using glass beads. Plates were air-dried for 5 min before incubation at 37 °C overnight.

2.6.5 Validation of assemblies

Level 1 acceptors (pICH47732 or pICH47742) contain the *β-GALACTOSIDASE* (*LacZ*) gene, and correct constructs for *CYP* and *ACT* candidate genes were identified by blue-white screening. The Level 1 acceptor (ppTRV2:GG_SP/CM) carries the *ccdB* gene coding for the toxic ccdB protein. Surviving colonies, lacking the ccdB cassette, were selected. Selected colonies were incubated at 37 °C shaking at 220 rpm overnight in 10 mL LB with 50 µg/mL appropriate antibiotics. Plasmids were purified using the Plasmid DNA Miniprep Kit (QIAGEN). DNA was eluted in 50 µL elution buffer and yield assessed using a NanoDrop One Microvolume UV-Vis Spectrophotometer (Thermo Scientific). Plasmids were diluted to 66 ng/µL for Sanger sequencing (Eurofins Genomics; http://www.eurofinsgenomics.eu/) (15 µL of 66 ng/µL DNA and 2 µL of primer). Sequencing primers are provided in **Supplementary Table S2.5.** Sequence-verified Level 1 assemblies were transformed into

A. tumefaciens GV3101 by electroporation. Sequence-verified VIGS constructs were transformed into *A. tumefaciens* AGL1 by electroporation.

2.6.6 Preparation of electrocompetent *A. tumefaciens*

A single colony was used to inoculate a 10 mL LB culture containing appropriate antibiotics (**Table 2.6.**). Cultures were grown for two nights at 28 °C with shaking (220 rpm) then 500 mL of LB was inoculated with 5-10 mL of saturated culture and incubated with shaking (28 °C, 220 rpm) until OD_{600} reached 0.5 - 1.0. The cultures were placed on ice for 15 min and centrifugated at 3,400 x g at 4 °C for 15 min. The supernatant was discarded, and cells were resuspended in 100 mL of ice-cold 10% glycerol. This was followed by two successive centrifugations at 3,400 x g at 4 °C for 15 min, and cells were finally resuspended in 1.5 mL ice-cold 10% glycerol. Aliquots were flash-frozen in liquid nitrogen and stored at -70 °C.

2.6.7 Transformation of *A. tumefaciens*

An aliquot of 40 µL electrocompetent *A. tumefaciens* was incubated on ice with ~200 ng of plasmid DNA for 2 min before adding to pre-chilled 2 mm electroporation cuvettes (Geneflow). Electroporation was performed using a MicroPulser Electroporator (Bio-Rad) with 2.2 kV with <1 s pulse duration. Immediately after electroporation, 400 µL of LB was added to cells and transferred to a 2 mL microcentrifuge tube. Cells were incubated at 28 °C for 2-3 h at 200 rpm and then 20 µL of each reaction was plated onto LB-agar with appropriate antibiotics (**Table 2.6.**), using 6 mm glass beads. Plates were dried for 5 min and incubated upside-down at 28 °C for 48 h.

2.6.8 Agroinfiltration of *N. benthamiana*

A single colony was used to inoculate 10 mL LB media with appropriate antibiotics (**Table 2.6.**). This mixture was incubated overnight at 28 °C and 220 rpm. The cultures were centrifuged at 3700 rpm for 20 min at room temperature, and the supernatant was discarded. Cell pellets were resuspended in 10 mL infiltration media (water, 10 mM $MgCl_2$, 10 mM of 2-(N-morpholino) ethanesulfonic acid (MES) pH 5.6 and 0.2 mM 3′,5′-Dimethoxy-4′-hydroxyacetophenone (acetosyringone)) and incubated at room temperature with low rotation speed for 3 h. OD_{600} was measured, and cultures were diluted to OD_{600} 0.8. Finally, for co-infiltrations, *A. tumefaciens* strains were combined in equal ratios.

Immature (no flower buds) *N. benthamiana* plants with three true leaves were used for infiltration. First, the underside of the leaf was pierced using a syringe needle, then *Agrobacterium* suspensions were pushed into the leaf using a 1 mL needleless syringe. Generally, half of a leaf was infiltrated with each mixture of strains. For candidate gene characterisation and mutagenesis studies, all cultures were co-infiltrated with *A. tumefaciens* GV3101 strains containing constructs for constitutive expression of (i) the p19 suppressor of gene silencing from Tomato Bushy Stunt Virus (TBSV) (pEPQD1CB0104; #177038) (Garabagi *et al.*, 2012a), (ii) a truncated, feedback-insensitive tHMGR (pEPQD1CB0817; #177039) to increase triterpene production (Reed *et al.*, 2017b), and (iii) a previously characterised pot marigold ψ-taraxasterol synthase (CoTXSS) (pEPMS1CB0001). For luciferase assays, an *A. tumefaciens* strain carrying an in-house vector with the coding sequence of firefly luciferase (LucF) under the control of the Cauliflower Mosaic Virus 35 s promoter (pEPCTαKN001; #187568) was used. Following infiltration, plants were grown at 25 °C/22 °C with a 16/8 hour day/night cycle for five days in an MLR-352-PE plant growth chamber (Panasonic Healthcare Co, Oizumi-Machi, Japan).

2.6.9 Agroinfiltration of pot marigold

Agroinfiltration of pot marigold was carried out using two methods. In the first, as described for *N. benthamiana*, leaves of four-week-old pot marigold were used for leaf infiltration. In the second method, *Agrobacterium* suspensions were injected into the leaf midrib and veins using a syringe with a Terumo Agani hypodermic 25 Mm needle (R & L Slaughter Ltd, Essex, UK). In both methods, three leaves per plant were infiltrated with the same mixture of strains. After infiltration, plants were returned to the glass house with natural day length and temperature conditions for 38 days before sample collection.

Table 2.5 Bacterial strains used. All bacteria stocks were stored as 1 mL aliquots at -70 °C.

Strain	**Antibiotic resistance**
E. coli, DH5α (Invitrogen)	-
A. tumefaciens GV3101	100 µg/mL rifampicin and 20 µg/mL gentamycin
A. tumefaciens LBA4404	100 µg/mL rifampicin and 50 µg/mL streptomycin
A. tumefaciens AGL1	100 µg/mL rifampicin and 50 µg/mL carbenicillin

Table 2.6 Antibiotics used for culturing bacteria. All antibiotic stocks were stored as 1 mL aliquots in the specified solvent at -20 °C.

Antibiotic	Stock	Dilution factor	Final concentration
Gentamicin	50 mg/mL in H2O	1/1000	50 µg/mL
Kanamycin	50 mg/mL in H2O	1/1000	50 µg/mL
Rifampicin	50 mg/mL in dimethylformamide	1/1000	50 µg/mL
Chloramphenicol	35 mg/mL in ethanol	1/1000	35 µg/mL
Carbenicillin	100 mg/mL in H2O	1/1000	100 µg/mL
Streptomycin	50 mg/mL in H2O	1:1000	50 µg/mL

2.7 Gene expression analysis

2.7.1 Luciferase assay

Firefly luciferase (*LucF*) expression was detected using the Nano-Glo® Dual-Luciferase® reporter assay system (Promega, Madison, WI, USA). A 1 cm disc was taken from the infiltrated leaf and homogenised in 180 µL passive lysis buffer (Promega) containing protease inhibitor (P9599, Sigma-Aldrich). Following incubation on ice for 15 min and centrifugation (100 × g, 2 min, 4 °C), the supernatant was diluted 1:5 in passive lysis buffer. Next, 10 µL of the dilution was mixed with 20 µL of passive buffer, which was then mixed with 30 µL ONE-Glo™ EX Luciferase Assay Reagent (Promega) and incubated at room temperature for 10 min. LucF luminescence was quantified using a GloMax 96 Microplate Luminometer (Promega) with a 10 second read time and 1 second settling time.

2.7.2 RNA extraction

Samples of plant tissue were collected into 2 mL microcentrifuge tubes with 3 mm tungsten carbide beads and flash-frozen in liquid nitrogen. Samples were ground using a TissueLyser II (Qiagen) for 1 min, 25 1/s. ~100 mg tissue was reserved for metabolic analyses and RNA was extracted using the Spectrum™ Plant Total RNA Kit according to the manufacturer's instructions. RNA concentrations and A280/A260 and A280/A230 ratios were assessed using a NanoDrop One Microvolume UV-Vis Spectrophotometer (ThermoFisher). Quality was verified on a 1% agarose gel.

2.7.3 cDNA synthesis

cDNA was synthesised from 50 ng of total RNA. In brief, 6 µL of master mix containing 1 µL of Oligo(dT), 1 µL of 10 mM dNTP Mix (10 mM each) and 4 µL of RNase-free water were added to 6 µL of 50 ng/µL of RNA. RNA was denatured at 65 °C and transferred to ice. After brief centrifugation, 7 µL RNaseOUT mix containing 4 µL of 5X First-Strand Buffer, 2 µL of 0.1 M DTT and 1 µL of RNaseOUT (40 units/µL) was added to the tube and mixed. Tubes were incubated at 37 °C for 2 min, and 1 µL M-MLV reverse transcriptase was added to make a total reaction volume of 20 µL. Reactions were incubated at 37 °C for 50 then inactivated at 70 °C for 15 min. cDNA was diluted 1:10 by the addition of 180 µL 1/2 Low TE buffer (5 mM Tris-HCl + 0.5 mM EDTA, pH 8.0) and stored at -20 °C until use.

2.7.4 RT-qPCR

Primers were designed using Primer3 and BLAST (Ye *et al.*, 2012). The following parameters were specified: PCR product size = 70-150 bp, Tm = 58-60 °C to design 20 primers. The pot marigold transcriptome dataset was used to identify potential off targets. The three best primers were chosen for further analysis. An efficiency check was performed using a serial dilution of cDNA (1:10). A trendline of Ct values was plotted, and the equation for the trendline was calculated (y=mx+b). The slope (m) of the equation was used to calculate the efficiency using the following formula: E=2^(-1/m). The efficiency (%) was calculated as %E=100(E-1). Primers resulting in the E closest to -3.32, and the %E closest to 100% were selected to use for qPCR amplification. Primer sequences are given in **Table S2.3.**

Amplifications were performed in 10 µl reactions with 0.2 µM of each primer, 6 µl cDNA template and 1 x SYBR Green Jumpstart™ Taq ReadyMix™ . Each amplification was repeated in duplicate (technical replicates) with at least 3 biological replicates on a QuantStudio™ 6 Pro Real-Time PCR system (Applied Biosystems A43182) in 384-well plates using the following cycling conditions:

		Step	Temp (°C)	Time
PCR	40 cycles	Denaturation	94 °C	2 min
		Denaturation	94 °C	15 sec
		Annealing	58 °C	1 min
		Extension	95 °C	15 sec
Melt curve	Continuous	Hold	60 °C	1 min
		Denaturation	95 °C	1 sec

Relative expression was quantified using the ΔΔCq method (Livak and Schmittgen, 2001) relative to the housekeeping gene *SAND* (SAND family protein). The resulting cross point (Ct) values from the qPCR reaction were averaged across technical replicates. ΔCt was calculated by subtracting the average *SAND* Ct value from the average Ct value of the target gene. ΔCt was normalised for each experimental sample to average Ct of control treatment to calculate the normalised expression of each biological replicate. The DeltaDeltaCt (ΔΔCt) was then calculated using the 2^(ΔCt) formula. No reverse transcriptase and no template controls had Cq values >33.

Chapter 3 - The anti-inflammatory properties of pot marigold

3.1 Introduction

Chronic wounds are a serious public health concern worldwide. They are defined as wounds that have not progressed or are taking longer to go through all stages of healing, which include inflammation (0–3 days), re-epithelisation (3–12 days) and tissue remodelling (3–6 months) (Kumar *et al.*, 2007, Schultz *et al.*, 2011). Recently, it has been estimated that about 2% of people in both developing and developed countries suffer from chronic wounds at any time (Sen, 2021). It is, therefore, important to find new drugs to treat chronic wounds and reduce the economic burden on healthcare systems and patients.

In this chapter, I focus on investigating the wound-healing activity of pot marigold flowers, which has been previously recorded in multiple *in vivo* (Givol *et al.*, 2019) and *in vitro* (Fronza *et al.*, 2009, Nicolaus *et al.*, 2017) studies. To assess the activity of pot marigold extract and its pure compounds, I predominantly focus on the first two stages of the wound healing process – the inflammatory and re-epithelisation phases.

The inflammation phase begins within a few minutes after the tissue damage has occurred (Criollo-Mendoza *et al.*, 2023). As discussed in the introduction, different stimuli are recognised by surface receptors, which activate various inflammatory signalling pathways. In these pathways, chains of biochemical reactions lead to the production of pro-inflammatory mediators such as proinflammatory cytokines (interleukins IL-1β, IL-6, IL-8 and TNF-α, chemokines (e.g. CXCL-8, CCL2, CCL3), and growth factors (e.g. PDGF, TGF-α, TGF-β, FGF) (Chen *et al.*, 2017, Criollo-Mendoza *et al.*, 2023) (**Figure 3.1.**).

If the optimal level of mediators is exceeded and continues, it can lead to the damage of healthy tissue, chronic inflammation and a delayed wound healing process. Thus, one of the common methods to assess the anti-inflammatory activity of potential treatments is to evaluate their ability to decrease the production of pro-inflammatory mediators (Chiswick *et al.*, 2012). A common model for studying monocyte/macrophage function, signalling pathways and mechanisms of drug actions is the human leukaemia monocytic cell line (THP-1), (Chanput *et al.*, 2014) (**Figure 3.1.**). Bacterial LPS can be used to simulate inflammation, which, in these cells, is recognised by a receptor complex composed of the

glycosylphosphatidylinositol (GPI)-anchored receptor (CD14), Toll-like receptor 4 (TLR4), and myeloid differentiation factor 2 (MD-2) (Park and Lee). The TLR4 receptor has been shown to activate the NF-κB, MAPK and JAK/STAT signalling pathways (Liu *et al.*, 2018, Reddy and Reddanna, 2009) (**Figure 3.1.**). The NF-κB pathway is a major inflammatory pathway that drives the production of critical regulators of immune responses, including TNF-α, IL-6, IL-8 and IL-1β (Webster and Vucic, 2020) (Liu *et al.*, 2018).

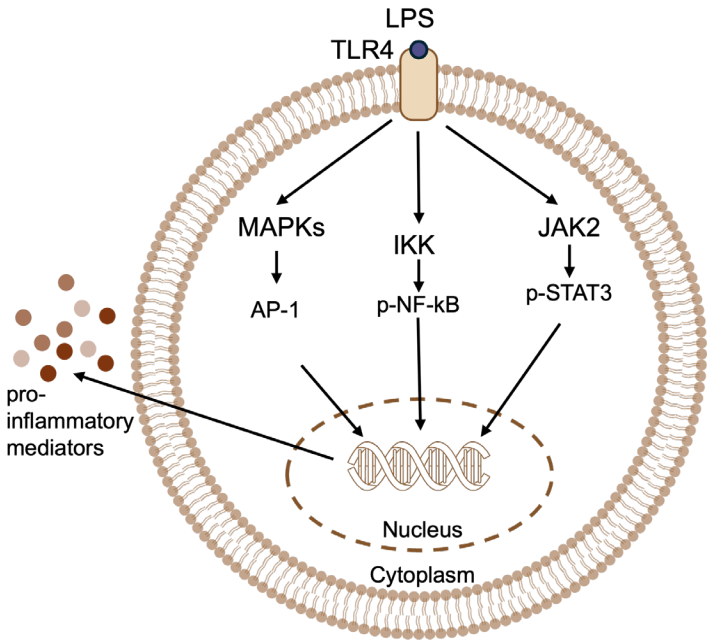

Figure 3.1 LPS-mediated induction of inflammation in monocytes. LPS is recognised by the TLR4 receptor, which activates IkappaB kinase (IKK), mitogen-activated protein kinase (MAPK) and Janus kinase (JAK) signalling pathways. In the pathways, transcription factors (activating protein-1 (AP-1) for MAPK, nuclear factor kappa B (NF-κB) for NF-κB, and STAT3 for JAK pathways are phosphorylated and bind to corresponding promoters to drive production of pro-inflammatory cytokines (tumour necrosis factor-alpha (TNF-α), interleukins IL-1β and IL-6).

After the inflammatory stage, the proliferative phase takes place, lasting a few days to weeks. In this stage, the epithelial cells (keratinocytes) proliferate and migrate to the wound to form a new epidermal barrier (Sinno and Prakash, 2013). At the same time, activated fibroblasts also migrate to the wound and create an extracellular protein matrix by synthesising collagen to provide structural support to the new tissues (Criollo-Mendoza *et al.*, 2023). One of the simplest and fastest methods to assess the wound-healing activity of potential drugs, aimed at assessing re-epithelialisation upon treatment with the target extract/compound, is performed by measuring fibroblast and keratinocyte proliferation and migration into the open wound (Liang *et al.*, 2007). A second common method is to determine the collagen content synthesised by fibroblasts by measuring soluble collagen in the cell culture supernatant (Szász *et al.*, 2023).

The human-immortalised keratinocyte (HaCaT) cell line has become a widely used model for studying wound healing activity using a so-called 'scratch' assay (Glady *et al.*, 2021, Liang *et al.*, 2007, Liu *et al.*, 2021) (**Figure 3.2.**). In this method, cells are grown to generate a monolayer, and a wound (or scratch) is generated using a mechanical item such as a pipette tip (Lampugnani, 1999), magnet (Fenu *et al.*, 2019), comb (Klemke *et al.*, 2013), or cell insert (Caesar *et al.*, 2013, Shih *et al.*, 2012). Cells are incubated for 24 h and wound closure is assessed by measuring wound area before and after treatment with the extract or compound being assessed (**method 2.4.6**).

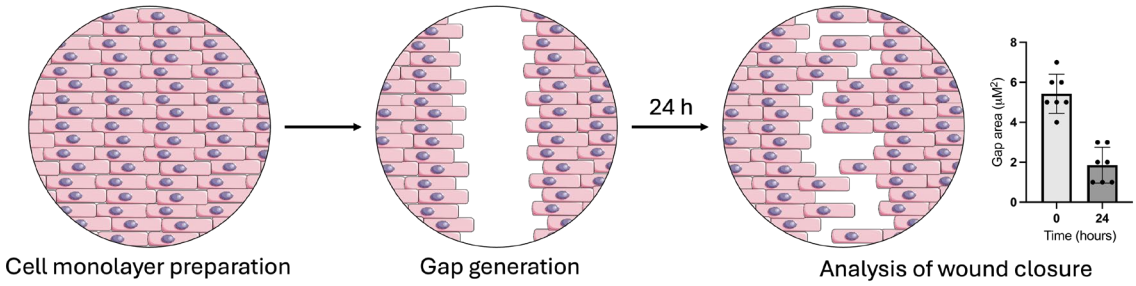

Figure 3.2 Schematic of a scratch assay. Cells are grown to generate a monolayer, and the artificial wound is generated. After treatment, cells are incubated for 24 h and wound closure is assessed by measuring the wound area before and after treatment.

The World Health Organization (WHO) estimates that almost 80% of the world's population uses traditional healthcare practices, with 85 % of these being plant-derived remedies (Criollo-Mendoza *et al.*, 2023). More than 100 plant species have been shown to have wound-healing properties (Malabadi *et al.*, 2022). However, plant extracts can often contain toxic compounds. This has led to a reduction in the use of whole plant extracts in many world regions. Instead, modern research has focused on the identification of individual compounds that exhibit strong activity with few side effects.

Numerous small molecules from plant extracts have been shown to be effective in all phases of the wound-healing process (Mehta *et al.*, 2016, Shah and Amini-Nik, 2017). Many of these compounds are considered to be safer than some synthetic molecules, and are often cheaper than conventional therapies (Monika *et al.*, 2022). Thus, the use of purified plant natural products is becoming more common in modern medicine. For example, in 2023, the first wound-healing gel (FILSUVEZ) for treating epidermolysis bullosa was approved by the Food and Drug Administration of the United States of America (FDA). This topical gel contains 100 mg of four anti-inflammatory triterpenoids (betulin, betulinic acid, oleanolic acid and lupeol) derived from the birch bark in an oil base of refined sunflower oil (Kindler *et al.*, 2016).

The global skincare industry, a major section of the beauty industry, valued at USD 109.71 billion in 2023 (Fortune Business Insights Report ID: FBI102544), is also a major consumer of plant natural products. These include flavonoids such as quercetin and catechins that exhibit strong anti-inflammatory and antioxidant activities and promote collagen synthesis and tissue repair (Zulkefli *et al.*, 2023). These compounds are included in skincare products such as 'Korres Quercetin Face Serum' and the FDA-approved 'EltaMD' sun protection factor (SPF).

This thesis is focused on pot marigold, which accumulates a variety of triterpenoids, some of which have already been associated with wound-healing and anti-inflammation. For example, in 1994, Della Loggia and colleagues performed a bioassay-oriented fractionation of the CO_2 extract of pot marigold flowers with the aim of identifying potential anti-inflammatory drugs (Della Loggia *et al.*, 1994). In this research, the inhibition of croton oil-induced dermatitis of the mouse ear by triterpene fractions or pure compounds was assessed. Unesterified faradiol, a C16 hydroxylated triterpene found in pot marigold, showed the strongest anti-inflammatory activity, while triterpene monols, including ψ-taraxasterol, lupeol and taraxasterol exhibited relatively weaker activity (**Figure 3.3.**). Faradiol monoesters are the most abundant compound in pot marigold extracts (19% of total CO_2 extract), but showed the weakest anti-inflammatory activity extract (Della Loggia *et al.*, 1994).

In 1997, the same group reported a separative method for two monoesters abundant in pot marigold extracts, faradiol myristate and faradiol palmitate, and tested them using the same *in vivo* model (Zitterl-Eglseer *et al.*, 1997). Both molecules exhibited similar dose-dependent anti-oedematous activity, with no significant synergistic effect. In a later study, Neukirch and colleagues showed that more-polar compounds exhibit stronger *in vivo* anti-oedematous activity than less-polar compounds (Neukirch *et al.*, 2005). This principle was demonstrated for lupeol and its hydroxylated analogues calenduladiol and heliantriol B_2; ψ-taraxasterol and its hydroxylated analogues faradiol and heliantriol B_0; and for taraxasterol and its hydroxylated analogue arnidiol (**Figure 3.3**.). In 2009, the wound-healing properties of pot marigold extracts were investigated using a scratch assay, concluding that faradiol myristate and palmitate have wound-healing activity but only partially contribute to the bioactivity of the extract, indicating contributions by other compounds (Fronza *et al.*, 2009).

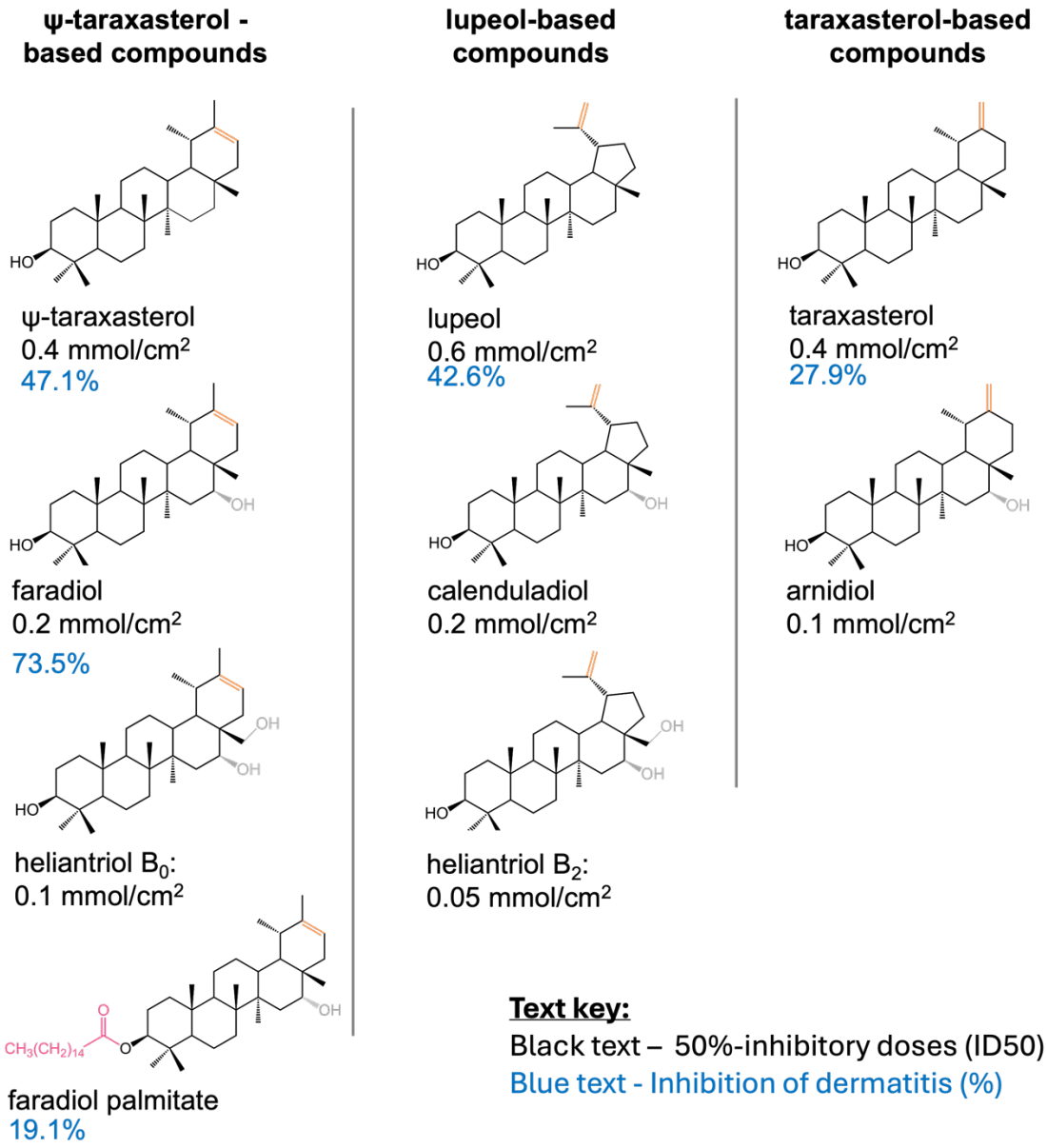

Figure 3.3 Anti-inflammatory triterpenes identified in pot marigold floral extracts. Figure 3.3 Anti-inflammatory triterpenes identified in pot marigold floral extracts. Chemical structures of pot marigold triterpenes. Blue numbers indicate the percentage inhibition of croton oil-induced dermatitis of the mouse ear following the application of 120 pg/cm^2 determined by (Della Loggia *et al.*, 1994). Black numbers indicate the 50%-inhibitory doses (ID50 in mg/ear) reported by (Neukirch *et al.*, 2005).

More recently, the anti-inflammatory potential of pot marigold flower extracts and compounds found within them have been investigated in *in vitro* studies. A study in gastric epithelial cells demonstrated that pot marigold triterpene diols and their esters exhibited significant and concentration-dependent inhibitory activity of NF-κB-driven transcription, with diols showing a stronger effect than esters (Colombo *et al.*, 2015). Other compounds (loliolide and fucoside acetates of *β*-eudesmol and viridiflorol) also exhibited intermediate inhibitory activity on NF-κB-driven transcription, indicating that multiple constituents may contribute to anti-inflammatory activity (Colombo *et al.*, 2015). A study in HaCaT cells

showed that pot marigold extracts influence the inflammatory phase by increasing levels of the chemokine IL-8 at both the transcriptional and protein levels (Nicolaus *et al.*, 2017). However, it was noted that activation of the NF-κB transcription factor was cell-specific. Moreover, while an ethanolic extract inhibited the activity of collagenase *in vitro* and enhanced the amount of collagen contributing to the wound-healing process, triterpenes only played a marginal role in new tissue formation. Thus, the authors concluded that more investigation is needed to understand which compounds contribute to the inflammatory stage of wound healing, and what is the underlying mechanism of action.

Prior to the experiments described in this thesis, Dr. Melissa Salmon, a postdoctoral researcher in the Patron group, performed GC-MS analysis on pot marigold extracts of leaf and flower tissues. A capitulum of Asteraceae consists of two types of florets: the ray floret that occupy the exterior of the head and the disc floret that are found in the centre (Figure X) (Zhang and Elomaa, 2024). Both of these tissues (ray and disc florets) were profiled by Dr. Melissa Salmon. These analyses showed that ψ-taraxasterol and its derivatives, including faradiol fatty acid esters, are only found in the floral tissues, predominantly in ray floret **(Figure 3.4).**

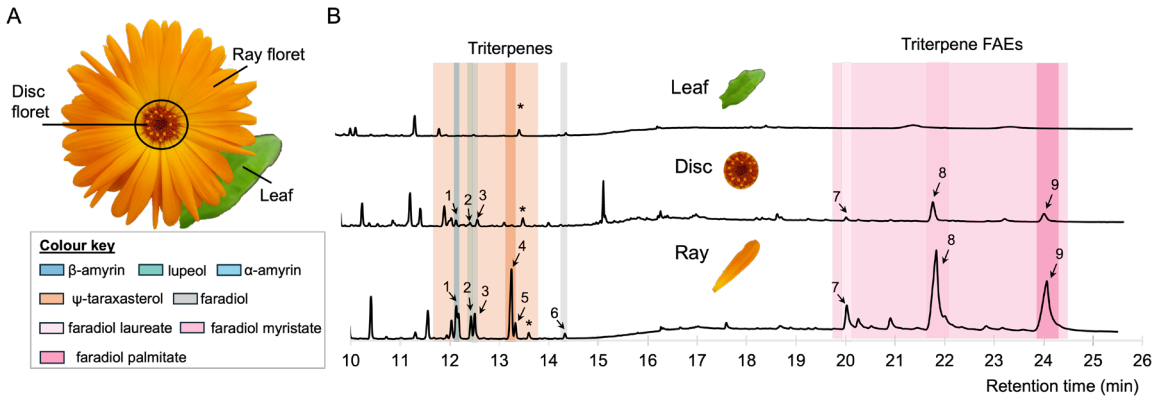

Figure 3.4. Metabolite analysis of Calendula officinalis (pot marigold) by GC-MS. Metabolite analysis of *Calendula officinalis* (pot marigold) by GC-MS. A. The structure of pot marigold capitulum. B. Total Ion Chromatogram (TIC) of derivatised leaf disc and ray extracts.

3.2 Aims

The overarching objective of this chapter is to identify which compounds found in flowers of pot marigold contribute to its anti-inflammatory activity, and to investigate a mechanism for this bioactivity via the following aims:

- Compare the metabolic profile of pot marigold ray tissue to other Asteraceae to investigate the prevalence of the proposed anti-inflammatory compounds, faradiol and faradiol FAEs

- Confirm the previously reported anti-inflammatory activity of pot marigold flower extracts and compare it with other Asteraceae
- Identify the key molecules responsible for pot marigold anti-inflammatory activity
- Investigate which structural features underly the bioactivity of triterpene FAEs
- Investigate the underlying mechanism of action of anti-inflammatory activity
- Compare the activity of pot marigold triterpenes to those used in commercial products
- Investigate the wound-healing activity of pot marigold

3.3 Contributions by other scientists

Experiments in this chapter were done by the author of this thesis, except that Professor Maria O'Connell and Solomon Awuni, an undergraduate student in the O'Connell lab, performed two replicates of the Western Blot analysis for p-NF-κB/NF-κB.

3.4 Results

3.4.1 Bioactivity of pot marigold extracts

3.4.1.1 Faradiol and faradiol FAEs are rare compounds

Previous literature suggests that faradiol FAEs contribute to the inflammatory activity of pot marigold. To investigate whether any of these compounds are unique to this species, comparative metabolomics was used to identify if other Asteraceae species also produce faradiol and its derivatives.

To investigate whether any of these compounds are unique to this species, comparative metabolomics was used to identify if other Asteraceae species also produce faradiol and its derivatives. To do this, 14 species were selected from the three largest Asteraceae subfamilies: Asteroideae, Cichorioideae and Carduoideae **(Table 3.1.).** Pot marigold belongs to the Calenduleae tribe of the largest Asteraceae subfamily, the Asteroideae. Therefore, two other species from the same tribe, field marigold and *C. suffruticosa,* were selected to determine if other species from this tribe also produce faradiol and its derivatives.

Sword-leaved inula has previously been reported to produce faradiol (Trendafilova *et al.*, 2021). Thus, two species that belong to the Inuleae tribe, sword-leaved inula, and British yellowhead, were also selected. C16 hydroxylated triterpenes maniladiol and faradiol have been also found in flowers of common sunflower from the Heliantheae alliance tribe (Yasukawa *et al.*, 1996). Thus, the common sunflower and another species from this tribe, hemp-agrimony, were selected. Both of these species are used in herbal medicine. Traditional uses of common sunflower date back three thousand years, with various parts of the plant, including seeds, leaves, flowers, and roots, used to treat the cold, heart disease, cough and respiratory infections (Singh *et al.*, 2022a). In India, edible sunflower flowers are also used against skin allergies (Xavier *et al.*, 2015). Aerial parts of hemp-agrimony are also used in traditional medicine. In Taiwan, they are utilised for the treatment of headache, diarrhea and hypertension, and worldwide as a detoxifying herb for the treatment of fevers, cold and flu (Al-Snafi, 2017).

In addition, two species from the Anthemideae tribe, chamomilla, and yarrow, recorded to produce ψ-taraxasterol (Chandler *et al.*, 1982, Ganeva *et al.*, 2003) were selected together with common daisy, which has not been reported to produce ψ-taraxasterol or its derivatives. Their use in traditional medicine is discussed in (**section 1.2.1)**. Finally, to cover species diversity and assess the prevalence of faradiol in the wider Asteraceae family, four additional species from two smaller Asteraceae subfamilies Cichorioideae and Carduoideae were selected: mouse-ear hawkweed which is known to produce ψ-taraxasterol based compounds (Jiao *et al.*, 2022), and milk thistle, common cat's ear and rush skeleton weed, which have not been recorded as producing ψ-taraxasterol or its derivatives. Milk thistle and common cat's ear are also commonly used herbs in traditional medicine. Leaf and flower extracts of these plants have been used to treat a wide range of illnesses, including liver, kidney and heart disorders for milk thistle, and as anticancer, anti-inflammatory and wound healing agents for common cat's ear (Riaz *et al.*, 2023, Senguttuvan *et al.*, 2014).

Table 3.1 Table of Asteraceae species studied in this chapter.

Subfamily	Tribe	Bionomial name	Common name
Asteroideae	Calenduleae	*Calendula officinalis*	pot marigold
		Calendula arvensis	field marigold
		Calendula suffruticosa	
	Inuleae	*Pentanema britannica*	British yellowhead
		Inula ensifolia	sword-leaved inula
	Heliantheae alliance	*Helianthus annuus*	common sunflower
		Eupatorium cannabinum	hemp agrimony
	Anthemideae	*Matricaria chamomilla*	chamomile
		Achillea millefolium	yarrow
	Astereae	*Bellis perennis*	common daisy
Cichorioideae	Hieraciinae	*Pilosella officinarum*	mouse-ear hawkweed
	Hypochaeridina	*Hypochaeris radicata*	common cat's ear
	Chondrillinae	*Chondrilla juncea*	rush skeleton weed
Carduoideae	Carduinae	*Silybum marianum*	milk thistle

For this, a common ethyl acetate extraction and subsequent N-Methyl-N-trimethylsilyltrifluoroacetamide (MSTFA) derivatisation methods, described by (Huang *et al.*, 2019, Reed *et al.*, 2017a, Stephenson *et al.*, 2018) were adapted for pot marigold ray tissues, with the subsequent analysis using GC-MS. Compounds were identified (A) by comparing retention time and mass spectra with commercially available standards, (B) by comparing mass spectra with spectra recorded in the NIST database or predicted (C) based on the fragmentation patterns, characteristic and molecular ions **(Supplementary Figure S3.1., Supplementary Table S3.3.).**

All 14 species were found to accumulate triterpene monols, including β-amyrin, α-amyrin, lupeol, ψ-taraxasterol and taraxasterol (**Figure 3.5.**, and **Supplementary Figure S3.1.**). Further, four species — pot marigold, sword-leaved inula, common sunflower and rush skeleton weed — were found to accumulate C:16 triterpene diols (faradiol and/or maniladiol) (**Figure 3.5.**, and **Supplementary Figure S3.1.**). Interestingly, despite accumulation of C:16 triterpene diols FAEs, unesterified C:16 triterpene diols were not detected in field marigold, *C. suffruticosa* and British yellowhead. Most species accumulated triterpene fatty acid esters based on β-amyrin, α-amyrin, lupeol, or ψ-taraxasterol, but triterpene diol FAEs were only identified in the *Calendula* genus, common sunflower, British yellowhead, sword-leaved inula and rush skeleton weed (**Figure 3.5.,** and **Supplementary Figure S3.1.**). In addition, common cat's ear, chamomilla, yarrow, milk thistle, and rush skeleton weed were observed

to accumulate ψ-taraxasterol and taraxasterol acetates and milk thistle also produced β-amyrin acetate and α-amyrin acetate (**Supplementary Figure S3.1.**). All identified compounds and their peak areas are detailed in the extended table (**Supplementary Table S3.1.).**

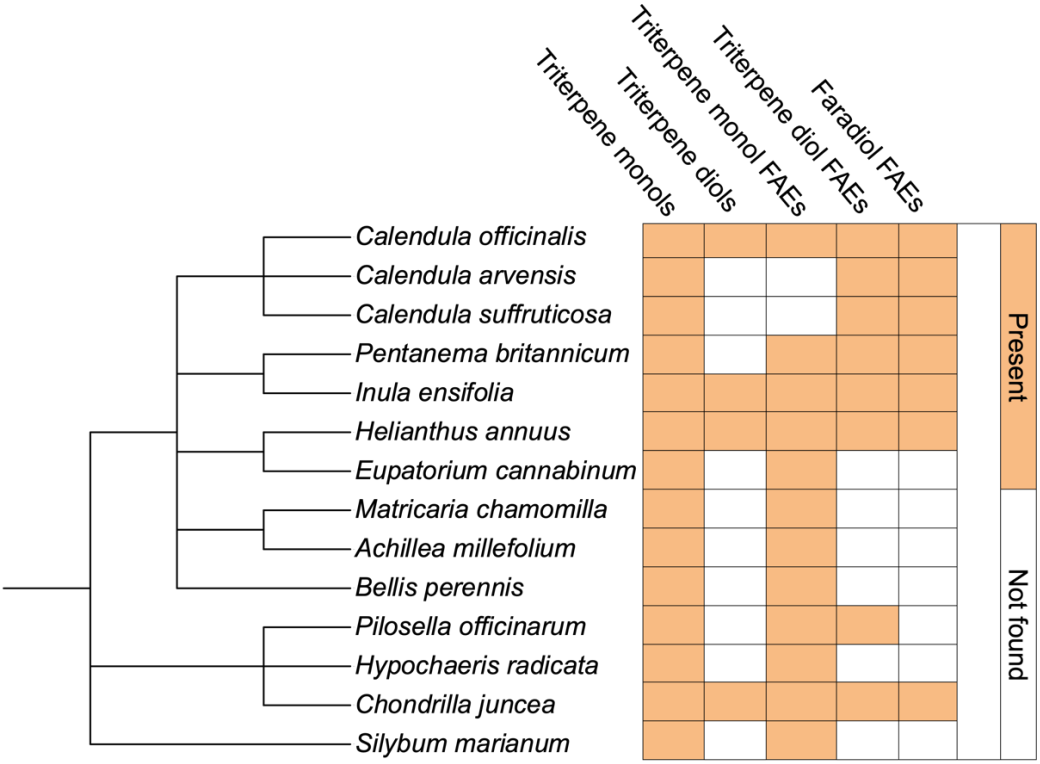

Figure 3.5 Phylogenetic tree and metabolite content of fourteen Asteraceae species. A phylogenetic tree of fourteen Asteraceae was generated using the NCBI Common Tree Taxonomy Tool (Schoch *et al.*, 2020). The presence of triterpenes identified using GC-MS is indicated in orange. A full table with peak areas of identified compounds is provided in Supplementary Figure S3.1. Common names of all species are shown in Table 3.1.

3.4.1.2 Most floral extracts of Asteraceae species are not cytotoxic

Prior to performing anti-inflammatory bioassays, the impact of floral extracts on cell proliferation must be determined. To do this, the anti-proliferative activity of 11 species - pot marigold, common sunflower, chamomile, yarrow, common daisy, British yellowhead, sword-leaved inula, mouse-ear hawkweed, common cat's ear, rush skeleton weed, and milk thistle - were compared using the human leukaemia cell lines, THP-1 and HL-60. Insufficient tissue was obtained from hemp agrimony, *C. suffruticosa*, and field marigold.

Due to the lipophilic nature of the many triterpenes, ethyl acetate extracts were dried down and re-dissolved in DMSO. To assess the ability of extracts to inhibit cell growth, a standard colourimetric method MTS was used (**methods 2.4.2.**). For the initial screen, a 72h MTS assay was performed on $3x10^5$ cells/mL and 200 µg/mL crude extract concentration for the

ray tissues. A cell-permeable alkaloid (1 µM staurosporine) isolated from *Streptomyces staurosporeus* and previously shown to exhibit anti-cancer activity was used as a positive control.

The results showed that 200 µg/mL of extracts from most Asteraceae species do not inhibit 50% of THP-1 cell growth. Only yarrow extract significantly inhibited THP-1 cell growth (80 % inhibition compared to the vehicle control (DMSO)) (**Table 3.2.**). More extracts inhibited the proliferation of HL-60 cells. Extracts of common daisy showed the strongest activity, inhibiting more than 95 % of cell growth at 200 µg/mL (**Table 3.2.**). This was followed by extracts from British yellowhead and yarrow, chamomile, and common sunflower, inhibiting 84 %, 60 %, 57 % and 51 % of growth, respectively (**Table 3.2.**). Further, pot marigold extract was observed to significantly stimulate the proliferation of THP-1 and HL-60 cell lines, with treated cells showing 68 % and 60 % higher cell viability than the vehicle control (DMSO), respectively. Extracts from other species, including common cat's ear, milk thistle, sword-leaved inula and rush skeleton weed, also showed similar trend in increasing cells proliferation but it was not significant (**Table 3.2.; Supplementary Table S3.4.**)

Table 3.2 Effect of the Asteraceae on THP-1 and HL-60 cell viability. Cells ($3x10^5$ cells/ mL) were plated and treated with extracts, vehicle control (DMSO) or 1 µM of staurosporine (positive control), and incubated for 72 h. Cell viability was measured in an MTS assay. Data is expressed as % of vehicle control. N=5. Mean ± SEM. Statistical significance of the cells treated with extracts was compared to vehicle control and analysed using one-way ANOVA with a post-hoc Dunnett test. *=p<0.0332, **=p<0.0021, ***=p<0.0002, ****=p<0.0001.

Treatment (extract)	**Cell viability (% DMSO control)**	
	THP1	**HL60**
pot marigold	167.7 ± 30.1	160.0 ± 19.2 *
yarrow	19.9 ± 12.6 *	29.8 ± 5.6 **
common sunflower	126.6 ± 23.0	48.5 ± 6.0
mouse-ear hawkweed	101.6 ± 16.5	65.7 ± 43.9
milk thistle	113.8 ± 35.0	120.1 ± 23.2
common cat's ear	157.0 ± 40.2	133.9 ± 44.5
common daisy	110.8 ± 57.9	4.4 ± 2.4 ***
rush skeleton weed	147.8 ± 30.5	119.9 ± 28.9
chamomile	95.6 ± 63.2	42.8 ± 13.9 *
British yellowhead	79.0 ± 52.5	15.8 ± 3.9 ***
sword-leaved inula	155.3 ± 59.9	106.1 ± 22.1

For extracts that showed more than 70 % cell growth inhibition compared to the vehicle control (DMSO), the IC_{50} value was determined. For this, a 72h MTS assay was performed on $3x10^5$ cells/mL using a serial dilution of the initial crude extract. The IC_{50} value was calculated using non-linear curve-fitting in Graph Pad Prizm (v.10.3.1) (**Table 3.3.**). Extracts of yarrow showed strong anti-proliferative activity with IC_{50}: 13.39 ± 8.67 µg/mL in THP-1 and 12.39 ± 2.40 µg/mL HL-60. British yellowhead and common daisy were mildly potent with similar IC_{50}s (~20 µg/mL) (**Table 3.3.**).

Table 3.3 IC50 of selected Asteraceae in THP-1 and HL-60. Cells ($3x10^5$ cells/mL) were plated and treated with a broad range of extract concentrations, DMSO (vehicle control) and incubated for 72 h. Cell viability was measured by MTS assay and IC_{50} was determined. N=3. Mean ± SEM.

Treatment	**IC_{50} (µg/mL)**	
	THP1	**HL60**
yarrow	13.39 ± 8.67	12.39 ± 2.40
common daisy		23.97 ± 2.52
British yellowhead		22.46 ± 1.54

3.4.1.3 Asteraceae species that produce faradiol FAEs exhibit anti-inflammatory activity

ELISA was used to assess the ability of extracts to inhibit the release of the pro-inflammatory cytokines TNF-α and IL-6 in LPS-induced THP-1 cells. Extracts of yarrow were not screened due to the cytotoxicity identified above.

Before testing extracts in the anti-inflammatory assays, a 24 h MTS assay was performed using 50 µg/mL crude extract of ray tissues on $3x10^5$ cells/mL to confirm that this is a suitable, non-toxic concentration, and to ensure observed effects are not due to cell death. These results indicated that ethyl acetate extracts of all species, except rush skeleton weed, have a negligible effect on cell viability compared to the vehicle control (DMSO) (**Figure 3.6., Supplementary Table S3.4.**). Rush skeleton weed extract has a light negative impact on the THP-1 cells viability.

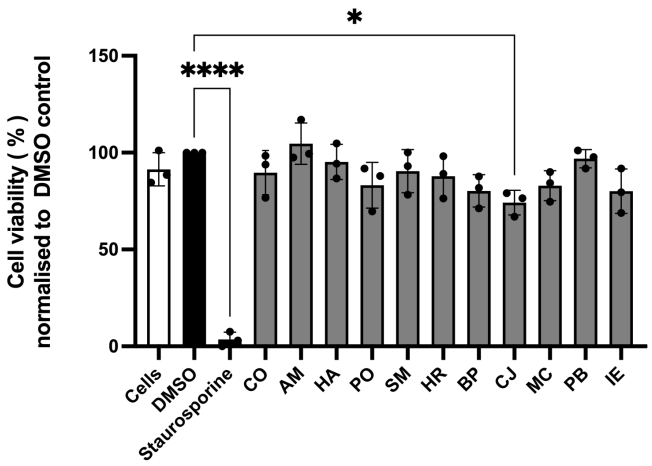

Figure 3.6 Effect of Asteraceae crude extracts (50 µg/mL) on THP-1 cell viability. Cells ($1x10^6$ cells/ mL) were plated and treated with extracts, vehicle control (DMSO) or 1 µM of staurosporine (positive control) and incubated for 24 h. Cell viability was measured using an MTS assay. Data is expressed as percentage of vehicle control, mean ± SEM. CO = pot marigold; AM = yarrow; HA = common sunflower; PO = mouse-ear hawkweed; SM = milk thistle; HR = common cat's ear; BP = common daisy; CJ = rush skeleton weed; MC = chamomile; PB = British yellowhead; IE = sword-leaved inula. N=3, Mean ± SEM. Statistical significance of the cells treated with extracts was compared to vehicle control and analysed by one-way ANOVA with a post-hoc Dunnett test. *=p<0.0332, **=p<0.0021, ***=p<0.0002, ****=p<0.0001.

The effect of LPS on TNF-α and IL-6 secretion and the use of the small NF-κB inhibitor, (E)-3-(4-methylphenylsulfonyl)-2-propenenitrile (BAY 11-7082), as a positive control was established. In these assays, previously optimised cell seeding density ($1x10^6$ cells/ mL) and incubation time point of LPS for 3 h (TNF-α) and 24 h (IL-6) were adopted from (di Gesso *et al.*, 2015). THP-1 cells were treated with 10µM BAY 11-7082 for 30 min prior to the addition of 10 ng/mL LPS for 3 h (for TNF-α) or 1 µg/mL of LPS for 24 h (for IL-6) after which, TNF-α and IL-6 secretion were measured in the media (**Figure 3.7.**). The results showed that cells treated with 10 ng/mL LPS secreted ~10 times more TNF-α compared to IL-6. Moreover, IL-6 secretion showed high day-to-day variability in terms of absolute concentration (pg/mL). Thus, values, normalised to vehicle control (DMSO) were used in all assays to minimise variation. BAY 11-7082 suppressed the secretion of both LPS-induced TNF-α and IL-6 significantly and was therefore used as a positive control for later experiments (**Figure 3.7.; Supplementary Table S3.4.**).

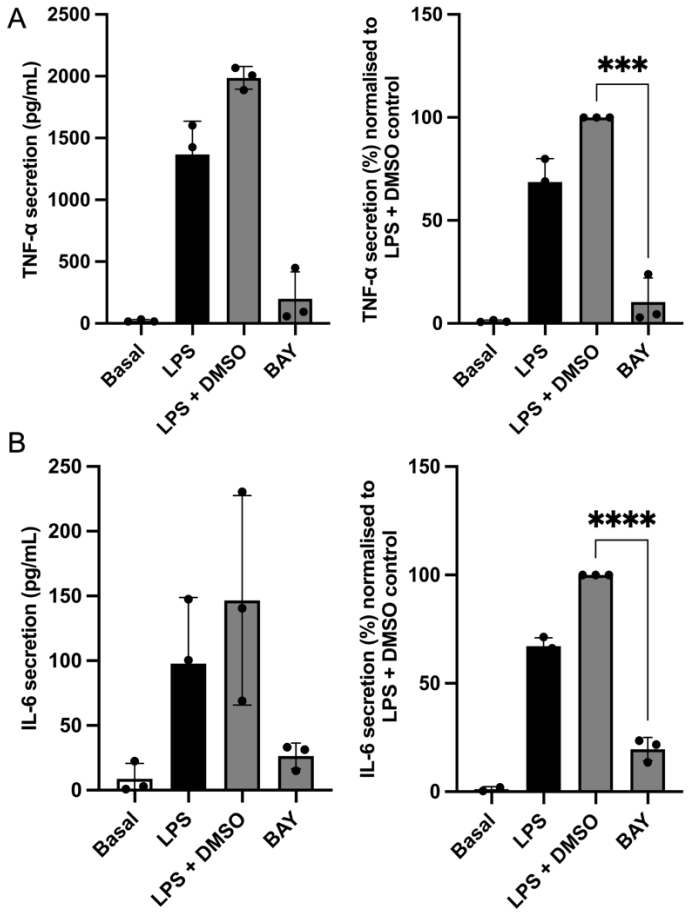

Figure 3.7 Effect of BAY 11-7082 (10 µM) on TNF-α (A) and IL-6 secretion (B) from LPS-stimulated THP-1 cells. 1x10^6 cells/ mL were incubated with vehicle control (DMSO) or 10µM BAY 11-7082 (BAY, positive control) for 30 min prior to LPS treatment for **(A)** 3 h (TNF-α) and **(B)** 24 h (IL-6). Cytokine release was measured by ELISA. Graphs show the concentration of secreted cytokine (pg/mL) (left panels) and as a percentage of vehicle control (LPS + DMSO) (right panels). N=3, Mean ± SEM. Statistical significance of the cells treated with BAY was compared to vehicle control and analysed by T-test. *=p<0.0332, **=p<0.0021, ***=p<0.0002, ****=p<0.0001.

The anti-inflammatory activity of selected extracts was quantified to confirm the previously reported activity of pot marigold extracts and compare its activity to extracts of other Asteraceae. For this purpose, floral extracts (50 µg/mL) were applied to THP-1 cells (1x10^6 cells/mL) 30 min prior to the addition of 10 ng/mL LPS for 3 h (for TNF-α) or 1 µg/mL of LPS for 24 h (for IL-6) after which the level of TNF-α and IL-6 in the supernatant was quantified. BAY 11-7082 was used as a positive control.

These experiments revealed that floral extracts of pot marigold reduced the release of TNF-α by 46%, compared to the vehicle control (DMSO). Interestingly, extracts of pot marigold had a stronger effect on the IL-6 pathway, inhibiting 56% of IL-6 secretion compared to the vehicle control (**Figure 3.8.; Supplementary Table S3.4.**). This assay also identified that extracts of British yellowhead had the strongest effect on both TNF-α and IL-6 cytokines, reducing secretion by 80% and 95%, respectively. Further, extracts of common daisy and chamomile showed anti-inflammatory potential through TNF-α suppression but had the

opposite effect on IL-6 secretion. Extracts of mouse-ear hawkweed also showed a pro-inflammatory effect, selectively stimulating the release of IL-6 but not TNF-α (**Figure 3.8.; Supplementary Table S3.4.**).

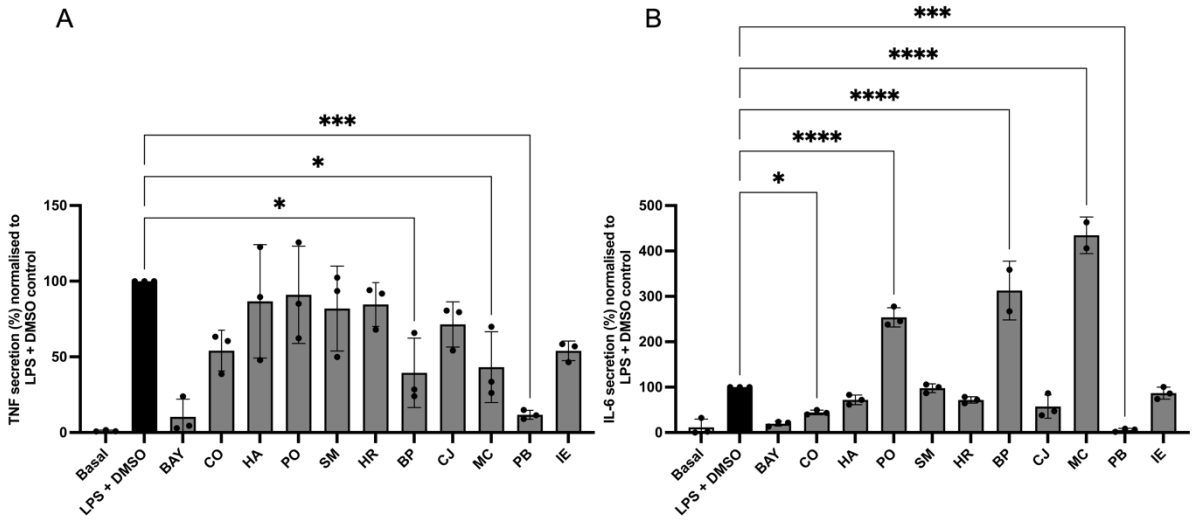

Figure 3.8 The effects of crude extracts of Asteraceae floral tissues on TNF-α and IL-6 secretion from LPS-stimulated THP-1 cells. 1x10^6 cells/ mL were incubated with DMSO (vehicle control), 10 µM BAY 11-7082 (BAY, positive control) or 50 µg/mL of extracts for 30 min prior to LPS treatment for **(A)** 3 h (TNF-α) and **(B)** 24 h (IL-6). Cytokine release was measured by ELISA. Graphs show the concentration of secreted cytokine (pg/mL) (left panels) and as a percentage of vehicle control (LPS + DMSO) (right panels). In both graphs, N=3, except for BP and CM (IL-6) N=2. Mean ± SEM. Statistical significance was analysed using one-way ANOVA with a post-hoc Dunnett test; *=p<0.0332, **=p<0.0021, ***=p<0.0002, ****=p<0.0001. CO = pot marigold; HA = common sunflower; PO = mouse-ear hawkweed; SM = milk thistle; HR = common cat's ear; BP = common daisy; CJ = rush skeleton weed; MC = chamomile; PB = British yellowhead; IE = sword-leaved inula.

3.4.1.4 Pot marigold triterpene content changes through flower development

The metabolic profile of pot marigold flowers was analysed through development to determine changes in metabolite content that might be linked to its anti-inflammatory activity. To do this, metabolites were extracted in ethyl acetate from three flowers at six development stages from the bud to the senescing flower and triterpene content was analysed using GC-MS (**Figure 3.9.**). To determine the concentration of metabolites 50 µg/mL of friedelin was added to extracts as an internal standard. Each compound was quantified as a proportion of the total ψ-taraxasterol based content.

The results showed that triterpene content changes through floral development (**Figure 3.9.**). At the first stage (S1 – bud), ψ-taraxasterol palmitate is the predominant compound comprising over 50 % of the total ψ-taraxasterol based triterpene content of ray tissues. However, this was observed to reduce through floral development, accounting for just ~2 % at stages S5 and S6. Ψ-taraxasterol stearate showed a similar accumulation pattern,

accumulating to 30 % at S1, but decreasing to ~5-10 % by S2/S3, and none was detected at later stages. At the same time, the proportion of faradiol myristate and palmitate increased through bud development from 0 % to 42 %, and 0% to 30%, respectively. Smaller increases from 0 % to 7 % and from 0 % to 3 % were observed for faradiol laurate and stearate, respectively. Finally, the availability of ψ-taraxasterol increased from 1 % at S1 to 8.5 % at S6, while faradiol content remained constant through development at around 0.5 % of total content.

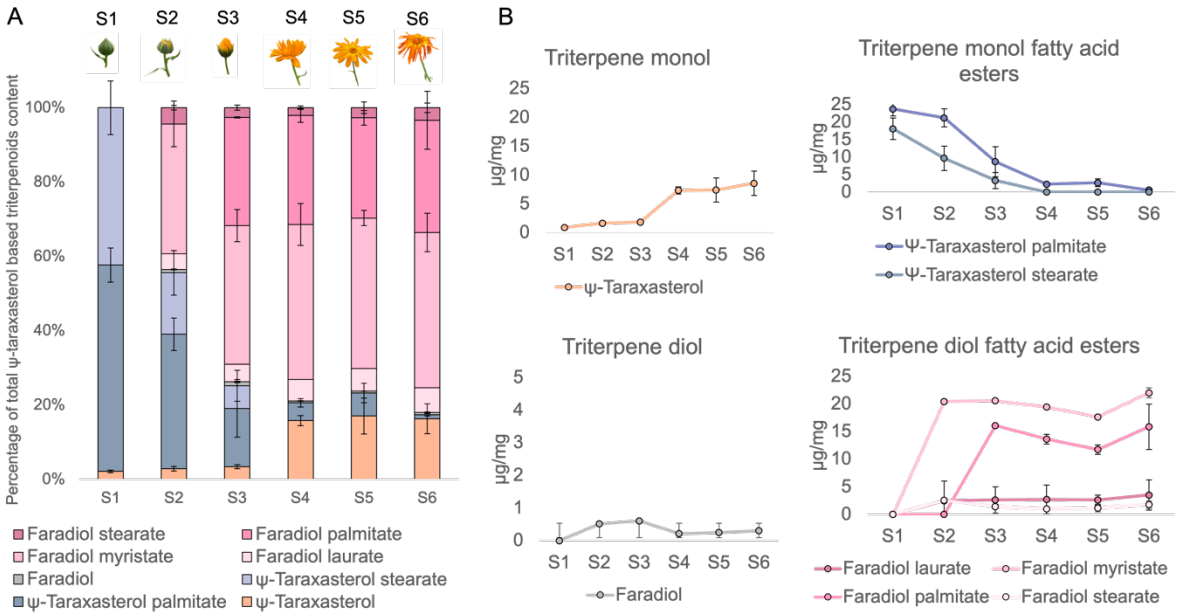

Figure 3.9 Triterpene content pot marigold ray tissues through floral development. Ethyl acetate extracts from six developmental stages of three individual flowers from different plants were analysed using GC-MS. To determine the concentration, the peak areas of eight target molecules were normalised to an internal standard (friedelin; 50 µg/mL). The quantity of each compound is shown as **(A)** a proportion of the total ψ-taraxasterol-based content and **(B)** as concentrations (µg/mg of dry weight). On the graphs, Mean ± SEM.

3.4.1.5 Anti-inflammatory activity of pot marigold does not change through floral development

To investigate if the observed differences in the content of faradiol FAEs between stages S1 and S6 of floral development **(Figure 3.10.)** correlate with anti-inflammatory activity, extracts from six developmental stages were compared in TNF-α and IL-6 ELISAs. As previously described, the viability of cells following the application of extracts (50 µg/mL) was verified, which confirmed that the concentration was suitable for use in anti-inflammatory assays (**Figure 3.10.; Supplementary Table S3.4.**). The results indicated that extracts from all stages were not cytotoxic to THP-1 cells.

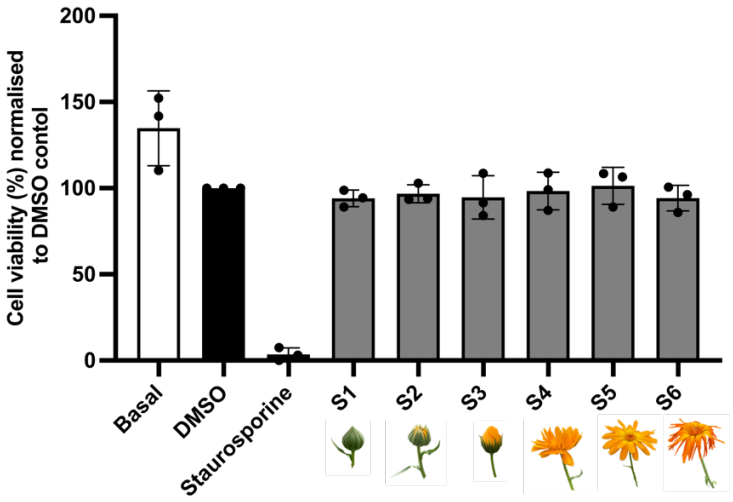

Figure 3.10 Effect of pot marigold extracts on THP-1 cell viability. Cells ($1x10^6$ cells/ mL) were plated and treated with extracts and vehicle control (DMSO) or 1 µM of staurosporine (positive control) and incubated for 24 h. Cell viability was measured by MTS assay. Values are expressed as a percentage of the vehicle control (DMSO). N=3, Mean ± SEM.

Next, floral extracts (50 µg/mL) from each development stage (S1-S6) were applied to THP-1 cells ($1x10^6$ cells/ mL) 30 min prior to the addition of 10 ng/mL LPS for 3 h (for TNF-α) or 1 µg/mL of LPS for 24 h (for IL-6), after which the levels of TNF-α and IL-6 in the supernatant were quantified. BAY 11-7082 was used as a positive control. This assay revealed no significant difference in the release of either TNF-α or IL-6 cytokines between different developmental stages (**Figure 3.11.; Supplementary Table S3.4.)**. Consistent with the initial results, pot marigold extracts had a greater effect on IL-6 than on TNF-α (**Figure 3.11.**).

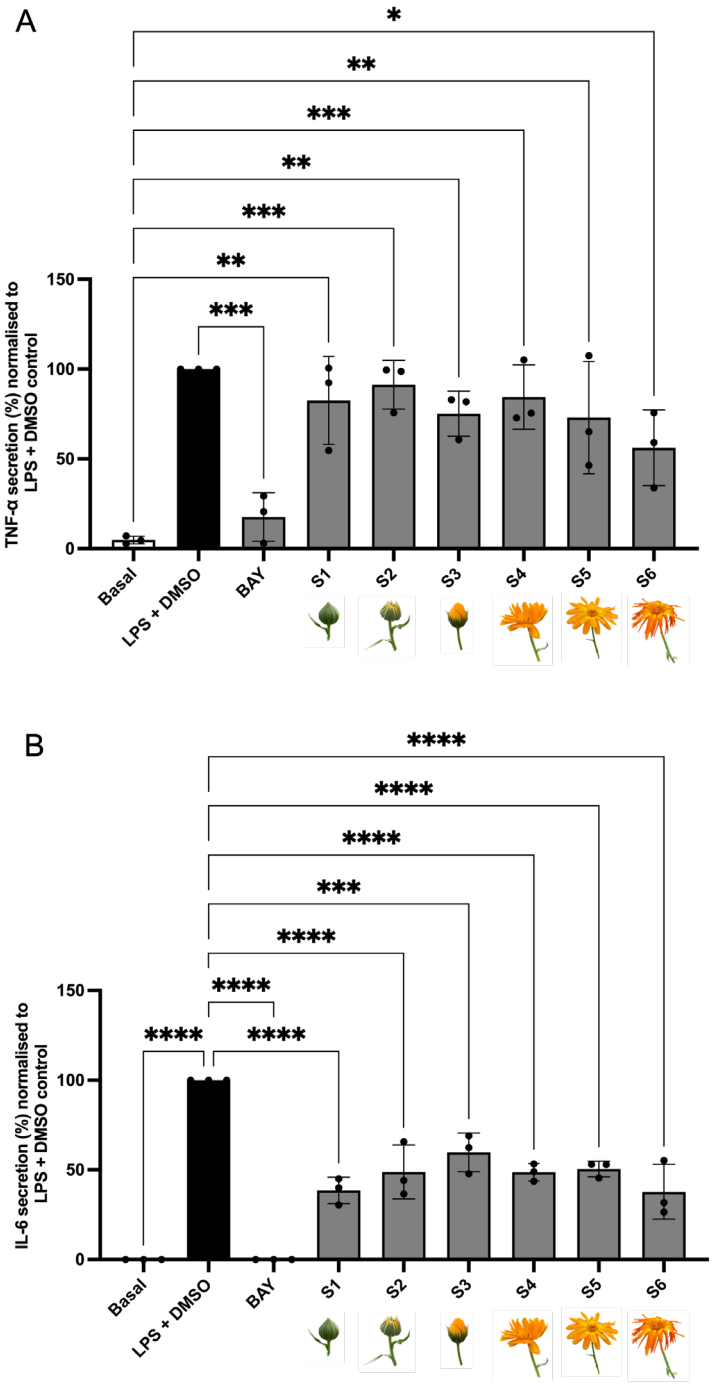

Figure 3.11 Effect of crude extracts from pot marigold flowers from six developmental stages on TNF-α and IL-6 secretion from LPS-stimulated THP-1 cells. 1x10^6 cells/ mL were incubated with the vehicle control (DMSO), 10 µM BAY 11-7082 (BAY, positive control) or 50 µg/mL of extracts for 30 min prior to LPS treatment for **(A)** 3 h (TNF-α) or **(B)** 24 h (IL-6). LPS concentration was 10 ng/mL for (A) TNF-α and 1 µg/mL for (B) IL-6 secretion. Secreted cytokines were quantified using ELISA and expressed as a percentage of vehicle control (LPS+DMSO) for (A) TNF-α and (B) IL-6. In both graphs, N=3, Mean ± SEM.

3.4.1.6 Pot marigold exhibit concentration-dependent anti-inflammatory activity

As it was determined that pot marigold extracts exhibit stronger activity through the IL-6 pathway than the TNF-α pathway (**Figure 3.8.** and **Figure 3.11.**), the next step was to investigate if suppression of IL-6 was concentration-dependent. To ensure concentrations of

compounds within the extract did not vary, all extracts were made from flowers at the S5 stage (open flower). Cell viability was checked at four concentrations 10 µg/mL, 25 µg/mL, 50 µg/mL and 100 µg/mL. Using 24 h MTS assays, it was confirmed that the extracts had a negligible effect on cell viability and could be used in ELISA (**Figure 3.12A.; Supplementary Table S3.4.**). Next, extracts were applied prior to the addition of 1 µg/mL of LPS for 24 h, after which the level of IL-6 in supernatants was quantified by ELISA. These experiments revealed that pot marigold extract has a concentration-dependent activity between 10 µg/mL and 100 µg/mL, significantly reducing IL-6 secretion at all tested concentrations (**Figure 3.12B.; Supplementary Table S3.4.**).

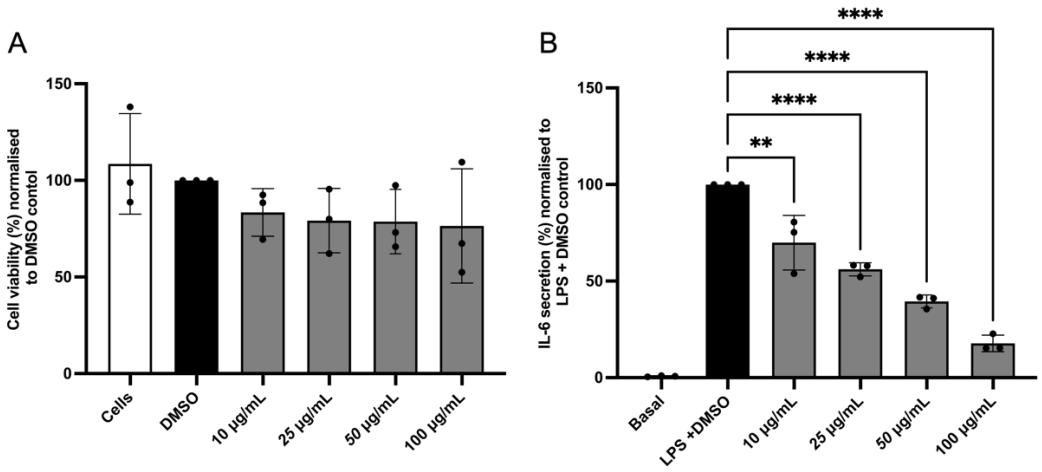

Figure 3.12 Effect of pot marigold extract on THP-1 cell viability and IL-6 secretion. (A) Cell viability was measured using an MTS assay. Cells ($1x10^6$ cells/ mL) were plated and treated with extracts and vehicle control (DMSO) and incubated for 24 h. Data is expressed as a percentage of vehicle control. **(B)** IL-6 was quantified using ELISA. Cells ($1x10^6$ cells/mL) were incubated with the vehicle control (DMSO) or 10 - 100 µg/mL of extracts for 30 min prior to LPS treatment for 24 h (IL-6). Values are expressed as a percentage of vehicle control (LPS+DMSO). Statistical significance to LPS+DMSO was analysed using one-way ANOVA with a post-hoc Dunnett test; *=p<0.0332, **=p<0.0021, ***=p<0.0002, ****=p<0.0001. In both graphs, N=3, Mean ± SEM.

3.4.2 Identification of candidate compounds

3.4.2.1 An optimised method for fractionation of pot marigold extracts

To investigate the contribution of triterpenes to the anti-inflammatory activity of pot marigold, extracts were fractionated using liquid chromatography (LC) to obtain seven fractions containing different classes of compounds. For this, a method developed in 2003 (Reznicek and Zitterl-Eglseer, 2003) was adapted for use on the liquid chromatography tandem mass spectrometer (LC-MS.MS) Shimadzu single-quad machine. Five gradient profiles were compared to identify the most suitable separation method (**Table 3.4.**).

Table 3.4 Five LC separation gradients for pot marigold fractionation. MeOH = methanol.

25%-100% MeOH		**50%-100% MeOH**		**75%-100% MeOH**		**85%-100% MeOH**		**90%-100% MeOH**	
Time (min)	% MeOH	Time (min)	% MeOH	Time (min)	% MeOH	Time (min)	% MeOH	Time (min)	% MeOH
0	25	0	25	0	50	0	50	0	90
2.5	25	1	50	2.5	75	2.5	85	2.5	90
20	100	20	100	20	100	20	100	20	100
22.5	100	22.5	100	22.5	100	22.5	100	22.5	100
22.5	25	22.5	50	22.5	50	22.5	50	22.5	90
28	25	28	50	28	50	28	50	28	90

The best gradient was 85-100 % methanol (MeOH) (**Table 3.4.**) as triterpene monols, triterpene FAEs and other compounds separated into different fractions (**Figure 3.13.**). Retention times were identified for lupeol (9.45 min); β-amyrin, α-amyrin, taraxasterol and ψ-taraxasterol (between 10.30 and 12.30 min); faradiol laureate (15.00 min; faradiol myristate (16.30 min), and faradiol palmitate (18.00 min) (**Figure 3.13.**).

For downstream analysis of bioactivity, three adjacent 600 µL fractions were pooled to make seven 1800 µL fractions (**Figure 3.13.**). Eight LC fractionation runs (14.4 mL), yielded the following masses: fraction 1 – 234 µg, fraction 2 – 253 µg, fraction 3 – 213 µg, fraction 4 – 325 µg, fraction 5 – 244 µg, fraction 6 – 593 µg, fraction 7 – 237 µg (**Figure 3.13.**).

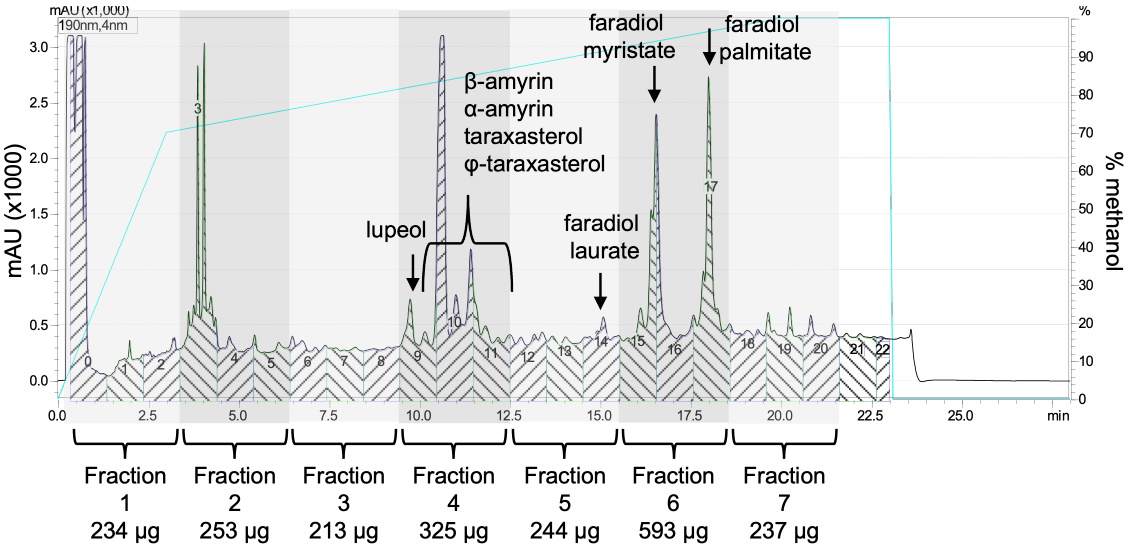

Figure 3.13 Semi-preparative uHPLC chromatograms of methanol extracts of pot marigold ray florets. The methanol gradient used for separation is shown as a cyan line. A total of 8 runs were performed and fractions were pooled into seven groups of three fractions and dried down for use in bioassays. The yield (µg) of each pooled fraction is shown below the x axis.

The content of the fractions was verified by GC-MS (**Figure 3.14.**). As expected, all triterpene monols were found in fraction 4, while faradiol myristate and faradiol palmitate were found in fraction 6. Faradiol laurate was found in fraction 5, in agreement with LC fractionation (**Figure 3.14.**). Fractions 1 and 2 predominantly contained fatty acids, mainly palmitic, stearic and arachidonic acids. In fractions 3 and 7, only small quantities of fatty acids were identified using GC-MS. A list of all compounds is provided in **Supplementary Table S3.2.**

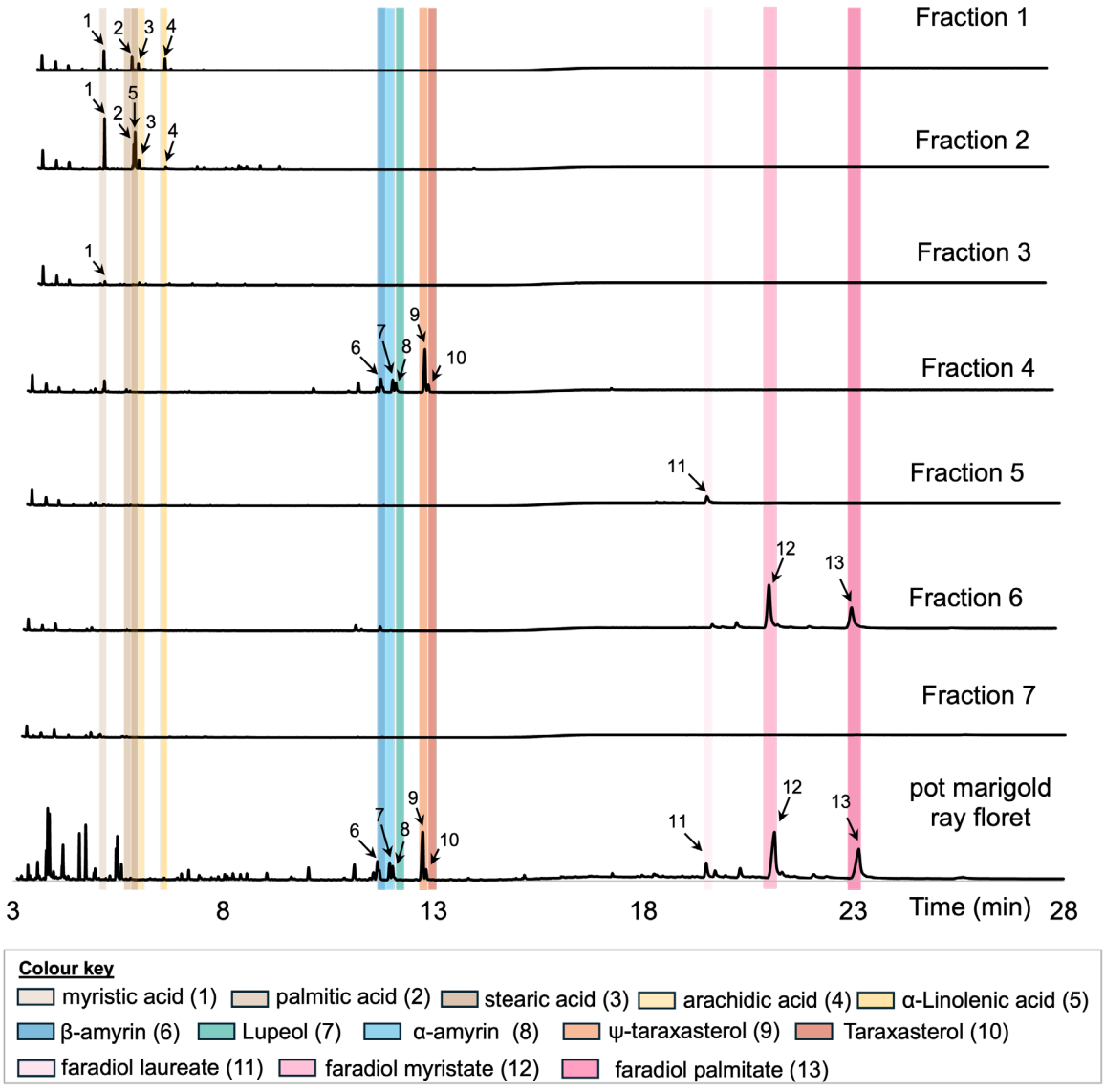

Figure 3.14 GC-MS analysis of pot marigold ray floret fractions. GC-MS chromatograms of TMS derivatised pooled fractions from the fractionation of extracts of pot marigold ray florets. Fatty acids were found in fractions 1 and 2 (yellow); triterpene monols in fraction 4 (peach) and triterpene fatty acid esters in fractions 5 and 6 (lilac). Compounds were identified by comparing retention times and mass fragmentation patterns with those of authentic standards.

3.4.2.2 Faradiol FAEs are major contributors to the anti-inflammatory activity of pot marigold

After obtaining fractions, anti-inflammatory assays were conducted using ELISA to investigate which fractions are major contributors to the anti-inflammatory activity of pot marigold floral extracts. Based on the yields of different fractions, it was estimated that faradiol FAEs represent ~ 28% of the total extract mass. Thus, to keep a similar concentration of faradiol FAEs as found in pot marigold extract (previously tested at 50 µg/mL) a concentration of 15 µg/mL was selected for Fraction 6. The concentration of all other fractions was normalised by volume to maintain an equal relative proportion as found in pot marigold extracts. The concentration of fractions 1 - 7 was therefore: Fraction 1 – 5.92 µg/mL, Fraction 2 – 6.4 µg/mL, Fraction 3 – 5.4 µg/mL, Fraction 4 – 8.22 µg/mL, Fraction 5 – 6.18 µg/mL, Fraction 6 – 15 µg/mL, Fraction 7 – 6 µg/mL.

As previously, a 24-hour cell viability assay was performed with $1x10^6$ cells/mL to confirm that these concentrates were suitable and non-toxic (**Figure 3.15A.; Supplementary Table S3.4.**). For the anti-inflammatory activity assays, fractions (concentrations detailed above) were applied to THP-1 cells prior to the addition of 1 µg/mL of LPS for 24 h after which the concentration of IL-6 in the supernatant was measured using ELISA. As previously, BAY 11-7082 was used as a positive control (**Figure 3.15B.**). The results of these experiments revealed that three fractions significantly reduced the release of IL-6: fraction 1, which predominately contained fatty acids; fraction 6, which contained faradiol myristate and faradiol palmitate; and fraction 7. Fraction 6 had the most significant effect, inhibiting 48% of IL-6 release, followed by fraction 7 with 46% inhibition and fraction 1 with 36% inhibition (**Figure 3.15B.; Supplementary Table S3.4.**).

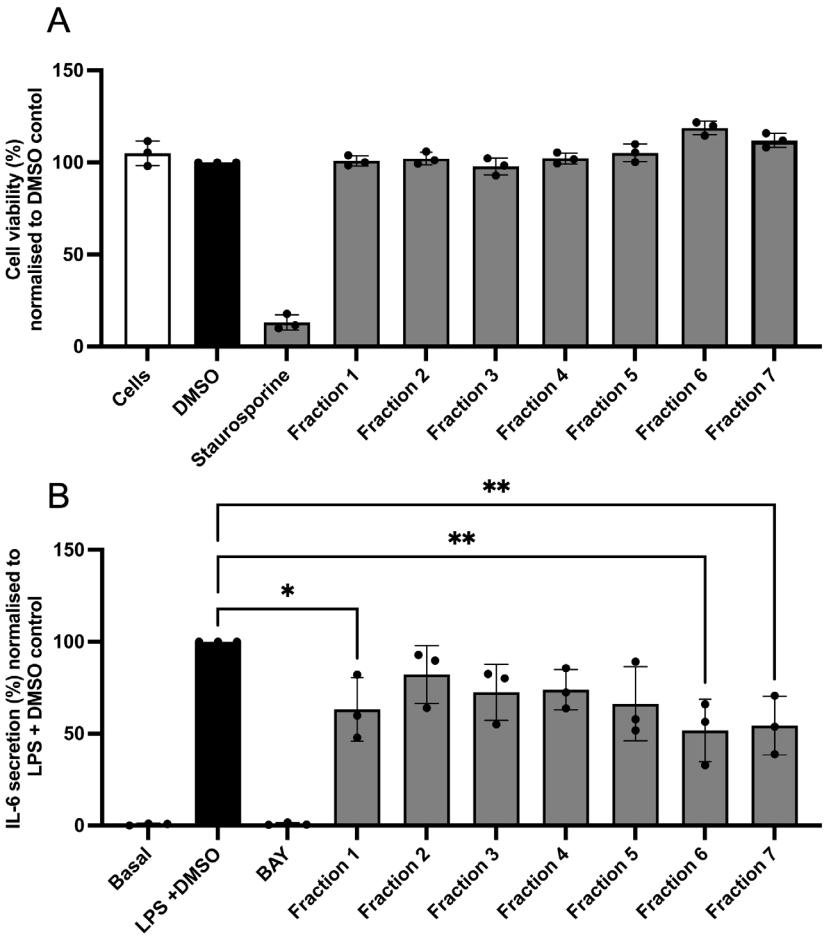

Figure 3.15 The effects of pot marigold fractions on cell viability and release of IL-6 in LPS-activated THP-1 cells. (A) Cell viability was measured using an MTS assay. Cells ($1x10^6$ cells/ mL) were plated and treated with extracts and vehicle control (DMSO), 1 µM of staurosporine (positive control) or fractions (concentration detailed above) and incubated for 24 h. Data is expressed as a percentage of LPS + vehicle control (DMSO). **(B)** IL-6 was quantified using ELISA. Cells ($1x10^6$ cells/mL) were incubated with DMSO, 10µM BAY 11-7082 (BAY, positive control) or fractions (concentration detailed above) for 30 min prior to LPS treatment for 24 h (IL-6). Values are expressed as a percentage of vehicle control (LPS+DMSO). Statistical significance to vehicle control was analysed using one-way ANOVA with a post-hoc Dunnett test; *=p<0.0332, **=p<0.0021, ***=p<0.0002, ****=p<0.0001. In both graphs, N=3, Mean ± SEM.

3.4.2.3 Purification of ψ-taraxasterol, faradiol myristate and faradiol palmitate

To investigate which structural features of faradiol FAEs might be important for anti-inflammatory activity, authentic standards of taraxasterol, faradiol and arnidiol were purchased and verified using GC-MS (**Supplementary Figure S3.1.**). As ψ-taraxasterol, faradiol myristate and faradiol palmitate could not be purchased, these were purified from pot marigold extracts. To do this, a previously reported LC method (Reznicek and Zitterl-Eglseer, 2003) was adapted for use on the LC-MS.MS Shimadzu single-quad machine and four gradient profiles were compared to identify the most suitable separation method (**Table 3.5.**).

Table 3.5 Five LC separation gradients were compared to assess their ability to separate triterpenes from pot marigold floral ray extracts. MeOH = methanol

92%-95% MeOH		93%-95% MeOH		90%-95% MeOH		90%-97% MeOH	
Time (min)	% MeOH	Time (min)	% MeOH	Time (min)	% MeOH	Time (min)	% MeOH
0	90	0	90	0	90	0	90
2.5	92	2.5	93	2.5	90	2.5	90
20	95	20	95	20	95	20	97
22.5	95	22.5	95	22.5	95	22.5	97
22.5	90	22.5	90	22.5	90	22.5	90
28	90	28	90	28	90	28	90

The most suitable gradient for isolation of ψ-taraxasterol, faradiol myristate and faradiol palmitate in the same run was found to be 90 - 97 % MeOH (**Figure 3.16.**). Retention times were identified for ψ-taraxasterol (5.15 min); faradiol myristate (between 12.00 min and 13.00 min), and faradiol palmitate (between 15.00 min and 16.00 min) (**Figure 3.16.**). Compounds were verified using GC-MS (**Supplementary Figure S3.1.**).

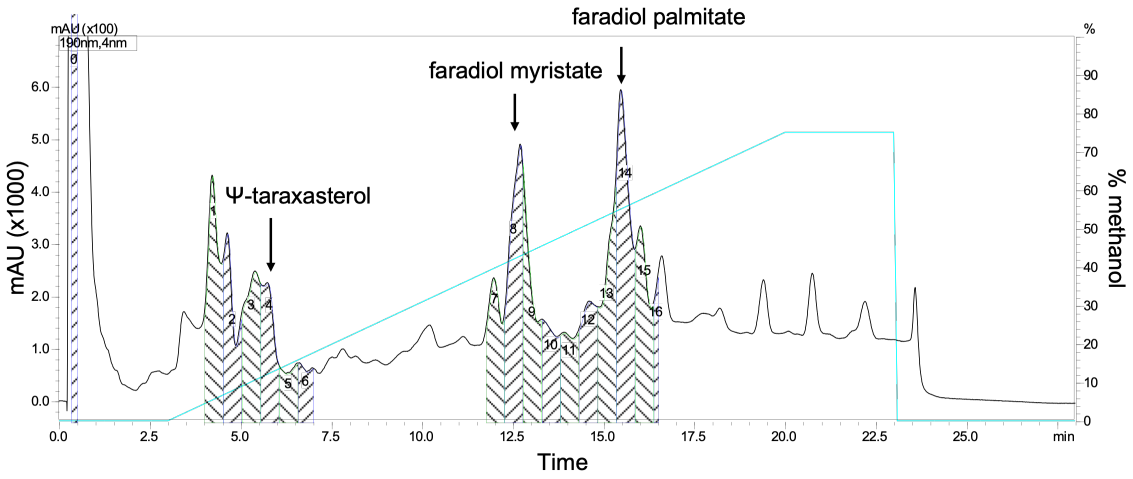

Figure 3.16 Representative semi-preparative uHPLC chromatogram of methanol extracts of pot marigold ray florets. Multiple runs were performed and fractions corresponding to compounds of interest were pooled and dried down for structural analysis by NMR. In this run, the following fractions were taken for the compounds of interest: ψ -taraxasterol (fraction 4); faradiol myristate (fractions 8 and 9); and faradiol palmitate (fraction 14).

One hundred LC runs yielded 850 µg ψ-taraxasterol, 2,000 µg faradiol myristate and 1,495 µg faradiol palmitate. It was found that the ψ-taraxasterol fraction contains a mixture of ψ-taraxasterol (62 %) and α-amyrin (19 %), while faradiol myristate and faradiol palmitate fractions are 96 % and 98 % pure, respectively (**Figure 3.17.**). The structure of faradiol palmitate was verified by NMR analysis by Dr. Sergey Nepogodiev (John Innes Centre).

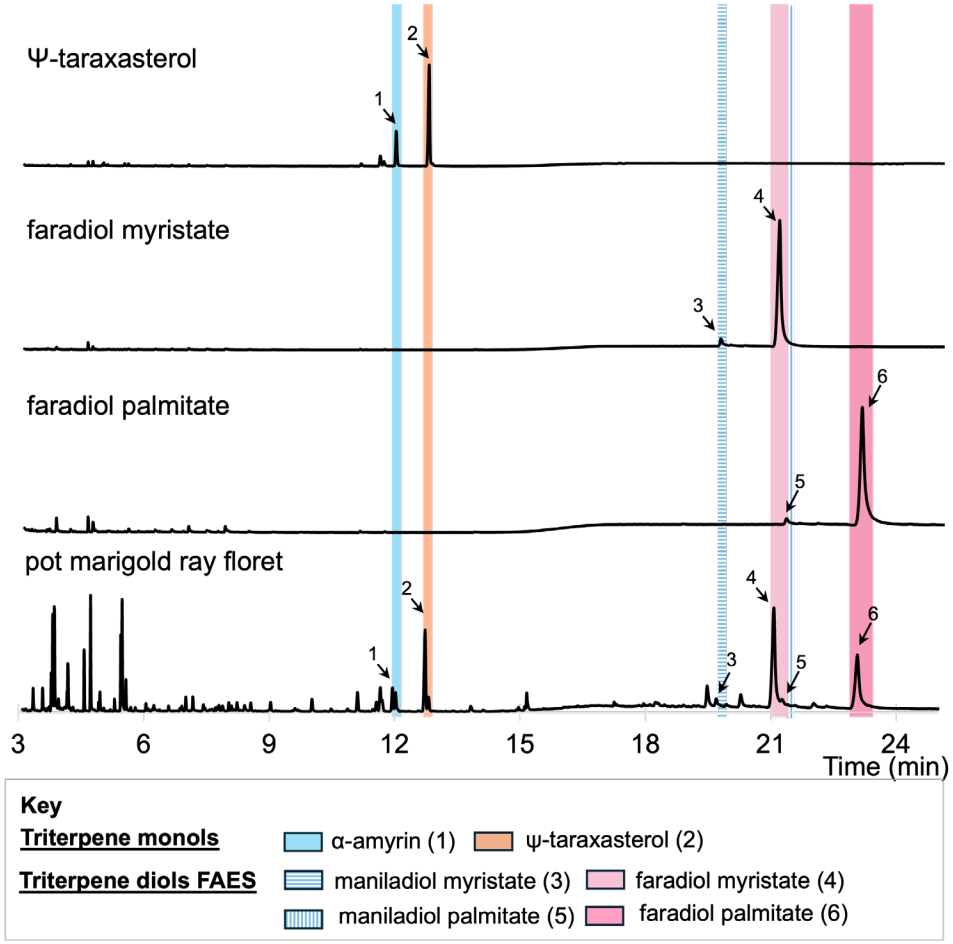

Figure 3.17 GC-MS analysis of compounds purified from pot marigold ray floret extract. GC-MS chromatograms of TMS derivatised pooled fractions from the LC purification of triterpene compounds from pot marigold ray floret extract.

3.4.2.4 C16 hydroxylated triterpenes exhibit the strongest anti-inflammatory activity

To identify which structural feature of faradiol FAEs might be important for anti-inflammatory activity, the activity of six triterpenoids (ψ-taraxasterol, taraxasterol, faradiol, arnidiol, faradiol myristate, faradiol palmitate and mixture of esters) was assessed by ELISA.

Again, a 24 h MTS proliferation assay was performed on $1x10^6$ cells/mL to confirm that 20 µM concentration is not toxic for THP-1 cells. The results indicated that all compounds tested had a negligible effect on the THP-1 cells viability at this concentration and can be used in further anti-inflammatory assays (**Figure 3.18A.**).

To perform anti-inflammatory assays, 20 µM triterpenoids were applied to THP-1 cells, followed by treatment with 1 µg/mL LPS. Cells were incubated for 24 h, and the secretion of IL-6 was quantified by ELISA. As previously, BAY 11-7082 was used as a positive control. Unexpectedly, taraxasterol showed strong pro-inflammatory activity, enhancing LPS-induced IL-6 secretion (**Figure 3.18B.; Supplementary Table S3.4.**). All other

compounds (ψ-taraxasterol, faradiol, arnidiol, faradiol myristate, faradiol palmitate and mixture of esters) displayed significant anti-inflammatory activity, reducing LPS-induced IL-6 secretion. The C:16 hydroxylated compounds (faradiol and arnidiol) showed the strongest anti-inflammatory activity, inhibiting IL-6 secretion by 59% and 61%, respectively. No synergistic effect was noted in cells treated with both faradiol myristate and faradiol palmitate (**Figure 3.18B.; Supplementary Table S3.4.**).

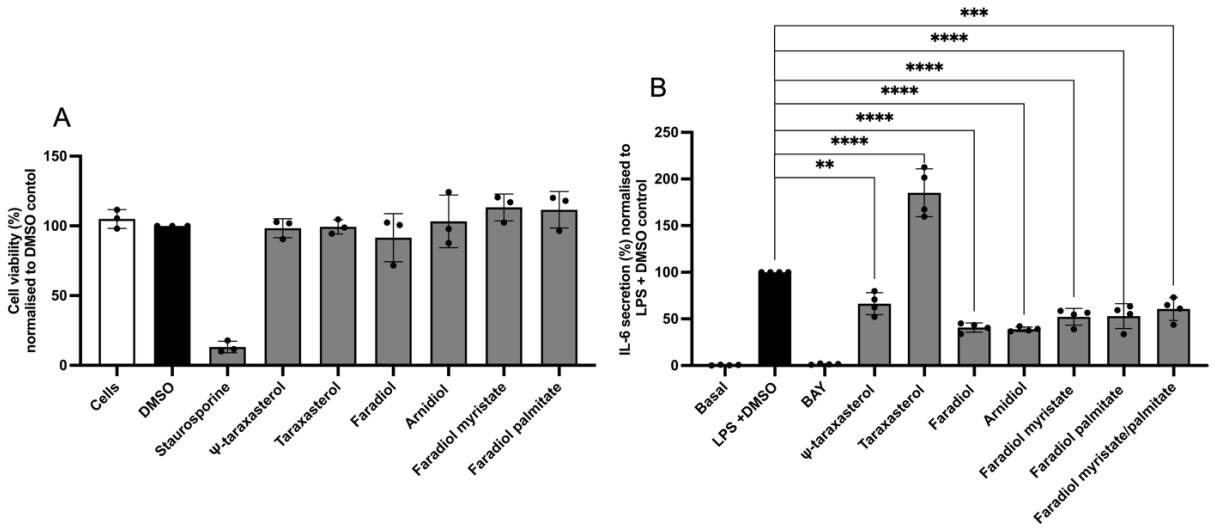

Figure 3.18 Effect of pure compounds on cell viability and IL-6 secretion from LPS-stimulated THP-1 cells. (A) Cell viability was measured using an MTS assay. Cells ($1x10^6$ cells/ mL) were plated and treated with extracts and vehicle control (DMSO), 1 µM of staurosporine (positive control) or 20 µM of target compounds and incubated for 24 h. Data is expressed as % vehicle control. N=3, Mean ± SEM. **(B)** IL-6 secretion was quantified using ELISA. Cells ($1x10^6$/mL) were incubated with the vehicle control, 10µM BAY (positive control) or 20 µM of target compounds for 30 min prior to the addition of LPS for 24 h (IL-6). Values are expressed as a percentage of vehicle control (LPS+DMSO). Statistical significance to LPS+DMSO was analysed using one-way ANOVA with a post-hoc Dunnett test; *=p<0.0332, **=p<0.0021, ***=p<0.0002, ****=p<0.0001. N=4, Mean ± SEM.

3.4.2.5 Faradiol exhibits concentration-dependent anti-inflammatory activity

As faradiol showed the most potent anti-inflammatory activity among ψ-taraxasterol derivatives, its activity through the IL-6 pathway was investigated for a 1 µM - 20 µM concentration range. To do this, cell viability at five concentrations 1 µM, 2.5 µM, 5 µM, 10 µM, and 20 µM was investigated in 24h MTS assays. It was confirmed that 1 µM - 20 µM faradiol has a negligible effect on cell viability (**Figure 3.19A.; Supplementary Table S3.4.**). However, high variability was noted at 20 µM.

Following this, the same extracts were tested in anti-inflammatory assays. Faradiol at 1 µM, 2.5 µM, 5 µM, 10 µM and 20 µM was applied prior to the addition of 1 µg/ml of LPS for 24 h, after which IL-6 secretion was measured in the media supernatants using ELISA. These

experiments revealed that faradiol shows concentration-dependent inhibition of the IL-6 pathway between 1 µM and 20 µM (**Figure 3.19B.; Supplementary Table S3.4.**). A significant reduction in IL-6 secretion was noted between 5 µM and 20 µM.

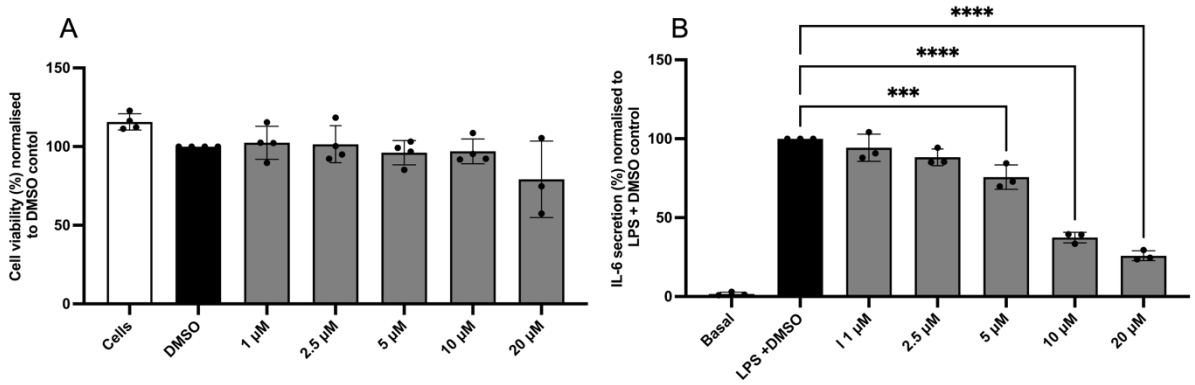

Figure 3.19 The effects of pot marigold fractions on THP-1 cell viability and IL-6 secretion. (A) Cell viability was measured using an MTS assay. Cells ($1x10^6$ cells/ mL) were plated and treated with extracts and vehicle control (DMSO), 1 µM of staurosporine (positive control) or 1 µM - 20 µM of faradiol and incubated for 24 h. Data is expressed as percentage of vehicle control (DMSO) N=4, Mean ± SEM. **(B)** IL-6 secretion was quantified using ELISA. Cells ($1x10^6$ cells/mL) were incubated with vehicle control (DMSO) or 1 µM - 20 µM of faradiol for 30 min prior to LPS (1 µg/mL) treatment for 24 h (IL-6). IL-6 release was measured by ELISA. Values are expressed as a percentage of vehicle control (LPS+DMSO). Significant IL-6 reduction compared to LPS+DMSO was analysed using one-way ANOVA with a post-hoc Dunnett test; *=p<0.0332, **=p<0.0021, ***=p<0.0002, ****=p<0.0001. N=3, Mean ± SEM.

3.4.3 Faradiol has a stronger effect on IL-6 release than the four triterpenes used in skincare

Faradiol showed strong anti-inflammatory activity in a wide range of concentrations (**Figure 3.19B.**). Thus, it was compared to triterpenes currently used in the pharmaceutical industry. Four triterpenes (betulin, betulinic acid, oleanolic acid and lupeol) were selected as ingredients of the FILSUVEZ topical wound-healing gel. All industry compounds were purchased from Merck (Darmstadt, Germany) and analysed by GC-MS (**Supplementary Figure S3.1.**).

As previously described, a 24 h MTS assay was performed with 20 µM of each compound. This showed that faradiol, lupeol, betulin, betulinic acid and oleanolic acid have a negligible effect on cell viability at 20 µM (**Figure 3.20A.; Supplementary Table S3.4.**). Next, 20 µM of each compound was applied to THP-1 cells, followed by the treatment with 1 µg/mL of LPS. Cells were incubated for 24 h and IL-6 release was measured by ELISA. As previously described, BAY 11-7082 was used as a positive control. No compounds except faradiol showed significant activity of IL-6 release (**Figure 3.20B.; Supplementary Table S3.4.**).

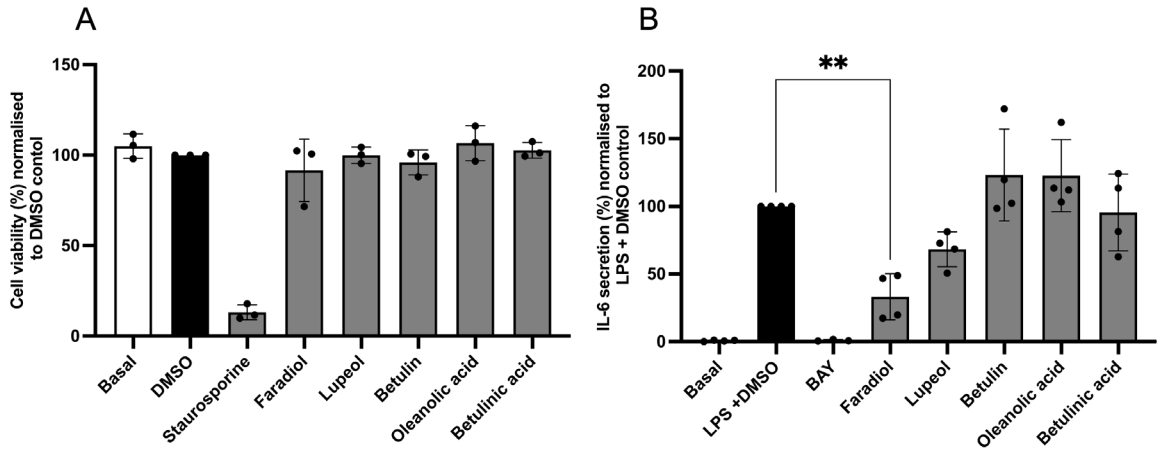

Figure 3.20 The effects of selected compounds on THP-1 cell viability and IL-6 secretion. (A) Cell viability was measured using an MTS assay. Cells ($1x10^6$ cells/ mL) were plated and treated with extracts, vehicle control (DMSO), 1 µM of staurosporine (positive control) or 20 µM of pure compounds and incubated for 24 h. Data is expressed as a percentage of vehicle control. N=3, Mean ± SEM. **(B)** IL-6 secretion was quantified using ELISA. Cells ($1x10^6$ cells/mL) were incubated with DMSO, 10µM BAY11-7082 (BAY, positive control) or 20 µM of pure compounds for 30 min prior to LPS (1 µg/mL) treatment for 24 h (IL-6). Values are expressed as a percentage of vehicle control (LPS+DMSO). N=4, Mean ± SEM. Significant IL-6 reduction compared to vehicle control (LPS+DMSO) was analysed using one-way ANOVA with a post-hoc Dunnett test; *=p<0.0332, **=p<0.0021, ***=p<0.0002, ****=p<0.0001.

3.4.4 Faradiol has an unusual mechanism of action

LPS is known to activate several pro-inflammatory pathways, including NF-κB, MAPK and JAK/STAT signalling pathways in THP-1 cells (**Figure 3.1.**). The production of IL-6 is regulated through the binding of phosphorylated transcription factors (NF-κB and STAT3) to the IL-6 promoter (Chang *et al.*, 2013). To investigate which pathway is primarily affected by faradiol and faradiol palmitate, the effect on phosphorylation of NF-κB and STAT3 was explored. To do this, 20 µM of faradiol or faradiol palmitate was applied to cells, followed by treatment with 1 µg/mL LPS for 2 h. Cells were lysed, and the total protein content was extracted and analysed by Western blot using antibodies to p-NF-κB/NF-κB or p-STAT3/STAT3.

Surprisingly, THP-1 cell treatment with 20 µM of faradiol affected phosphorylation of STAT3 but not p65 NF-κB, suggesting that faradiol influences the JAK2/STAT3 pathway without affecting phosphorylation of NF-κB (**Figure 3.21A.; Supplementary Table S3.4.**).Treatment with 20 µM of faradiol palmitate did not affect the phosphorylation of either STAT3 or NF-κB p65 (**Figure 3.21A.; Supplementary Table S3.4.**).

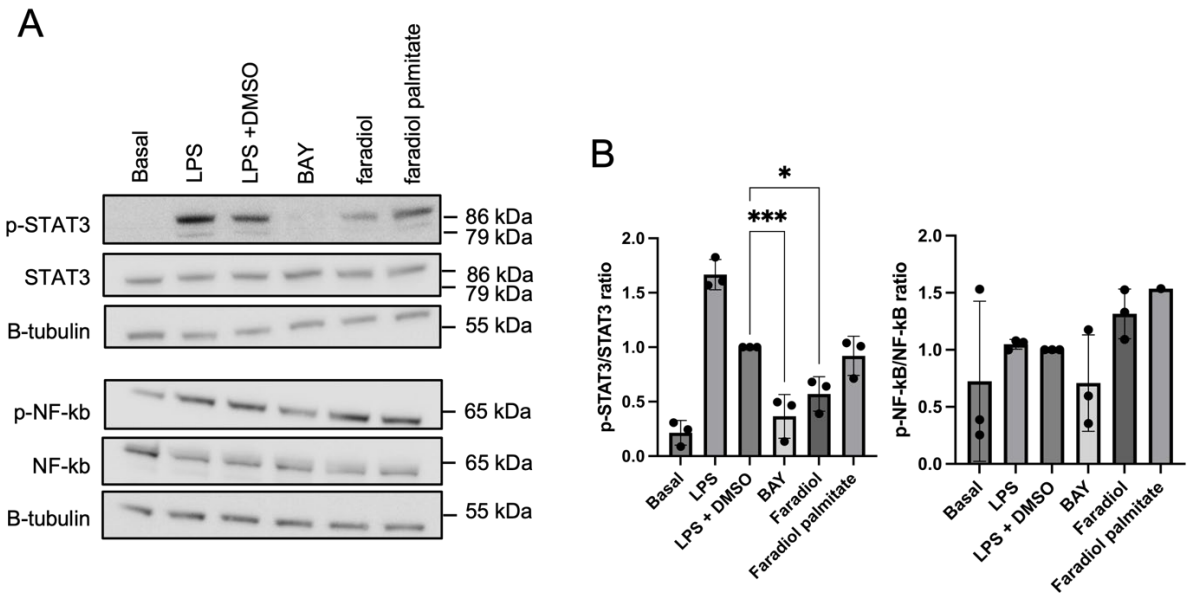

Figure 3.21 Effect of faradiol and faradiol palmitate (20 µM) on NF-κB and STAT3 signalling pathways in LPS-induced THP-1 cells. (A) Western blot analysis of cells treated with faradiol and faradiol palmitate (representative of 3 independent experiments). Cells ($1x10^6$ cells/mL) were incubated with vehicle control (DMSO), 10µM BAY 11-7082 (BAY), or 20 µM of pure compounds for 30 min before LPS (1 µg/mL) treatment for 2 h. Top panel: signal transducer and activator of transcription 3 (STAT3) was detected using primary antibodies against unphosphorylated and phosphorylated proteins: STAT3; and pSTAT3 (Tyr705). Bottom panel: nuclear factor NF-kappa-B p65 subunit (NF-κB p65) was detected using primary antibodies to unphosphorylated and phosphorylated protein: NF-κB p65; and p-NF-κB p65 (Ser536). Antibodies to β-Tubulin were used as a loading control. **(B)** Densitometry of protein detection levels normalised to tubulin control and relative fold change to vehicle control (LPS +DMSO), expressed as p-STAT3/ STAT3 ratio. The bands on each individual gel image were measured using gel analysis software in Fiji Just Image J (v2.14.0). The band density of proteins was normalised to the β-tubulin, and then the ratio of phospho/non-phospho protein expressions was calculated using Excel. N=3, Mean ± SEM. A significant difference to the vehicle control (LPS + DMSO) was analysed using one-way ANOVA with a post-hoc Dunnett test; *=p<0.0332, **=p<0.0021, ***=p<0.0002, ****=p<0.0001.

3.4.5 Selected triterpenes are not responsible for wound healing activity of pot marigold

Epithelial cell proliferation and migration into the wound is part of the second phase of the normal wound-healing process. Thus, the effect of pot marigold extracts, and the triterpenes found within those extracts, on proliferation and migration of human keratinocyte line - HaCaT was investigated. Proliferation was assessed using 24 h MTS assay, while the ability to contribute to the closure of a mechanically induced gap (wound) in the cells monolayer through stimulation of migration was assessed using would heling scratch assay (**Figure 3.2.**).

An MTS assay for HaCaT cells was seeded at $3.5x10^5$ cells/mL and incubated overnight at 37 °C; 5% CO_2 to allow the formation of monolayer (**methods 2.4.6.**). Cells were then treated with 12.5 µg/mL, 25 µg/mL and 50 µg/mL concentrations of pot marigold extracts,

or 20 µM of pure compound. This experiment showed that none of the tested compounds or extract concentrations could significantly increase HaCaT cells proliferation (**Figure 3.22.; Supplementary Table S3.4.**).

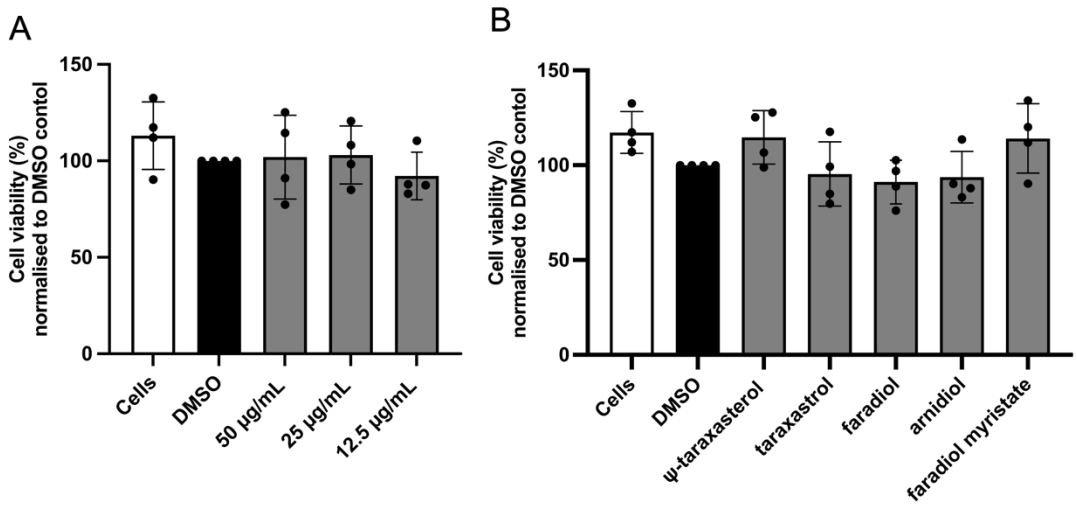

Figure 3.22 The effects of (A) pot marigold extract and (B) selected compounds on HaCaT cell proliferation. Cell proliferation was measured using an MTS assay. Cells ($3.5x10^5$ cells/ mL) were plated and treated with 12.5 µg/mL, 25 µg/mL and 50 µg/mL of pot marigold extracts, 20 µM of pure compounds or vehicle control (DMSO) for 24 h. Data is expressed as a percentage of vehicle control. N=4, Mean ± SEM.

Before testing extracts and pure compounds in the wound healing assay, the use of human epithelial growth factor (hEGF) as a positive control for wound closure was verified. To do this, HaCaT cells were seeded at $3.5x10^5$ cell/mL into culture inserts and incubated overnight at 37 °C; 5% CO_2. (**methods 2.4.6.**). The next day, a gap was generated by removing the cell culture insert, and the monolayer was treated with 5 µg/mL of mitomycin C for two h to inhibit cell proliferation (**methods 2.4.6.**) (**Figure 3.23.**). Standard media contains 10 % of fetal bovine serum (FBS), which has several growth factors such as insulin-like growth factor-1 (IGF-1), vascular endothelial growth factor (VEGF), FGF, and epidermal growth factor (EGF), which are needed for mammalian cell growth and proliferation (Mohamed *et al.*, 2020). Thus, standard media was replaced with FBS-free media to assess if extracts or pure compounds can influence HaCaT cell migration independently from proliferation. For the positive control, 50 ng/mL hEGF was applied for 24 h. The results showed a significant wound closer after 24 h with the addition of the hEGF, compared to untreated cell control. Thus, hEGF was used in the following assays (**Figure 3.23.; Supplementary Table S3.4.**).

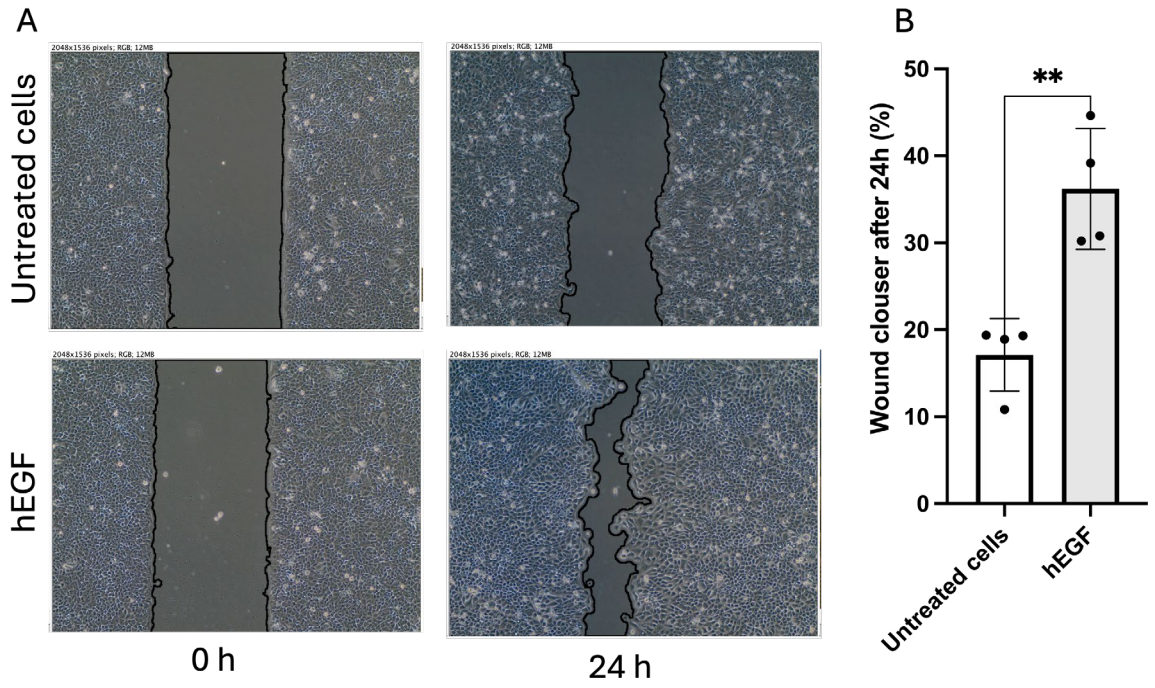

Figure 3.23 Effect of hEGF on wound closure in HaCaT cells. (A) Representative pictures of wound closure with or without hEGF. Cells ($3.5x10^5$ cell/mL) were seeded and left overnight. A HaCaT monolayer was treated with 5 µg/mL of mitomycin C for two h, and 10% FBS media was replaced with FBS-free media. Cells were treated with 50 ng/mL of human epithelial growth factor (hEGF) for 24 h. The top panels show untreated cells, and the lower panels show cells treated with hEGF. **(B)** Wound closure with or without hEGF. Each dot represents one of the four wounds created by cell insert removal. N=4, Mean ± SEM. Statistical significance was analysed using a student's T-test. *=p<0.0332, **=p<0.0021, ***=p<0.0002, ****=p<0.0001.

Once the wound healing assay was optimised, the wound-closure activity of pot marigold extracts and five triterpenes was investigated. A HaCaT monolayer was treated with 5 µg/mL of mitomycin C for two h. As previously described, standard media (10% FBS) was then replaced with FBS-free media. 12.5 µg/mL, 25 µg/mL and 50 µg/mL of extract, or 20 µM triterpenes was applied for 24 h. The results showed a significant wound closure after 24 h with the addition of 25 µg/mL of the extract compared to the vehicle control (DMSO) (**Figure 3.24.;Supplementary Table S3.4.**). However, no effect of wound healing was observed with cells treated with any of the triterpenes. Interestingly, arnidiol had a significant wound-opening effect, generating a bigger gap than vehicle control (DMSO).

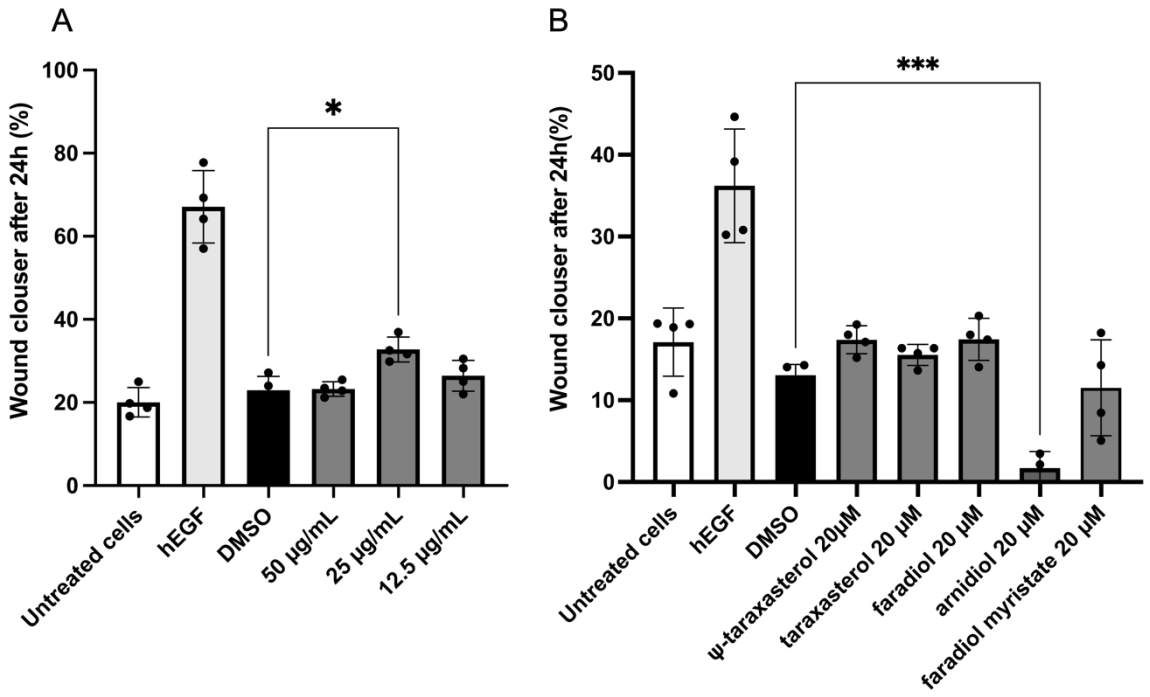

Figure 3.24 Effect of pot marigold extracts and triterpenes on wound closure in HaCaT cell monolayer after 24h. Cells ($3.5x10^5$cells/mL) were seeded and left overnight. The HaCaT monolayer was treated with 5 µg/mL of mitomycin C for two h and 10% FBS media was replaced with FBS-free media. Cells were treated with 50 ng/mL hEGF, vehicle control (DMSO), and **(A)** 12.5 µg/mL, 25 µg/mL and 50 µg/mL of pot marigold extracts, **(B)** 20 µM triterpenes for 24h. Wound closure was measured as a percentage of wound area after 24h (µM^2) divided by the initial wound area (µM^2). Mean ± SEM, N=3. Significant reduction in wound area compared to vehicle control (DMSO) was analysed using one-way ANOVA with a post-hoc Dunnett test. *=p<0.0332, **=p<0.0021, ***=p<0.0002, ****=p<0.0001.

3.5 Discussion

Pot marigold is a medicinal herb which has been used in traditional medicine for its wound healing and anti-inflammatory activities for many centuries (Macht, 1955). Faradiol fatty acid esters have previously been proposed to contribute to the anti-inflammatory activity of pot marigold extracts (Della Loggia *et al.*, 1994, Zitterl-Eglseer *et al.*, 1997). However, further research was needed to confirm the specific constituents responsible and to identify a molecular mechanism for this bioactivity.

3.5.1 Production of faradiol and faradiol FAEs is not restricted to a single subfamily

To determine if the use of pot marigold as a medicinal plant is justified, and to provide more evidence for the hypothesis that faradiol esters are responsible for this activity, the triterpene content and anti-inflammatory activity of pot marigold were compared to other Asteraceae.

These experiments revealed that faradiol derivatives are present in all tested species in the *Calendula* genus but also in four other Asteraceae (British yellowhead, sword-leaved inula, common sunflower, and rush skeleton weed) (**Figure 3.5.**). Interestingly, no unesterified C:16 hydroxylated triterpenes were detected in field marigold, *C. suffruticosa* and British yellowhead only, which might either indicate that faradiol is a reactive intermediate which is rapidly converted to faradiol FAEs. Alternatively, it might also indicate that enzymes that add C:16 hydroxyl on triterpenes have higher preference for esterified triterpenes over triterpene monols.

The presence of faradiol and faradiol palmitate in sword-leaved inula and common sunflower were previously reported (Trendafilova *et al.*, 2021, Yasukawa *et al.*, 1996). However, no previous studies have reported the production of these compounds in British yellowhead or rush skeleton weed. Sword-leaved inula and British yellowhead belong to the Inuleae tribe. Thus, other species in this tribe may also produce faradiol and its derivatives. Further, since it was confirmed that common sunflower produces both faradiol and maniladiol (a C16 hydroxylated β-amyrin), it might be worth conducting metabolite analysis of other maniladiol-producing Asteraceae. For example, *Euphorbia myrsinites* (myrtle spurge) and *Billardiera heterophylla* (bluebell creeper), could be analysed to determine if they produce ψ-taraxasterol, faradiol and its derivatives. Finally, surprisingly, rush skeleton weed, which belongs to the Cichorioideae sub-family, was also found to produce faradiol/faradiol FAEs, indicating that although faradiol is an uncommon triterpene diol, its production is not restricted to any individual Asteraceae subfamily or tribe. The ability to synthesise these compounds by distant plant lineages could be a result of convergent evolution through the independent development of biosynthetic enzymes, or selective maintenance of faradiol biosynthetic pathway in several plants due to similar environmental pressures (Ono and Murata, 2023). The genetic basis of faradiol production in pot marigold is investigated in Chapter 4.

One of the limitations of current experiment was the restricted number of tested tissues. Despite that faradiol and its derivatives have, to date, only been reported to accumulate in floral tissues, decorated compounds such as glucosides based on a structurally similar pentacyclic triterpene scaffold (β-amyrin) are found in the root and leaf tissues of pot marigold (Olennikov and Kashchenko, 2022). Thus, although ψ-taraxasterol-glycosides have never been reported, more detailed investigations of other pot marigold tissues, such as root and seed, may reveal the presence of new compounds.

Further, although ethyl acetate is suitable for extracting a broad range of non-polar to moderately polar triterpenes, this extraction could not give a full picture of present compounds. For instance, only faradiol monoesters were detected using this method, while faradiol diesters have been previously reported in floral tissues (Olennikov and Kashchenko, 2022). Thus, other solvents such as hexane and chloroform, suitable for extracting highly lipophilic triterpenes, or those containing sugars could complement compounds identification within the extracts.

In addition to investigating different tissues and using different solvents, the use of other techniques is also likely to reveal additional molecules. GC-MS only detects volatile or semi-volatile organic compounds (Cappelaro and Yariwake, 2015). However, pot marigold has also been reported to accumulate non-volatile triterpenes (Olennikov and Kashchenko, 2022), including faradiol diesters such as faradiol 3,16-dimyristate and -dipalmitate, as well as mixed diesters faradiol 3-myristate,16-palmitate and faradiol 3-palmitate,16-myristate (Nicolaus *et al.*, 2016). The presence of these compounds can be analysed using liquid chromatography. Thus, future experiments using LC–MSMS, followed by molecular network analysis would allow the alignment of experimental spectra against one another, connecting related molecules by their spectral similarity into molecular families, which could be compared across species (Nothias *et al.*, 2020). This approach would give a better picture of unique or unusual compounds present in the extracts of different species.

Further, a quantitative analysis could be valuable for comparing the abundance of the target compounds in the extracts. In the initial experiments described in this chapter, it was not possible to compare the abundance of target metabolites between extracts due to the lack of an internal standard and variation between experiments conducted on tissues harvested at different times.

3.5.2 Accumulation of faradiol FAEs in floral extracts does not correlate with anti-inflammatory activity

Interestingly, a direct correlation between the strength of anti-inflammatory activity and the accumulation of faradiol FAEs in Asteraceae was not found. Each species that accumulated faradiol FAEs displayed different levels of anti-inflammatory activity, ranging from low activity (common sunflower, rush skeleton weed and sword-leaved inula), moderate activity in the case of pot marigold, and high activity in the case of British yellowhead (**Figure 3.8.).** As observed in pot marigold fractionation experiments (**Figure 3.15.**), other compounds may

contribute to anti-inflammatory bioactivity. Fractionation of all faradiol-producing extracts might help to determine its contribution to the overall activity of the extracts, as well as the contribution of other compounds. Supporting this, previous studies have reported that other secondary metabolites present in the flowers of British yellowhead have anti-inflammatory activity. For example, the sesquiterpene lactone, ergolide, demonstrated suppression of NF-κB activation (Whan Han *et al.*, 2001). Further, inulanolides B and D also exhibited a potent inhibitory effect on the LPS-induced NF-κB activation and were shown to reduce TNF-α production in the RAW264.7 mouse macrophage cell line (Khan *et al.*, 2010). However, no studies have tested if the faradiol FAEs present in the floral extract of British yellowhead contribute to its activity. In future, an investigation of the compounds unique to British yellowhead extracts would be valuable.

3.5.3 Extracts from pot marigold and three other Asteraceae exhibit proliferative activity

Pot marigold extracts exhibited the strongest cell proliferative activity in THP-1. This result is consistent with the previous study that demonstrated that pot marigold stimulates the proliferation of mouse embryonic fibroblasts via the expression of growth factors - transforming growth factor beta 1 (TGFβ1) and fibroblast growth factor 2 (bFGF2) (Hormozi *et al.*, 2019). Extracts from common cat's ear, rush skeleton weed and sword-leaved inula also exhibited proliferative activity, with a slightly higher effect on THP-1 than on IL-6 (**Table 3.2.**), which has not been recorded before.

Although most studies are focused on the anti-proliferative activity of plant extracts and the identification of the potent anti-proliferative compounds that can be further developed into anti-cancer drugs, it has recently been demonstrated that the proliferative activity of plant extracts can be used in stem cell therapy and immune cell therapy (Li *et al.*, 2022a). For example, it was shown that a few plant extracts, such as *Foeniculum vulgare* (common fennel) (Mahmoudi *et al.*, 2013), *Malus pumila* (apple) (Lee *et al.*, 2016), *Tinospora cordifolia* (guduchi) and *Withania somnifera* (ashwagandha) (Sanap *et al.*, 2017) could significantly increase proliferation of the adult mesenchymal stem cells (MSCs) which are utilised in immune cell therapy for further differentiation into osteocytes, neurons, and angiogenesis. Thus, further studies could include testing the proliferative activity of common cat's ear, rush skeleton weed and sword-leaved inula extract on MSCs, as well as fractionation of these plant extracts to enable the identification of compound(s) responsible for this promising activity.

3.5.4 Three Asteraceae species exhibit moderate anti-proliferative activity

Extracts of three Asteraceae species (yarrow, common daisy and British yellowhead) showed moderate cytotoxicity on one or both cell lines and were investigated further to determine IC_{50} values (**Table 3.2.** and **Table 3.3.**). Extracts of yarrow flowers exhibited moderate cell growth inhibition. Previously, anti-proliferative activities of n-hexane, chloroform, aqueous-methanol and aqueous extracts of the aerial parts of yarrow were previously tested in three other human tumour cell lines (HeLa cervical cancer, MCF-7 breast cancer and A431 epidermoid carcinoma) in a similar anti-proliferative assay – 3-(4, 5-dimethylthiazolyl-2)-2, 5-diphenyltetrazolium bromide) MTT assay (Csupor-Löffler *et al.*, 2009). This study demonstrated that extracts, the flavonoids centaureidin and casticin, and the sesquiterpenoid paulitin, were highly effective against HeLa and MCF-7 cells and had moderate effect on A431 cells.

Similarly, ethyl acetate extracts of common daisy flowers were previously shown to have moderate levels of cytotoxic activity against human lung carcinoma cells (A549) and colon adenocarcinoma cells (DLD-1) cells, with similar IC_{50} values - 25 ± 8 µg/mL and 20 ± 4 µg/mL, respectively (Karakas *et al.*, 2017) that was determined in current study – 23.97 ± 2.52 µg/mL for HL-60 (**Table 3.3**). In addition, seven oleanane-type triterpene saponins isolated from a methanol extract of common daisy flowers, were also evaluated for their anti-proliferative activity against squamous carcinoma cells (HSC-2), tongue squamous cell carcinoma cells (HSC-4), and gastric adenocarcinoma cells (MKN-45) cells (Ninomiya *et al.*, 2016). This study identified that perennisaponin O has moderate to strong cytotoxicity (IC_{50} = 11.2 µM, 14.3 µM, and 6.9 µM, respectively).

Lastly, in comparison to sword-leaved inula which showed proliferative activity, British yellowhead, which belongs to the same Inuleae tribe, exhibited anti-proliferative activity. Previous research has focused on sesquiterpene lactones from the floral extracts of British yellowhead which were isolated and tested for cytotoxicity using human colon carcinoma cells (COLO 205), colorectal adenocarcinoma cells (HT-29), HL-60, and gastric epithelial adenocarcinoma cells (AGS) cancer cells (Bai *et al.*, 2006). Neobritannilactone B and acetyl neobritannilactone B were observed to be the most active although the IC_{50} values varied between 5 µM - 60 µM across cell lines. In the future, comparative metabolomics between sword-leaved inula and British yellowhead could be used to identify potent proliferative or anti-proliferative compounds. In addition, extracts identified in this chapter to have anti-

proliferative activity could be screened against other cancer cell lines, and fractionation experiments could be conducted to identify molecules responsible for anti-proliferative activity.

3.5.5 Changes in metabolite content through floral development do not affect anti-inflammatory activity

Experiments to quantify triterpene FAEs during pot marigold flower development revealed patterns in metabolite content (**Figure 3.9.**). The most noticeable change was a gradual reduction of ψ-taraxasterol FAEs and a gradual increase of faradiol FAEs through bud development, while triterpene monol and diol content remained almost constant. The changes in content over time are expected as many metabolites are involved in flower induction, floral organ development and growth (Chakraborty *et al.*, 2022). For example, a recent study conducted to identify metabolite changes in edible flowers of *Magnolia kobus* (mokryeon) at different developmental stages revealed that phenolic and flavonoid contents were most abundant in the buds and decreased with ageing (Choi *et al.*, 2024).

Changes in metabolite content can be associated with changes in the bioactivity (Yang *et al.*, 2018). However, while the metabolite content of pot marigold changed during flower development, no significant difference in either TNF-α or IL-6 cytokine release between the six developmental stages was found. This might be an indication of similar levels of activity of ψ-taraxasterol FAEs and faradiol FAEs. As only faradiol esters were tested for their anti-inflammatory (**Figure 3.18.**) in this study, further analysis will be needed to compare it to monol FAEs. Alternatively, this might also indicate that either the major contributor to this activity remains unchanged, which is consistent with diol content being relatively unchanged through development, or that multiple compounds contribute to the overall activity of the extract, which the fractionation studies also support (**Figure 3.15.**)

3.5.6 Fractions containing faradiol FAEs exhibit the strongest anti-inflammatory activity

Ethyl acetate extracts of pot marigold flowers reduced the levels of TNF-α and IL-6 cytokines. This is consistent with a previous study in which the effects of pot marigold extract on IL-1β, IL-6 and TNF-α in the blood serum of LPS-induced animals was investigated (Preethi *et al.*, 2009). All screened cytokines were significantly reduced in animals treated with 50 mg/mg, 100 mg/mg and 200 mg/mg of pot marigold extract for six

days. In that study, the effect on the TNF-α release was slightly stronger than on IL-6, with about 80 % and 68 % cytokine reduction, respectively, at the top concentration. Whereases in this study, a slightly stronger effect on IL-6 secretion than on TNF-α secretion was observed (**Figure 3.8.** and **Figure 3.11.**). This difference might occur due to the difference in the experimental conditions, where the (Preethi *et al.*, 2009) study was conducted on an animal model while our study was performed *in vitro*.

Subsequent fractionation of pot marigold extracts identified three fractions with significant anti-inflammatory activity (**Figure 3.15.**). One fraction, containing faradiol myristate and faradiol palmitate, displayed the highest anti-inflammatory activity and inhibited 48 % of IL-6 release. This is consistent with the previous research in which fractions containing faradiol FAEs were found to affect NF-κB-driven transcription using a luciferase reporter assay in which AGS cells transiently transfected with a plasmid-containing promoter with NF-κB binding sites driving a reporter. This is not a direct readout of anti-inflammatory activity, and the work described in this chapter represents an advance as it quantifies the release of IL-6 cytokines.

A second fraction significantly exhibiting anti-inflammatory activity predominantly contained myristic, palmitic, stearic and arachidonic acids (**Figure 3.25.**). Arachidonic acid, a major component of Fraction 1, has been previously found to inhibit the LPS-induced inflammatory response in THP-1 cells by downregulation of IL-6 and IL-1β in a concentration-dependent manner (Hung *et al.*, 2023). Also, the other study demonstrated that myristic acid significantly inhibits the LPS-induced inflammatory response in microglial cells (BV-2) through the NF-κB pathway (Huang *et al.*, 2023). In contrast, multiple studies have shown that palmitic acid has a pro-inflammatory effect through the activation of the NF-κB pathway and subsequent release of IL-1β and TNF-α cytokines (Korbecki and Bajdak-Rusinek, 2019). Finally, stearic acid was also reported to stimulate THP-1 cells to secrete all three major pro-inflammatory cytokines (TNF-α, IL-1β, and IL-6) (Hung *et al.*, 2023).

The two notable (by GC-MS) differences between Fraction 2 compared to Fraction 1, were the reduction of arachidonic acid and the additional presence of α-linolenic acid in Fraction 2 (**Figure 3.25.**), which might explain the stronger anti-inflammatory activity of Fraction 1. Although previous research has shown that α-linolenic acid, like arachidonic acid, has a concentration-dependent anti-inflammatory response in THP-1 cells through inhibition of IL-6 release, the same study demonstrated that arachidonic acid is slightly more potent

(Hung *et al.*, 2023). Thus, further studies will be needed to determine if arachidonic and α-linolenic acids are key anti-inflammatory compounds, and how the proportion of different fatty acids affects monocyte inflammatory response.

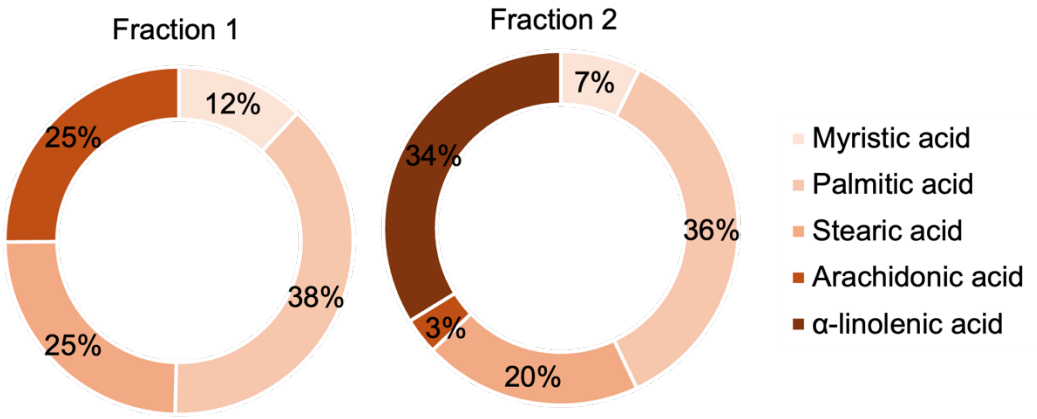

Figure 3.25 Fatty acids identified in Fraction 1 and Fraction 2. Proportions are the peak area of each compound divided by the peak area of all compounds.

Finally, Fraction 7 also exhibited anti-inflammatory activity (**Figure 3.15.**). Due to time constraints, I was unable to investigate this. Previous studies have identified loliolide, fucoside acetates of β-eudesmol and viridiflorol (Colombo *et al.*, 2015), and oleanane-type triterpene glycosides (Ukiya *et al.*, 2006) are present in pot marigold extracts and may have anti-inflammatory activity. Thus, further investigations are required.

3.5.7 C16 hydroxylation is a key structural feature important for the anti-inflammatory activity of faradiol and its FAEs

A comparison of the anti-inflammatory activity of purified triterpenoids identified faradiol and arnidiol as the most potent compounds, highlighting the importance of C:16 hydroxylation for enhancing anti-inflammatory activity (**Figure 3.18.**). This finding is consistent with previous studies, which reported that more-polar compounds such as faradiol and arnidiol exhibit stronger *in vivo* anti-oedematous activity than less-polar primary triterpene monols (ψ-taraxasterol and taraxasterol), and their FAEs (Neukirch *et al.*, 2005, Zitterl-Eglseer *et al.*, 1997) (**Figure 3.3.**).

A comparison between faradiol, the most potent compound in the faradiol FAEs pathway, and other triterpenes which compile a part of wound-healing gel (lupeol, betulin, oleanolic acid, betulinic acid) showed that only faradiol exhibited significant activity through the IL-6 pathway (**Figure 3.20.**). Among the tested compounds, lupeol was previously shown to

decrease the generation of pro-inflammatory cytokines (TNFα) and IL-1β in LPS-stimulated macrophages at a wide range of concentrations (10–100 μM) (Fernández *et al.*, 2001). Similarly, oleanolic acid was shown to decrease the release of TNF-α via NF-κB pathway in primary endothelial cells (Yang *et al.*, 2012) and TNF-α mRNA expression in RAW264.7 macrophages (Li *et al.*, 2021a). In the future, it will be important to compare the effect of faradiol and other triterpenes on other cytokines, including TNFα and IL-1β in THP-1, to determine the level of specificity. Further, betulin and betulinic acid have been shown to inhibit IL-6 secretion in murine monocyte/macrophage cells (P388D1) (Szlasa *et al.*, 2023), which indicates that the response seen in our studies might be cell-specific. Future studies should, therefore, be performed in a few different cell lines to investigate this effect.

Consistent with previous research, both faradiol myristate and faradiol palmitate showed significant anti-inflammatory activity (**Figure 3.18.**). With their high abundance and activity, it can now be concluded that these compounds are major contributors to the activity of the whole extract, as previously proposed (Della Loggia *et al.*, 1994). No synergistic effect was noted between faradiol myristate and faradiol palmitate, also reported previously (Zitterl-Eglseer *et al.*, 1997). Esterification of hydroxyl, amino acid, or carboxylic acid-containing drug molecules can increase their lipophilicity, improving intestinal drug permeability (Chen *et al.*, 2022). Esterification is, therefore, a widely applied chemical modification for drug uptake and absorption and an emerging method to improve the uptake and absorption of bioactive compounds. Further studies could include cell permeability research with esterified or non-esterified faradiol to investigate how these compounds are transported into immune cells and whether esterification is important for their bioavailability.

Finally, an unexpected difference between ψ-taraxasterol and taraxasterol was found at 20 μM (**Figure 3.18.**), with the former being anti-inflammatory and the latter pro-inflammatory. Since taraxasterol has previously been shown to have anti-inflammatory activity through inhibition of TNF-α, IL-1β and IL-6 production in LPS-induced RAW264.7 cells (Piao *et al.*, 2015), we hypothesised that taraxasterol might have an unusual U-shape IL-6 activity that has been previously reported for other natural products such as monounsaturated and polyunsaturated fatty acids (Huang *et al.*, 2023). Future concentration-activity studies are needed to confirm or reject this hypothesis.

3.5.8 Faradiol inhibits IL-6 release by preventing STAT3 phosphorylation

The investigation of the mechanism by which faradiol regulates IL-6 production in LPS-stimulated monocytes revealed inhibition of STAT3 phosphorylation without affecting NF-κB p65 (**Figure 3.21.**). While chromatin immunoprecipitation (ChIP) results have shown that both recognition sites (STAT3 and NF-κB p65) are present on the IL-6 promoter (Chang *et al.*, 2013), our result suggests that faradiol can selectively prevent IL-6 release by preventing STAT3 phosphorylation and binding to IL-6 promoter. This finding complements the recent discovery of independent regulation of the JAK2/STAT3 pathway by lncRNA brain and reproductive organ-expressed protein (BRE) antisense RNA 1 (BRE-AS1) in LPS-stimulated THP-1 cells (Shin *et al.*, 2024). In this study, the authors showed that specific knockdown of BRE-AS1 via siRNA transfection enhances LPS-induced expression of IL-6 and IL-1β, without affecting TNF-α, confirming independent regulation of NF-κB and JAK/STAT3 pathways in LPS-induced THP-1 cells. At the time of writing, faradiol is the first natural compound that has been shown to suppress IL-6 production by inhibiting JAK2/STAT3 pathway. Further, more work is needed to understand which part of the JAK2/STAT3 pathway is affected and which structural features of faradiol are important for this activity. To do this, the phosphorylation profile of JAK2 after faradiol treatment should be investigated.

Further, although we did not not detect inhibition of NF-κB p65 phosphorylation, previous work reported that faradiol and faradiol palmitate affects NF-κB-driven transcription (Colombo *et al.*, 2015). Thus, these compounds may be active though multiple inflation pathways, and more work is needed to clarify which part of the LPS signalling pathway leading to NF-κB-driven transcription is influenced by faradiol and its derivatives, and to what extent the effect on the NF-κB pathway seen in previous work is cell-specific.

3.5.9 Selected triterpenes are not responsible for pot marigold wound healing activity

Re-epithelisation is a complex process that involves the coordinated work of two cell types -fibroblasts and keratinocytes. A few *in vivo* studies continuedly demonstrated the strong wound healing activity of pot marigold extracts (Givol *et al.*, 2019). However, to date, compounds that can significantly influence re-epithelisation and tissue remodelling stages of the wound-healing process have not been identified.

In this research, the effect of pot marigold and selected triterpenes on keratinocyte proliferation and migration was investigated. Thes experiments revealed a slight effect on the cell migration (wound closure) after 24h following the addition of 25 µg/ml of pot marigold extract (**Figure 3.24.**). However, no effect was observed with the triterpenoids (**Figure 3.24.**). Also, no effect was observed with the extracts or triterpenoids for HaCaT cell proliferation (**Figure 3.22.)**This is broadly consistent with a previous study in which the migration of keratinocytes during new tissue formation was marginally influenced by α-amyrin, β-amyrin, lupeol and taraxasterol acetate derived from pot marigold extract (Nicolaus *et al.*, 2017). Thus, further studies are needed to determine if the combination of individual triterpenes or other components of pot marigold extract can stimulate keratinocyte migration and proliferation.

Moreover, investigating the proliferation and migration of fibroblasts may help to determine if pot marigold and our target compounds have a stronger stimulation effect on fibroblasts than on keratinocytes. A study differentiating between cell proliferation and cell migration using mitomycin C demonstrated that pot marigold extracts (10 µg/ml) stimulated the proliferation and migration of Swiss 3T3 albino mouse fibroblasts (Fronza *et al.*, 2009). This work further showed that the effect is mainly due to the stimulation of migration rather than proliferation. Further, faradiol myristate and palmitate enhanced fibroblast stimulation although, as the effect was small, the authors concluded that faradiol FAEs contribute only partially to the wound healing effects of pot marigold extract (Fronza *et al.*, 2009).

In addition, it was previously shown that ethanolic extracts of pot marigold inhibited the activity of collagenase and enhanced the amount of collagen in the supernatant of fibroblasts (Nicolaus *et al.*, 2017). Thus, the impact of faradiol and its derivatives on the collagen content could also be investigated.

Finally, although the majority of wound healing studies that investigate the effect of natural products *in vitro* look into anti-inflammatory and re-epithelisation stages (Criollo-Mendoza *et al.*, 2023), the tissue remodelling phase could also be investigated. One recent study demonstrated that myricetin-3-*O*-β-rhamnoside and chlorogenic acid, two main phenolic compounds found in *Parrotia persica* (Persian ironwood) extracts, are effective in wound repair and scar remodelling due to their ability to stimulate capillary-like tube formation (Moghadam *et al.*, 2017).

3.6 Conclusion

In this Chapter, the anti-inflammatory activity of pot marigold was investigated. First, the prevalence of faradiol FAEs, which were proposed to be responsible for this activity, revealed that these are rare compounds, but their presence is not restricted to specific Asteraceae sub-family. Ethyl acetate extracts of pot marigold were shown to repress the release of TNF-α and IL-6 cytokines with a stronger effect on IL-6. Subsequent fractionation of pot marigold extracts revealed that faradiol FAEs are major contributors to anti-inflammatory activity via the IL-6 pathway. Analysis of the activity of specific compounds present in these extracts identified that the polar triterpene diols are the most potent, highlighting the importance of C:16 hydroxylation for anti-inflammatory activity. Further investigation of the mechanism of action revealed that faradiol regulates IL-6 production in LPS-stimulated monocytes in an unusual mechanism in which phosphorylation of STAT3 is inhibited without affecting phosphorylation of NF-κB. Finally, wound-healing activity confirmed the ability of pot marigold extract to stimulate keratinocyte migration, but selected triterpenes were not responsible for this effect. This research provides a base for further investigation of the mechanism of action of faradiol and the potential development of novel, clinically useful anti-inflammatory and wound-healing agents.

Chapter 4 - Elucidation and reconstruction of the faradiol palmitate biosynthetic pathway

In Chapter 3, faradiol fatty acid esters (FAEs) were identified as major contributors to the anti-inflammatory activity of pot marigold. This chapter describes an investigation into the genetic basis of these compounds, elucidating their biosynthetic pathways to enable production in heterologous hosts.

4.1 Introduction

Triterpene FAEs are found in many Asteraceae species, including in species of *Chrysanthemum, Inula, Pulicaria, Calendula,* and *Centaurea* genera (Abdallah *et al.*, 2019, Ayaz *et al.*, 2017, Khan *et al.*, 2010, Ukiya *et al.*, 2001). The most common are based on unmodified triterpene scaffolds such as β-amyrin, α-amyrin and lupeol with long-chain fatty acids (C ≥ 6) (Liu *et al.*, 2024a). The predominant site of acylation in triterpene esters is C3, with almost 70 % of all triterpene FAEs acylated at this position. However, multiple acylation sites can also occur on the same triterpene scaffold, with fatty acids found at other positions (C16, C21, C28 and C29) (Liu *et al.*, 2024a).

The most abundant TFAEs found in *Calendula* species are esters of faradiol (**Figure 4.1.**). Arnidiol, α-amyrin, lupeol, β-amyrin, ψ-taraxasterol and taraxasterol FAEs (**Figure 4.1.**), can also be found, but in smaller amounts (Niżyński *et al.*, 2015). In this genus, laureate (C12), myristate (C14) and palmitate (C16) are most frequently found at the C3 position of both triterpene monols and diols.

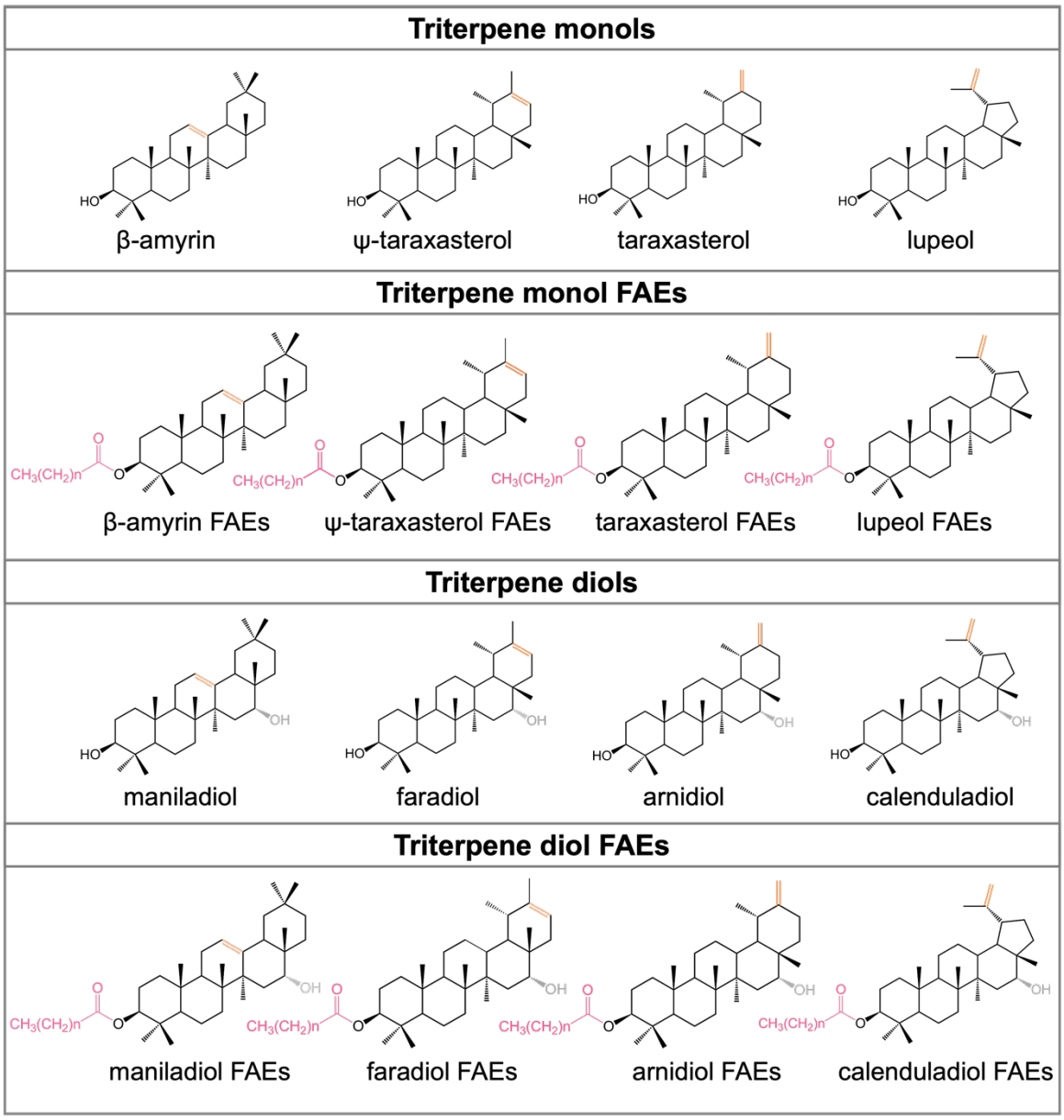

Figure 4.1 Chemical structure of pot marigold pentacyclic triterpenes and their C16 hydroxylated and C3 acylated derivatives.

Most triterpene scaffolds are biosynthesised from 2,3-oxidosqualene by OSCs. These scaffolds are then decorated by enzymes of different classes to produce a large diversity of triterpenoids. Faradiol FAEs consist of a ψ-taraxasterol scaffold with two modifications: C16 hydroxylation and C3 esterification. To date, it is unknown which modification, hydroxylation or esterification, takes place first.

Previous research in Patron lab identified an enzyme from pot marigold that produces the triterpene scaffold, ψ-taraxasterol, from which faradiol and its FAEs are derived. This chapter describes the identification of C16 CYPs that can hydroxylate ψ-taraxasterol to make faradiol, and C3 fatty acid acyl transferases (ACTs) that make faradiol FAEs.

To date, more than 170 plant CYPs that modify triterpenes have been characterised (Ghosh, 2017b, Miettinen *et al.*, 2017a, Wang *et al.*, 2021a). Among them are three pentacyclic triterpene C16β-hydroxylases: AsCYP51H10 from *Avena strigosa* (black oat), a member of the CYP51H subfamily, which appears to be restricted to monocots (Ghosh, 2017b), AcCYP716A111 from *Aquilegia coerulea* (Rocky Mountain columbine) and PgCYP716A141 from *Platycodon grandifloras* (Chinese bellflower), which belong to the CYP716 family considered the main contributor to the diversification of eudicot triterpenoid biosynthesis (Miettinen *et al.*, 2017a). It has been suggested that many eudicot CYPs in the CYP716 family evolved to catalyse the production of defence compounds (Miettinen *et al.*, 2017a).

Interestingly, both AsCYP51H10 and PgCYP716A141 have additional C12-C13β-epoxidase and C28 oxidase functions, respectively. Further, AcCYP716A111, AsCYP51H10 and PgCYP716A141 have been reported to act on the same triterpene scaffold, β-amyrin. However, substrate promiscuity is commonly observed for CYPs and the reported data is often limited by the number and the range of compounds tested in the studies (Hansen *et al.*, 2021). This flexibility of substrate acceptance is believed to promote the retention of duplicated genes and their evolution into new functional roles, enabling the acquisition of novel biochemical reactions (Hansen *et al.*, 2021). Although promiscuity contributes to the breadth of specialised metabolites found in plants, non-specific enzymes may be less desirable for metabolic engineering, particularly when only one specific product is of value. Thus, it is desirable to identify residues important for substrate specificity, as these can be used to inform engineering strategies to reduce promiscuity.

The acyltransferase enzyme family is not well-characterised. To date, only one C3 fatty acid triterpene acyltransferase capable of catalysing the addition of FAEs onto a triterpene scaffold has been identified and characterised. This is AtTHAA3 acyl transferase, which was identified in Arabidopsis and adds C10, C12 and C14 fatty acid groups to thalianol, a tricyclic triterpene (Huang *et al.*, 2019).

Overall, the biological function of triterpene FAEs is poorly understood. However, thalianol FAEs were shown to have a role in modulating microorganisms in the rhizosphere (Huang *et al.*, 2019), and other triterpene FAEs have been shown to have roles in plant defence (Huang *et al.*, 2019, Liu *et al.*, 2024a). For example, avenacin, a glycosylated triterpene ester, exhibits anti-fungal activity in *Avena strigose* (lopsided oat) (Nützmann *et al.*, 2016),

and acylated derivatives of boswellic acid protect against pests and pathogens in *Boswellia serrata* (Indian frankincense) (Kumar *et al.*, 2021).

Methyl jasmonate (MeJA) is known to be a significant activator of defence mechanisms in response to pathogens or wounding, as well as response to abiotic conditions such as low/high temperature or drought (Cheong and Do Choi, 2003, Wang *et al.*, 2021d). Further, inducible defence responses in plants can be activated through the exogenous application of MeJA. This approach has been widely used to study gene expression and corresponding defence metabolite accumulation in many plants (Morcillo *et al.*, 2022, Wang *et al.*, 2021d, Yang *et al.*, 2022, Yi *et al.*, 2016). In this chapter, the regulation of pathway genes in response to MeJA is investigated.

Prior to the experiments described in this thesis, Dr. Melissa Salmon, a postdoctoral researcher in the Patron group, performed GC-MS analysis on extracts of leaf, disc and ray tissues of pot marigold **(Figure 3.4)**. This analysis confirmed that ψ-taraxasterol and its derivatives, including faradiol fatty acid esters, are only found in the floral tissues. It also identified the presence of smaller quantities of other C16 hydroxylated triterpene FAEs (**Figure 4.1.**). Further, prior to the start of my project, the genome and transcriptome from leaf, ray and disc tissues of pot marigold were sequenced and assembled by Dr. David Swarbreck group (core bioinformatic group) at Earlham Institute. In addition, the transcriptomes of leaf, ray and disc tissues of field marigold were also sequenced. Dr. Salmon has mined these datasets to identify pot marigold *OSCs* expressed in floral tissues. Heterologous expression in *N. benthamiana* identified a multifunctional enzyme in pot marigold that produced ψ-taraxasterol as the major product with smaller quantities of taraxasterol, lupeol and β-amyrin. The pot marigold gene was named *Ψ-TARAXASTEROL SYNTHASE* (*CoTXSS*). In this chapter, I utilise the same datasets and approach to identify and characterise CYPs and ACTs able to modify ψ-taraxasterol/faradiol as Dr. Salmon used for identification of *CoTXSS*. I also use CoTXSS in heterologous expression in *N. benthamiana* to characterise candidate CYPs and ACTs.

4.2 Aims

The aims of this chapter are to:

- Identify pot marigold C16 CYPs that hydroxylate ψ-taraxasterol
- Investigate the substrate specificity of these C16 CYPs

- Identify pot marigold C3 fatty acid acyltransferases that modify faradiol/ψ-taraxasterol
- Investigate the expression profiles of pathway genes to determine if they are co-regulated and upregulated by defence hormone MeJA

4.3 Contributions by other scientists

All experiments described in this chapter were done by me except that Dr. Melissa Salmon previously extracted RNA from (i) flowers at six developmental stages, from the bud to open flower; (ii) flowers and leaves 0h, 6h and 24h after application of 100 μM MeJA. In addition, Dr. Connor Tansley characterised four additional ACTs (CoACT4-CoACT7) and quantified metabolites produced by CoACT1-CoAC7.

4.4 Results

4.4.1 Identification of candidate ψ-taraxasterol C16 hydroxylases

4.4.1.1 Nine candidate members of the CYP716A family were identified in pot marigold

Due to its mono-functionality as a C16 hydroxylase, AsCYP716A111 was used as a query to identify candidate genes in the pot marigold genome and field marigold transcriptome (**methods 2.5.1.**). This identified nine candidate genes encoding CYPs from the pot marigold genome and nine from the field marigold transcriptome. The translated protein sequences were aligned with 68 uncharacterised candidate CYPs mined from publicly available genomes, and 171 previously characterised CYPs (Ghosh, 2017b, Miettinen *et al.*, 2017a, Wang *et al.*, 2021a).

The CYP alignment was trimmed and used to reconstruct a maximum likelihood phylogenetic tree (**methods 2.5.1.**) in which CYPs grouped predominantly by substrate specificity (**Figure 4.2.**). All nine candidate CoCYPs resolved in a clade with members of the CYP716A family, containing CYPs known to modify pentacyclic triterpene scaffolds, including α-amyrin, β-amyrin and lupeol. These included the C16 hydroxylases, AsCYP716A111 and PgCYP716A141 (**Figure 4.2.** and **Figure 4.6.**).

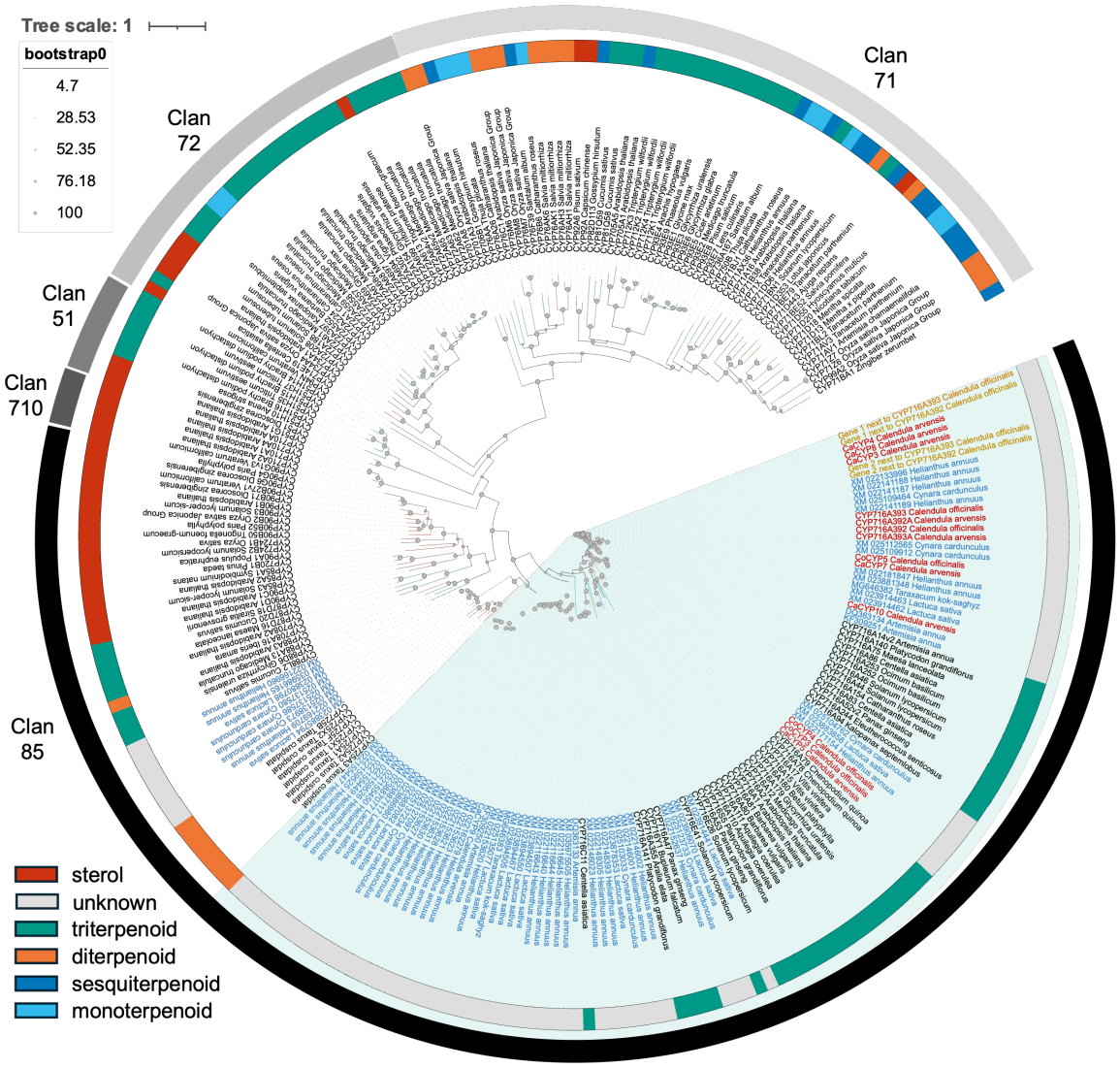

Figure 4.2 Maximum-likelihood tree of plant cytochrome p450s (CYPs). A maximum likelihood tree was constructed in IQ-Tree using the LG+F+I+G4 matrix-based model and visualised using Interactive Tree of Life (iTOL) v6. Substrate specificity is shown in the inner ring; CYPs clans are shown in the outer ring, CYP716 family triterpenoid modifying clade is highlighted in light teal. Filled grey circles indicate bootstrap supports for each node. The scale bar represents the number of substitutions per site. Functionally characterised taxa are shown in black. CYPs sequences mined from the publicly available genomes of Asteraceae, pot marigold genome and transcriptome datasets, and field marigold transcriptome, are shown in blue. Genes found next to the *CoCYP716A392* and *CoCYP716A393* in the genome are shown in yellow. Pot marigold and field marigold candidate C16 ψ-taraxasterol hydroxylases are shown in red.

Sequences corresponding to five out of nine candidates were identified in the pot marigold transcriptome data. Using previously generated differential gene expression data, I found two candidate genes (*CoCYP1* and *CoCYP5*) that were highly expressed (>10,000 normalised counts) in at least one tissue. *CoCYP1* and *CoCYP2* were predominantly expressed in ray tissues, while *CoCYP5* was mainly expressed in leaves (**Figure 4.3.**). The expression patterns of *CoCYP1-CoCYP4* were consistent with previous metabolic profiling analyses, in which faradiol and faradiol FAEs were found to predominantly accumulate in the ray florets, with low levels in the disc and florets, and none in the leaves. The candidate genes were named *CoCYP1 (CoCYP716A392), CoCYP2 (CoCYP716A393), CoCYP3*

(CoCYP716A429), CoCYP4 (CoCYP716A430) and *CoCYP5 (CoCYP716A431),* with official nomenclature provided by Professor David Nelson.

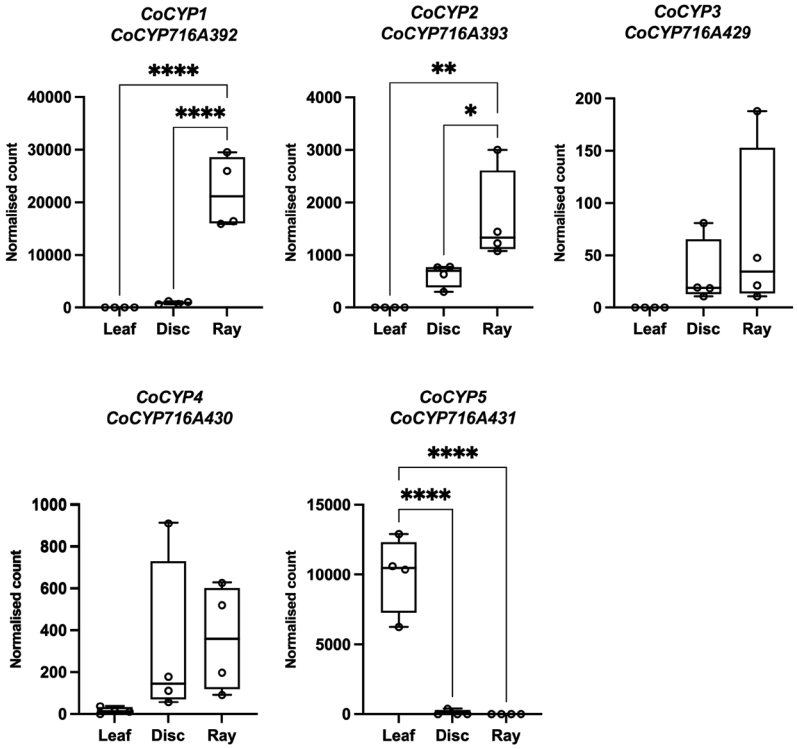

Figure 4.3 Differential expression of pot marigold candidate *CoCYPs* genes in leaf, disc and ray floret tissues. Gene expression for each tissue is displayed in a box plot as normalised counts with the centre line of the boxplot denoting the median, the box denotes the 25th to 75th percentiles of the data and the whiskers show the minimum and maximum of the data. Significant difference in normalised transcript count was analysed using one-way ANOVA with a post-hoc Tukey's test; *=p<0.0332, **=p<0.0021, ***=p<0.0002, ****=p<0.0001.

4.4.1.2 Pot marigold *CoCYP716A392* and *CoCYP716A393* encode ψ-taraxasterol C16 hydroxylases

To investigate if the enzymes encoded by these genes were able to hydroxylate taraxasterol, ψ-taraxasterol or lupeol at the C16 position, the coding sequences were synthesised and cloned into a MoClo Level l acceptor plasmid (pICH47742; **methods 2.6.1.**) between the strong constitutive promoter CaMV35s and a terminator. After sequence confirmation, plasmids were transformed into *Agrobacterium tumefaciens* GV3101 before agroinfiltration of *N. benthamiana* leaves (**methods 2.6.7.**). Each strain was co-infiltrated with strains carrying similar plasmids constitutively overexpressing CoTXSS and a truncated version of the rate-limiting enzyme HMG-CoA reductase 1 (tHMGR) to enhance the levels of squalene precursors (Liao *et al.*, 2018). Finally, strains carrying a plasmid for expression of the p19 suppressor of gene silencing from Tomato Bushy Stunt Virus were co-infiltrated to increase gene expression (Kontra *et al.*, 2016). Five days after infiltration, leaves were harvested, and extracts were analysed by GC-MS.

Co-expression of CoTXSS, with either CoCYP716A392 or CoCYP716A393 resulted in new peaks (13.6 min), accompanied by a decrease in ψ-taraxasterol compared to controls, suggesting that much of the ψ-taraxasterol had been converted (**Figure 4.4.**). The new peak had a signature 189 m/z ion for ψ-taraxasterol/taraxasterol-based compounds and a molecular ion of 586 m/z, which corresponds to trimethylsilyl derivatised faradiol. The mass spectrum also matched the commercially obtained faradiol standard (**Supplementary Figure S3.1.**). In addition, two smaller peaks also appeared at 12.1 min and 12.9 min. These peaks also had a molecular mass of m/z 586, and characteristic ions at m/z 216 and m/z 189, which corresponded to maniladiol and calenduladiol, respectively (**Supplementary Figure S3.1.**). This coincided with a significant reduction of the substrate molecules (β-amyrin and lupeol).

Noticeably, the peak areas of the triterpene diols (faradiol, arnidiol, calenduladiol, and maniladiol) were not equivalent to the areas depleted from the substrates. Further, although the taraxasterol peak was depleted, the corresponding peak of arnidiol was not detected. Finally, co-expression of CoTXSS with either CoCYP716A392 or CoCYP716A393 also resulted in the accumulation of a small quantity of faradiol palmitate (**Figure 4.4.**).

Co-infiltration of strains expressing CoTXSS and CoCYP716A431 resulted in the depletion of all substrate molecules (ψ-taraxasterol, taraxasterol, β-amyrin and lupeol) and yielded four new products. All the new peaks had m/z 585 molecular ions, indicating the addition of a hydroxyl group (**Figure 4.4.**). The two peaks at 13.6 min and 13.7 and had signature m/z 189 ions for ψ-taraxasterol/taraxasterol-based compounds, but their mass spectra did not match any known compounds (**Figure 4.4.**). The two peaks at 13.3 min and 13.4 min had fragmentation patterns that matched those of commercially obtained standards for oleanolic and betulinic acids (**Supplementary Figure S3.1.**).

Co-infiltration of strains expressing CoTXSS with CoCYP716A429 or CoCYP716A430 did not yield any new peaks (**Figure 4.4.**).

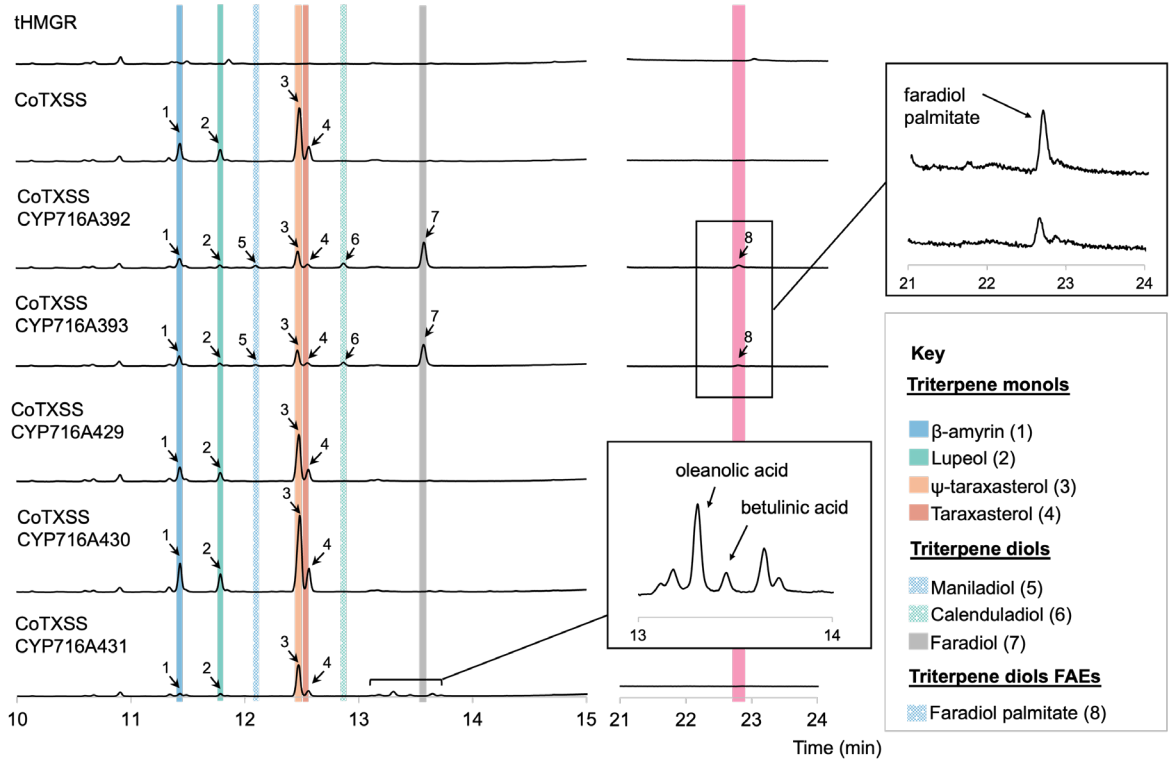

Figure 4.4 GC-MS total ion chromatogram of *N. benthamiana* leaves expressing candidate pot marigold cytochrome P450s (CYPs). Representative total ion chromatograms of ethyl acetate extracts of *N. benthamiana* leaves transiently expressing pot marigold ψ-taraxasterol synthase CoTXSS and candidate C16 hydroxylases (CoCYP*s*).

4.4.1.3 *CoCYP716A392* and *CoCYP716A393* are located in genomic regions with conserved synteny

To investigate if *CoCYP716A392* and *CoCYP716A393* are homeologues, the synteny between the regions of the genome in which they are located was analysed. The genomic locations of these genes were annotated on pseudo-chromosomes from the pot marigold genome assembly and compared using the whole genome alignment function of Geneious Prime (2021.1.1) (**methods 2.5.3.**)

This analysis showed that synteny in the regions flanking *CoCYP716A392* and *CoCYP716A393* is generally conserved, providing additional evidence that the sequences comprising contigs 6 and 8 are likely homeologous (**Figure 4.5.**).

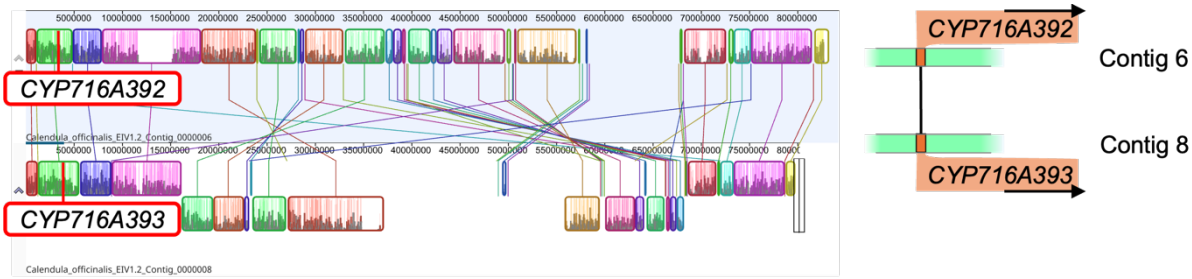

Figure 4.5 Genomic location and synteny of pot marigold CoCYP716A392 and CoCYP716A393 genes. Chromosome synteny and graphical representation of the contig positions of candidate *CoCYP716A392* and *CoCYP716A393* genes. Contigs are paired to show synteny between genes found on homeologous contigs. A graphical representation of the relative position, orientation and similarity of genes within each contig pair is shown to the right of the contig synteny plot.

Further investigation of the genes adjacent to *CoCYP716A392* and *CoCYP716A393* (**Figure 4.6.A**) revealed that these encode CYPs that belong to the CYP716A family, which are very closely related within the phylogenetic tree (**Figure 4.6.B**).

Figure 4.6 Genomic regions containing CoCYP716A392/CoCYP716A393 and maximum-likelihood tree of CYP716 family. (A) Genomic location of *CoCYP716A392/CoCYP716A393*. (B) CYP716 family. The red text indicated C16 ψ-taraxasterol hydroxylases, and the blue text indicated other CYPs made from pot marigold genome, field marigold transcriptome and publicly available Asteraceae genomes. Genes found next to the *CoCYP716A392* and *CoCYP716A393* in the genome are shown in yellow.

4.4.1.4 Field marigold also has genes encoding a ψ-taraxasterol synthase and ψ-taraxasterol C16 hydroxylases

CoCYP716A392 and CoCYP716A393 are clustered in the phylogenetic tree, forming a sub-clade with two CYPs from field marigold (CaCYP716A392 and CaCYP716A393) and another CYP from common sunflower (XM 022141189) (**Figure 4.2.** and **Figure 4.6.**). To confirm that other enzymes from this sub-clade can also hydroxylate ψ-taraxasterol at C16, *CaCYP716A392* was also cloned and characterised.

In addition, a ψ-taraxasterol synthase was identified using the previously characterised CoTXSS as a query to identify candidate CaTXSS gene in field marigold. This identified a protein with 95.0% pairwise identity to CoTXSS, which was renamed in CaTXSS (**Figure 4.7.**).

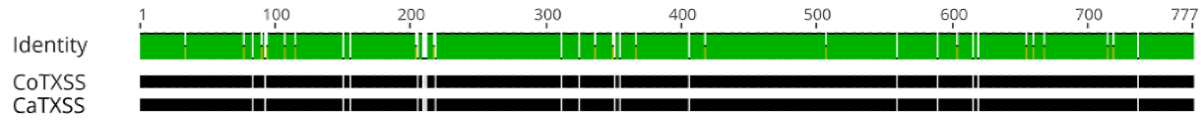

Figure 4.7 Protein sequence alignment of CoTXSS and CaTXSS candidate genes. TXSS = taraxasterol synthase; Co = *Calendula officinalis* (pot marigold) Ca = *Calendula arvensis* (field marigold)

The coding sequences of *CaTXSS* and *CaCYP716A392A* were synthesised and cloned as above. Plasmids were transformed into *A. tumefaciens* GV3101 and expressed in *N. benthamiana* together with tHMGR and p19. Five days after infiltration, leaves were harvested, and extracts were analysed by GC-MS.

When CaTXSS was expressed, it yielded a major peak at 12.1 mins and three smaller peaks (11.1 min, 11.3 min and 12.2 min). The mass spectra and retention time of these peaks matched those produced by CoTXSS (**Figure 4.4.**), the identities of which were confirmed by comparison with commercially obtained standards (lupeol and taraxasterol), or the NIST database (β-amyrin), or predicted based on the fragmentation patterns, characteristic and molecular ions (ψ-taraxasterol) (**Supplementary Figure S3.1.**; **Supplementary Table S3.3.**).

The co-expression of CaTXSS with CaCYP716A392A yielded four new peaks. The mass spectra and retention time of these peaks matched those produced by the co-expression of CoTXSS and CoCYP716A392. The major peak had a signature 189 m/z ion for ψ-taraxasterol/taraxasterol-based compounds and a molecular ion of 586 m/z, which corresponds to trimethylsilyl derivatised faradiol and matched the commercially obtained

faradiol standard (**Figure 4.8.**). In addition, two smaller peaks were identified (calenduladiol and maniladiol), indicating that CaCYP716A392A is also a promiscuous C16 hydroxylase. Again, the peak areas of the terpene diols (faradiol, calenduladiol, and maniladiol) were not equivalent to the areas depleted from the triterpene scaffold substrates, and arnidiol was not detected despite a reduction in the taraxasterol peak.

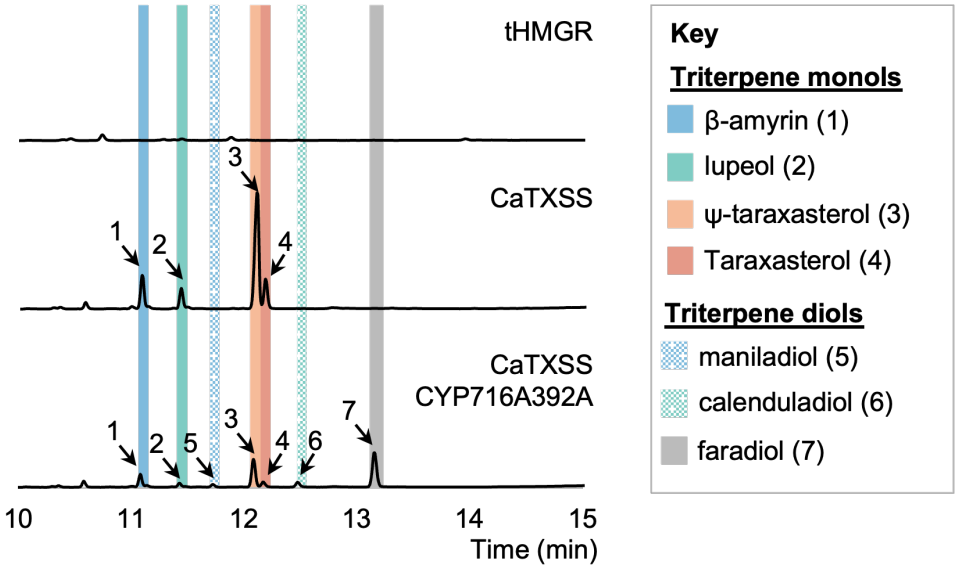

Figure 4.8 GC-MS total ion chromatogram of *N. benthamiana* leaves expressing candidate field marigold ψ-taraxasterol synthase (CaTXSS) and candidate cytochrome P450 (CaCYP716A292A). Representative total ion chromatograms of ethyl acetate extracts of *N. benthamiana* leaves transiently expressing genes encoding a candidate ψ-taraxasterol synthase and CYPs identified in the field marigold transcriptome.

4.4.2 Investigation of the substrate specificity of CoCYP716A392 and CoCYP716A393

4.4.2.1 Structural modelling indicates three residues involved in the substrate specificity of CoCYP716A392 and CoCYP716A393.

To investigate the substrate specificity of CoCYP716A392 and CoCYP716A393, the amino acid sequence and structure were compared to other CYP716 family CYPs that modify other triterpene scaffolds.

To predict the active sites of CoCYP716A392 and CoCYP716A393 3D structural models were first inferred using Phyre2 (**methods 2.5.4.**). For both CoCYP716A392 and CoCYP716A393, the two best homology models were based on the crystal structure of the putative substrate-free cytochrome CYP120A1 from cyanobacteria (PDB ID: 2VE4) and CYP90B1A in complex with 1,6-hexandiol from Arabidopsis (PDB ID: 6A18). CoCYP716A392 had a slightly higher similarity to CYP120A1 (RMSD: 1.202) than to

CYP90B1A (RMSD: 1.283). In contrast, CoCYP716A393, had a slightly higher similarity to CYP90B1A (RMSD: 1.235) than to CYP120A1 (RMSD: RMSD:1.259). CYP90B1A-based models were selected for both pot marigold CYPs as this enzyme is of plant origin and acts on sterols, which are closely related to triterpenes (**Figure 4.9.A**).

The models of CoCYP716A392 and CoCYP716A393 were aligned with the available crystal structure of CYP90B1 in a complex with cholesterol (PDB:6A15) (**Figure 4.9.A**). Then, ψ-taraxasterol (PubChem ID: 115250) was manually docked into the active site based on the location of cholesterol in 6A15. Energy minimisation was performed using the YASARA force field (Land and Humble, 2018a). This placed the ligand in a similar position and with a 5.1 Å distance between C16 of ψ-taraxasterol and the heme molecules (**Figure 4.9.B**).

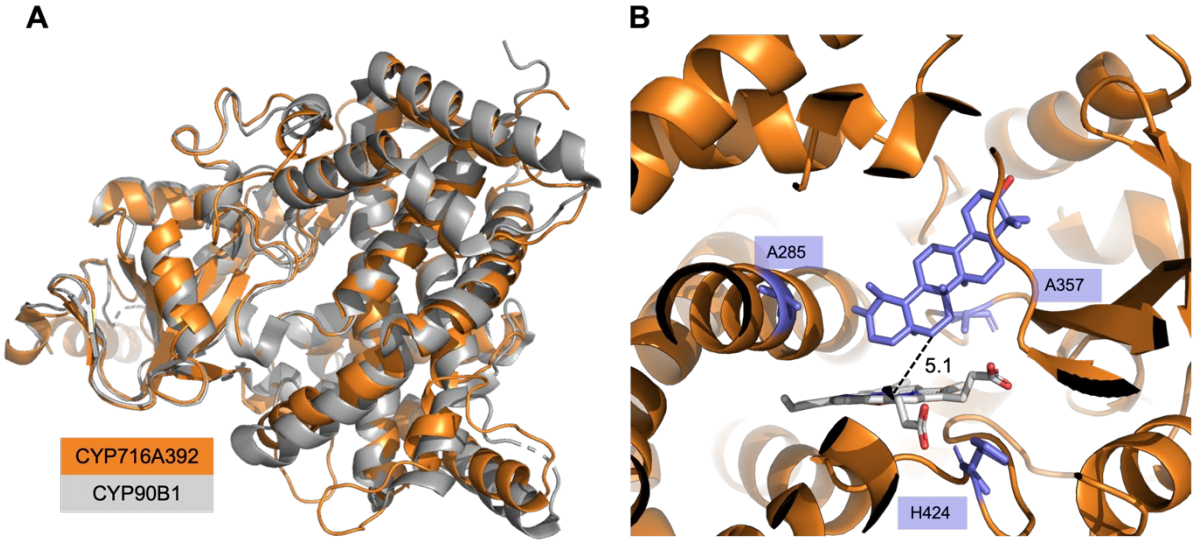

Figure 4.9 Structural models illustrating the alignment of Phyre2 structural model of CoCYP716A392 and crystal structure of CYP90B1 and the predicted position of the ψ-taraxasterol in the active site of CoCYP716A392. (A) Alignment CoCYP716A392 and CYP90B1 (PDB:6A15). CoCYP716A392 is shown in orange; CYP90B1 is shown in grey. **(B)** Predicted position of the ψ-taraxasterol in the active site of CoCYP716A392. The CoCYP716A392 is shown in orange; ψ-taraxasterol and residues selected for mutagenesis are shown in violet; heme is shown in grey.

To select candidate residues that might impact the substrate specificity of CoCYP716A392 and CoCYP716A393, a sequence alignment of (i) 30 known plant CYPs that belong to that CYP716A (with two of them being C16-hydroxylases - CYP716A111 and CYP716A141), (ii) CoCYP716A392, CoCYP716A393, CaCYP716A392A and CaCoCYP716A393A, and (iii) a predicted ψ-taraxasterol C16-hydroxylase (XM 022141189) mined from common sunflower, was performed using MUSCLE V3.8.425 (**methods 2.5.1.**).

Residues within 12 Å of C16 were annotated as the “active site”. Among the 64 residues that comprise the active site, three amino acids, A285, A357 and H424, identified in conserved

regions of the sequence alignment were found to differ from those found in CYPs that modify β-amyrin, α-amyrin and lupeol (**Figure 4.10.**).

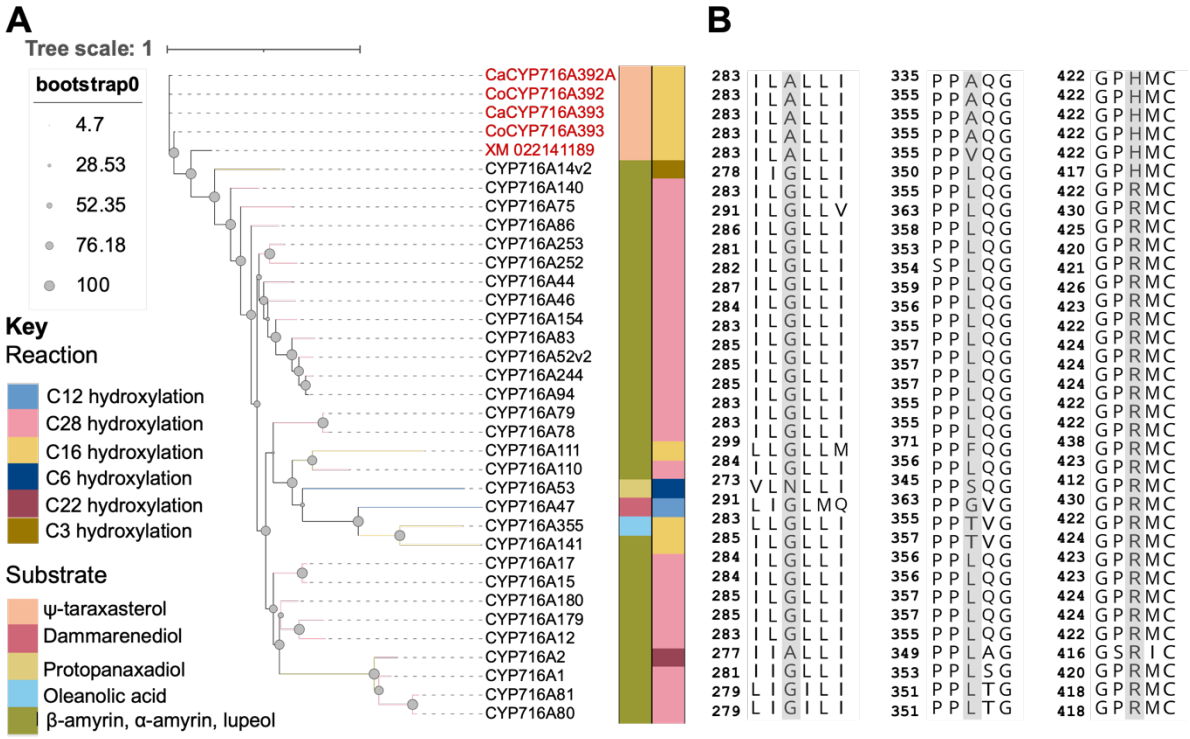

Figure 4.10 Maximum-likelihood phylogenetic tree and a sequence alignment of CYP716A clade. (A) A maximum likelihood tree of CYP716A clade was constructed in IQ-Tree using the LG+F+I+G4 matrix-based model and visualised using Interactive Tree of Life (iTOL) v6. Substrate specificity is shown in the inner bar; reactions catalysed by CYPs are shown in the outer bar. Grey circles indicate bootstrap supports for each node. The scale bar represents the number of substitutions per site. ψ-taraxasterol modifying CYPs sequences are shown in red. **(B)** Protein sequence alignment of the CYP716A clade. Residues selected for mutagenesis are highlighted in grey.

4.4.2.2 All tested residues are important for substrate specificity and activity of CoCYP716A392 and CoCYP716A393

To establish whether any of these residue mutations impacted the substrate specificity of CoCYP716A392 or CoCYP716A393, mutations were introduced into the genes and mutants were screened in the *N. benthamiana*.

The candidate amino acids in CoCYP716A392/CoCYP716A393 were substituted with the corresponding consensus amino acid from CYPs that modify other triterpene scaffolds - A285G, A357L and H424R (**Figure 4.10.**). Moreover, an additional mutation was made to explore if the size of hydrophobic amino acid at position A285 facilitates the shift in enzyme specificity. For this, alanine (88.6 $Å^3$) was replaced with another aliphatic amino acid - valine V (140.0 $Å^3$) to increase the amino acid size at this position.

These mutations were introduced into the level 1 plant expression plasmids (pEPMS1CB0018) and (pEPMS1CB0019) using site-directed mutagenesis (**methods 2.6.7.**). After sequence confirmation, plasmids were transformed into *A. tumefaciens* GV3101 and expressed in *N. benthamiana* with CoTXSS, tHMGR, and p19, as described above. Five days after infiltration, leaves were harvested, and extracts were analysed by GC-MS. Metabolites were quantified by peak area analysis using friedelin as an internal standard.

As observed with the wild-type enzymes, the peak area of the terpene diols (faradiol, calenduladiol, and maniladiol) was not equivalent to the area depleted from the triterpene scaffold substrates (ψ-taraxasterol, taraxasterol and β-amyrin), and arnidiol was not detected in any samples despite a reduction in the taraxasterol peak. Therefore, the reduction of the ψ-taraxasterol and β-amyrin substrates was quantified.

β-amyrin co-eluted with isofucosterol, for which the amount remained similar in all samples. Thus, both peaks were integrated, and the average was subtracted from the β-amyrin peak area in each sample after normalisation to the internal standard, friedelin. Friedelin co-eluted with one of the reaction products, calenduladiol. These were separated by removing 13.3 % of the peak area using automatic MassHunter ion-based calculator (v B.08.00; Agilent). (**Figure 4.11.**).

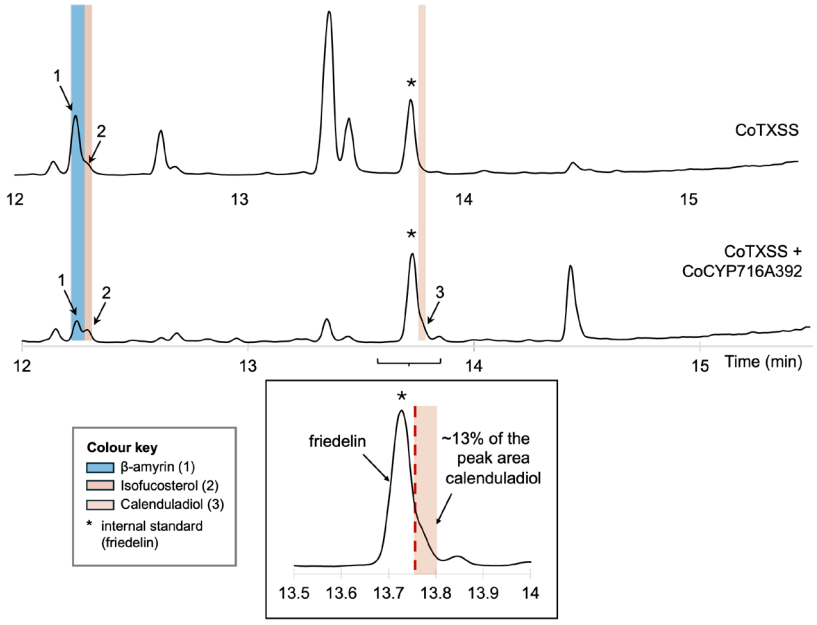

Figure 4.11 Co-elution of β-amyrin with isofucosterol, and friedelin with calenduladiol. Representative total ion chromatograms of ethyl acetate extracts of *N. benthamiana* leaves transiently expressing ψ-taraxasterol synthase and ψ-taraxasterol hydroxylase genes. β-amyrin co-elutes with isofucosterol produced by endogenous *N. benthamiana* enzymes. Friedelin co-elutes with calenduladiol produced by CoCYP16A392.

The highest specificity shift was observed from A285V mutations of both CoCYP716A392 and CoCYP716A393 (**Figure 4.12. ;Supplementary Table S3.4.**). Interestingly, the A285G mutation did not show a change in specificity but, instead, resulted in a slight loss in the activity of both enzymes. Mutation of A357L in both CoCYP716A392 or CoCYP716A393 shifted specificity towards β-amyrin but caused partial activity loss in CoCYP716A393. The H424R mutation shifted activity towards β-amyrin for CoCYP716A393 alone, but this was accompanied by a reduction in activity. The H424R mutation of CoCYP716A392 did not impact either the specificity or activity of the enzyme.

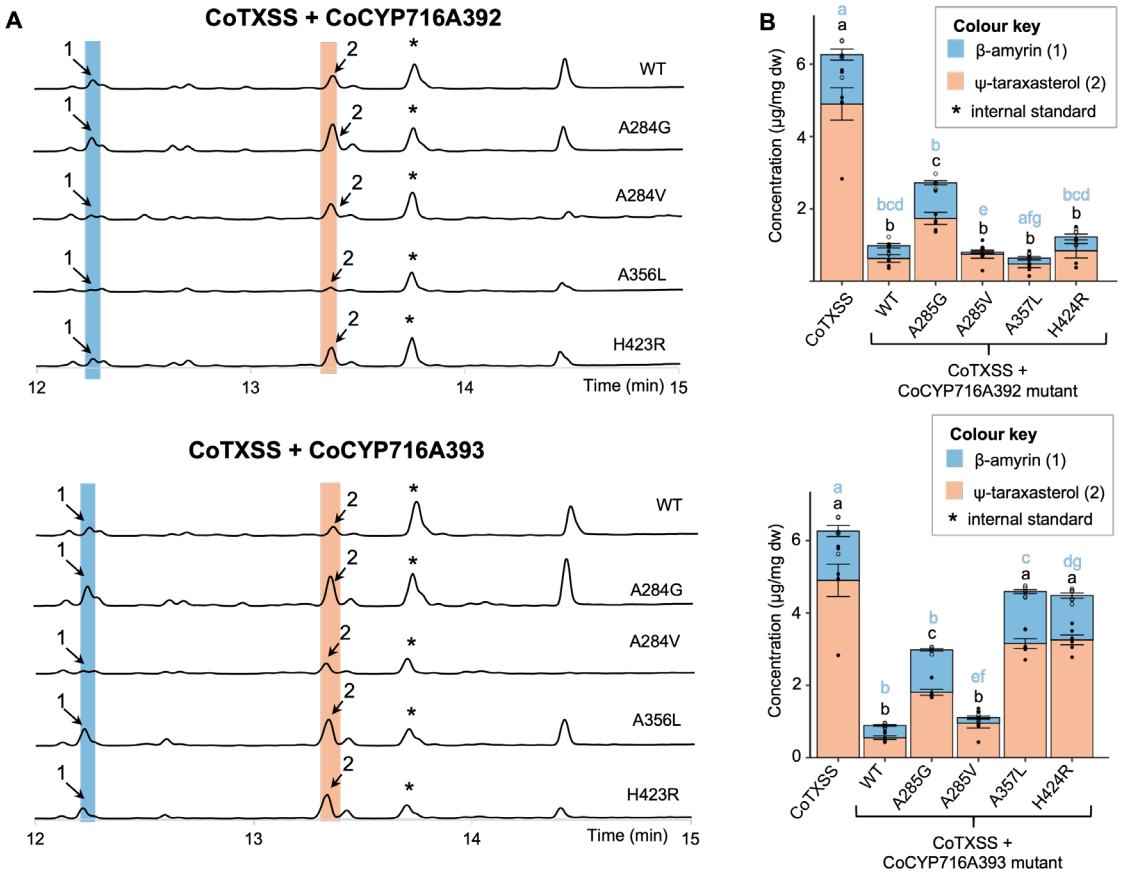

Figure 4.12 GC-MS analysis and quantification of triterpenes in *N. benthamiana* leaves expressing mutants of CoCYP716A392 and CoCYP716A393. (A) Representative total ion chromatograms of extracts of *N. benthamiana* leaves transiently co-expressing CoTXSS with wild-type and mutated pot marigold CoCYPs (CoCYP716A392 and CoCYP716A393). **(B)** Quantification of triterpenes depleted by wild type and mutated CoCYP716A392 and CoCYP716A393; n=6; error bars indicate standard error. Significant differences in total ψ-taraxasterol/β-amyrin content compared to wild-type CoCYP716A392 or CoCYP716A393 (black lowercase letters), and significant differences in taraxasterol/β-amyrin ratio compared to wild-type CoCYP716A393 (blue lowercase letters) were analysed using a Kruskal-Wallis test followed by post-hoc Wilcoxon rank sum test with a Benjamin-Hochberg correction. Samples that do not share the same lower-case letter are significantly different from each other ($p<0.05$).

4.4.3 Identification of candidate genes encoding C3 fatty acid acyl transferases

4.4.3.1 Thirteen candidate ACTs in the MBOAT family were identified in pot marigold

To identify candidate C3 fatty acid acyl transferase genes, a previously characterised AtTHAA3 from Arabidopsis was used as a query to search the genome of pot marigold and publicly available Asteraceae species as before (method 2.5.1). This search identified 13 candidate pot marigold *ACTs* genes coding for CoACTs 1-13, which were predicted to be members of the membrane-bound O-acyltransferase (MBOAT) superfamily. Two of these genes contained missense mutations (**Figure 4.13.**).

The protein sequences of all candidate genes from pot marigold were aligned with 80 uncharacterised candidate ACTs from the publicly available genomes and 50 previously characterised ACTs (D'Auria, 2006). The alignment was trimmed and used to reconstruct a maximum likelihood phylogenetic tree (**methods 2.5.1.**). As with the CYPs, many candidates were observed to pair in the phylogeny. In these cases, one candidate from the pair was selected for functional characterisation (CoACT1-7).

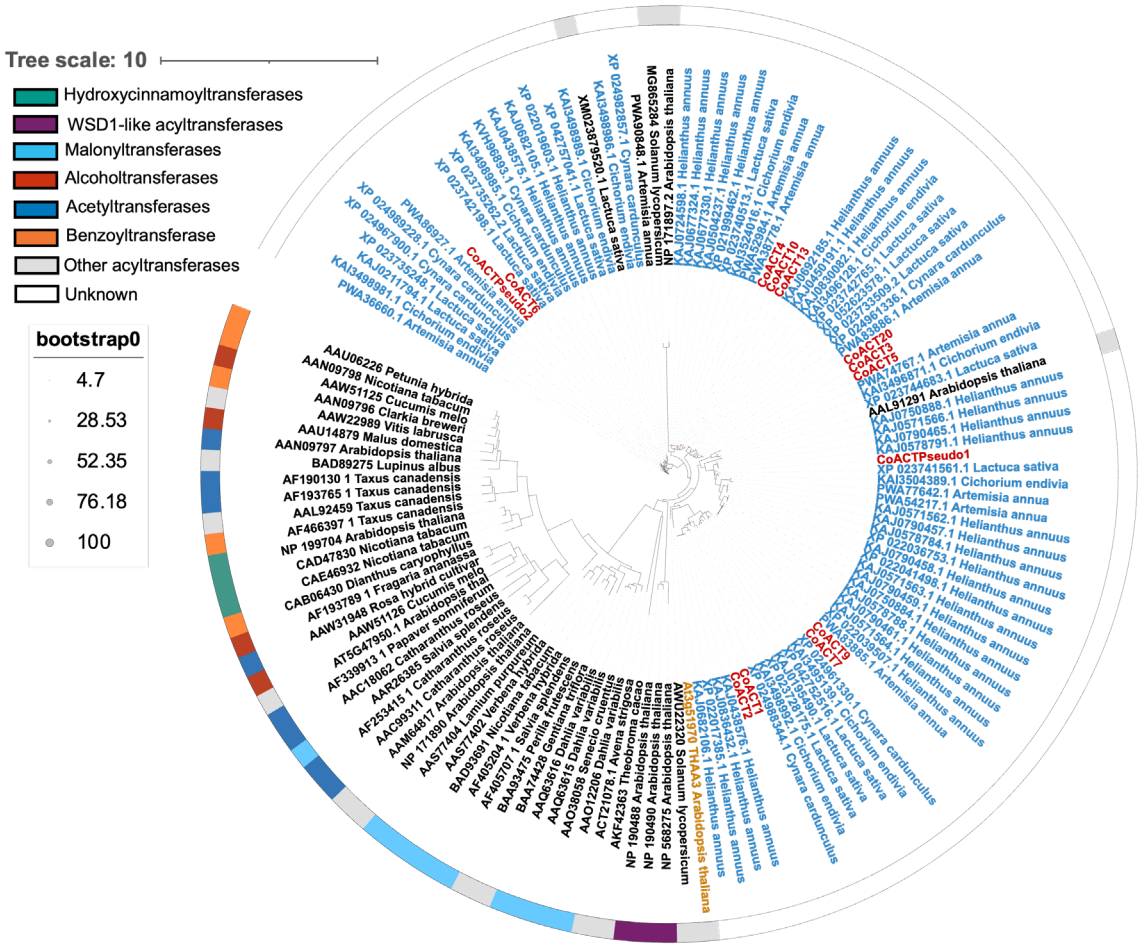

Figure 4.13 Maximum-likelihood tree of plant acyltransferases (ACTs). A maximum likelihood tree was constructed in IQ-Tree using the LG+F+I+G4 matrix-based model and visualised using Interactive Tree of Life (iTOL) v6. Substrate specificity is shown in the ring; Filled grey circles indicate bootstrap supports for each node. The scale bar represents the number of substitutions per site. Functionally characterised ACTs are shown in black. ACTs sequences mined from the publicly available genomes of Asteraceae, pot marigold genome and transcriptome datasets are shown in blue. Pot marigold candidate C3 fatty acid acyl transferases are shown in red. Arabidopsis fatty acid acyltransferase (AtTHAA3) is shown in orange.

Differential gene expression data showed that *CoACT2* had a similar pattern to *CoCYP716A392/CoCYP716A393* and were upregulated in ray floret compared to disk floret and leaf (**Figure 4.14.**). Whereas *CoACT1, CoACT3, CoACT4, CoACT5, CoACT6* and *CoACT7* were expressed at similar levels in all three tissues.

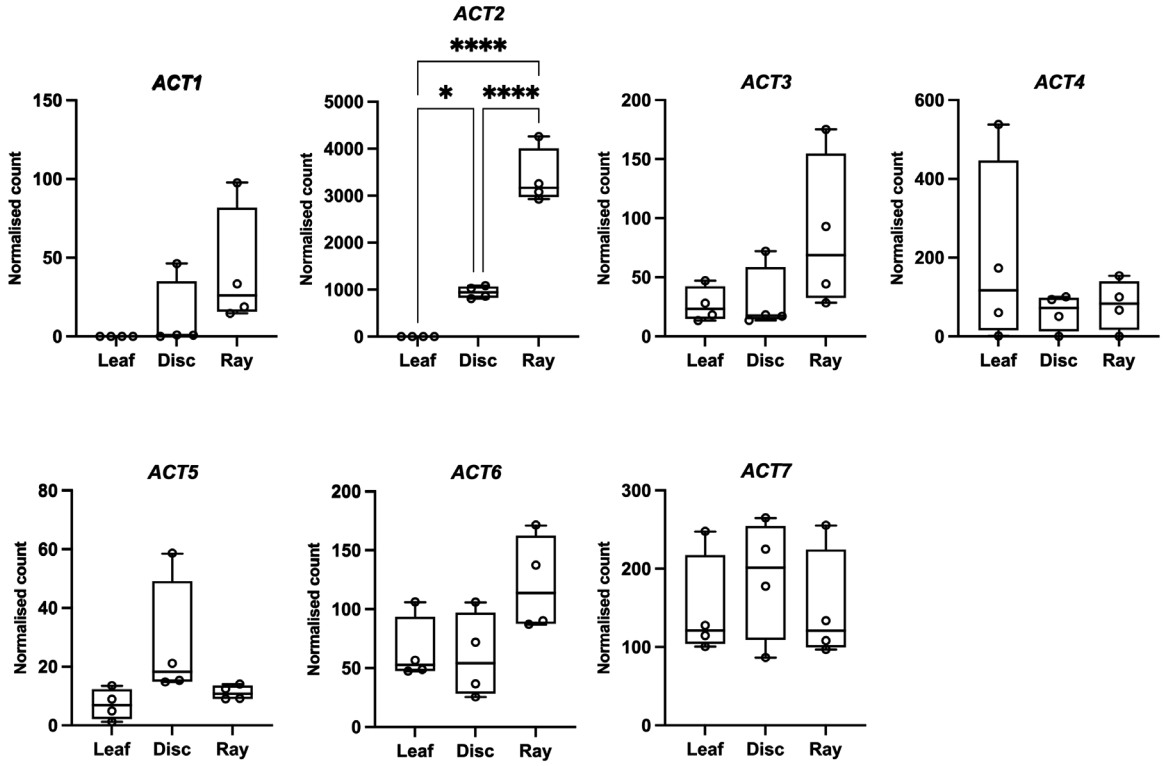

Figure 4.14 Differential expression of pot marigold candidate *CoACT* genes in leaf, disc and ray floret tissues. Gene expression for each tissue is displayed in a box plot as normalised counts with the centre line of the boxplot denoting the median, the box denotes the 25th to 75th percentiles of the data and the whiskers show the minimum and maximum of the data. Significant difference in normalised transcript count was analysed using one-way ANOVA with a post-hoc Tukey's test; *=p<0.0332, **=p<0.0021, ***=p<0.0002, ****=p<0.0001.

4.4.3.2 Pot marigold CoACT1 and CoACT2 are faradiol C3 fatty acid acyltransferases

In this section, I describe the characterisation of CoACT1-CoACT3. The other candidates (CoACT4-CoACT7) were characterised by Dr. Connor Tansley.

To establish if the enzymes encoded by the candidate ACTs were able to add fatty acids to faradiol at the C3 position, *CoACT1-CoACT3* were synthesised and cloned into the Level 1 pICH47732 acceptor plasmid as described for the CYP candidates. After sequence confirmation, plasmids were transformed into *A. tumefaciens* GV3101 and co-infiltrated into *N. benthamiana* with strains expressing *CoTXSS, CoCYP716A392, tHMGR,* and *p19*, as described above. Five days after infiltration, leaves were harvested, and extracts were analysed by GC-MS.

Co-expression of CoTXSS with CoACT3, yielded a peak at 21.0 min with a molecular ion of 665 and characteristic ion of 189, with the retention time matching ψ-taraxasterol palmitate (**Supplementary Figure S3.1.**), confirming that CoACT3 can add fatty acid to the

ψ-taraxasterol triterpene scaffold (**Figure 4.15.**). In addition, three smaller peaks with a molecular ion of m/z 665 were also observed following expression of CoACT3, corresponding to β-amyrin, α-amyrin and lupeol palmitate, suggesting that these enzymes can add fatty acid groups to other pentacyclic triterpene scaffolds. Interestingly, when CoTXSS and CoCYP716A392 were co-expressed with CoACT3, all substrates (ψ-taraxasterol, taraxasterol, β-amyrin and lupeol) were significantly depleted, but only small quantities of faradiol and ψ-taraxasterol palmitate were detected in the samples.

Co-expression of CoTXSS with CoACT1 and CoACT2 did not yield any peaks. However, when CoACT1 and CoACT2 were co-expressed with CoTXSS and CoCYP716A392, it led to the production of a peak matching the retention time (21.6 min) and fragmentation of faradiol palmitate (molecular ion of m/z 753 and characteristic ion of 189), indicating their function as faradiol C3 fatty acid ester acyl transferases (**Figure 4.15.**). In addition, trace quantities of maniladiol- calenduladiol- and arnidiol- palmitates were also detected in these samples.

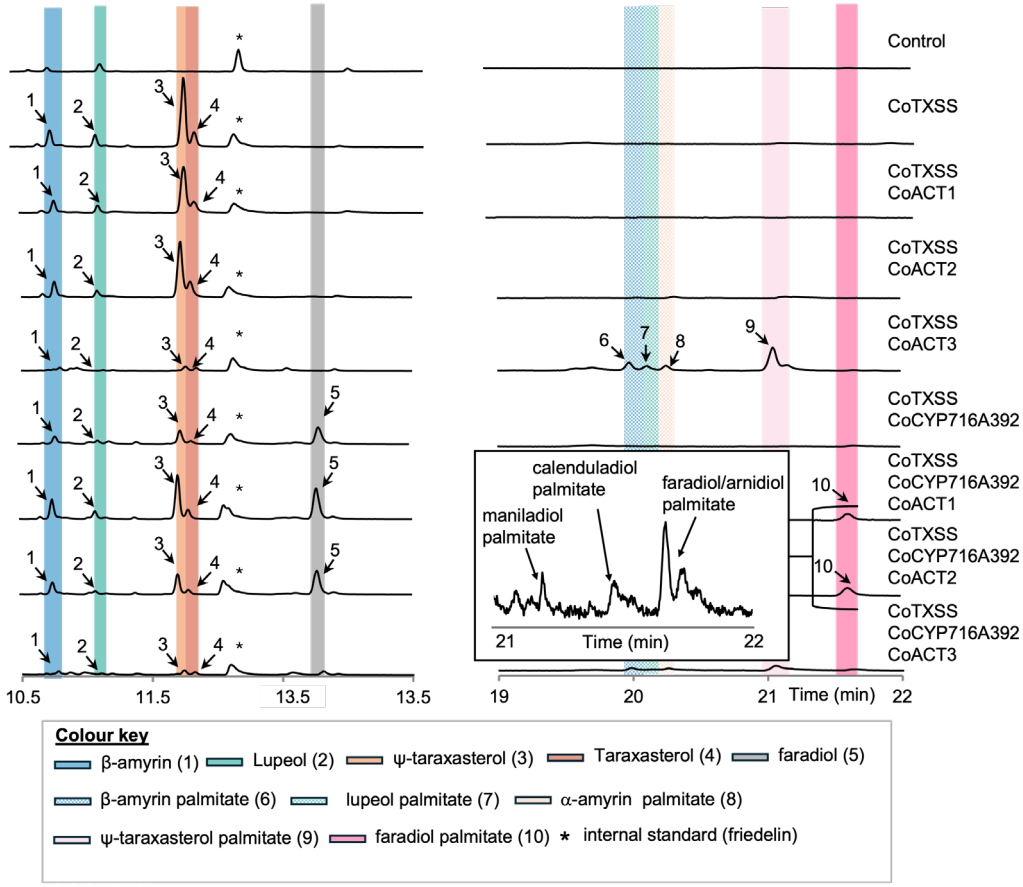

Figure 4.15 GC-MS total ion chromatogram of *N. benthamiana* leaves expressing candidate acyltransferases. Representative total ion chromatograms of ethyl acetate extracts of *N. benthamiana* leaves transiently expressing pot marigold ψ-taraxasterol synthase CoTXSS, CoCYP716A392 and CoACT candidates. CoTXSS = pot marigold ψ-taraxasterol synthase; CoCYP716A392 = pot marigold ψ-taraxasterol C16 hydroxylase; CoACT = candidate faradiol C3 fatty acid transferase.

4.4.3.3 *CoACT1* and *CoACT2* are located in genomic regions with conserved synteny

To investigate if *CoACT1* and *CoACT2* are homeologous, the synteny between the genomic regions in which they are located was analysed. As before, the genomic locations of these genes were annotated on pseudo-chromosomes from the pot marigold genome assembly and compared using the whole genome alignment function of Geneious Prime (2021.1.1) (**methods 2.5.3.**)

As found for *CoCYP716A392* and *CoCYP716A393, CoACT1* and *CoACT2* were also found to be located in genomic regions with conserved synteny (contigs 5 and 10), indicating that they are likely homeologues (**Figure 4.16.**).

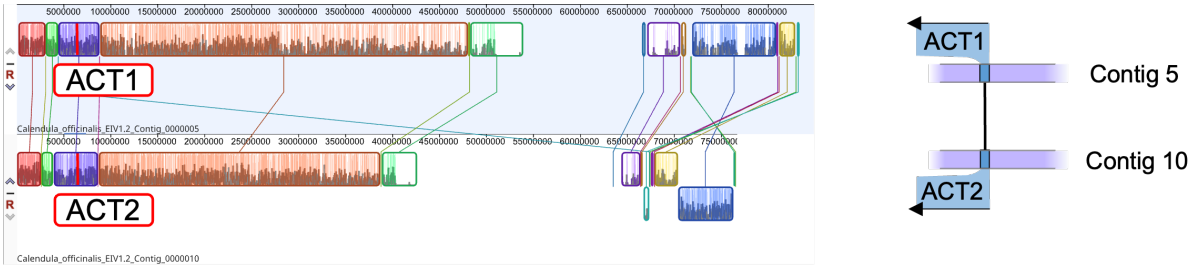

Figure 4.16 Genomic location and synteny of pot marigold *ACYLTRANSFERASES (ACTs).* A graphical representation of the relative genomic position, orientation and similarity of *CoACT1* and *CoACT2,* which add fatty acid groups to faradiol C3.

4.4.4 Investigation of faradiol palmitate biosynthetic pathway genes expression during floral development and in response to methyl jasmonate (MeJA)

4.4.4.1 Faradiol palmitate pathway genes are not co-expressed during floral development

The genes encoding the three pathway steps are not co-located or clustered in the pot marigold genome. However, all pathway genes showed higher expression in floral tissues than in leaves. To determine if these genes also show temporal co-expression, their relative expression patterns during flower development were determined. To do this, RNA that had previously been extracted from flowers sampled at six developmental stages (S1-S6) was obtained from Dr Salmon. After cDNA synthesis, the expression of each pathway gene was compared by quantitative reverse-transcription PCR qRT-PCR. As previously determined by Dr. Salmon, *SAND* was used as a control gene for relative quantification as its expression does not alter through floral development.

This analysis revealed that the expression of pathway genes is not synchronous. *CoTXSS* displays a similar expression profile as *CoACT1* and *CoACT2*, all being most highly expressed in young buds (S1) with limited expression later in development (**Figure 4.17.; Supplementary Table S3.4.**). In contrast, the expression of *CoACT3* was higher at the end of floral development (S5), while *CoCYP716A392* and *CoCYP716A393* were expressed at similar levels throughout development.

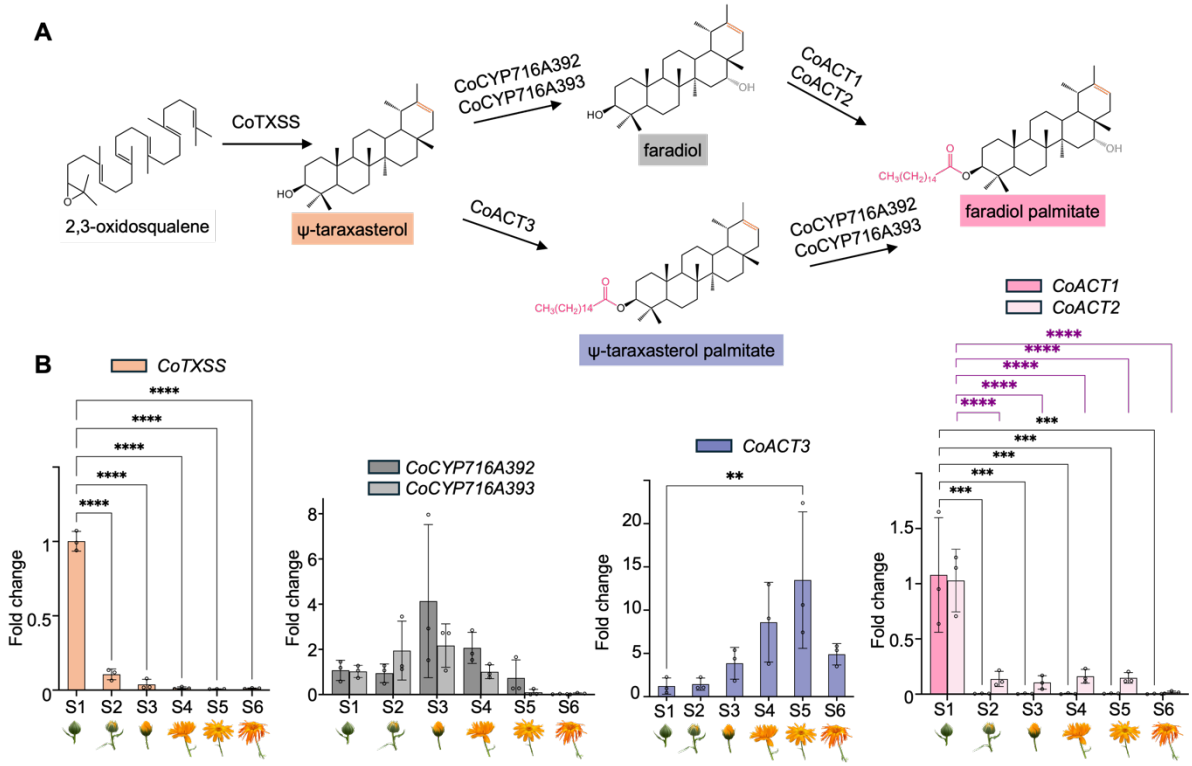

Figure 4.17 Proposed biosynthetic pathway and relative gene expression analysis of faradiol palmate pathway genes through flower development. (A) Proposed biosynthetic pathway of faradiol palmitate. TXSS = oxidosqualene cyclase; CYP = C16 hydroxylase; ACT = C3 fatty acid acyl transferase. **(B)** Relative expression of *CoTXSS*, *CoCYP716A392, CoCYP716A393, CoACT1, CoACT2* and *CoACT3* through six stages of floral development (S1-6); n=3; error bars indicate standard deviation. Statistical significance to S1 was analysed using one-way ANOVA with a post-hoc Dunnett test; *=p<0.0332, **=p<0.0021, ***=p<0.0002, ****=p<0.0001. Pink stars (*) represent statistics for CoACT2.

4.4.4.2 Expression of faradiol palmitate pathway genes is increased after methyl jasmonate (MeJA) treatment

Hydroxylated and esterified triterpenes are known to play a critical role in plant defence against biotic and abiotic factors (Liu *et al.*, 2024a). To investigate if faradiol palmitate might be involved in pot marigold defence, the expression of faradiol palmitate pathway genes was quantified in plants treated with 100 µM MeJa. Gene expression was quantified in RNA samples taken at 0 h, 6 h, and 24 h after MeJa treatment (RNA was extracted by Dr Melissa Salmon). As before, *CoSAND* was used for relative expression.

Relative gene expression analysis showed that there was no significant gene expression increase in leaf or disc tissues for any of the target genes after MeJa treatment (**Figure 4.18.; Supplementary Table S3.4.**). Expression in the disc floret was also highly variable, with some replicates showing 5-40 times higher expression than other replicates. Further, in the ray floret, an increase in expression after 6 h after MeJA was observed only for one pathway gene, *CoACT1*. Even though other pathway gene expression profiles showed a similar trend, it was not significant.

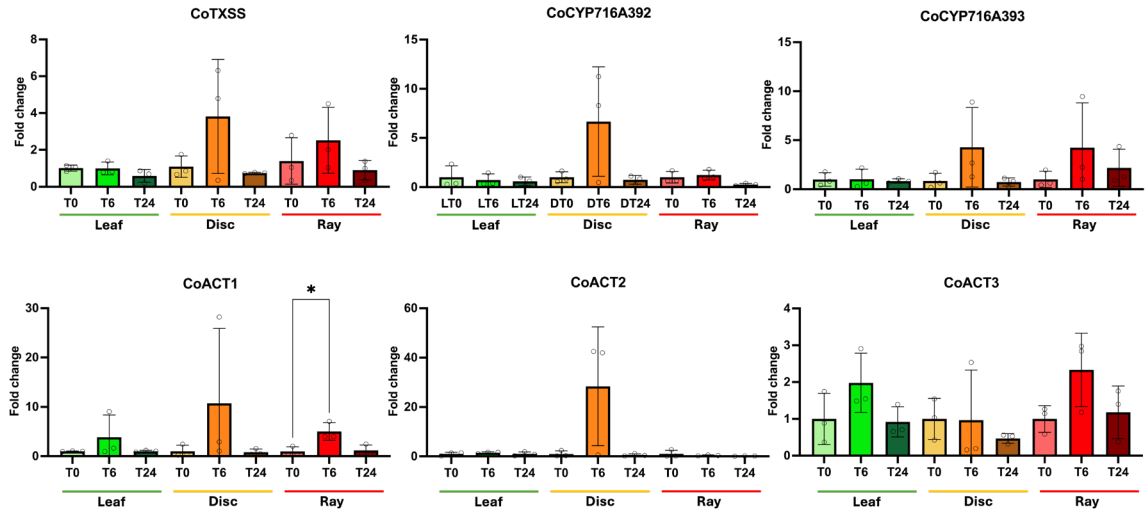

Figure 4.18 Expression analysis of faradiol palmate pathway genes after MeJa treatment. Relative expression of *CoTXSS*, *CoCYP716A392, CoCYP716A393, CoACT1*, *CoACT2* and *CoACT3* after 6 h and 24 h after MeJa treatment; n=3; error bars indicate standard deviation. Statistical significance to T0 for each of the tissues was analysed using one-way ANOVA with a post-hoc Dunnett test; *=p<0.0332, **=p<0.0021, ***=p<0.0002, ****=p<0.0001.

4.4.4.3 Additional Relevant Results

Due to time limitations, Dr. Connor Tansley performed the cloning and characterisation of *CoACT4-CoACT7* in *N. benthamiana*. GC-MS analysis showed that CoAC4, CoACT5 and CoACT7 are ψ-taraxasterol C3 fatty acid acyl transferases that produce ψ-taraxasterol palmitate. CoACT6 was not active on any of the triterpene scaffolds (ψ-taraxasterol, taraxasterol, β-amyrin, and lupeol) synthesised by CoTXSS. Further, Dr. Connor Tansley further quantified metabolites produced by co-expression of CoTXSS+CoACT1/2/3 compared to CoTXSS+CoCYP716A392+CoACT1/2/3. This confirmed that the production of faradiol palmitate is significantly increased in CoTXSS+CoCYP716A392+CoACT1/2 compared to CoTXSS+CoCYP716A392. It also confirmed that the amount of ψ-taraxasterol palmitate obtained by co-expression of CoTXSS+CoACT3 is significantly less that that obtained by co-expression of CoTXSS+CoCYP716A392+CoACT3.

4.5 Discussion

Elucidating the biosynthetic pathways of natural products enables their production in heterologous hosts. This chapter described the elucidation of the pot marigold pathway for the production of the anti-inflammatory compounds faradiol and faradiol palmitate for which the bioactivity was described in Chapter 3.

4.5.1 Two pot marigold C16 hydroxylases can catalyse the production of faradiol

To identify candidate C16 CYPs, phylogenetics was combined with metabolomics and transcriptomics. This search identified genes encoding two candidate CYPs: CoCYP716A392 and CoCYP716A393 subsequently shown to catalyse the production of faradiol by C16 hydroxylation of ψ-taraxasterol (**Figure 4.4.**). These enzymes, as well as C16 hydroxylases from field marigold, and common sunflower form a distinct subclade within the CYP71A family (**Figure 4.6.B**). Phylogenetic analysis indicates that they are most closely related to genes within the CYP71A family that are adjacent to *CoCYP716A392/CoCYP716A393* (**Figure 4.6.A** and **Figure 4.6.B**). This suggests a tandem gene duplication and neofunctionalization event.

Although, the order by which the adjacent genes and *CoCYP716A392/CoCYP716A393* have evolved in is not clear, the conservation of gene order in the homeologous chromosome indicates that this gene duplication occurred before the allopolyploidisation event that gave rise to the pot marigold. This is also supported by the existence of these genes in field marigold. Thus, to understand whether adjacent genes are duplicates of *CoCYP716A392/CoCYP716A393*, or might be ancestral genes, the function and substrate-specificity of these CYPs would need to be investigated. Further, although it is not clear how CoCYP716A392/CoCYP716A393 may have evolved, its sister clade contains CYP716A14v2, a β-amyrin C3 oxidase, and CoCYP716A431 which was characterised here to be a promiscuous C28 oxidase. This might also suggest an evolution from CYPs that are active on other positions/triterpene scaffolds (**Figure 4.6.B**).

Interestingly, a putative C16 ψ-taraxasterol hydroxylase from a common sunflower was also found to be closely related (bootstrap 99.9). Common sunflower is a diploid and, expectedly, only encoded a single C16 ψ-taraxasterol hydroxylase, whereas the tetraploid *Calendula* species have retained genes from both parental chromosomes. These data suggest that C16 ψ-taraxasterol hydroxylases were likely present in a common ancestor of the sunflower and

Calendula lineages, which diverged 42–37 mya (Mandel *et al.*, 2019). Synteny analysis between the pot marigold and common sunflower genomes might be used to determine whether these C16 ψ-taraxasterol hydroxylases are of the same origin. If this is the case, the genomes of related Asteraceae lineages may also encode homologues C16 ψ-taraxasterol hydroxylases. Further investigations are required to confirm this.

The same experiment also identified CoCYP716A431 as a promiscuous C28 hydroxylase that can make two known triterpenes (oleanolic and betulinic acids) and two novel compounds – C28 hydroxylated ψ-taraxasterol and taraxasterol (**Figure 4.4.**). In the future, NMR analysis will be required to confirm the structure of these new compounds.

One of the main challenges encountered during characterisation of the candidate CYPs is that the peak areas of the C16 (faradiol, arnidiol, calenduladiol, and maniladiol) and C28 (oleanolic, betulinic, ψ-taraxasterol and taraxasterol acids) products were not equivalent to the areas lost from the substrate peaks (**Figure 4.4.**). This may be due to the derivatisation of the products by *N. benthamiana* enzymes, as has been reported for other compounds, including monoterpene indole alkaloids and sesquiterpene lactones (Dudley *et al.*, 2022a, Liu *et al.*, 2014). No additional peaks were observed by GC-MS, but it is likely that compounds derivatised with groups such as hexose sugars would not be detectable using this method. Further, the presence of small quantities of faradiol palmate was observed when CoTXSS was co-expressed with either CoCYP716A392 or CoCYP716A393, indicating the presence of endogenous fatty acid acyltransferase (**Figure 4.4.**).

For more accurate characterisation of compounds produced by pathway CYPs, alternative strategies could be employed: Experiments could be conducted in other heterologous hosts such as brewer's yeast. Numerous CYPs have been characterised in this species (Bureau *et al.*, 2023). However, despite the advantage of a simpler metabolic background, production of triterpenes in yeast requires more extensive host engineering. For example, the production of friedelin (the triterpene monol used as an internal standard in this study) required (i) the integration of four mevalonate (MVA) pathway genes and (ii) knocking down genes of competing pathways (Gao *et al.*, 2022). Further, testing required heterologous expression of a cytochrome P450 reductase to facilitate electron transfer from NADPH to cytochrome P450 during the reaction (Miettinen *et al.*, 2017a).

An alternative route might be the identification and silencing of predicted genes coding for decorating enzymes. This approach was used to identify and mutate *N. benthamiana* genes

encoding enzymes that derivatised heterologously produced monoterpenes (Dudley *et al.*, 2022a). However, these enzymes are unlikely to be active on triterpenes, and a new search will be required. Finally, groups added by promiscuous enzymes might be removed by acidic hydrolysis or through enzymatic reactions. Acidic hydrolysis was also previously used to convert less biologically active flavonoid glycosides of hesperidin and naringin into the more active aglycones of hesperetin and naringenin (König *et al.*, 2023).

4.5.2 Substitutions at A285 impact the substrate specificity of CoCYP716A392 and CoCYP716A393

As one of the goals of engineering biology is to enable the production of bioactive compounds without side products, the residues important for substrate specificity were investigated. These experiments revealed that small changes in amino acid size impact both the substrate specificity and activity of CoCYP716A392 and CoCYP716A393. The substitution of A285 (88.6 $Å^3$) to glycine G (60.1 $Å^3$), which is found in almost all β-amyrin modifying CYPs, did not alter the substrate preference of CoCYP716A392 or CoCYP716A393 towards β-amyrin. However, it reduced the activity of both enzymes. In contrast, substitution with valine V (140.0 $Å^3$) resulted in an increased preference for β-amyrin (**Figure 4.12.**).

Although there were similarities in mutations that impacted the activity of CoCYP716A392 and CoCYP716A393, there was no clear trend, and more detailed investigations are required. These might include combinations of mutations, investigating the preferences for alternative substrates such as taraxasterol and lupeol, and reciprocal mutations of b-amyrin hydroxylases, e.g., AsCYP716A111 or AcCYP716A141. Previously, segment-directed mutagenesis was successfully employed to study the substrate specificity of human CYP1A1 by generating a library of random combinatorial mutants limited to a ten amino acid region (Urban *et al.*, 2001). Site-directed mutagenesis of non-active site residues has also been shown to be efficient at altering CYP specificity: systematic investigation of unique, non-active site residues in crystal structures of P450 2B4 revealed that single amino acid substitution could lead to 50 times higher specificity towards certain substrates than the wild type (Wilderman *et al.*, 2012).

As noted above, the inability to accurately quantify faradiol, arnidiol calenduladiol, and maniladiol in *N. benthamiana* due to potential derivatisation was problematic. Identification of derivatised products using liquid chromatography-mass spectrometry (LC-MS) may be

useful. However, as derivatisation of heterologous compounds by *N. benthamiana* enzymes such as uridine diphosphate (UDP)-glucosyl transferases has been reported to result in numerous products, quantification is likely to remain challenging, and the use of alternative hosts may provide a better option.

Another challenge was the co-elution of the target compounds with background peaks or products of the reaction (**Figure 4.11.**). In the future, alternative compounds with different retention times should be selected, for example, triterpene acids, which elute later than the monols (**Supplementary Figure S3.1.**).

4.5.3 C3 fatty acid acyltransferases are likely to be involved in the production of faradiol palmitate in pot marigold

Similar approaches were used to identify two CoACTs that catalysed the production of faradiol palmitate (**Figure 4.15.**). Interestingly, trace quantities of other triterpene diols FAEs (maniladiol- calenduladiol- and arnidiol- palmitates), but not triterpene monol FAEs (ψ-taraxasterol, taraxasterol, β-amyrin and lupeol - palmitates), were detected in the samples, suggesting high specificity of CoACT1 and CoACT2 for triterpene diols.

A previous analysis of the evolution of ACT (*AWU22320)* from tomato, indicated that sterol and triterpene fatty acid ACTs diverged from a gene duplication event that gave rise to enzymes that add fatty acids to the cycloartenol sterol scaffold (Sun and Shi, 2021). The phylogenetic analysis of ACTs presented in this chapter (**Figure 4.13.**) found that triterpene fatty acid ACTs, including AtTHAA3 and the CoACTs are closely related and the genes encoding them may have arisen by duplication and neofunctionalization of sterol ACTs. Interestingly ACTs that modify triterpene monols (CoACT7) and those that show a preference for diols (CoACT1 and CoACT2) are in distinct subclades, the latter of which has a sister clade containing four genes from common sunflower. This is interesting because common sunflower was also found to encode a ψ-taraxasterol C16 hydroxylase (**Figure 4.6B**). Characterisation of the enzymes from this sister clade may provide insights into whether they modify C16-hydroxylated triterpenes and their substrate preferences.

The overall quantity of faradiol palmitate produced in *N. benthamiana* was small, with minimal depletion of the faradiol substrate (**Figure 4.15.**). This indicates that CoACT1/CoACT2 may express poorly in *N. benthamiana,* have a slow turnover, or that the pool of fatty acids is limiting in this species.

With regard to the fatty acid content, notably, although faradiol myristate, -palmitate and -stearate are all detected in pot marigold, only faradiol palmitate was detected in *N. benthamiana* (**Figure 4.15.**). Thus, to investigate if the fatty acid pool is limiting, they could be co-infiltrated concurrent with pathway expression, as described for the production of novel cannabinoid derivatives (Reddy *et al.*, 2022). Alternatively, transient silencing of an *N. benthamiana* gene encoding beta-ketoacyl-ACP synthase II (KasII), was shown to shift carbon flux from C18 fatty acids to C16, significantly increasing the production of palmitate and wax esters (Aslan *et al.*, 2015), and could be explored to manipulate the fatty acid pool. This, as well as the expression of CoACT1/CoACT2 in the other heterologous hosts, could shed light on what might be limiting factors for the production of faradiol FAEs in *N. benthamiana.*

The experiments also identified CoACT3 as a promiscuous C3 fatty acid acyl transferase that can modify triterpene monols (ψ-taraxasterol, taraxasterol, β-amyrin and lupeol) but not triterpene diols. In the future, it would be interesting to perform structure-function studies to determine what underlies this difference in substrate specificity between CoACT1/2 and CoACT3.

Experiments in this chapter also found that CoCYP716A392 is likely able to hydroxylate ψ-taraxasterol palmitate (**Figure 4.15.**). Thus, there may be two routes to the production of faradiol palmitate. One, in which hydroxylation of ψ-taraxasterol occurs first to make faradiol, which is acylated by CoACT1 and CoACT2 to make faradiol palmate, or the other in which acylation of ψ-taraxasterol occurs first, catalysed by CoACT3 to make ψ-taraxasterol palmitate, and then hydroxylation occurs to make faradiol palmitate. To investigate this, further research is needed.

An alternative hypothesis as to how pot marigold accumulates large quantities (~20 µg/gm dry weight of faradiol myristate and ~11.5 µg/gm dry weight of faradiol palmitate) of faradiol FAEs, compared to how much can be produced in *N. benthamiana* (1 µg/gm dry weight of faradiol palmitate) is that the fatty acid substrates may be concentrated around the enzyme. An early study suggested that triterpene diols and their FAEs are enriched in the floral chromoplasts (Wilkomirski and Kasprzyk, 1979). However, there is no evidence for plastid-targeting sequences on any of the CoACTs or any of the other pathway enzymes. Thus, further studies are required to investigate if TFAEs or their precursors are sequestered into pot marigold chromoplasts. It is unknown how this might occur, but suggestions include

via direct membrane contact between the endoplasmic reticulum (ER) membrane and the chromoplast membrane. This mechanism has been proposed to facilitate the exchange of different lipids and hydrophobic metabolites between organelles (Prinz *et al.*, 2020).

4.5.4 Gene expression of pathway genes through floral development reflects metabolite accumulation

Although genes for some plant metabolites, including triterpenoids, are clustered in plant genomes (Nützmann *et al.*, 2016), faradiol palmitate biosynthetic genes were not co-located (**Figure 4.5.** and **Figure 4.16.**). Further, the expression levels differed through floral development (**Figure 4.17.**).

The expression profile through flower development is partially aligned with the metabolic profile shown in Chapter 3 (**Figure 3.9.**), ψ-taraxasterol FAEs accumulate at the S1 bud, potentially resulting from the activity of CoTXSS and CoACT3. Transcripts of *CoTXSS* are highest at S1 and, although transcripts of *CoACT3* peak later, it was relatively efficient at converting ψ-taraxasterol to ψ-taraxasterol palmitate (**Figure 4.15.**). Further, other acyl transferases that were found to act on ψ-taraxasterol (CoACT4, CoACT5 and CoACT7) could potentially contribute to the accumulation of ψ-taraxasterol FAEs pool.

The accumulation of faradiol and faradiol FAEs between S1 and S3 correlates with the accumulation of transcripts of *CoCYP716A392* and *CoCYP716A393*. The production of faradiol FAEs via hydroxylation of ψ-taraxasterol palmitate is also supported by the observation that co-expression of CoTXSS and CoACT3 leads to the production of the ψ-taraxasterol palmitate, while additional co-expression of CoCYP716A392 leads to the depletion of this peak (**Figure 4.15.**). This finding is consistent with early work in which radioactive labelling was used to show that triterpene monol FAEs are the precursors of triterpene diol FAEs (Wiłckomirski, 1987).

4.5.5 The biological function of faradiol FAEs remains unclear

There are numerous examples in the literature supporting the role of specific hydroxylated and esterified triterpenes in plant defence against biotic and abiotic factors. Often, the genes underlying the biosynthesis of these compounds are upregulated following treatment with MeJA, a hormone involved in mediating defence responses (Morcillo *et al.*, 2022, Wang *et al.*, 2021d, Yang *et al.*, 2022, Yi *et al.*, 2016). In these experiments, treatment with MeJA,

only resulted in the upregulation of one of the pathway genes (*CoACT1*) in ray tissues (**Figure 4.18.**). This indicates a transcriptional activation of pathway genes and provides preliminary evidence that faradiol/faradiol FAEs might have a function in defence. However, further work is required to investigate this.

It is known that induction of some biosynthetic pathways occurs remarkably early (within 1–4 h) after MeJA treatment (Pauwels *et al.*, 2009). Thus, a time course experiment with samples taken more frequently might help to determine if faradiol FAEs pathway genes are upregulated earlier after MeJA treatment and if their expression decreases rapidly after a certain point in time. Further, investigating the impact on the metabolic profile might help to determine if and when the target compounds increase after the application of MeJA. Finally, systems-level analyses, for example, transcriptomics, could be used to investigate if the faradiol palmate pathway is specifically upregulated, or if this is the result of a more general upregulation of secondary metabolism.

If these compounds have a role in defence, it might be expected that they show anti-fungal or anti-bacterial bioactivity. It has previously been shown that methanol and ethanol extracts of pot marigold petals have anti-microbial activity against clinical gram-negative (*E. coli*) and gram-positive (*Bacillus subtilis* (hay bacillus) and *Staphylococcus aureus* (golden staph)) bacteria, and well as fungi from *Candida, Aspergillus and Exophiala* genera (Efstratiou *et al.*, 2012). However, the metabolic profile of these extracts was not reported, and concentrations of triterpenes were unknown. Further, to date, there have been no reports of equivalent studies performed with any plant pathogens. Thus, future studies could investigate (i) the activity of faradiol FAEs against selected plant pathogens and (ii) the gene expression profile of faradiol FAEs pathway genes after the treatment of pot marigold with these pathogens. For this, broad-spectrum pathogens, for example, *Pseudomonas syringae* (bacterial canke) (Xin *et al.*, 2018), or *Phytophthora cryptogea* (foot rot of tomato) (Martin *et al.*, 2012) could be used. In addition, experiments could be done with the necrotrophic fungal, *Sclerotinia sclerotiorum* (cottony rot), which has recently been shown to infect Asteraceae species (Underwood *et al.*, 2022).

Further, if faradiol and its derivatives are defence compounds, they might be protecting the plant from pests or exhibit insecticidal and/or antifeedant activities. A recent review highlighted 102 triterpenoids with insecticidal activity from the Meliaceae family (Lin *et al.*, 2021). This included two pentacyclic triterpenoids, oleanolic and oleanonic acids, from *Cedrela fissilis* (Argentine cedar) , which were tested against *Atta sexdens rubropilosa* (leaf-

cutting ants). Both compounds showed antifeedant activities at 100 µg/mL on this insect, with survival medians (S_{50}) of 6 days and 8 days, respectively (Leite *et al.*, 2005). Thus, in the future, petals of pot marigold, their extracts or individual compounds found in these extracts, might be tested in antifeedant experiments, either by supplementing artificial insect diet as was done for tetranortriterpenoids from *Trichilia pallida* (Simmonds *et al.*, 2001) and triterpenoid saponins from *Diploknema butyracea* (Indian butter tree) and *Sapindus mukorossi* (Indian soapberry) (Saha *et al.*, 2010), or by soaking leaf discs in floral extracts or compounds solutions as was demonstrated for the total ginsenosides contract from *Panax ginseng* (Asian ginseng) (Zhang *et al.*, 2015a). Alternatively, the biosynthetic pathway of faradiol and faradiol FAEs could be expressed in leaves of *N. benthamiana,* which could then be assessed in antifeeding experiments. This latter method was successfully employed for the reconstitution of saponin monoglucosides biosynthesis in *N. benthamiana* and identification of hederagenin monoglucosides as potent insecticides, reducing larval feeding by up to 90% and causing 75% larval mortality (Liu *et al.*, 2019a).

Finally, pathway expression following abiotic stresses such as heat or physical damage could be investigated to gain insights into the biological function of these molecules.

4.6 Conclusion

This chapter describes the identification and characterisation of five pot marigold enzymes involved in the biosynthesis of triterpene fatty acid esters. Two CYPs (CoCYP716A392 and CoCYP716A393) were identified that can hydroxylate ψ-taraxasterol at the C16 position making faradiol, and three fatty acid acyl transferases were identified that can add palmitate to the C3 position of faradiol (CoACT1 and CoACT2) or ψ-taraxasterol (CoACT3). In addition, two enzymes involved in faradiol biosynthesis in field marigold (CaTXSS and CaCYP716A392) were characterised. Structural analysis and site-directed mutagenesis of CoCYP716A392 and CoCYP716A393 revealed amino acids important for their substrate specificity. Further, gene expression analysis through flower development revealed that the expression of *CoTXSS* and *CoACT1/CoACT2* is asynchronous with *CoCYP716A392*, *CoCYP716A393* and *CoACT3.* Finally, relative expression analysis also showed that *CoACT1* was upregulated in response to MeJA treatment, though the biological function of these molecules remains unknown. These findings represent an important advance in elucidating the biosynthesis of anti-inflammatory triterpenes in pot marigold and provide blueprints for access via biomanufacturing.

Chapter 5 - Development and exemplification of virus-induced gene silencing in pot marigold

In Chapter 4, I identified genes encoding two CYPs and two ACTs, involved in the biosynthesis of faradiol palmitate in pot marigold. Although their function was characterised, it is desirable to validate the functions of biosynthetic genes in their native species. To address this, in this chapter, I describe the development of a VIGS method for pot marigold.

5.1 Introduction

Although the Asteraceae family is the largest and most diverse family of land plants, methods for genetic transformation are limited to a few species and were achieved later than in many other families (Darqui *et al.*, 2021). Gene-delivery and/or transformation techniques were first described for species such as *Chrysanthemum morifolium* (chrysanthemum), lettuce, and *Helianthus annus* (common sunflower), which are widely used in agriculture and horticulture (Darqui *et al.*, 2021). For example, the first report of *Agrobacterium*-mediated stable transformation of common sunflower was in 1999, where cotyledons of two-day-old seedlings were infected with a strain of *A. tumefaciens* LBA4404 carrying a plasmid encoding genes for constitutive expression of the *β-glucuronidase* (*GUS*) and *NEOMYCIN PHOSPHOTRANSFERASE* (*NPT II*) genes (Rao and Rohini, 1999). *Agrobacterium*-mediated transformation of lettuce was described in 2007 (Ahmed *et al.*, 2007). More recently, *Agrobacterium*-mediated transformation methods have been developed and optimised for the medicinal plant sweet wormwood to enhance the production of the anti-malarial drug artemisinin (Suhandono and Chahyadi, 2014). That study compared three *A. tumefaciens* strains, showing that the highest frequency of transformation was obtained using AGL1 (70.91%), compared to GV3101 (49.25%) and LBA4404 (45.45%). To date, there is only one report of the genetic transformation of pot marigold, in which *Agrobacterium rhizogenes* was used to initiate so-called hairy root cultures for the production of oleanolic acid glucosides (Długosz *et al.*, 2013).

RNA silencing is a key mechanism for regulating gene expression in eukaryotes. In plants, it occurs through two mechanistically distinct routes: transcriptional gene silencing (TGS) and post-transcriptional gene silencing (PTGS), both of which are mediated by small RNAs (sRNAs) (Zhan and Meyers, 2023, Zhang *et al.*, 2015b). In TGS, non-coding RNA molecules direct the addition of methyl groups to specific nuclear DNA sequences which is

termed RNA-directed DNA methylation (RdDM). DNA methylation patterns in plants are heritable, and one role of RdDM is the transgenerational suppression of transposable elements (Guo *et al.*, 2021). In contrast, PTGS acts on messenger RNAs (mRNAs) and, therefore, is cytoplasm localised.

PTGS is triggered by sRNAs that result either from endogenously encoded miRNA transcripts (pri-miRNAs) or from *trans*-acting small interfering RNAs (siRNA). The latter of these are produced by RdRp, which converts single-stranded RNA into double-stranded RNA (dsRNA). The dsRNAs are cleaved by a protein known as DICER to release small interfering RNAs (siRNAs) initiating silencing (Molnár *et al.*, 2005). The siRNAs are bound by a member of the Argonaute (AGO) protein family and incorporated into the RNA-induced silencing complex (RISC). Once incorporated into RISC, the siRNAs serve as guides to target RNAs with sequence similarity. The target RNAs are then cleaved within the base-paired region (Sheu-Gruttadauria and MacRae, 2017) resulting in RNA degradation (or translation repression), causing silencing (**Figure 5.1.**).

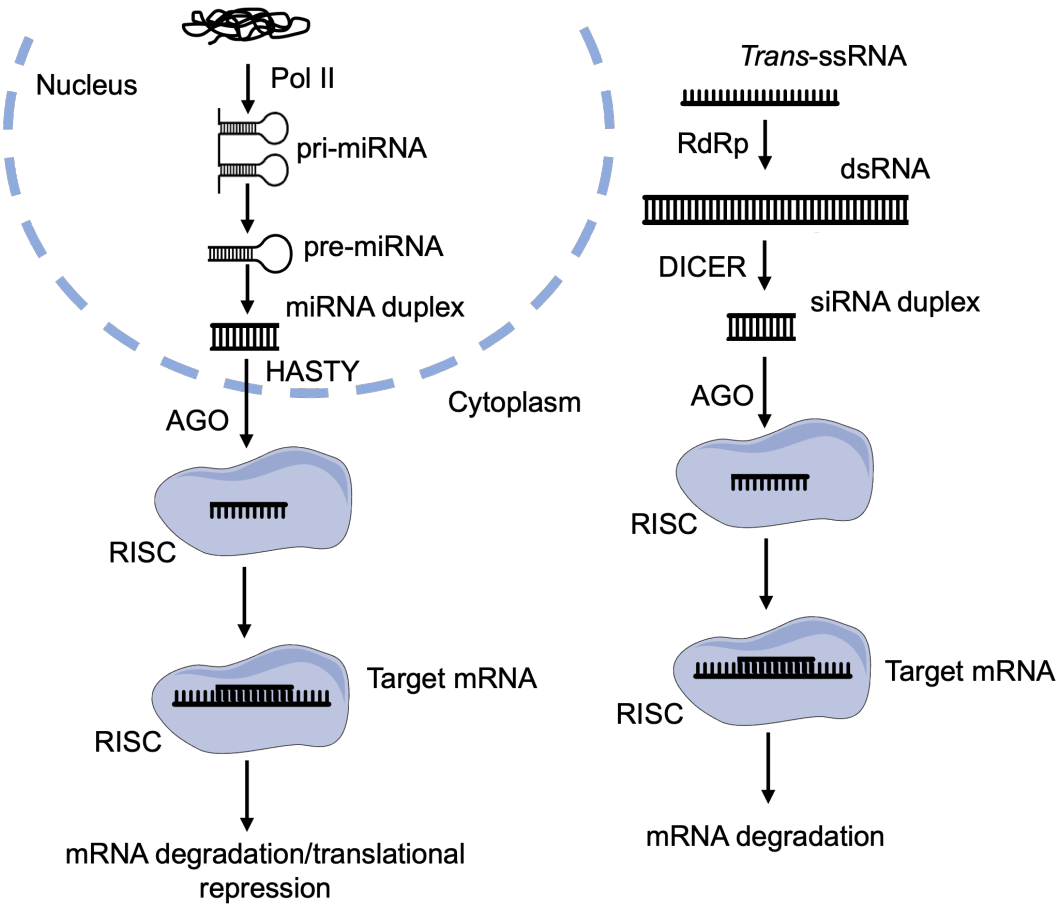

Figure 5.1 Schematic representation of post-transcriptional gene silencing (PTGS). Pri-miRNAs are processed from the genome and form pre-miRNAs. miRNA duplexes are transported from the nucleus to the cytoplasm by the karyopherin family member protein (HASTY). In the cytoplasm, miRNA binds with the argonaute family protein (AGO) and is incorporated into the RNA-induced silencing complex (RISC). The miRNA directs RISC towards complementary mRNAs, causing degradation or translation repression. *Trans* single-stranded RNAs (ssRNAs) are transcribed into double-stranded dsRNAs by RNA-Dependent RNA polymerase (RdRp). DICER proteins slice dsRNAs into siRNA duplexes, which are incorporated into RISC via AGO. siRNAs then direct RISC to target mRNAs for degradation. Figure adapted from (Zhang *et al.*, 2015b).

An important function of PTGS is viral defence. Highly expressed viral transcripts are processed by RdRp, resulting in siRNAs with sequence identity to the virus. This is termed VIGS and has been adapted for the silencing of endogenous genes using viral vectors encoding viral proteins and short (~300 bp) sequences of the target gene (**Figure 5.2**.). VIGS has been used to interrogate gene function in many model and non-model plants including *N. benthamiana* (Kumagai *et al.*, 1995) and other *Solanaceae* (Senthil-Kumar *et al.*, 2007), Arabidopsis (Jupin, 2013), *Gossypium* (cotton) species (Tian *et al.*, 2024), and food crop species such as *Oryza sativa* (rice) (Ding *et al.*, 2007), *Hordeum vulgare* (barley) (Hein *et al.*, 2005), and maize (Wang *et al.*, 2016).

VIGS has been extensively used for *in vivo* characterisation of gene function, including genes involved in biotic and abiotic stress responses, development and metabolism (Zulfiqar *et al.*, 2023). In addition, several studies have reported the use of VIGS for the discovery

and characterisation of genes involved in specialised metabolism, including alkaloid metabolism in Madagascar periwinkle (Caputi *et al.*, 2018, Liscombe and O'Connor, 2011, Yamamoto *et al.*, 2021) and multifunctional CYPs that catalyse sequential three-step oxidation of α-amyrin and β-amyrin to produce ursolic and oleanolic acids in sweet basil (Misra *et al.*, 2017). It has also been employed to study *CYCLOARTENOL SYNTHASE (CAS)* in the cholesterol pathway in tomato (Sonawane *et al.*, 2017). In this study, silencing of *SlCAS* led to a significant decrease in *α*-tomatine, cholesterol, stigmasterol, *β*-sitosterol, isofucosterol and cycloartenol. At the same time, the level of *β*-amyrin, which depends on 2,3-oxidosqualene as a precursor compound, significantly increased in *SlCAS*-silenced leaves.

The efficiency of VIGS in different species depends on several factors, including plant growth conditions, the efficiency of *Agrobacterium* infection, and the ability of the viral vector to infect the host (Zulfiqar *et al.*, 2023). Over the past years, multiple plant viruses (e.g. tobacco mosaic virus (TMV), potato virus X (PVX), and tomato golden mosaic virus (TGMV)) were used to develop viral vectors for VIGS. Of these, tobacco rattle virus (TRV) has the broadest host range, with results reported from a wide variety of angiosperms (Dommes *et al.*, 2019). The TRV VIGS vectors comprise two plasmids: pTRV1, which encodes a viral RdRp, movement protein (MP) and a cysteine-rich protein (SCP), and pTRV2, which encodes a capsid protein (CP) and a multiple cloning site into which sequences with to the target gene(s) are inserted (Senthil-Kumar and Mysore, 2014) (**Figure 5.2.**).

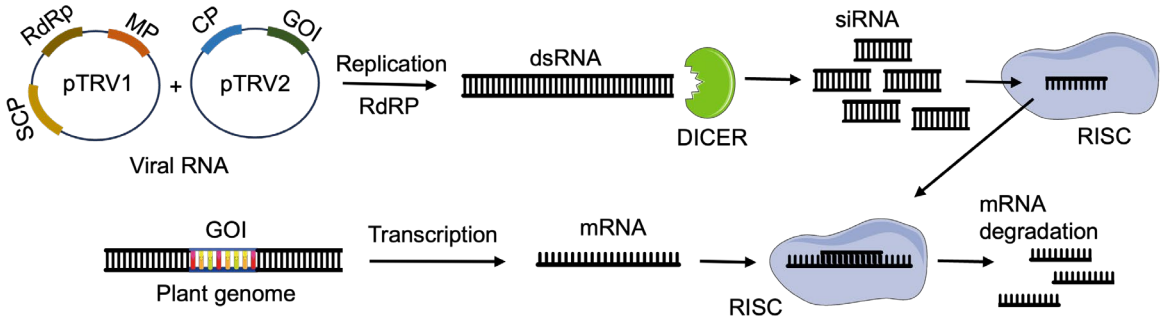

Figure 5.2 VIGS Mechanism. The pTRV1 vector encodes an RNA-dependent RNA polymerase (RdRp), movement protein (MP) and cysteine-rich protein (SCP). The pTRV2 vector encodes a fragment of the target gene and a capsid protein (CP). The viral RNA forms double-stranded RNA (dsRNA), which is recognised by DICER. DICER cleaves the dsRNA into fragments called small interfering RNAs (siRNAs), which are recognised by the RNA-induced silencing complex (RISC). This siRNA guides the RISC complex to transcripts of the target gene(s), which are degraded, preventing translation.

Although VIGS has been shown to be successful in a wide range of plants, in the Asteraceae, there are only three studies that have reported VIGS. One study in *Gerbera hybrida* (African

daisy) silenced *PHYTOENE DESATURASE (PDS)*, *MAGNESIUM-CHELATASE SUBUNIT H (GCHL-H)* and *SUBUNIT I* (*GCHL-I)* genes using a TRV vector (Deng *et al.*, 2012). Another, conducted in 2016, targeted genes encoding hydroxycinnamate-CoA quinate hydroxycinnamoyl transferases (HQT)-like enzymes involved in caffeoylquinic acid synthesis in cardoon (Moglia *et al.*, 2016). Finally, a recent study was conducted to develop robust VIGS in common sunflower (Mardini *et al.*, 2024). In this study several factors that affect the efficiency of VIGS, including the method of agroinfiltration, genotype dependency and mobility of TRV in different tissues were elucidated.

In this thesis, the target biosynthetic pathway genes predominantly show floral expression. To date, there have been a few reports of VIGS applied to floral tissues. For example, VIGS was established and optimised for *Rosa chinensis* (China rose) (Yan *et al.*, 2020). In this study, axillary sprouts were vacuum infiltrated with *Agrobacterium* and the inoculated scions were then grafted back onto the plants and allowed to flower. This way, *DIHYDROFLAVONOL 4-REDUCTASE 1 (DFR1), a* gene involved in the biosynthesis of anthocyanin was silenced using the TRV system. This led to the production of white flowers instead of the original bright pink.

Further, several studies have demonstrated that applying *Agrobacterium* cultures to leaves just beneath developing floral tissues wresults in the migration of the virus into the flowers and facilitates VIGS in floral tissues. For instance, *Agrobacterium* suspensions carrying a VIGS vector were injected into leaves of *Phalaenopsis equestris* (horse moth orchid) just above the inflorescence emergence site. This resulted in the successful silencing of multiple transcription factors and led to changes in floral structures such as sepals and petals (Hsieh *et al.*, 2013). Similarly, leaves of *Cleome violacea* were injected with *Agrobacterium* cultures containing a TRV-based VIGS vector with a fragment of the transcription factor *FRUITFULL (FUL)* gene to investigate fruit development. The silencing of the *CvFUL* led to disruptions in fruit morphology, suggesting that the VIGS had an effect in both leaves and flower tissues (Carey *et al.*, 2021).

Other examples of VIGS in flowers, include the infiltration of Agrobacterium cultures into the leaves of *Petunia hybrida* (petunia) to investigate floral senescence (Chen *et al.*, 2004). Infection with TRV containing a fragment of the *PDS* gene resulted in typical photobleaching of leaf tissues, while infection with TRV containing a *CHALCONE SYNTHASE (CHS)* gene fragment led to a reduction in anthocyanin production in infected flowers, resulting in bleached flowers. Further, infection with TRV containing a tandem

construct that included fragments of both *PDS* and *CHS* resulted in simultaneous photobleaching of leaves and white patterns on the flowers. Later, two other studies also demonstrated efficient silencing of the *PDS* gene in Arabidopsis, which led to bleaching phenotype in both leaf and flower tissues using similar method (Burch-Smith *et al.*, 2006, Pflieger *et al.*, 2008).

Some plant mRNAs are mobile and can move between cells or organs to transmit environmental signals into developmental programs (Luo *et al.*, 2024). For example, the mRNA of *FLOWERING TIME* (*FT*), which encodes for a mobile protein that mediates the onset of flowering (Pin and Nilsson, 2012), was shown to move from leaves to the shoot apical meristem (SAM) through the phloem (Yu *et al.*, 2022). In 2020, (Ellison *et al.*, 2020) used TRV to agroinfiltrate the leaves of transgenic *N. benthamiana* constitutively expressing Cas9 with single guide RNAs (sgRNA) tagged with FT. This enabled sgRNAs to move from the site of infiltration to the SAM and allowed the generation of seeds with heritable CRISPR-induced mutations. In this chapter, the use of FT to improve the efficacy of VIGS in floral tissues is investigated.

5.2 Aims

The aims of this chapter were to:

- Develop a method for *Agrobacterium*-mediated transient expression in pot marigold
- Demonstrate VIGS of endogenous visual maker genes
- Demonstrate VIGS of leaf and flower-expressed OSCs
- Investigate if FT can be used to improve VIGS in floral tissues.

5.3 Contributions by other scientists

Experiments in this chapter were performed in collaboration with Dr. Connor Tansley and Dr. Melissa Salmon, post-doctoral researchers in the Patron lab. All experiments were done by me except that Dr. Tansley developed an improved method for *Agrobacterium*-mediated delivery to pot marigold described in (**methods 2.6.9.**), which I used in subsequent experiments. He also assisted by (i) cloning fragments of the visual control genes *CoPDS* and *CoCHL-H* into pTRV2 and co-infiltrating *N. benthamiana* with these control constructs; (ii) cloning fragments of *CoPDS_CoTXSS* and *CoPDS_CoTXSS_FT* fragments into pTRV2**.** Dr. Salmon assisted with large-scale experiments, providing an extra set of hands for (i) agroinfiltration of pot marigolds in the experiments with dual gene knockdown and (ii) RNA extraction for gene expression analysis.

5.4 Results

5.4.1 Pot marigold is amenable to agroinfiltration

To investigate if pot marigold is amenable to *Agrobacterium*-mediated expression agroinfiltration, an in-house vector encoding a chimeric gene for constitutive expression of firefly luciferase (LucF) was selected: pEPCTαKN001 (CaMV35Sp:LucF:T). This plasmid was used to transform three *A. tumefaciens* strains: GV3101, LBA4404 and AGL1 (**Table 5.1.**). *A. tumefaciens* suspensions (OD600 = 0.8) were then used to infiltrate the leaves of four-week-old pot marigold plants by piercing the leaves using a syringe needle and pushing the cell suspensions into the abaxial surface using a needleless syringe. Four-week-old *N. benthamiana* plants were infiltrated with the same strains. As a positive control for agroinfiltration of pot marigold, constructs with sequences to orthologues of the target genes were used to infect the LAB strain of *N. benthamiana* used in previous chapters, which carries a disruptive insertion in its *Rdr1* gene, weakening its immunity and enhancing its susceptibility to *A. tumefaciens* agroinfiltration (Bally *et al.*, 2015).

Table 5.1. Agrobacterium strains used in this study and their characteristics.

Strains	Chromosomal background	Ti plasmids	Resistance gene
AGL1	C58, *RecA*	pEHA105 (pTiBo542DT-DNA)	rif, carb
LBA4404	*Ach5*	pAL4404	rif, strep
GV3101	C58	pMP90 (pTiC58DT-DNA)	rif, gent

Five days post-infiltration, eight 0.8 cm diameter leaf discs were collected per plant (x3) and luciferase expression was quantified (method 2.7.1). Expectedly, the results showed that, in comparison with *N. benthamiana,* expression was significantly lower in pot marigold (**Figure 5.3.; Supplementary Table S3.4.**). However, compared to control samples (infiltration media), luciferase expression was significantly greater in plants infected with *Agrobacterium* strains (**Figure 5.3.**). For pot marigold, the highest expression level was obtained using *Agrobacterium* AGL1.

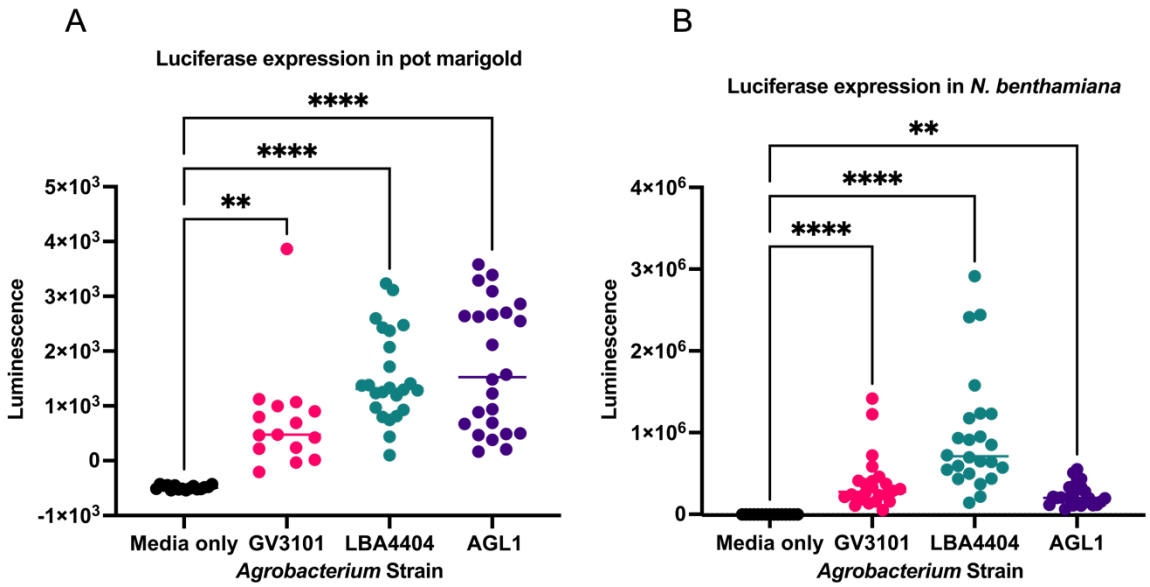

Figure 5.3 Quantification of luciferase expression in (A) *N. benthamiana* and (B) pot marigold. Leaves were infiltrated with three *Agrobacterium* strains (GV3101, LBA4404 and AGL) carrying constructs for constitutive expression of Firefly luciferase (*LucF)*. N=3, except pot marigold GV3101 (N=2). Dots represent eight leaf discs taken from three individual plants. Significant differences in luminescence between leaves discs that we treated with *Agrobacterium* strains and infiltration media were analysed using Kruskal–Wallis with a post-hoc Dunn test; *=p<0.0332, **=p<0.0021, ***=p<0.0002, ****=p<0.0001.

5.4.2 Silencing of *CoPDS* and *CoCHL-H*

5.4.2.1 Two *CoPDS* and three *CoCHL-H* genes were identified in pot marigold

To enable a visual phenotype, the *PDS* gene, which codes for a rate-limiting enzyme in the carotenoid biosynthetic pathway, was selected (**Figure 5.4.**). Silencing of *PDS* results in a bleaching phenotype in many plant species, including Asteraceae (Senthil-Kumar *et al.*, 2007). The *CHL-H* gene, encoding the H subunit of magnesium chelatase, an enzyme involved in chlorophyll biosynthesis (Hiriart *et al.*, 2002) was also selected as silencing has also been reported to result in a bleaching phenotype (Deng *et al.*, 2012) (Liscombe and O'Connor, 2011 (Palmer *et al.*, 2022) (**Figure 5.4.**).

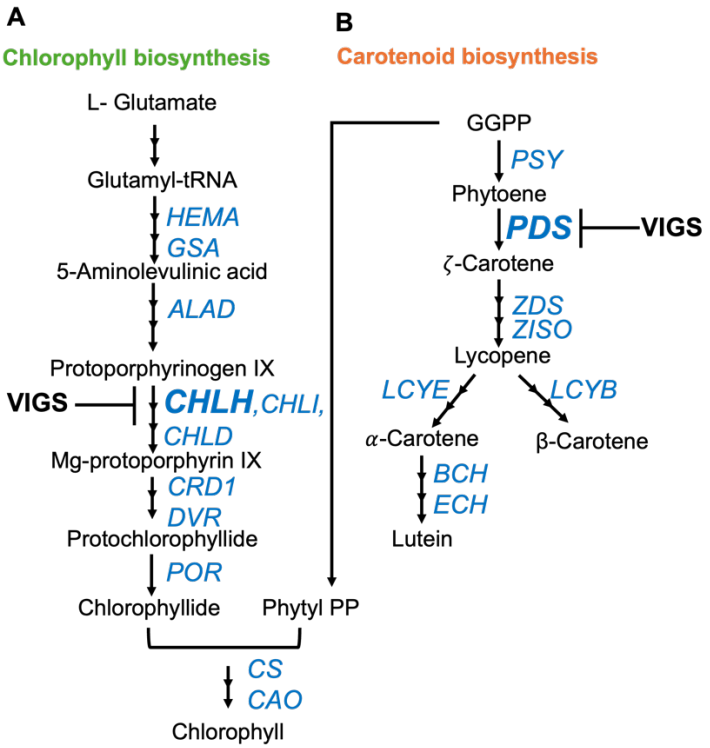

Figure 5.4 Schematic of chlorophyll and carotenoid biosynthesis in plants, showing intermediates and genes. (A) Chlorophyll biosynthetic pathway. *HEMA*=Glu-tRNA reductase; *GSA*=Aminotransferase; *ALAD*=ALA dehydratase, *CHLH*=Mg-cheletase H subunit; *CHLI*= Mg-cheletase I subunit; *CHLD*=Mg-cheletase D subunit; *CRD1*=Cardiolipin synthase; *DVR*=3, 8-divinyl pchlide a 8-vinyl reductase; POR=Protochlorophyllide oxidoreductase; *CS*=Chlorophyll synthase; *CAO*=Chlorophyll *a* oxygenase; **(B)** Carotenoid biosynthetic pathway. *PSY*=Phytoene synthase; *PDS*=Phytoene desaturase; *ZDS*=ζ-carotene desaturase; *ZISO*=ζ-carotene Isomerase; *LCYE*=Lycopene-ε-cyclase; *LCYB*= Lycopene-β-cyclase; *BCH*=β-carotene hydroxylase; *ECH*=ε-carotene hydroxylase. Figure adapted from (Park *et al.*, 2017).

To identify pot marigold *PDS* genes, the *N. benthamiana* gene *NbPDS* (Gene Bank ID: LC543532.1) was used as a query in a BLAST search of the combined multiorgan pot marigold transcriptome. Candidates with at least 80% coverage and pairwise identity were selected. Two candidate *CoPDS* genes were found with 80.7% and 81.0% sequence identity, respectively (**Table 5.2.**). Differential gene expression analysis showed that the *CoPDS_2* gene has a slightly higher expression level in every tissue (leaf, ray and disc) than *CoPDS_1* (**Figure 5.5.**). Both genes were more highly expressed in the ray tissue, compared to leaf and disc tissues.

To identify candidate pot marigold *CHL-H* genes, *Nicotiana tabacum* (common tobacco) *NtCHL-H* (Gene Bank ID: NM_001325713.1) was used as a query in a BLAST search of the pot marigold transcriptome using the parameters described above. Three candidate *CHIL-H* genes were identified (**Table 5.2.**). Phylogenetic analysis with seven previously characterised *CHL-H* genes revealed that all three candidates are closely related to each other and *CHL-H* genes found in other species (**Figure 5.5.**). The differential gene expression

analysis of these candidates showed that all candidates are more highly expressed in leaves than in ray or disc tissues. Further, in leaf tissue, *CoCHL-H_2* and *CoCHL-H_3* show greater expression than *CoCHL-H_1*. All three candidates were used in subsequent analyses.

Table 5.2 Candidate *CoPDS* and *CoCHL-H* genes. E-value denotes the number of hits that could be found by chance. Pairwise Identity (%) denotes the percentage of amino acids identical to the BLAST query. Sequence coverage is the percentage of the query length that aligns with the BLAST hit.

Name	Associated protein/transcript number	Transcript length (bp)	E-value	Pairwise Identity (%)	Sequence coverage (%)
CoPDS_1	585040	1491	0.00E+00	80.7	84.67
CoPDS_2	254110	1493	0.00E+00	81	84.67
CoCHL-H_1	120600	4160	0.00E+00	77.3	90.72
CoCHL-H_2	382320	4157	0.00E+00	77.3	90.63
CoCHL-H_3	261260	4151	0.00E+00	77.7	90.5

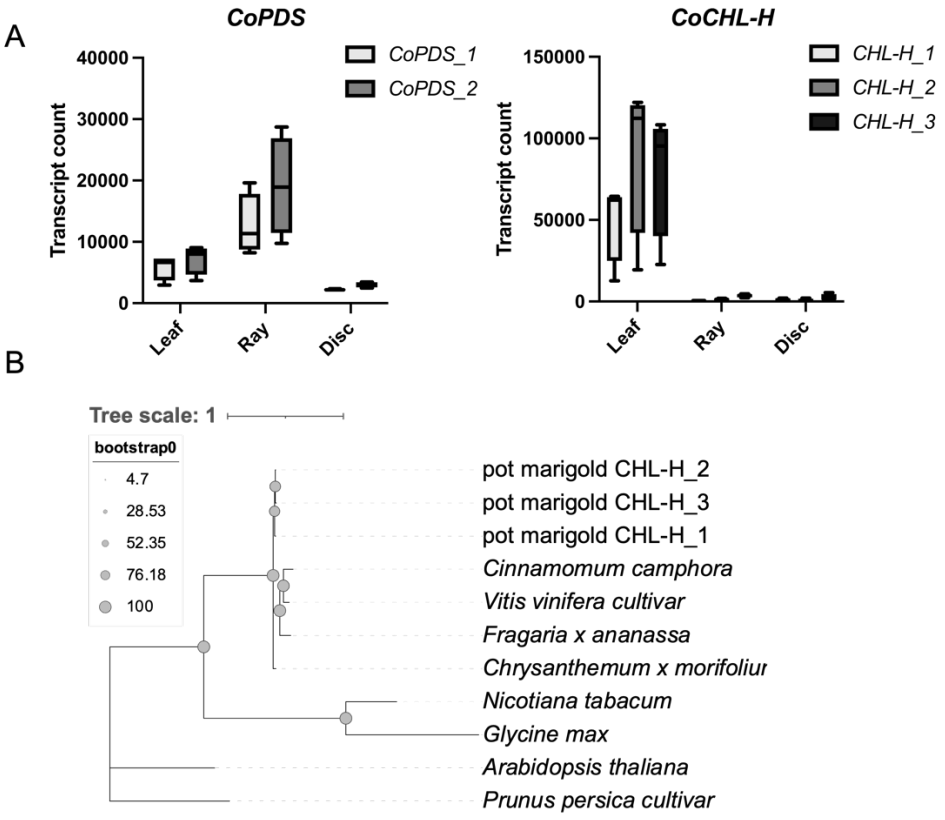

Figure 5.5 Gene expression and phylogenetic analysis of *CoPDS* and *CoCHL-H* candidate genes. (A) Expression levels of candidate *CoPDS* and *CoCHL-H* genes in pot marigold leaf, ray and disc tissues. **(B)** Phylogenetic relationship of *CoCHL-H* candidates and previously characterised *CoCHL-H* genes. *CoPDS* =Pot marigold phytoene desaturase; *CoCHL-H*=Pot marigold H subunit of Mg-chelatase. The scale bar indicates the number of substitutions.

5.4.2.2 Identification of target sequences within *CoPDS* and *CoCHL-H*

Previous studies focused on increasing VIGS efficiency showed that DNA fragments longer than 250 bp help to reduce viral symptoms and are sufficient for silencing target genes (Broderick and Jones, 2014, Wu *et al.*, 2011). To construct VIGS vectors for silencing *CoPDS* and *CoCHL-H*, fragments of 250-300 bp were selected from the CDS sequences. Where possible, regions with a high sequence similarity between two or more candidate genes were selected. For the *CoPDS* genes, a region of 291 base pairs was selected with only one nucleotide difference (**Figure 5.6.A**). As *CoPDS_2* is more highly expressed in leaf and floral tissues, a fragment with 100% identity to *CoPDS_2* was selected and synthesised. No region with ~300 nucleotides of high similarity was identified in the three candidate *CoCHL-H* genes (**Figure 5.6.B**). Thus, three separate 300 bp sequences were designed and synthesised.

Furthermore, empty pTRV1/pTRV2 vectors were shown to cause necrosis, stunting and delaying floral development in petunia (Broderick and Jones, 2014). In that study, the inclusion of 265 and 383 bp fragments of the gene encoding green fluorescent protein (GFP) eliminated necrosis and lesions and nearly eliminated stunting without affecting flowering time. Thus, a 300 bp fragment of the GFP coding sequence was included in the negative or 'empty vector' control (**Figure 5.6.C**).

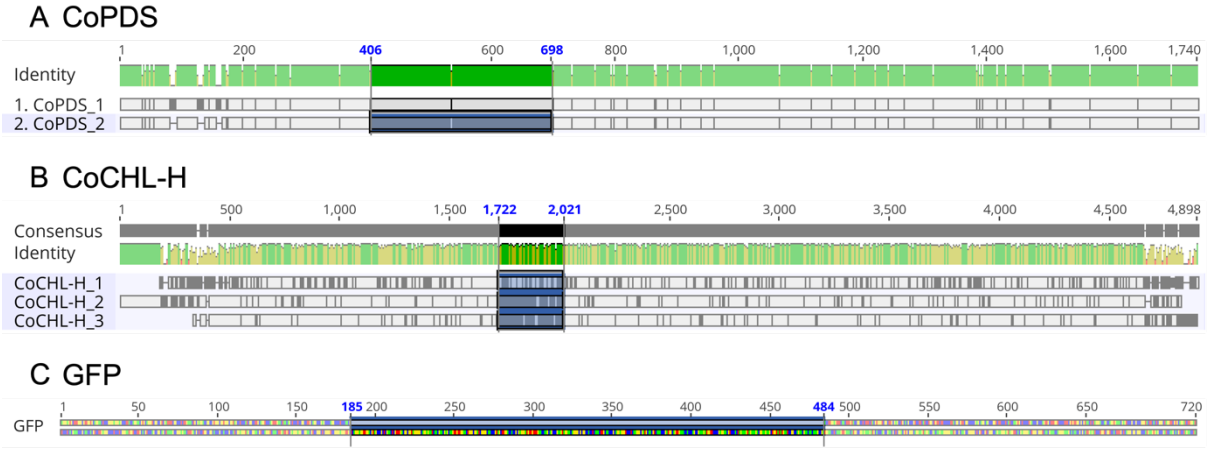

Figure 5.6 Sequence alignment of (A) *CoPDS* and (B) *CoCHL-H* gene candidates. The highlighted region was selected for cloning into the VIGS vector. *CoPDS*=Pot marigold phytoene desaturase; *CoCHL-H*=Pot marigold H subunit of the Mg-chelatase; GFP=green fluorescent protein.

5.4.2.3 VIGS of *CoPDS* and *CoCHL-H* result in bleaching phenotypes

The TRV vector system was selected as it has previously been demonstrated in other Asteraceae species: gerbera, globe artichoke and common sunflower (Deng *et al.*, 2012, Mardini *et al.*, 2024, Moglia *et al.*, 2016).

pTRV1 plasmids, together with pTRV2 plasmids carrying the viral genes and fragments of pot marigold *CoPDS* and *CoCHL-H* were co-infiltrated into the leaves of the 4-weeks-old pot marigold using a method previously described for *N. benthamiana* and *Pisum sativum* (peas) in which the suspension is injected into the midrib and veins (Xiong *et al.*, 2019). pTRV1 plasmids and pTRV2 plasmids with fragments of *NbPDS* or *NbCHL-H* were co-infiltrated into 4-week-old *N. benthamiana* on the same date. Phenotypes of both *N. benthamiana* and pot marigold plants were assessed after three weeks post-infiltration.

In *N. benthamiana*, plants infiltrated with constructs targeting either *NbPDS* or *NbCHL-H* displayed large sectors of white (**Figure 5.7.**), with silencing of *NbPDS* resulting in a more robust bleaching phenotype. In pot marigold, plants infiltrated with constructs targeting *CoPDS_1/2, CoCHL-H_1* and *CoCHL-H_2* showed yellow patches on the leaves. However, the phenotype was not systemic and affected ~30% of leaves (*CoPDS*), or ~1 % and 10% of leaves (*CoCHL-H_1* and *CoCHL-H_2,* respectively). Leaves with constructs targeting *CoCHL-H_3* remained fully green (**Figure 5.7.**). Overall, pot marigold plants infiltrated with *Agrobacterium*-carrying constructs with the *CoPDS* fragment had the strongest phenotype. Thus, *CoPDS* was selected as a visual control in subsequent experiments where the aim was to silence the expression of genes encoding OSCs.

From this experiment, it was also observed that the effects of VIGS began to appear after 14 days post-inoculation in leaf tissue and after 35 days post-inoculation in floral tissue (**Figure 5.7.** and **Figure 5.10.**). Thus, 35 days as a sampling time point was selected for future experiments allowing the virus to spread through the plant and silence the target gene in both tissues. Also, since injection into the midrib and veins was successful, it was used in further experiments.

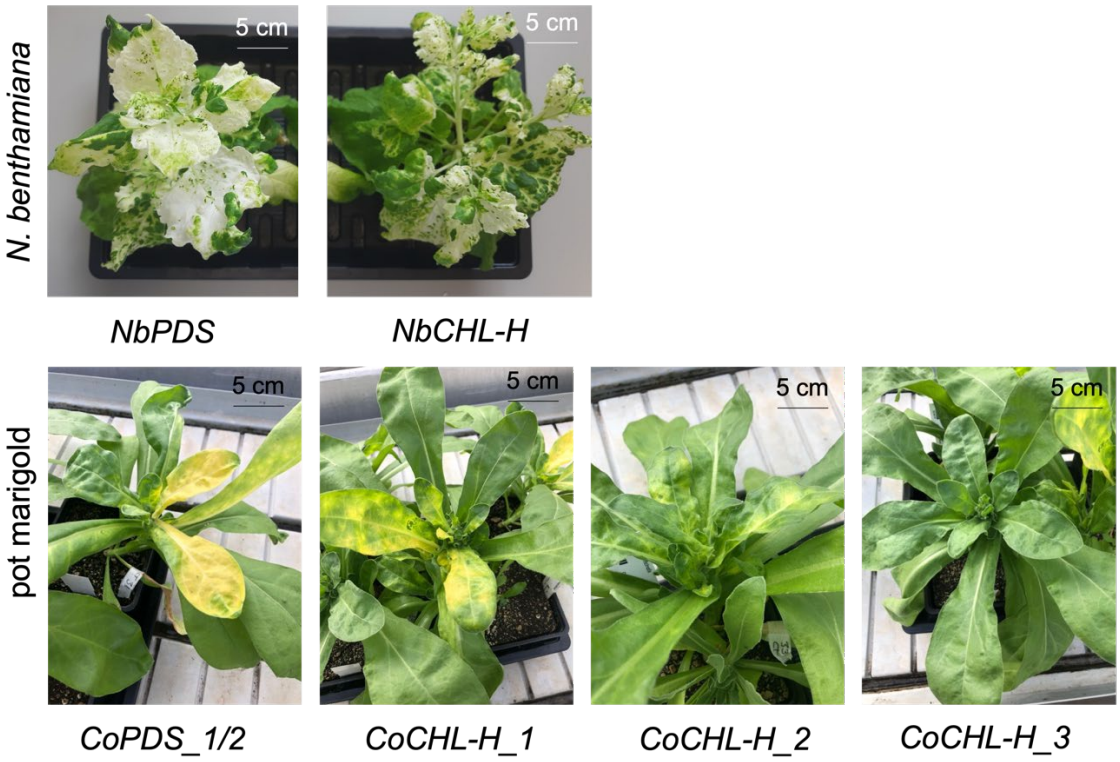

Figure 5.7 Images of N. benthamiana and pot marigold, 38 days after the delivery of VIGS constructs carrying fragments of *PDS* and *CHL-H*. *PDS*=Phytoene desaturase; *CHL-H*=H subunit of the Mg-chelatase.

5.4.3 VIGS of pot marigold OSCs

5.4.3.1 Identification of target sequences within *CoTXSS* and *CoCAS*

The main target gene of this study was *CoTXSS*, an oxidosqualene cyclase that catalyses the production of ψ-taraxasterol, the substrate for the CYPs and ACTs identified in the previous chapter. A 300 bp fragment of CoTXSS was chosen in a variable region, to limit the potential of altering the expression of other OSCs (**Figure 5.8.**).

To enable verification of VIGS of biosynthetic genes in non-floral tissues, a leaf-expressed cycloartenol synthase gene, *CoCAS4,* was additionally selected as a target gene. This enzyme is involved in the biosynthesis of cycloartenol, which is a precursor of molecules such as isofucsterol and sigmasterol (**Figure 5.15.**), which can be detected in extracts of pot marigold leaves and flowers by GC-MS.

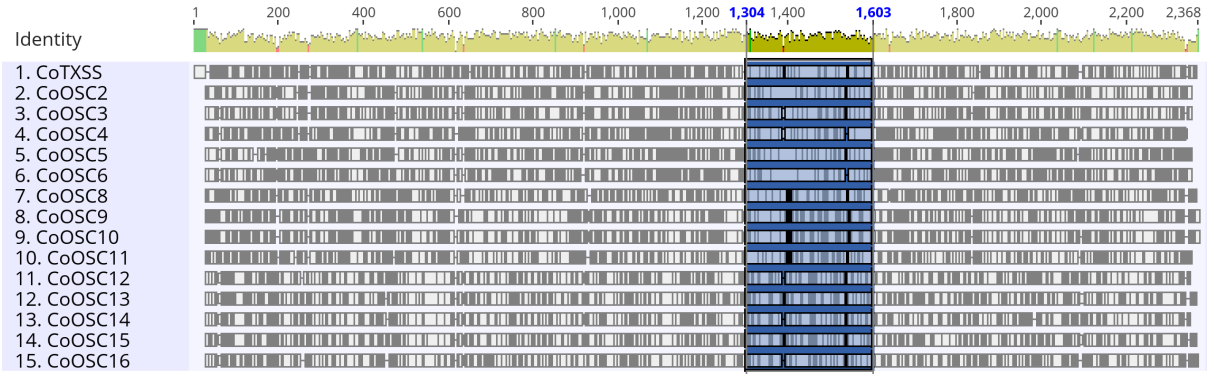

Figure 5.8 Sequence alignment of pot marigold *OSCs* including *CoTXSS*. The highlighted region was selected for inclusion in the VIGS vector. *CoTXSS*=Pot marigold ψ-taraxasterol synthase.

5.4.3.2 Design of dual VIGS vectors to simultaneously target visual control and target genes.

To enable the visual identification of tissues in which the virus is replicating for the target metabolite knockdown assessment, a dual-targeting VIGS vector based on previously reported systems (Palmer *et al.*, 2022, Yamamoto *et al.*, 2021) was developed. Also, to investigate if the use of mobile RNAs could be used to improve the efficiency of VIGS in floral tissues, FT was fused to the RNA fragments of target genes. Target gene fragments were amplified from existing clones or cDNA, and FT was amplified from an in-house plasmid (pEPQDKN0760; Addgene #185629), introducing BsaI sites that generate a four bp overhang complementary to the pTRV2:GG_SP/CM (Addgene #105349) vector plasmid (**Figure 5.9.**). Fragments were inserted using Golden Gate assembly (**methods 2.6.1.**). In total, five constructs were made, each targeting *CoPDS* and a target gene, with or without an FT tag: PDS_TXSS; PDS_CAS; PDS_GFP; PDS_TXSS_FT, and PDS_GFP_FT (**Figure 5.9.**).

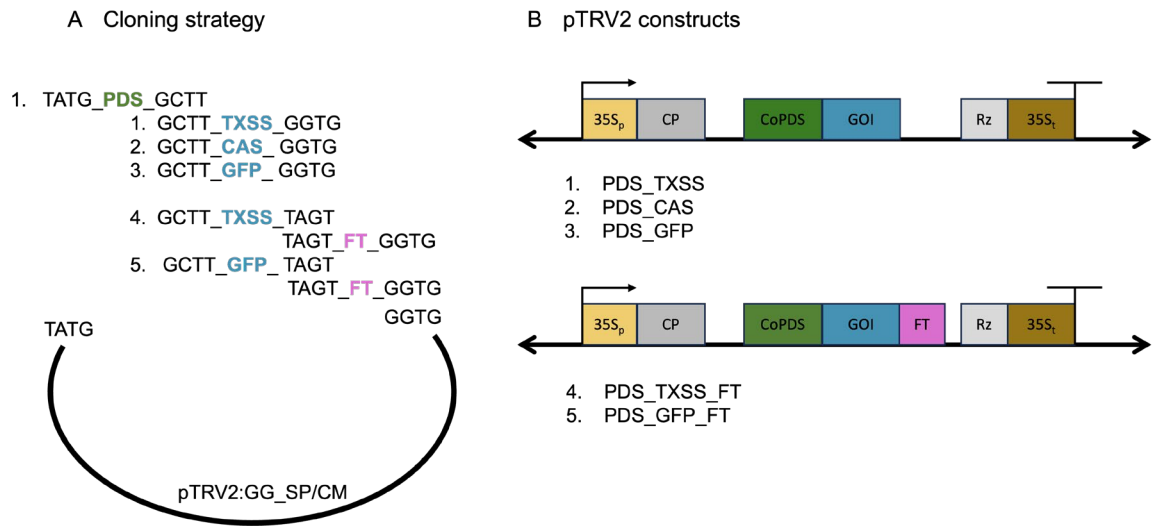

Figure 5.9 Construction of vectors for virus-induced gene silencing (VIGS). (A) Schematic showing the insertion of fragments into the pTRV2:GG_SP/CM vector. Fragments of the target genes are cloned into the BsaI cloning site of the pTRV2 vector together with fragments of CoPDS and FT. **(B)** Schematic of pTRV2 VIGS constructs. $35S_p$=CaMV 35S promoter; CP=coat protein; FT=flowering locus T tag; Rz=self-cleaving ribozyme; $35S_t$=CaMV 35S terminator.

5.4.3.3 Transcripts of *CoPDS* were reduced in the leaves but not the flowers of plants infected with dual knockdown VIGS vectors

To assess the efficiency of dual knockdown vectors in leaf and floral tissues, *Agrobacterium* carrying plasmids with tandem *PDS_GOI* fragments were co-infiltrated into the leaves of 4-weeks-old pot marigold using the agroinfection method described in (**methods 2.6.9.**). After 38 days, leaf and flower samples were collected for analysis of *CoPDS* gene expression using reverse-transcriptase quantitative polymerase chain reaction (RT-qPCR). Floral tissues only showed indications of possible bleaching on a few ray florets and, therefore, two whole flowers were collected at random from each of the four plants infiltrated with each plasmid. Leaves were also sampled at random, except that samples from leaves of VIGS-treated plants were collected from tissues showing a bleached phenotype (**Figure 5.10.**).

Figure 5.10 Representative images of pot marigold plants 38 days after infiltration with VIGS vectors targeting *CoPDS*, in comparison to wild-type plants. *CoPDS*=Pot marigold phytoene desaturase.

First, the presence of the TRV movement protein was confirmed in leaf and floral tissues. For this, total RNA was extracted for three randomly selected leaves and flowers of WT plants and those infected with the 'empty vector' pTRV2 (PDS_GFP) control plasmid. Following cDNA synthesis, the presence of the TRV movement protein was assessed using PCR and gel electrophoresis. A band of the expected size (759 bp) was detected in replicate samples of leaf and floral tissues of plants infected with the empty vector control pTRV2 (PDS_GFP) but not in wild type plants (**Figure 5.11.**).

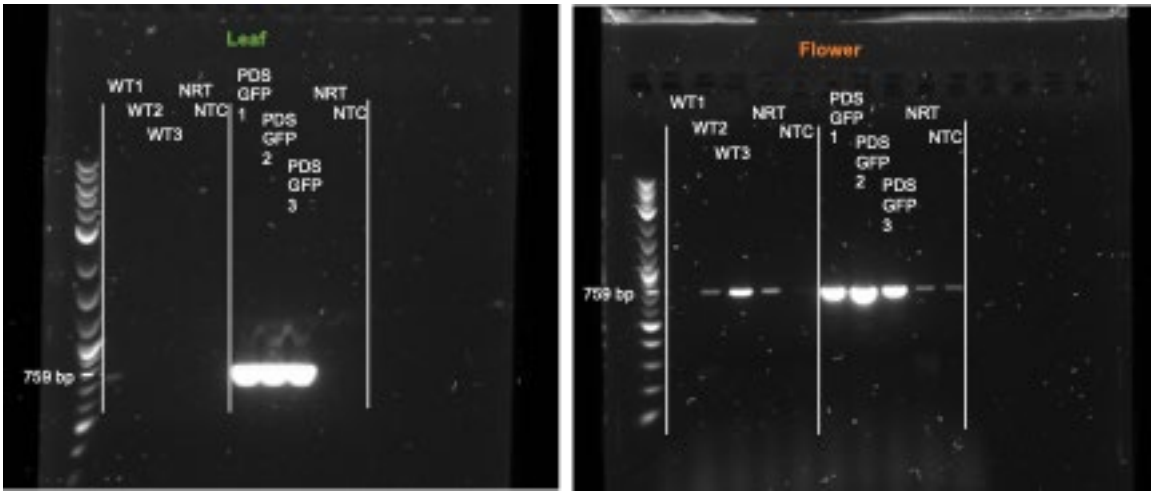

Figure 5.11 Agarose gel electrophoresis (1% agarose) of amplicons of the TRV movement protein gene from leaves and flowers of pot marigold. WT=Wild type; NRT=No reverse transcriptase control; NTC=No template control; PDS_GFP=Plants infected with *Agrobacterium* carrying empty vector control plasmid pTRV2 (PDS_GFP).

To verify that the *CoPDS* transcript was reduced in regions of the leaf in which the bleaching phenotype was observed, gene expression was quantified using RT-qPCR. This analysis revealed that *CoPDS* transcripts were significantly reduced in the leaves of plants infected with VIGS vectors containing an empty pTRV2 vector (PDS_GFP) with fragments of the *CoPDS* and *GFP* genes in comparison to wild-type plants. However, the expression of *CoPDS* was not reduced in the flowers (**Figure 5.12.**; **Supplementary Table S3.4.**).

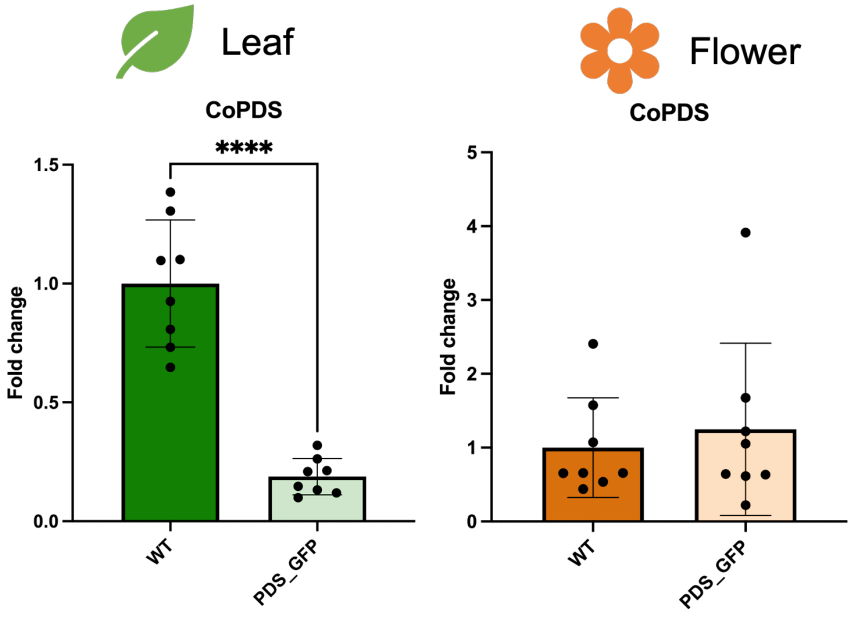

Figure 5.12 Gene expression analysis of *CoPDS* in pot marigold plants infiltrated with VIGS vectors. Graphs show the Ct values (fold change) from reverse-transcriptase quantitative PCR (RT-qPCR) analyses of plants infiltrated with VIGS vectors encoding a fragment of the *CoPDS* gene compared to plants infiltrated with an empty vector control (PDS_GFP), normalised to non-infected wildtype plants (WT). Bars show the mean of 8 biological replicates. Error bars show the standard error of the mean. Significant difference in Ct values between empty vector treatment and WT control analysed using T-test. *=p<0.0332, **=p<0.0021, ***=p<0.0002, ****=p<0.0001.

5.4.3.4 VIGS of *CoCAS*

5.4.3.4.1 Transcripts of *CoCAS* were reduced in the leaves but not the flowers of plants infected with VIGS vectors

First, the relative expression of *CoCAS* in plants infected with *A. tumefaciens* containing a pTRV2 vector encoding fragments of *CoPDS* and *CoCAS* was compared to lines infected with the empty vector control, revealing a significant reduction in expression (**Figure 5.13.; Supplementary Table S3.4.**). Although there was a slight reduction in *CoCAS* expression in floral tissues, it was not statistically significant compared to control samples, where only *CoPDS* was silenced.

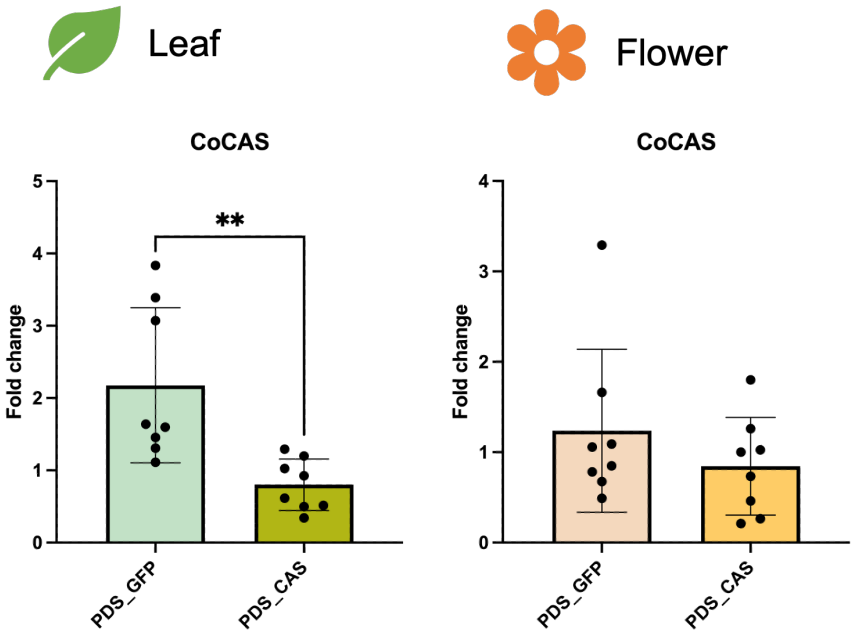

Figure 5.13 Gene expression analysis of *CoCAS* in plants infiltrated with VIGS vectors. Graphs show the Ct values (fold change) from reverse-transcriptase quantitative PCR (RT-qPCR) analyses of plants infiltrated with VIGS vectors encoding a fragment of the *CoPDS* and *CoCAS* genes (PDS_CAS) compared to plants infiltrated with an empty vector control (PDS_GFP), normalised to empty vector control. Bars show the mean of 8 biological replicates. Error bars show the standard error of the mean. Significant difference in Ct values between PDS_CAS treatment and empty vector control was analysed using T-test. *=p<0.0332, **=p<0.0021, ***=p<0.0002, ****=p<0.0001.

5.4.3.5 VIGS of *CoTXSS* gene

5.4.3.5.1 The addition of the FT aids VIGS in floral tissues

To examine gene silencing in floral tissues, the expression of *CoPDS* and *CoTXSS* was compared in plants infiltrated with VIGS constructs targeting these genes with ((PDS_GFP_FT) and (PDS_TXSS_FT)), or without ((PDS_GFP) and (PDS_TXSS)) the

inclusion of the flowering time (FT) tag. RNA was extracted from two randomly selected flower heads of each plant (x4). As previously, no visual phenotype was observed.

As above, there was no statistically significant difference in the expression level of *CoPDS* expression level compared to the plants infiltrated with the empty vector control (PDS_GFP) control or plants infiltrated with (PDS_TXSS) (**Figure 5.14.; Supplementary Table S3.4.**). Similarly, there was no statistically significant difference in the expression level of *CoPDS* in plants infected with the equivalent vectors containing an FT tag (PDS_GFP_FT) and (PDS_TXSS_FT) (**Figure 5.14.; Supplementary Table S3.4.**). Plants infiltrated with the vectors to silence *CoTXSS* (PDS_TXSS) without an FT tag did not show a significant reduction in *CoTXSS* expressions, however, those with the FT tag (PDS_TXSS_FT) showed a significant reduction in *CoTXSS* expression in comparison to flowers of plants infected with the empty vector control (PDS_GFP_FT) (**Figure 5.14.; Supplementary Table S3.4.**). There was also a significant difference in *CoTXSS* expression between plants infected with constructs that included FT (PDS_TXSS_FT) and without FT (PDS_TXSS) (**Figure 5.14.; Supplementary Table S3.4.**).

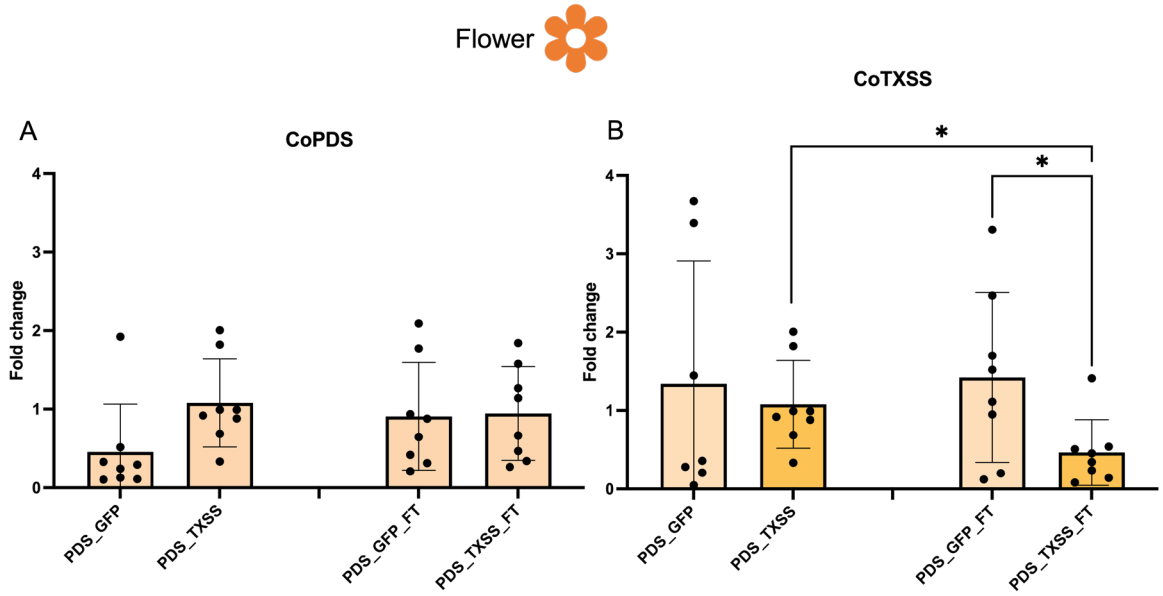

Figure 5.14 Gene expression analysis of *CoPDS* and *CoTXSS* in flowers of pot marigold infiltrated with VIGS vectors. Graphs show the Ct values (fold change) from reverse-transcriptase quantitative PCR (RT-qPCR) analyses of (A) CoPDS and (B) CoTXSS in plants infiltrated with VIGS vectors encoding a fragment of CoPDS and/or CoTXSS compared to plants infiltrated with an empty vector control (PDS_GFP), normalised to empty vector control. Bars show the mean of 8 biological replicates. Error bars show the standard error of the mean. Significant difference in Ct values between PDS_TXSS or PDS_TXSS_FT treatments and empty vector control was analysed using T-test. *=p<0.0332, **=p<0.0021, ***=p<0.0002, ****=p<0.0001.

5..4 Additional Relevant Results

Due to time limitations, I was unable to perform metabolic profiling of plants infiltrated with VIGS constructs. Metabolite extraction and GC-MS analysis were completed by Dr. Tansley, who showed that bleached leaf tissues from plants transfected with VIGS vectors containing fragments of *CoPDS* and *CoCAS* showed a statistically significant decrease in stigmasterol content and a significant increase in the level of isofucosterol. Levels of campesterol and stigmast-5-ene remained unchanged. In floral tissues, there were no significant differences in any of these four metabolites. Further, silencing of *CoPDS* and *CoCAS* led to a significant increase in ψ-taraxasterol in floral tissues, but no difference in the content of α-amyrin, β-amyrin, or lupeol. Surprisingly, silencing *CoPDS* and *CoTXSS* with FT tag resulted in a significant increase in the content of ψ-taraxasterol, faradiol myristate, faradiol palmitate, α-amyrin, β-amyrin, stigmasterol and isofucosterol in floral tissues. Without an FT-tag, significant changes were only found in stigmasterol and isofucosterol.

5.5 Discussion

VIGS is a powerful method for studying the function of newly discovered genes or validating the candidate genes. Thus, in this chapter, I explored (i) the amenability of pot marigold to *Agrobacterium*-mediated transformation, (ii) the identification of control genes with visual phenotypes for VIGS, and (iii) the applicability of this method for silencing *OSC*s expressed in leaf and floral tissues.

5.5.1 A method for agroinfiltration of pot marigold

Agroinfiltration of pot marigold with constitutively expressed reporter constructs expectedly resulted in lower levels of *LucF* expression compared to *N. benthamiana*. However, all *A. tumefaciens* GV3101, LBA4404, and AGL1 were able to deliver T-DNAs encoding LucF, indicating that pot marigold can be infected by all three strains (**Figure 5.3.**). Overall, there was little difference in luminescence between strains, but slightly higher levels were observed for AGL1 and LBA4404 compared to GV3101. AGL1 has a similar chromosomal background to the wild-type strain C58, containing a 2.8-Mb circular and a 2-Mb linear chromosome plus the pTiBo542 Ti plasmid and the 0.54-Mb pAtC58 accessory plasmid (De Saeger *et al.*, 2021). The main difference between the GV3101 and AGL1 strains is the

presence of hypervirulent Ti plasmid, pTiBo542, carrying additional *vir* genes in the case of AGL1 (Jones *et al.*, 2005). A higher efficiency of transformation with strains containing pTiBo542 plasmid has been observed in both dicots (Dönmez *et al.*, 2019, Komari, 1990) and monocots (Chen *et al.*, 2004). Further, AGL1 carries an insertion mutation in its *recA* general recombination gene (Lazo *et al.*, 1991), which may also impact plasmid integrity and therefore efficiency of transformation.

A. tumefaciens LBA4404 has an Ach5 chromosomal background, which is also similar to C58, consisting of a 2.8-Mb circular chromosome, a 2-Mb linear chromosome, a 0.2-Mb Ti pAL4404 plasmid, and a 0.55-Mb megaplasmid (De Saeger *et al.*, 2021). This strain has also been shown to be efficient for dicot transformation (Petti *et al.*, 2009), showing a three-fold greater backbone integration compared to *A. tumefaciens* AGL1 in potato. Overall, based on the result of the experiment, *A. tumefaciens* AGL1 was taken and used in the subsequent VIGS experiments.

In the future, agroinfiltration of pot marigold could be improved. For example, a recent study (Mardini *et al.*, 2024) in common sunflower investigated factors that affect silencing efficiency, including plant growth stage and method of agroinfiltration. They infiltrated plants with syringes, rubbing or using a vacuum at the third true leaf stage, two-day-old sprouts, or seeds. This research identified vacuum infiltration of common sunflower seeds as the best method for VIGS. Following this, they explored the length of co-cultivation on VIGS efficacy, establishing that 6 h of co-cultivation with *A. tumefaciens* was optimal (Mardini *et al.*, 2024).

Further, treatments of both *Agrobacterium* and plants before infiltration could be explored. For instance, culturing *Agrobacterium* with acetosyringone, which is known to induce the expression of virulence genes, has been shown to improve the agrotransformation efficiency of a commercially used rootstock ‘Carrizo’ citrange (*Citrus sinensis* × *Poncirius trifoliata*) (Li *et al.*, 2022b), *Eustoma grandiflorum* (prairie gentian) (Nakano, 2017), and *Tamarix hispida* (Kashgar tamarisk) (Zhao *et al.*, 2020a). Similarly, the use of surfactants was explored in common sunflower (Suhandono and Chahyadi, 2014). Researchers demonstrated that two organosilicon surfactants (Silwet L-77 and Silwet S-408) enhanced the transient expression of *GUS*.

Finally, comparatively poor VIGS has previously been reported in floral tissue compared to leaves (Yan *et al.*, 2020). VIGS may be affected by sampling date as the reported optimal

date for sampling leaf tissues following VIGS varies by species: 12 days post-infection for *Triticum aestivum* (bread wheat) (Scofield *et al.*, 2005), *Antirrhinum majus* (snapdragon) and *Misopates orontium* (linearleaf snapdragon) (Tan *et al.*, 2020); 10 days post-infection for several cotton cultivars (Gao *et al.*, 2011); and 5-6 weeks post-inoculation for Arabidopsis. However, a long delay between agro-inoculation and flowering was reported to lead to attenuated efficiency of gene silencing in flowers (Yan *et al.*, 2020). An alternative method was proposed for China rose plants, in which axillary sprouts were excised and vacuum infiltrated with *Agrobacterium*. The inoculated scions were then grafted back onto the plants and allowed to flower. Silencing phenotypes were then observed within 5 weeks, post-infiltration, compared to about 34 days with traditional agroinfiltration methods (Yan *et al.*, 2018). These strategies could be explored in pot marigold.

5.5.2 Challenges of silencing *CoPDS* and *CoCHL-H* in pot marigold

Two *CoPDS* and three *CoCHL-H* genes were identified in the pot marigold transcriptome dataset and used as targets for VIGS silencing (**Figure 5.5.**). This experiment showed that the expected bleaching phenotype could be observed in plants infected with VIGS vectors targeting *CoCHL-H_1* and *CoCHL-H_2*. However, the phenotype was not systemic (**Figure 5.10.**). In the case of *CoCHL-H*, this might be an indication of metabolic compensation by other *CoCHL-H* genes since, in each of the given plants, only one *CoCHL-H* gene was silenced. Thus, in future research, simultaneous silencing of *CoCHL-H_1* and *CoCHL-H_2* might achieve a more robust phenotype. This could be done by either co-infiltration of the two plasmids tested here, or by dual VIGS vector containing a fusion of *CoCHL-H_1*and *CoCHL-H_2*. A bleaching phenotype was not observed in plants infected with VIGS vectors targeting *CoCHL-H_3*, an indication of either strong compensation, or a different function for this gene **Figure 5.10.**). In contrast, it is likely that, because of the high sequence similarity between two *CoPDS* genes, one VIGS construct may have silenced transcripts from both *CoPDS* genes, resulting in phenotype on about 30% of leaves. *CoPDS* was therefore selected as a visual control marker for subsequent experiments in which the silencing of *OSCs* was attempted.

Bleaching phenotypes were extremely limited in floral tissues. From the phenotype alone, this could be an indication of the low efficiency of VIGS in floral tissues, or due to the difficulty of observing this phenotype in these tissues. While analysis indicated the presence of virus in the floral tissues (**Figure 5.11.**), qPCR analysis showed that *CoPDS* expression level correlates with the level of the bleaching phenotype (**Figure 5.12.**). This indicates the

inefficiency of VIGS in floral tissues rather than an inability to observe the phenotype in floral tissues.

To improve the efficiency of VIGS in pot marigold floral tissues, it may be worth exploring viruses that have been shown to be effective in other species. For example, A cucumber mosaic virus (CMV)-derived VIGS vector was demonstrated in Arabidopsis, snapdragon, and *N. benthamiana*. Similarly, a PVX-based VIGS vector was developed for *Nicotiana and Solanum* species (Faivre-Rampant *et al.*, 2004, Lacomme and Chapman, 2008).

Alternative visual marker genes involved in the biosynthesis of floral pigments could also be targeted. For example, *CHS* was targeted in the leaves of Arabidopsis, snapdragon, and *N. benthamiana* (Inaba *et al.*, 2011). This gene codes for the first key enzyme in flavonoid biosynthesis, which catalyses the synthesis of naringenin chalcone from three molecules of 4-malonyl-CoA, and one molecule of p-coumaroyl CoA (Tanaka *et al.*, 2008). This gene has been targeted in floral tissues, limiting anthocyanin production in flowers of petunia, resulting in bleaching phenotype (Broderick and Jones, 2014, Chen *et al.*, 2004). Further, in African daisy, VIGS of *CHS* resulted in one out of three inflorescences showing milky white petals compared with the original bright purple (Deng *et al.*, 2014). Other genes involved in anthocyanin production could also be explored; China rose *DFR1*, involved in the biosynthesis of anthocyanin in China rose flowers, was silenced to produce a bleached phenotype (Yan *et al.*, 2018). The efficiency of this method was further improved in 2020, with 46% of flowers showing effects of silencing compared to 10–30% with the previously reported method (Yan *et al.*, 2020).

Pot marigold accumulates at least 39 known flavonoid glycosides, including anthocyanins, among which cyanidin derivatives are predominant (Olennikov and Kashchenko, 2013). Thus, targeting *CHS* or *DFR1* could be explored to achieve a more robust silencing phenotype. Pot marigold flowers are also rich in carotenoids, which are found in both free and esterified forms (Olennikov and Kashchenko, 2013). Although lutein is the most abundant carotenoid, approximately a hundred different carotenoids have also been identified. Thus, similarly to *PDS*, other genes in the carotenoid biosynthetic pathway, such as *PSY* could be considered as future targets for visual markers of silencing.

Finally, indirect markers could be used to guide the harvesting of plant tissues. As recently shown, the presence of TRV is not limited to tissues with observable silencing events

(Mardini *et al.*, 2024). An indirect marker such as chlorophyll/carotenoid content could be a useful indication of silencing. This strategy of quantifying chlorophyll content in leaf tissues was used to assess *PDS* silencing efficiency in Arabidopsis (Burch-Smith *et al.*, 2006). In floral tissues, carotenoid content could be equivalently used for assessing *PDS* silencing.

5.5.3 Challenges of biosynthetic gene silencing in floral tissues

In the next step, the *CoCAS* gene was selected as a control *OSC* as it is more highly expressed in leaf tissues than in ray or disc tissues. In these experiments, a fragment of *CoPDS* was fused to a fragment of *CoCAS* to enable the simultaneous silencing of both genes. As above, the plants developed persistent but non-systemic bleaching of leaf tissues but extremely limited bleaching of floral tissues, with only a couple of petals becoming fully white. Consistent with the data obtained for *CoPDS*, there was a reduction in the expression in leaf tissues but not in flowers (**Figure 5.12.**).

Metabolic analysis of these plants, performed subsequently by Dr Tansley, found a decrease of ~20% in stigmasterol and ~10% in stigmast-5-ene content, plus an increase of ~50% in isofucosterol and campesterol. *CoCAS* is a key gene in plant sterol biosynthesis, which catalyses the conversion of 2,3-oxidosqualene to cycloartenol (Silvestro *et al.*, 2013) (**Figure 5.15.**). The pathway then branches off to make campesterol and isofucosterol from 24-methylene lophenol. Isofucosterol then gives rise to sitosterol, which is further converted to stigmasterol and stigmast-5-ene (**Figure 5.15.**). Insistingly, silencing of the *CoCAS* gene led to an increased level of isofucosterol, a precursor compound to stigmasterol and stigmast-5-ene, of which levels decreased. From this, it could be suggested that *CoCAS* knockdown results in compensation by other enzymes in the pathway (e.g. sterol C24 methyltransferase (SMT2)) (**Figure 5.15.**). The relationship between genes in the pathway could be investigated by combinatorial knockdown of different pathway steps and subsequent metabolic profiling.

Consistent with a previous study (Sonawane *et al.*, 2017), where silencing of the *CAS* gene led to a decrease in sterol content and a simultaneous increase in β-amyrin content in tomato leaves, we found a significant increase in both α-amyrin and β-amyrin. This could indicate that *CoCAS* silencing leads to increased availability in precursor compound 2,3-oxidosqualene, which is directed towards triterpene biosynthesis. Further, a decrease in the availability of cycloartenol could unpredictably affect the regulation of upstream and

downstream genes in the pathway. For example, it has been shown before that secondary metabolites are often under feedback control by pathway intermediates or products (Li *et al.*, 2024b). In future, it will be worthwhile investigating the expression levels of other genes involved in sterol biosynthesis (*3-HYDROXY-3-METHYLGLUTARYL-COA REDUCTASE (HMGR), STEROL C24 METHYLTRANSFERASEs* (*SMT1* and *SMT2*)) and triterpene biosynthesis (other *CoOSCs*) in wild-types and VIGS plants to gain a better insight into feedback control and flux through these pathways (**Figure 5.15.**).

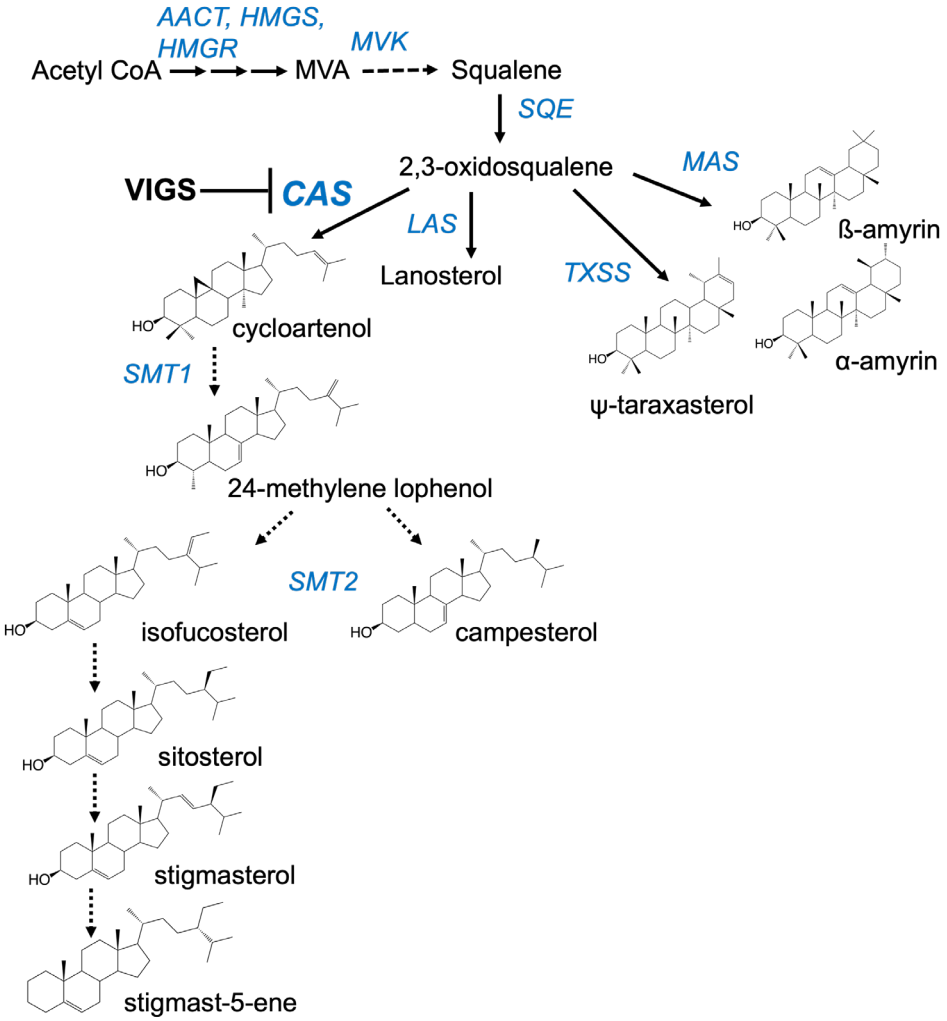

Figure 5.15 Sterol biosynthesis in plants, showing intermediates and genes. Figure adapted from (Silvestro *et al.*, 2013). *AACT*=Acetyl CoA acetyltransferase; *HMGS* =3-hydroxy-3-methylglutaryl-CoA synthase; *HMGR*= 3-hydroxy-3-methylglutaryl-CoA reductase; *MVK*=Mevalonate kinase; *SQE*=Squalene epoxidase, *CAS* =Cycloartenol synthase; *LAS*=Lanosterol synthase, *SMT*=Sterol C-24 methyltransferase; MAS=Mixed amyrin synthase; TXSS=ψ-taraxasterol synthase.

Finally, the use of a FT tag was investigated to determine if it could improve VIGS in floral tissues. In this set of experiments, two sets of constructs were compared. The first set included a tandem fusion of fragments of *CoPDS* and *CoTXSS*, and an empty vector control (*CoPDS_GFP*), while the second set of constructs included a tandem fusion of *CoPDS* and *CoTXSS* and *FT,* and an equivalent empty vector control (*CoPDS_GFP_FT*). Gene

expression analysis of plants infected with these constructs showed that the *CoPDS* gene was not significantly silenced in the flowers (**Figure 5.14.**). However, *CoTXSS* expression was significantly reduced in plants infected with *A. tumefaciens* carrying a plasmid with *CoPDS_CoTXSS_FT*. Although it is difficult to be conclusive about why floral expression of *CoTXSS* but not *CoPDS* was reduced, it may simply be due to the inefficient and stochastic movement to floral tissues.

At the metabolite level, plants infected with *CoPDS_CoTXSS_FT* also showed an increase in ψ-taraxasterol, faradiol myristate and faradiol palmitate as well as stigmasterol, isofucosterol, α-amyrin and β-amyrin. This again suggests the potential for feedback regulation, where a decrease in *CoTXSS*, leads to the upregulation of other biosynthetic genes (Erb and Kliebenstein, 2020, Li *et al.*, 2024b). However, the increase in ψ-taraxasterol is difficult to explain; previous work in Patron laboratory by Dr. Salmon identified that while pot marigold encodes a multifunctional amyrin synthase that produces a small quantity of taraxasterol, no other enzymes were identified that produce large quantities of ψ-taraxasterol. To investigate these changes to metabolite content, the gene expression levels of all pathway genes, as well as genes in the upstream pathway, and genes encoding enzymes that compete for these precursors need to be assessed. Lastly, it is worth mentioning that, although the fragment used to silence *CoTXSS* was selected from a region that varied from other *OSCs*, there is still a risk that it may have affected the expression of other genes.

5.5.4 VIGS methodology improvement

Future improvements to VIGS could include optimisation of the timing of tissue harvesting and plant growth conditions. In these experiments, leaf and floral tissues were sampled after 38 days post-infiltration. This time was selected following initial experiments in which the bleaching phenotype was observed to peak.

However, in the future, an improved strategy to determine the optimal harvesting time could be the conduction of a time course experiment in which gene expression in different tissues is monitored, a similar experiment was performed in *Panicum virgatum* (switchgrass) (Tiedge *et al.*, 2022). Further, in Madagascar periwinkle, successful infiltration of the VIGS plants was confirmed by the detection and monitoring of pTRV2-derived TRV coat protein transcript using qPCR, (Liscombe and O'Connor, 2011). Moreover, it has been shown that VIGS is affected by plant growth conditions and can vary depending on photoperiod, humidity, and temperature (Burch-Smith *et al.*, 2006, Fei *et al.*, 2021, Fu *et al.*, 2006). Thus,

these experiments may have been influenced by variable conditions in the summer glasshouse in which plants were grown, as temperature and day length were not controlled. Growth in controlled conditions was used for experimental variation in VIGS of potato, *Papaver somniferum* (opium poppy) (Chen *et al.*, 2020b), *Styrax japonicus* (Japanese snowbell) (Sun *et al.*, 2024a), *Nicotiana attenuata* (coyote tobacco), *Solanum nigrum* (nightshade) (Galis *et al.*, 2013) and other species (Arce-Rodríguez and Ochoa-Alejo, 2020, Bomzan *et al.*, 2020, Zhao *et al.*, 2020b). Thus, to improve the robustness of future experiments, it could be performed in controlled conditions.

Overall, although it was possible to silence a pot marigold visual marker and biosynthetic target gene genes in leaves, VIGS of floral tissues was inefficient. A combination of optimising plant growth conditions and sampling times, as well as alternate viral vectors and visual marker genes may be investigated to improve VIGS efficiency.

5.6 Conclusion

In this Chapter, methods for *Agrobacterium*-mediated transient expression and VIGS were developed in pot marigold. For *Agrobacterium* transformation, three *A. tumefaciens* strains were compared, showing that *A. tumefaciens* AGL was the most efficient. To develop a VIGS method, two commonly reported VIGS markers (*PDS* and *CHL-H*) were compared; silencing of *CoPDS* provided a more robust visual phenotype. Finally, a dual knockdown system for simultaneous silencing of *CoPDS* and target genes was trialled together with the addition of a *FT* tag to aid mobility to floral tissues. This VIGS system was successful in leaf tissues, enabling the silencing of *CoCAS* and providing a base for further development and establishment of robust functional genomics tools.

Chapter 6 - General Discussion and Future Directions

6.1 Introduction

In 2019, the WHO estimated that around 60% of the world's population uses herbal medicine, with approximately 80% of the population in developing countries relying almost entirely on it for their primary healthcare needs (Khan and Ahmad, 2019). In this context, the Asteraceae family, the largest among flowering plants, plays a significant role. Extracts from Asteraceae species are widely used in traditional medicine products, including creams, balms, tinctures, and orally administered preparations (Lakshman *et al.*, 2014).

However, the use of plant extracts has several limitations compared to the use of purified bioactive compounds. These include yield variability between harvests, leading to difficulties in standardising dosages (de Lacerda *et al.*, 2017, Ekor, 2014). Moreover, excessive harvesting of medicinal plants can lead to the depletion of natural resources and biodiversity loss (Cazar Ramirez *et al.*, 2020). Finally, the use of crude extracts can be problematic as some contain toxic or antagonistic compounds, posing health risks or leading to reduced efficacy (Vaou *et al.*, 2022).

Where bioactivity has been associated with a specific molecule, that compound can be isolated and used as a drug. However, many compounds are present in low abundance, and their complex structure and stereochemistry can make chemical synthesis economically unfeasible (Wawrosch and Zotchev, 2021). Thus, the identification of bioactive compounds, followed by the identification of their biosynthetic pathways in native species, provides options for large-scale biomanufacturing.

The work in this thesis described the integration of comparative metabolic profiling with bioactivity assays to identify faradiol and faradiol fatty acid esters (FAEs) as anti-inflammatory compounds in pot marigold flower extract (Chapter 3). Further, by combining metabolomics, genomics, and transcriptomics with transient expression in *N. benthamiana*, the biosynthetic enzymes involved in the synthesis of these compounds were identified and characterised (Chapter 4). Finally, a method was developed for perturbing gene expression in pot marigold (Chapter 5). This work highlights how integrated studies of bioactivity and biosynthesis can unlock the therapeutic potential of medicinal plants.

6.2 Towards pot-marigold-based products and therapies

Comparative metabolic profiling of extracts from Asteraceae species identified faradiol and faradiol FAEs as compounds only abundant in a few species, mainly in the *Calendula* genus (Chapter 3). Bioactivity assays confirmed previously reported suggestions that faradiol FAEs are major contributors to the overall bioactivity of pot marigold extracts but that faradiol, which does not accumulate at high levels within pot marigold, is the most potent compound. The work also found that pot marigold extracts are not cytotoxic. These results support further research into the use of either pot marigolds extracts or individual compounds for treating inflammation. Further work is required to investigate the synergistic effects of faradiol/faradiol FAEs with other compounds present in the pot marigold extract. This can aid the development of more potent formulations, replicating the anti-inflammatory activity of pot marigold extract with only a selected number of pure compounds.

The work in Chapter 3 also highlighted the importance of C16 hydroxylation for anti-inflammatory activity. This finding complements a recent study which showed that certain modifications of β-amyrin-based triterpenes enhanced anti-proliferative effects, while others improved anti-inflammatory properties (Casson, 2022). Thus, in the future, faradiol and its FAEs could be further modified at other positions via chemical synthesis or via co-expressing biosynthetic genes with other enzymes in *N. benthamiana*. The strategy of co expressing OSCs and decorating enzymes from different plant species was previously exploited to produce new-to-nature variants of triterpenes (Reed *et al.*, 2017a), some of which demonstrated potent anti-inflammatory activity (Casson, 2022). This method could also be applied to combine multiple decorations associated with enhanced anti-inflammatory properties on different triterpene scaffolds to produce more potent molecules.

Chapter 3 revealed that faradiol (C16-hydroxylated ψ-taraxasterol) has an unusual mechanism for suppression of LPS-induced inflammation in THP-1 cells. It works through inhibition of interleukin 6 (IL-6) release by preventing the phosphorylation of STAT3. This discovery provides a foundation for further exploration. First, it is unclear whether faradiol directly targets the JAK2/STAT3 pathway, or if it targets the LPS signalling pathway that leads to the JAK2/STAT3 pathway, which has recently been shown to include long non-coding RNAs (lncRNAs) and suppressor of cytokine signalling (SOCS) (Shin *et al.*, 2024).

The former could be investigated by analysing the phosphorylation profile of JAK2, which acts upstream of STAT3, to pinpoint the level at which faradiol affects this pathway. Once

the target is identified, the ability of faradiol (and potentially structurally similar arnidiol) to interact with its target could be investigated. For example, if the primary target is within the JAK2/STAT3 cascade, the ability of faradiol to bind the active site of JAK2 or interact directly with STAT3 could be assessed.

On the other hand, all the natural triterpenes capable of suppressing STAT3 phosphorylation have been shown to lead to cell apoptosis through the targeting of downstream apoptosis inhibitors or survival genes (Khan *et al.*, 2024). In contrast, no cytotoxicity of the human leukemia monocytic cell line (THP-1) cells was observed after faradiol application. This might be an indication of LPS-specific inhibition of the pathway rather than direct targeting of JAK2/STAT3. To investigate this, the effect of faradiol on the expression levels of lncRNA, BRE-AS1, and on the expression level of *SOCS* gene, which have shown to have a regulatory function in modulating the inflammatory activation of THP-1 could be assessed.

It would then be important to determine the specificity of faradiol to its target, as, for example, it has previously been noted that many JAK2/STAT3 inhibitors exhibit poor selectivity due to the shared similarity in the active sites of these proteins (Lv *et al.*, 2024). Further, wider "off-target" protein interactions might need to be investigated to exclude potential side effects. This can be laborious and time-consuming (Lomenick *et al.*, 2011), but several new technologies are emerging (Tabana *et al.*, 2023). For example, affinity-based pull-down methods have been used to identify protein targets of many compounds, including the triterpenoid, 20-protopanaxadiol (Chen *et al.*, 2023a, Tabana *et al.*, 2023). These advanced methods could help in identifying protein targets and off-target interactions, proving the way for the safe and effective development of faradiol-based therapeutics

The other aspect of drug development is the investigation and improvement of the "druggability" of promising candidates. The physicochemical limitations of faradiol/faradiol FAEs, such as relatively poor water solubility, which currently hinders the development of many triterpenoids into drug leads, could also be explored (Faustino *et al.*, 2023). Improving water solubility often requires the incorporation of functional groups such as carboxylic acid, hydroxyl, or amino groups (Smułek and Kaczorek, 2022). Further, while fatty acids can improve compound solubility, ester components are viewed as less desirable for drug prospects, due to their potential decomposition by proteolytic enzymes (Smułek and Kaczorek, 2022). Thus, continued exploration of structural optimisation, potentially using *N. benthamiana* for the construction of these novel compounds, might result in molecules that are better suited to pharmaceutical applications.

Despite the broad range of bioactivities, the traditional uses of pot marigold are most strongly associated with the skin, and the extracts are still used in many skincare products. Thus, the advancement of pot-marigold-based products and therapies will require an assessment of the anti-inflammatory effect of the extracts/pure compounds *in situ* on human skin models. This could include, for example, incorporation into a sunflower oil base, for the direct comparison with the FDA-approved wound-healing gel, FILSUVEZ and its component ingredients. This would help to assess the feasibility of wound-healing or anti-inflammatorily products based on pot marigold.

Finally, alternative bioactivities of pot marigold extract could be investigated. Previous studies have demonstrated strong anti-microbial activity against clinical pathogens (Efstratiou *et al.*, 2012), but the specific contributions of individual compounds or classes of compounds remain unclear. Thus, the activity of purified triterpenes could be tested against common wound pathogens, such as *Pseudomonas aeruginosa* and golden staph (Ge and Wang, 2023, Tom *et al.*, 2019). Evaluating these contributions could reveal additional uses for the molecules studied here and other pot marigold-derived compounds. Further, faradiol and faradiol FAEs have also been observed to show anti-inflammatory activity *in vitro* in gastric cells (Colombo *et al.*, 2015). Thus, further studies validating this effect *in situ* or *in vivo* might result in applications for the treatment of inflammatory gut conditions such as irritable bowel syndrome (IBS), for which other plant-derived compounds such as phytothymol and resveratrol have already been tested (Zhang *et al.*, 2024).

6.3 Insights into the evolution and function of faradiol FAE biosynthesis

In this study, enzymes involved in the biosynthesis of faradiol FAEs were functionally characterised (Chapter 4). The pot marigold pathway consists of an OSC (CoTXSS) that synthesises ψ-taraxasterol, two functionally redundant C16 hydroxylases (CoCYP716A392, CoCYP716A393), and two faradiol fatty acid acyl transferases (CoACT1 and CoACT2). In addition, a C28 hydroxylase (CoCYP716A431) that produces C28 ψ-taraxasterol carboxylic acid was identified, as well as a ψ-taraxasterol fatty acid acyl transferase (CoACT3) that produces ψ-taraxasterol FAEs.

Triterpene FAEs are abundant and widespread across Asteraceae, which highlights their crucial role in plant survival. Metabolic profiling of Asteraceae species in Chapter 3 revealed that all species that were tested accumulated triterpene monol FAEs. This is consistent with

the finding that over 50 distinct triterpene FAEs have been identified in various plant species (Liu *et al.*, 2024a), with the majority derived from β-amyrin, α-amyrin, and lupeol scaffolds. However, biological functions have only been assigned to a few of these molecules, which range from microbiome modulation in the case of thalianol (Huang *et al.*, 2019), to autotoxin codonopilate A (Xie *et al.*, 2017) and FAEs based on α-amyrin, ursolic acid, and uvaol, which are part of cuticle and thought to play a major role in preventing water loss and regulating the exchange of organic and inorganic substances (Müller and Riederer, 2005, Poirier *et al.*, 2018).

In contrast, triterpene diol FAEs (faradiol, maniladiol, and calenduladiol) were detected in only six species within the Asteroideae subfamily. Unlike triterpene monol FAEs, which are distributed across multiple plant tissues, triterpene diol FAEs were exclusively found in floral tissues. Similarly, unlike the genes encoding ACTs that modify triterpene monols, those that modify faradiol, *CoACT1/CoACT2* were found to be exclusively expressed in flowers together with the earlier pathway genes.

C16 ψ-taraxasterol hydroxylases from pot marigold, field marigold and common sunflower formed a sub-clade within the CYP71A family (Chapter 4). This discovery of a closely related gene in sunflower suggested that these enzymes may have evolved in a common ancestor of the *Calendula* and sunflower lineages, which lived around 42–37 mya before the formation of most Asteroidea tribes (Mandel *et al.*, 2019). Although it was not possible to say how CoCYP716A392/CoCYP716A393 have evolved, the characterisation of adjusted genes and those found in the sister clade could provide further clarification on this.

Further, sunflower was also found to encode an ACT closely related to the pot marigold ACTs that modify faradiol (Chapter 4). This is consistent with the observations made in Chapter 3 that faradiol is produced in Asteraceae species that belong to three different tribes of the Asteroidea subfamily, all of which trace back to this common ancestor. However, while some species have retained the biosynthetic pathway for faradiol production, others appear to have lost the ability to produce faradiol. The maintenance of a pathway for faradiol palmitate in selected lineages may mean that these lineages occupy ecological niches where triterpene diols and their FAEs confer a selective advantage and rely on similar biochemical defences.

While the biological function of faradiol compounds remains unknown, *CoACT1*, one of the key pathway genes, was upregulated in response to MeJA, a hormone known to play a role

in defence against resistance against insects and necrotrophic pathogens such as *Botrytis cinerea* (grey mold), and cottony rot (Macioszek *et al.*, 2023, Monte, 2023). Notably, a recent study showed that cottony rot can infect at least eight Asteraceae species, including common sunflower (Underwood *et al.*, 2022). Furthermore, it has been demonstrated that in many crops, cottony rot initially infects flowers before spreading to leaves, stems, fruits, pods, and seeds (Wang *et al.*, 2023). Thus, one hypotheses that could be investigated in the future is that faradiol FAE biosynthesis evolved to enhance resistance to necrotrophic floral pathogens. Alternatively, numerous triterpenoids have been shown to have antifeedant and insecticidal activities (Lin *et al.*, 2021). Thus, further studies could investigate whether faradiol and its derivatives are anti-herbivory agents that protect pot marigold from florivores.

The biological function of these molecules could potentially be investigated using VIGS (Chapter 5). This method was shown to be successful in reducing gene expression of *CoTXSS*. However, as discussed in Chapter 5, further work is required to optimise this method to enable the reduction of floral metabolites. Alternative experimental strategies, such as the use of gene editing tools for pathway disruption or over-expression in heterologous plant species may be required for functional characterisation.

6.4 The advantages and limitations of *N. benthamiana* for pathway discovery and bioproduction

Although *N. benthamiana* has proven useful for pathway elucidation, many studies have reported the derivatisation of enzyme products (Brückner and Tissier, 2013, Dudley *et al.*, 2022b, Liu *et al.*, 2014, Miettinen *et al.*, 2014). In Chapter 4, the likely derivatisation of some target compounds was observed, which complicated enzyme characterisation. Interestingly, this only affected C16, and C28 hydroxylated triterpenes, including faradiol and faradiol FAEs, oleanolic and betulinic acids. In contrast, the production of triterpene monol FAEs corresponded with reductions of the substrate. Further, no faradiol palmitate peak was observed following co-expression of CoTXSS, CoCYP716A392 and CoACT3, but the quantity of ψ-taraxasterol palmitate reduced, indicating possible derivatisation of the product by an endogenous enzyme. This indicates that if derivatisation occurs, the enzymes likely require hydroxyl groups. As hydroxyl groups are often associated with biological activity, derivatisation may indicate a general pathway for plant defence against bioactive xenochemicals.

Countermeasures for overcoming the challenge of triterpene derivatisation could involve the identification and silencing/knockdown of the endogenous *N. benthamiana* enzymes that might act on triterpene diols and their FAEs. Endogenous *N. benthamiana* glucosyl transferases that modify monoterpenes have been identified (Dudley *et al.*, 2022b). However, these enzymes are unlikely to be active on triterpenes. Thus, further research would be required to identify and remove candidate enzymes.

It should also be noted that when genes to produce faradiol were expressed (*CoTXSS* and *CoCYPA392/CoCYP716A393*), a small quantity of faradiol palmitate was also observed. This suggests that *N. benthamiana* encodes endogenous fatty acid ACTs capable of modifying C16 hydroxylated triterpenes. A better understanding of *N. benthamiana* fatty acids pools and endogenous ACTs would be useful. While many studies report on the lipid profiles of *N. benthamiana* (El Tahchy *et al.*, 2017, Koiwai *et al.*, 1983, Reynolds *et al.*, 2015), to date, there have been no studies detailing the fatty acid ester composition in this species, and no fatty acid ACTs have been identified in this species.

Despite these challenges, substantial quantities of the target triterpenes were present in the expected form, enabling enzyme characterisation. Importantly 5.3 times more faradiol was produced per g dry weight in *N. benthamiana* than accumulates in pot marigold, establishing a foundation for further yield optimisation.

In this study, precursor availability was boosted by overexpression of a truncated version of the HMGR, a rate-limiting enzyme in the mevalonate (MVA) pathway (Chapter 4). To further increase yields, overexpression of other enzymes involved in the MVA pathway, such as 3-hydroxy-3-methyl-glutaryl-CoA synthase (HMGS), squalene synthase (SQS), squalene epoxidase (SQE), and farnesyl diphosphate synthase (FPPS), could be explored. For example, recent studies showed that co-expression of SQEs with four different OSCs, either transiently in *N. benthamiana* or constitutively in yeast, increased triterpene production (Dong *et al.*, 2018). Similarly, *Panax ginseng* (Korean ginseng) hairy roots overexpressing farnesyl phosphate synthase (FPS) showed a 2.4-fold increase in ginsenosides production (Kim *et al.*, 2014). Several other studies also demonstrated that overexpression of HMGR, FPPS, and SQS can increase triterpene yields (Kim *et al.*, 2010, Reed and Osbourn, 2018, Wu *et al.*, 2012).

The possibility of increasing the yields of faradiol and its derivatives could be exported via spatial control strategies previously employed to direct metabolism towards triterpene and sesquiterpene biosynthesis in microorganisms. For instance, fusing OCSs and CYPs significantly increased the yield of hydroxylated triterpenes in *E. coli* (Wang *et al.*, 2021c). Similarly, fusing farnesyl diphosphate synthase (FPPS) and patchoulol synthase (PTS) enhanced sesquiterpene yields in yeast (Albertsen *et al.*, 2011).

Tactics employed to increase the production of other molecules that are biosynthesised though MVA pathway, such as sesquiterpenes, could also be adapted for faradiol compounds. For example, a translational fusion of FPPS and HMGR increased the yields of sesquiterpenes in *N. benthamiana* (van Herpen *et al.*, 2010) and enhanced the FPP production in plastids by overexpressing the fusion protein of 1-deoxy-d-xylulose 5-phosphate synthase (DXS) and FPPS allowed the accumulation of a high yield of sesquiterpene, patchoulol, in tomato fruit (Chen *et al.*, 2023b). A similar strategy was trialled to increase squalene synthesis in the plastid in *N. benthamiana*, but did not impact yields of triterpenes (Reed, 2016). Finally, yields of heterologous sesquiterpenes were boosted by silencing *N. benthamiana* genes involved in the competing pathways (Cankar *et al.*, 2015). A combination of these approaches might have significant impacts on the yields of triterpenes, such as faradiol and its derivatives.

Finally, recent advancements in synthetic biology offer further strategies for yield optimisation. For instance, it was recently shown that an increase in target metabolites can be achieved by controlling and balancing gene expression through the use of synthetic regulatory elements and construct architecture (Kallam *et al.*, 2023b). Investigating how these factors influence the accumulation of faradiol/faradiol FAEs in *N. benthamiana* could provide new opportunities for maximising yields.

Conclusions

Hundreds of plant extracts exhibit valuable biological activities and are widely used in herbal medicine. Harnessing their value through the identification and production of bioactive compounds is key for overcoming the limitations and challenges associated with crude extracts and advancing plant-based drugs development. This thesis integrates comparative metabolic profiling, bioactivity assays, and multi-omics approaches to identify and produce anti-inflammatory compounds from pot marigold in a heterologous host, establishing a base for their potential use in pharmaceutical applications. First, faradiol and faradiol FAEs were identified as key anti-inflammatory compounds, revealing a mechanism of action for faradiol in which IL-6 release is suppressed via inhibiting phosphorylation of STAT3 phosphorylation (Chapter 3). Biosynthetic genes involved in the production of faradiol FAEs were identified and characterised in *N. benthamiana*, shedding light on the evolution and potential function of these compounds within the Asteraceae family (Chapter 4). Lastly, a method for virus-induced gene silencing was developed for pot marigold (Chapter 5). Together, these findings advance our understanding of plant-derived therapeutics, and provide the foundations for drug development, sustainable biomanufacturing, and investigations of the biological function of these metabolites.

References

Abdallah, H. M., Mohamed, G. A., Ibrahim, S. R. M., Asfour, H. Z. & Khayat, M. T. (2019) Undulaterpene A: A New Triterpene Fatty Acid Ester from Pulicaria Undulata. *Pharmacognosy Magazine,* 15.

Acharya, K. R. & Lloyd, M. D. (2005) The Advantages and Limitations of Protein Crystal Structures. *Trends in Pharmacological Sciences,* 26**,** 10-14.

Ahamad, J., Ali, F., Sayed, M. A., Ahmad, J. & Nollet, L. M. (2022) Basic Principles and Fundamental Aspects of Mass Spectrometry. *Mass Spectrometry in Food Analysis.* CRC Press.

Ahmed, M., Akhter, M., Hossain, M., Islam, R., Choudhury, T.*, et al.* (2007) An Efficient Agrobacterium-Mediated Genetic Transformation Method of Lettuce (Lactuca Sativa L.) with an Aphidicidal Gene, Pta (Pinellia Ternata Agglutinin). *Middle-East Journal of Scientific Research,* 2**,** 155-160.

Al-Snafi, A. E. (2017) Chemical Constituents, Pharmacological and Therapeutic Effects of Eupatorium Cannabinum-a Review. *Indo American Journal of Pharmaceutical Sciences,* 4**,** 160-168.

Albertsen, L., Chen, Y., Bach, L. S., Rattleff, S., Maury, J.*, et al.* (2011) Diversion of Flux toward Sesquiterpene Production in Saccharomyces Cerevisiae by Fusion of Host and Heterologous Enzymes. *Applied and Environmental Microbiology,* 77**,** 1033-1040.

Alves, J. S., De Castro, J. C., Freire, M. O., Da-Cunha, E. V. L., Barbosa-Filho, J. M.*, et al.* (2000) Complete Assignment of the 1h and 13c Nmr Spectra of Four Triterpenes of the Ursane, Artane, Lupane and Friedelane Groups. *Magnetic Resonance in Chemistry,* 38**,** 201-206.

Arce-Rodríguez, M. L. & Ochoa-Alejo, N. (2020) Virus-Induced Gene Silencing (Vigs) in Chili Pepper (Capsicum Spp.). *Virus-Induced Gene Silencing in Plants: Methods and Protocols***,** 27-38.

Arendt, P., Miettinen, K., Pollier, J., De Rycke, R., Callewaert, N.*, et al.* (2017) An Endoplasmic Reticulum-Engineered Yeast Platform for Overproduction of Triterpenoids. *Metabolic Engineering,* 40**,** 165-175.

Arendt, P., Pollier, J., Callewaert, N. & Goossens, A. (2016) Synthetic Biology for Production of Natural and New-to-Nature Terpenoids in Photosynthetic Organisms. *The Plant Journal,* 87**,** 16-37.

Arora, D., Rani, A. & Sharma, A. (2013) A Review on Phytochemistry and Ethnopharmacological Aspects of Genus Calendula. *Pharmacognosy reviews,* 7**,** 179.

Arulselvan, P., Fard, M. T., Tan, W. S., Gothai, S., Fakurazi, S.*, et al.* (2016) Role of Antioxidants and Natural Products in Inflammation. *Oxidative medicine and cellular longevity,* 2016**,** 5276130.

Aslan, S., Hofvander, P., Dutta, P., Sitbon, F. & Sun, C. (2015) Transient Silencing of the Kasii Genes Is Feasible in Nicotiana Benthamiana for Metabolic Engineering of Wax Ester Composition. *Scientific reports,* 5**,** 11213.

Atsaves, V., Leventaki, V., Rassidakis, G. Z. & Claret, F. X. (2019) Ap-1 Transcription Factors as Regulators of Immune Responses in Cancer. *Cancers,* 11**,** 1037.

Ayaz, F., Ozcan, M., Kurt, A., Karayigit, B., Ozogul, Y.*, et al.* (2017) Fatty Acid Composition and Antioxidant Capacity of Cypselas in Centaurea Sl Taxa (Asteraceae, Cardueae) from Ne Anatolia. *South African Journal of Botany,* 112**,** 474-482.

Badshah, S. L., Ullah, A., Ahmad, N., Almarhoon, Z. M. & Mabkhot, Y. (2018) Increasing the Strength and Production of Artemisinin and Its Derivatives. *Molecules,* 23**,** 100.

Bai, N., Lai, C.-S., He, K., Zhou, Z., Zhang, L.*, et al.* (2006) Sesquiterpene Lactones from Inula B Ritannica and Their Cytotoxic and Apoptotic Effects on Human Cancer Cell Lines. *Journal of Natural Products,* 69**,** 531-535.

Balandrin, M. F. (1996) Commercial Utilization of Plant-Derived Saponins: An Overview of Medicinal, Pharmaceutical, and Industrial Applications. *Saponins used in traditional and modern medicine***,** 1-14.

Bally, J., Nakasugi, K., Jia, F., Jung, H., Ho, S. Y.*, et al.* (2015) The Extremophile Nicotiana Benthamiana Has Traded Viral Defence for Early Vigour. *Nature plants,* 1**,** 1-6.

Bao, S., Yi, M., Xiang, B. & Chen, P. (2024) Antitumor Mechanisms and Future Clinical Applications of the Natural Product Triptolide. *Cancer Cell International,* 24**,** 150.

Barberis, M., Calabrese, D., Galloni, M. & Nepi, M. (2023) Secondary Metabolites in Nectar-Mediated Plant-Pollinator Relationships. *Plants,* 12**,** 550.

Bardwell, L. (2006) Mechanisms of Mapk Signalling Specificity. *Biochemical Society Transactions,* 34**,** 837-841.

Barker, M. S., Kane, N. C., Matvienko, M., Kozik, A., Michelmore, R. W.*, et al.* (2008) Multiple Paleopolyploidizations during the Evolution of the Compositae Reveal Parallel Patterns of Duplicate Gene Retention after Millions of Years. *Molecular Biology and Evolution,* 25**,** 2445-2455.

Barnes, P. (2006) Corticosteroid Effects on Cell Signalling. *European Respiratory Journal,* 27**,** 413-426.

Barreda, V. D., Palazzesi, L., Tellería, M. C., Olivero, E. B., Raine, J. I.*, et al.* (2015) Early Evolution of the Angiosperm Clade Asteraceae in the Cretaceous of Antarctica. *Proceedings of the National Academy of Sciences,* 112**,** 10989-10994.

Bartwal, A., Mall, R., Lohani, P., Guru, S. & Arora, S. (2013) Role of Secondary Metabolites and Brassinosteroids in Plant Defense against Environmental Stresses. *Journal of Plant Growth Regulation,* 32**,** 216-232.

Benjamin, O., Goyal, A. & Lappin, S. L. (2018) Disease Modifying Anti-Rheumatic Drugs (Dmard).

Boachon, B., Burdloff, Y., Ruan, J.-X., Rojo, R., Junker, R. R.*, et al.* (2019) A Promiscuous Cyp706a3 Reduces Terpene Volatile Emission from Arabidopsis Flowers, Affecting Florivores and the Floral Microbiome. *The Plant Cell,* 31**,** 2947-2972.

Bokelmann, J. M. (2022) Calendula (Calendula Officinalis): Flower. *Jean M, Bokelmann, eds. Medicinal Herbs in Primary Care. Philadelphia: Elsevier***,** 263-267.

Bomzan, D. P., Shilpashree, H., Anjali, P., Kumar, S. R. & Nagegowda, D. A. (2020) Virus-Induced Gene Silencing for Functional Genomics in Withania Somnifera, an Important Indian Medicinal Plant. *Virus-Induced Gene Silencing in Plants: Methods and Protocols.* Springer.

Borges, A., Abreu, A. C., Ferreira, C., Saavedra, M. J., Simões, L. C.*, et al.* (2015) Antibacterial Activity and Mode of Action of Selected Glucosinolate Hydrolysis Products against Bacterial Pathogens. *Journal of food science and technology,* 52**,** 4737-4748.

Borrelli, G. M. & Trono, D. (2016) Molecular Approaches to Genetically Improve the Accumulation of Health-Promoting Secondary Metabolites in Staple Crops—a Case Study: The Lipoxygenase-B1 Genes and Regulation of the Carotenoid Content in Pasta Products. *International Journal of Molecular Sciences,* 17**,** 1177.

Borsini, A., Di Benedetto, M. G., Giacobbe, J. & Pariante, C. M. (2020) Pro-and Anti-Inflammatory Properties of Interleukin in Vitro: Relevance for Major Depression and Human Hippocampal Neurogenesis. *International Journal of Neuropsychopharmacology,* 23**,** 738-750.

Broderick, S. R. & Jones, M. L. (2014) An Optimized Protocol to Increase Virus-Induced Gene Silencing Efficiency and Minimize Viral Symptoms in Petunia. *Plant molecular biology reporter,* 32**,** 219-233.

Brückner, K. & Tissier, A. (2013) High-Level Diterpene Production by Transient Expression in Nicotiana Benthamiana. *Plant Methods,* 9**,** 1-10.

Burch-Smith, T. M., Schiff, M., Liu, Y. & Dinesh-Kumar, S. (2006) Efficient Virus-Induced Gene Silencing in Arabidopsis. *Plant Physiology,* 142**,** 21-27.

Bureau, J.-A., Oliva, M. E., Dong, Y. & Ignea, C. (2023) Engineering Yeast for the Production of Plant Terpenoids Using Synthetic Biology Approaches. *Natural Product Reports*.

Byers, K. J., Bradshaw Jr, H. & Riffell, J. A. (2014a) Three Floral Volatiles Contribute to Differential Pollinator Attraction in Monkeyflowers (Mimulus). *Journal of Experimental Biology,* 217**,** 614-623.

Byers, K. J., Vela, J. P., Peng, F., Riffell, J. A. & Bradshaw Jr, H. D. (2014b) Floral Volatile Alleles Can Contribute to Pollinator-Mediated Reproductive Isolation in Monkeyflowers (M Imulus). *The Plant Journal,* 80**,** 1031-1042.

Caesar, M., Zach, S., Carlson, C. B., Brockmann, K., Gasser, T.*, et al.* (2013) Leucine-Rich Repeat Kinase 2 Functionally Interacts with Microtubules and Kinase-Dependently Modulates Cell Migration. *Neurobiology of disease,* 54**,** 280-288.

Cai, Y.-M., Carrasco Lopez, J. A. & Patron, N. J. (2020) Phytobricks: Manual and Automated Assembly of Constructs for Engineering Plants. *Methods in molecular biology (Clifton, N.J.),* 2205**,** 179-199.

Cambier, S., Gouwy, M. & Proost, P. (2023) The Chemokines Cxcl8 and Cxcl12: Molecular and Functional Properties, Role in Disease and Efforts Towards Pharmacological Intervention. *Cellular & Molecular Immunology,* 20**,** 217-251.

Cankar, K., Jongedijk, E., Klompmaker, M., Majdic, T., Mumm, R.*, et al.* (2015) (+)-Valencene Production in Nicotiana Benthamiana Is Increased by down-Regulation of Competing Pathways. *Biotechnology journal,* 10**,** 180-189.

Cappelaro, E. A. & Yariwake, J. H. (2015) Hs-Spme-Gc-Ms Analysis of Volatile and Semi-Volatile Compounds from Dried Leaves of Mikania Glomerata Sprengel. *Química Nova,* 38**,** 427-430.

Caputi, L., Franke, J., Farrow, S. C., Chung, K., Payne, R. M. E.*, et al.* (2018) Missing Enzymes in the Biosynthesis of the Anticancer Drug Vinblastine in Madagascar Periwinkle. *Science,* 360**,** 1235-1238.

Carey, S., Higuera-Díaz, M., Mankowski, P., Rocca, A. & Hall, J. C. (2021) Virus-Induced Gene Silencing as a Tool for Functional Studies in Cleome Violacea. *Applications in plant sciences,* 9.

Casson, R. (2022) *Directing Biosynthesis of Bioactive Triterpenes for Pharmaceutical Applications.* University of East Anglia.

Castell, J. V., Gómez-Lechón, M. J., David, M., Andus, T., Geiger, T.*, et al.* (1989) Interleukin-6 Is the Major Regulator of Acute Phase Protein Synthesis in Adult Human Hepatocytes. *FEBS Letters,* 242**,** 237-239.

Cazar Ramirez, M. E., Howes, M. J. & Lughadha, E. N. (2020) Molecules from Nature: Reconciling Biodiversity Conservation and Global Healthcare Imperatives for Sustainable Use of Medicinal Plants and Fungi.

Chakraborty, A., Chaudhury, R., Dutta, S., Basak, M., Dey, S.*, et al.* (2022) Role of Metabolites in Flower Development and Discovery of Compounds Controlling Flowering Time. *Plant Physiology and Biochemistry,* 190**,** 109-118.

Chandler, R. F., Hooper, S., Hooper, D., Jamieson, W., Flinn, C.*, et al.* (1982) Herbal Remedies of the Maritime Indians: Sterols and Triterpenes of Achillea Millefolium L.(Yarrow). *Journal of Pharmaceutical Sciences,* 71**,** 690-693.

Chandran, S., Leung, J., Hu, C., Laszik, Z. G., Tang, Q.*, et al.* (2021) Interleukin-6 Blockade with Tocilizumab Increases Tregs and Reduces T Effector Cytokines in Renal Graft Inflammation: A Randomized Controlled Trial. *American Journal of Transplantation,* 21**,** 2543-2554.

Chang, Q., Bournazou, E., Sansone, P., Berishaj, M., Gao, S. P.*, et al.* (2013) The Il-6/Jak/Stat3 Feed-Forward Loop Drives Tumorigenesis and Metastasis. *Neoplasia,* 15**,** 848-IN45.

Chanput, W., Mes, J. J. & Wichers, H. J. (2014) Thp-1 Cell Line: An in Vitro Cell Model for Immune Modulation Approach. *International Immunopharmacology,* 23**,** 37-45.
Che, C.-T. & Zhang, H. (2019) Plant Natural Products for Human Health. MDPI.
Chen, F., Liu, D.-L., Wang, W., Lv, X.-M., Li, W.*, et al.* (2020a) Bioactive Triterpenoids from Sambucus Javanica Blume. *Natural Product Research,* 34**,** 2816-2821.
Chen, F., Zhang, W., Xu, S., Zhang, H., Chen, L.*, et al.* (2023a) Discovery and Validation of Pura as a Transcription Target of 20 (S)-Protopanaxadiol: Implications for the Treatment of Cognitive Dysfunction. *Journal of Ginseng Research,* 47**,** 662-671.
Chen, G., Kang, W., Li, W., Chen, S. & Gao, Y. (2022) Oral Delivery of Protein and Peptide Drugs: From Non-Specific Formulation Approaches to Intestinal Cell Targeting Strategies. *Theranostics,* 12**,** 1419.
Chen, J., Tan, J., Duan, X., Wang, Y., Wen, J.*, et al.* (2023b) Plastidial Engineering with Coupled Farnesyl Diphosphate Pool Reconstitution and Enhancement for Sesquiterpene Biosynthesis in Tomato Fruit. *Metabolic Engineering,* 77**,** 41-52.
Chen, J. C., Jiang, C. Z., Gookin, T. E., Hunter, D. A., Clark, D. G.*, et al.* (2004) Chalcone Synthase as a Reporter in Virus-Induced Gene Silencing Studies of Flower Senescence. *Plant Molecular Biology,* 55**,** 521-530.
Chen, L., Deng, H., Cui, H., Fang, J., Zuo, Z.*, et al.* (2017) Inflammatory Responses and Inflammation-Associated Diseases in Organs. *Oncotarget,* 9**,** 7204.
Chen, Q., Lai, H., Hurtado, J., Stahnke, J., Leuzinger, K.*, et al.* (2013) Agroinfiltration as an Effective and Scalable Strategy of Gene Delivery for Production of Pharmaceutical Proteins. *Advanced techniques in biology & medicine,* 1.
Chen, R., Chen, X., Hagel, J. M. & Facchini, P. J. (2020b) Virus-Induced Gene Silencing to Investigate Alkaloid Biosynthesis in Opium Poppy. *Virus-Induced Gene Silencing in Plants: Methods and Protocols.* Springer.
Cheong, J.-J. & Do Choi, Y. (2003) Methyl Jasmonate as a Vital Substance in Plants. *Trends in Genetics,* 19**,** 409-413.
Chiswick, E. L., Duffy, E., Japp, B. & Remick, D. (2012) Detection and Quantification of Cytokines and Other Biomarkers. *Leucocytes: Methods and Protocols***,** 15-30.
Choi, H. S., Han, J. Y., Cheong, E. J. & Choi, Y. E. (2022) Characterization of a Pentacyclic Triterpene Acetyltransferase Involved in the Biosynthesis of Taraxasterol and ψ-Taraxasterol Acetates in Lettuce. *Frontiers in Plant Science,* 12**,** 788356.
Choi, M., Kim, J. K., Yoon, J., Lim, J., Kim, K.*, et al.* (2024) Identification of Metabolite Changes and Evaluation of Biological Activities in Edible Flowers of Magnolia Kobus at Different Developmental Stages. *Chemical and Biological Technologies in Agriculture,* 11**,** 98.
Collins, S. L., Koo, I., Peters, J. M., Smith, P. B. & Patterson, A. D. (2021) Current Challenges and Recent Developments in Mass Spectrometry–Based Metabolomics. *Annual review of analytical chemistry,* 14**,** 467-487.
Colombo, E., Sangiovanni, E., D'ambrosio, M., Bosisio, E., Ciocarlan, A.*, et al.* (2015) A Bio-Guided Fractionation to Assess the Inhibitory Activity of Calendula Officinalis L. On the Nf-κb Driven Transcription in Human Gastric Epithelial Cells. *Evidence-Based Complementary and Alternative Medicine,* 2015**,** 727342.
Cravens, A., Payne, J. & Smolke, C. D. (2019) Synthetic Biology Strategies for Microbial Biosynthesis of Plant Natural Products. *Nature Communications,* 10**,** 2142.
Criollo-Mendoza, M. S., Contreras-Angulo, L. A., Leyva-López, N., Gutiérrez-Grijalva, E. P., Jiménez-Ortega, L. A.*, et al.* (2023) Wound Healing Properties of Natural Products: Mechanisms of Action. *Molecules,* 28**,** 598.
Csupor-Löffler, B., Hajdú, Z., Zupkó, I., Réthy, B., Falkay, G.*, et al.* (2009) Antiproliferative Effect of Flavonoids and Sesquiterpenoids from Achillea Millefolium Sl on Cultured Human Tumour Cell Lines. *Phytotherapy Research: An International Journal Devoted to Pharmacological and Toxicological Evaluation of Natural Product Derivatives,* 23**,** 672-676.

D’ambrosio, C., Stigliani, A. L. & Giorio, G. (2018) Crispr/Cas9 Editing of Carotenoid Genes in Tomato. *Transgenic Research,* 27**,** 367-378.
D'auria, J. C. (2006) Acyltransferases in Plants: A Good Time to Be Bahd. *Current Opinion in Plant Biology,* 9**,** 331-340.
D’auria, J. C. (2006) Acyltransferases in Plants: A Good Time to Be Bahd. *Current Opinion in Plant Biology,* 9**,** 331-340.
Da Silva, L. C. N., Sahal, D. & Panda, S. K. (2023) Developing Medicines (Drugs) Derived from the Asteraceae—an Opportunity in Ethnopharmacology, Volume Ii. *Frontiers in Pharmacology,* 14**,** 1285815.
Dale, M. P., Moses, T., Johnston, E. J. & Rosser, S. J. (2020) A Systematic Comparison of Triterpenoid Biosynthetic Enzymes for the Production of Oleanolic Acid in Saccharomyces Cerevisiae. *Plos One,* 15**,** e0231980.
Dang, C. V., O’donnell, K. A., Zeller, K. I., Nguyen, T., Osthus, R. C*., et al.* The C-Myc Target Gene Network. Seminars in Cancer Biology, 2006. Elsevier, 253-264.
Darling, A. C. E., Mau, B., Blattner, F. R. & Perna, N. T. (2004) Mauve: Multiple Alignment of Conserved Genomic Sequence with Rearrangements. *Genome Research,* 14**,** 1394-1403.
Darqui, F. S., Radonic, L. M., Beracochea, V. C., Hopp, H. E. & Bilbao, M. L. (2021) Peculiarities of the Transformation of <I>Asteraceae</I> Family Species: The Cases of Sunflower and Lettuce. *Frontiers in Plant Science,* 12.
De Lacerda, G. M., Da Silva, L. G., Haiele, M., Alves, A., Monteiro, À. B*., et al.* (2017) Use of Medicinal Plants: Benefits, Risks, Limitations and Perspectives. *Imp J Interdiscip Res,* 3**,** 67-70.
De Saeger, J., Park, J., Chung, H. S., Hernalsteens, J. P., Van Lijsebettens, M*., et al.* (2021) <I>Agrobacterium</I> Strains and Strain Improvement: Present and Outlook. *Biotechnology Advances,* 53.
Della Loggia, R., Tubaro, A., Sosa, S., Becker, H., Saar, S*., et al.* (1994) The Role of Triterpenoids in the Topical Anti-Inflammatory Activity Of. *Calendula officinalis***,** 516-20.
Demurtas, O. C., Nicolia, A. & Diretto, G. (2023) Terpenoid Transport in Plants: How Far from the Final Picture? *Plants,* 12**,** 634.
Deng, X., Elomaa, P., Nguyen, C. X., Hytönen, T., Valkonen, J. P*., et al.* (2012) Virus-Induced Gene Silencing for Asteraceae—a Reverse Genetics Approach for Functional Genomics in Gerbera Hybrida. *Plant Biotechnology Journal,* 10**,** 970-978.
Deng, X. B., Bashandy, H., Ainasoja, M., Kontturi, J., Pietiäinen, M*., et al.* (2014) Functional Diversification of Duplicated Chalcone Synthase Genes in Anthocyanin Biosynthesis of <I>Gerbera Hybrida</I>. *New Phytologist,* 201**,** 1469-1483.
Dhingra, G., Dhakad, P. & Tanwar, S. (2022) Review on Phytochemical Constituents and Pharmacological Activities of Plant Calendula Officinalis Linn. *Biological Sciences,* 2**,** 216-228.
Di Gesso, J. L., Kerr, J. S., Zhang, Q., Raheem, S., Yalamanchili, S. K*., et al.* (2015) Flavonoid Metabolites Reduce Tumor Necrosis Factor-α Secretion to a Greater Extent Than Their Precursor Compounds in Human Thp-1 Monocytes. *Molecular Nutrition & Food Research,* 59**,** 1143-1154.
Dinarello, C. A. (2010) Anti-Inflammatory Agents: Present and Future. *Cell,* 140**,** 935-950.
Ding, X. S., Srinivasa Rao, C. & Nelson, R. S. (2007) Analysis of Gene Function in Rice through Virus-Induced Gene Silencing. *Plant-Pathogen Interactions: Methods and Protocols***,** 145-160.
Dixon, R. A. & Dickinson, A. J. (2024) A Century of Studying Plant Secondary Metabolism—from “What?” to “Where, How, and Why?”. *Plant Physiology,* 195**,** 48-66.

Długosz, M., Wiktorowska, E., Wiśniewska, A. & Pączkowski, C. (2013) Production of Oleanolic Acid Glycosides by Hairy Root Established Cultures of Calendula Officinalis L. *Acta Biochimica Polonica,* 60**,** 467-473.

Dommes, A. B., Gross, T., Herbert, D. B., Kivivirta, K. I. & Becker, A. (2019) Virus-Induced Gene Silencing: Empowering Genetics in Non-Model Organisms. *Journal of Experimental Botany,* 70**,** 757-770.

Dong, L., Pollier, J., Bassard, J.-E., Ntallas, G., Almeida, A.*, et al.* (2018) Co-Expression of Squalene Epoxidases with Triterpene Cyclases Boosts Production of Triterpenoids in Plants and Yeast. *Metabolic Engineering,* 49**,** 1-12.

Dönmez, B. A., Dangol, S. D. & Bakhsh, A. (2019) Transformation Efficiency of Five Agrobacterium Strains in Diploid and Tetraploid Potatoes.

Dudley, Q., Jo, S., Guerrero, D., Chhetry, M., Smedley, M.*, et al.* (2022a) Reconstitution of Monoterpene Indole Alkaloid Biosynthesis in Genome Engineered Nicotiana Benthamiana. Communications Biology, 5 (1), 949.

Dudley, Q. M., Cai, Y.-M., Kallam, K., Debreyne, H., Lopez, J. a. C.*, et al.* (2021) Biofoundry-Assisted Expression and Characterization of Plant Proteins. *Synthetic Biology,* 6.

Dudley, Q. M., Jo, S., Guerrero, D. a. S., Chhetry, M., Smedley, M. A.*, et al.* (2022b) Reconstitution of Monoterpene Indole Alkaloid Biosynthesis in Genome Engineered Nicotiana Benthamiana. *Communications biology,* 5**,** 949.

Edgar, R. C. (2004) Muscle: Multiple Sequence Alignment with High Accuracy and High Throughput. *Nucleic Acids Research,* 32**,** 1792-1797.

Edmunds, N. S. & Mcguffin, L. J. (2021) Computational Methods for the Elucidation of Protein Structure and Interactions. *Structural Proteomics: High-Throughput Methods***,** 23-52.

Efstratiou, E., Hussain, A. I., Nigam, P. S., Moore, J. E., Ayub, M. A.*, et al.* (2012) Antimicrobial Activity of Calendula Officinalis Petal Extracts against Fungi, as Well as Gram-Negative and Gram-Positive Clinical Pathogens. *Complementary Therapies in Clinical Practice,* 18**,** 173-176.

Ekor, M. (2014) The Growing Use of Herbal Medicines: Issues Relating to Adverse Reactions and Challenges in Monitoring Safety. *Frontiers in Pharmacology,* 4**,** 177.

El Chami, D., Daccache, A. & El Moujabber, M. (2020) What Are the Impacts of Sugarcane Production on Ecosystem Services and Human Well-Being? A Review. *Annals of Agricultural Sciences,* 65**,** 188-199.

El Tahchy, A., Reynolds, K. B., Petrie, J. R., Singh, S. P. & Vanhercke, T. (2017) Thioesterase Overexpression in Nicotiana Benthamiana Leaf Increases the Fatty Acid Flux into Triacylglycerol. *FEBS Letters,* 591**,** 448-456.

Ellison, E. E., Nagalakshmi, U., Gamo, M. E., Huang, P.-J., Dinesh-Kumar, S.*, et al.* (2020) Multiplexed Heritable Gene Editing Using Rna Viruses and Mobile Single Guide Rnas. *Nature plants,* 6**,** 620-624.

Engler, C., Youles, M., Gruetzner, R., Ehnert, T.-M., Werner, S.*, et al.* (2014) A Golden Gate Modular Cloning Toolbox for Plants. *Acs Synthetic Biology,* 3**,** 839-843.

Erb, M. & Kliebenstein, D. J. (2020) Plant Secondary Metabolites as Defenses, Regulators, and Primary Metabolites: The Blurred Functional Trichotomy. *Plant Physiology,* 184**,** 39-52.

Esmaeili, G., Van Laere, K., Muylle, H. & Leus, L. (2020) Artificial Chromosome Doubling in Allotetraploid Calendula Officinalis. *Frontiers in Plant Science,* 11**,** 622.

Faivre-Rampant, O., Gilroy, E. M., Hrubikova, K., Hein, I., Millam, S.*, et al.* (2004) Potato Virus X-Induced Gene Silencing in Leaves and Tubers of Potato. *Plant Physiology,* 134**,** 1308-1316.

Fang, X. (2024) Identification of Secondary Metabolites by Multi-Omics Methods. MDPI.

Farré-Armengol, G., Filella, I., Llusia, J. & Peñuelas, J. (2016) Bidirectional Interaction between Phyllospheric Microbiotas and Plant Volatile Emissions. *Trends in Plant Science,* 21**,** 854-860.

Faustino, C., Duarte, N. & Pinheiro, L. (2023) Triterpenes Drug Delivery Systems, a Modern Approach for Arthritis Targeted Therapy. *Pharmaceuticals,* 17**,** 54.

Fei, Y., Pyott, D. E. & Molnar, A. (2021) Temperature Modulates Virus-Induced Transcriptional Gene Silencing Via Secondary Small Rnas. *New Phytologist,* 232**,** 356-371.

Fenu, M., Bettermann, T., Vogl, C., Darwish-Miranda, N., Schramel, J.*, et al.* (2019) A Novel Magnet-Based Scratch Method for Standardisation of Wound-Healing Assays. *Scientific reports,* 9**,** 12625.

Fernández, M. A., De Las Heras, B., Garcia, M. D., Sáenz, M. T. & Villar, A. (2001) New Insights into the Mechanism of Action of the Anti-Inflammatory Triterpene Lupeol. *Journal of Pharmacy and Pharmacology,* 53**,** 1533-1539.

Fernández, P., Hidalgo, O., Juan, A., Leitch, I. J., Leitch, A. R.*, et al.* (2022) Genome Insights into Autopolyploid Evolution: A Case Study in Senecio Doronicum (Asteraceae) from the Southern Alps. *Plants,* 11**,** 1235.

Ferreira, T., Faustino-Rocha, A. I., Gaspar, V. M., Medeiros, R., Mano, J. F.*, et al.* (2024) Contribution of Non-Steroidal Anti-Inflammatory Drugs to Breast Cancer Treatment: In Vitro and in Vivo Studies. *Veterinary World,* 17.

Field, B. & Osbourn, A. E. (2008) Metabolic Diversification—Independent Assembly of Operon-Like Gene Clusters in Different Plants. *Science,* 320**,** 543-547.

Figueroa-Suárez, M. Z., Christen, J. G., Cardoso-Taketa, A. T., Villafuerte, M. D. C. G. & Rodríguez-López, V. (2019) Anti-Inflammatory and Antihistaminic Activity of Triterpenoids Isolated from Bursera Cuneata (Schldl.) Engl. *Journal of Ethnopharmacology,* 238**,** 111786.

Foster, C. S. The Evolutionary History of Flowering Plants. Journal and Proceedings of the Royal Society of New South Wales, 2016. 65-82.

Freeling, M. (2009) Bias in Plant Gene Content Following Different Sorts of Duplication: Tandem, Whole-Genome, Segmental, or by Transposition. *Annual Review of Plant Biology,* 60**,** 433-453.

Fronza, M., Heinzmann, B., Hamburger, M., Laufer, S. & Merfort, I. (2009) Determination of the Wound Healing Effect of Calendula Extracts Using the Scratch Assay with 3t3 Fibroblasts. *Journal of Ethnopharmacology,* 126**,** 463-467.

Fruman, D. A., Chiu, H., Hopkins, B. D., Bagrodia, S., Cantley, L. C.*, et al.* (2017) The Pi3k Pathway in Human Disease. *Cell,* 170**,** 605-635.

Fu, D.-Q., Zhu, B.-Z., Zhu, H.-L., Zhang, H.-X., Xie, Y.-H.*, et al.* (2006) Enhancement of Virus-Induced Gene Silencing in Tomato by Low Temperature and Low Humidity. *Molecules and Cells,* 21**,** 153-160.

Funk, V. A., Bayer, R. J., Keeley, S., Chan, R., Watson, L.*, et al.* (2005) Everywhere but Antarctica: Using a Supertree to Understand the Diversity and Distribution of the Compositae. *Biol. Skr. 55: 343-373*.

Gabay, C. (2006) Interleukin-6 and Chronic Inflammation. *Arthritis Research & Therapy,* 8**,** 1-6.

Galis, I., Schuman, M. C., Gase, K., Hettenhausen, C., Hartl, M.*, et al.* (2013) The Use of Vigs Technology to Study Plant–Herbivore Interactions. *Virus-induced gene silencing: Methods and Protocols***,** 109-137.

Ganeva, I., Chr, C., Denchev, T., Ganeva, Y., Chr, C.*, et al.* (2003) Triterpenoids and Sterols from Matricaria Chamomilla L. *Asteraceae). Farmatsiya (Sofia, Bulgaria),* 50**,** 3-5.

Gao, H., Kang, N., Hu, C., Zhang, Z., Xu, Q.*, et al.* (2020) Ginsenoside Rb1 Exerts Anti-Inflammatory Effects in Vitro and in Vivo by Modulating Toll-Like Receptor 4 Dimerization and Nf-Kb/Mapks Signaling Pathways. *Phytomedicine,* 69**,** 153197.

Gao, H.-Y., Zhao, H., Hu, T.-Y., Jiang, Z.-Q., Xia, M.*, et al.* (2022) Metabolic Engineering of Saccharomyces Cerevisiae for High-Level Friedelin Via Genetic Manipulation. *Frontiers in Bioengineering and Biotechnology,* 10**,** 805429.

Gao, X. Q., Wheeler, T., Li, Z. H., Kenerley, C. M., He, P., *et al.* (2011) Silencing <I>Ghndr1</I> and <I>Ghmkk2</I> Compromises Cotton Resistance to Verticillium Wilt. *Plant Journal,* 66**,** 293-305.

Garabagi, F., Gilbert, E., Loos, A., Mclean, M. D. & Hall, J. C. (2012a) Utility of the P19 Suppressor of Gene-Silencing Protein for Production of Therapeutic Antibodies in Nicotiana Expression Hosts. *Plant Biotechnology Journal,* 10**,** 1118-28.

Garabagi, F., Gilbert, E., Loos, A., Mclean, M. D. & Hall, J. C. (2012b) Utility of the P 19 Suppressor of Gene-Silencing Protein for Production of Therapeutic Antibodies in N Icotiana Expression Hosts. *Plant Biotechnology Journal,* 10**,** 1118-1128.

Gasperini, D. & Howe, G. A. (2024) Phytohormones in a Universe of Regulatory Metabolites: Lessons from Jasmonate. *Plant Physiology,* 195**,** 135-154.

Gates, P. J. (2021) Atmospheric Pressure Chemical Ionisation Mass Spectrometry for the Routine Analysis of Low Molecular Weight Analytes. *European Journal of Mass Spectrometry,* 27**,** 13-28.

Ge, Y. & Wang, Q. (2023) Current Research on Fungi in Chronic Wounds. *Frontiers in molecular biosciences,* 9**,** 1057766.

Geetha, R., Roy, A. & Subramanian, A. K. Yarrow (Achillea Millefolium Linn.) a Herbal Medicinal Plant with Broad Therapeutic Use-a Review.

Geetha, T. & Varalakshmi, P. (2001) Anti-Inflammatory Activity of Lupeol and Lupeol Linoleate in Rats. *Journal of Ethnopharmacology,* 76**,** 77-80.

Ghosh, S. (2016) Biosynthesis of Structurally Diverse Triterpenes in Plants: The Role of Oxidosqualene Cyclases.

Ghosh, S. (2017a) Triterpene Structural Diversification by Plant Cytochrome P450 Enzymes. *Frontiers in Plant Science,* 8.

Ghosh, S. (2017b) Triterpene Structural Diversification by Plant Cytochrome P450 Enzymes. *Frontiers in Plant Science,* 8**,** 1886.

Givol, O., Kornhaber, R., Visentin, D., Cleary, M., Haik, J., *et al.* (2019) A Systematic Review of Calendula Officinalis Extract for Wound Healing. *Wound repair and regeneration,* 27**,** 548-561.

Glady, A., Vandebroek, A. & Yasui, M. (2021) Human Keratinocyte-Derived Extracellular Vesicles Activate the Mapkinase Pathway and Promote Cell Migration and Proliferation in Vitro. *Inflammation and regeneration,* 41**,** 1-9.

Golubova, D., Salmon, M., Su, H., Tansley, C., Kaithakottil, G., *et al.* (2025) Biosynthesis and Bioactivity of Anti-Inflammatory Triterpenoids in Calendula Officinalis (Pot Marigold). *bioRxiv***,** 2025.01. 11.632544.

Golubova, D., Tansley, C., Su, H. & Patron, N. J. (2024) Engineering<I> Nicotiana</I><I> Benthamiana</I> as a Platform for Natural Product Biosynthesis. *Current Opinion in Plant Biology,* 81.

González-Candelas, L., Alamar, S., Sánchez-Torres, P., Zacarías, L. & Marcos, J. F. (2010) A Transcriptomic Approach Highlights Induction of Secondary Metabolism in Citrus Fruit in Response to Penicillium Digitatum Infection. *BMC Plant Biology,* 10**,** 1-17.

Goossens, A., Häkkinen, S. T., Laakso, I., Seppänen-Laakso, T., Biondi, S., *et al.* (2003) A Functional Genomics Approach toward the Understanding of Secondary Metabolism in Plant Cells. *Proceedings of the National Academy of Sciences,* 100**,** 8595-8600.

Goossens, J., Fernández-Calvo, P., Schweizer, F. & Goossens, A. (2016) Jasmonates: Signal Transduction Components and Their Roles in Environmental Stress Responses. *Plant Molecular Biology,* 91**,** 673-689.

Goulet, M.-C., Gaudreau, L., Gagné, M., Maltais, A.-M., Laliberté, A.-C., *et al.* (2019) Production of Biopharmaceuticals in Nicotiana Benthamiana—Axillary Stem Growth as a Key Determinant of Total Protein Yield. *Frontiers in Plant Science,* 10**,** 735.

Guo, H., Chen, T., Zhu, H., Wang, H. & Huo, Y.-X. (2024) Engineering Amino Acid Residues of Pentacyclic Triterpene Synthases for Improving the Activity. *Applied Microbiology and Biotechnology,* 108**,** 195.

Guo, H., Wang, H. & Huo, Y.-X. (2020) Engineering Critical Enzymes and Pathways for Improved Triterpenoid Biosynthesis in Yeast. *Acs Synthetic Biology,* 9**,** 2214-2227.

Guo, W., Wang, D. & Lisch, D. (2021) Rna-Directed DNA Methylation Prevents Rapid and Heritable Reversal of Transposon Silencing under Heat Stress in Zea Mays. *PLoS Genetics,* 17**,** e1009326.

Guo, Y. L. (2013) Gene Family Evolution in Green Plants with Emphasis on the Origination and Evolution of a Rabidopsis Thaliana Genes. *The Plant Journal,* 73**,** 941-951.

Hamberger, B. & Bak, S. (2013) Plant P450s as Versatile Drivers for Evolution of Species-Specific Chemical Diversity. *Philosophical Transactions of the Royal Society B: Biological Sciences,* 368**,** 20120426.

Han, J.-Y., Kim, H.-J., Kwon, Y.-S. & Choi, Y.-E. (2011) The Cyt P450 Enzyme Cyp716a47 Catalyzes the Formation of Protopanaxadiol from Dammarenediol-Ii during Ginsenoside Biosynthesis in Panax Ginseng. *Plant and Cell Physiology,* 52**,** 2062-2073.

Hansen, C. C., Nelson, D. R., Møller, B. L. & Werck-Reichhart, D. (2021) Plant Cytochrome P450 Plasticity and Evolution. *Molecular Plant,* 14**,** 1244-1265.

Hansen, N. L., Miettinen, K., Zhao, Y., Ignea, C., Andreadelli, A.*, et al.* (2020) Integrating Pathway Elucidation with Yeast Engineering to Produce Polpunonic Acid the Precursor of the Anti-Obesity Agent Celastrol. *Microbial Cell Factories,* 19**,** 1-17.

Hassan Mir, R., Godavari, G., Siddiqui, N. A., Ahmad, B., Mothana, R. A.*, et al.* (2021) Design, Synthesis, Molecular Modelling, and Biological Evaluation of Oleanolic Acid-Arylidene Derivatives as Potential Anti-Inflammatory Agents. *Drug Design, Development and Therapy***,** 385-397.

Hein, I., Pacak, M. B., Hrubikova, K., Williamson, S., Dinesen, M.*, et al.* (2005) Virus-Induced Gene Silencing-Based Functional Characterization of Genes Associated with Powdery Mildew Resistance in Barley. *Plant Physiology,* 138**,** 2155-2164.

Hiriart, J. B., Lehto, K., Tyystjärvi, E., Junttila, T. & Aro, E. M. (2002) Suppression of a Key Gene Involved in Chlorophyll Biosynthesis by Means of Virus-Inducing Gene Silencing. *Plant Molecular Biology,* 50**,** 213-224.

Ho, C. S., Lam, C., Chan, M. H., Cheung, R., Law, L.*, et al.* (2003) Electrospray Ionisation Mass Spectrometry: Principles and Clinical Applications. *The Clinical Biochemist Reviews,* 24**,** 3.

Hong, B., Grzech, D., Caputi, L., Sonawane, P., López, C. E. R.*, et al.* (2022) Biosynthesis of Strychnine. *Nature,* 607**,** 617-622.

Hormozi, M., Gholami, M., Babaniazi, A. & Gharravi, A. M. (2019) Calendula Officinalis Stimulate Proliferation of Mouse Embryonic Fibroblasts Via Expression of Growth Factors Tgfβ1 and Bfgf. *Inflammation and regeneration,* 39**,** 1-7.

Hossain, M. A. & Ismail, Z. (2013) Isolation and Characterization of Triterpenes from the Leaves of Orthosiphon Stamineus. *Arabian Journal of Chemistry,* 6**,** 295-298.

Hsieh, M.-H., Pan, Z.-J., Lai, P.-H., Lu, H.-C., Yeh, H.-H.*, et al.* (2013) Virus-Induced Gene Silencing Unravels Multiple Transcription Factors Involved in Floral Growth and Development in Phalaenopsis Orchids. *Journal of Experimental Botany,* 64**,** 3869-3884.

Hsu, C.-L., Fang, S.-C., Huang, H.-W. & Yen, G.-C. (2015) Anti-Inflammatory Effects of Triterpenes and Steroid Compounds Isolated from the Stem Bark of Hiptage Benghalensis. *Journal of functional foods,* 12**,** 420-427.

Hu, Q., Bian, Q., Rong, D., Wang, L., Song, J.*, et al.* (2023) Jak/Stat Pathway: Extracellular Signals, Diseases, Immunity, and Therapeutic Regimens. *Frontiers in Bioengineering and Biotechnology,* 11**,** 1110765.

Hu, X., Li, J., Fu, M., Zhao, X. & Wang, W. (2021) The Jak/Stat Signaling Pathway: From Bench to Clinic. *Signal transduction and targeted therapy,* 6**,** 402.

Huang, A. C., Jiang, T., Liu, Y.-X., Bai, Y.-C., Reed, J.*, et al.* (2019) A Specialized Metabolic Network Selectively Modulates Arabidopsis Root Microbiota. *Science,* 364**,** eaau6389.

Huang, C.-H., Zhang, C., Liu, M., Hu, Y., Gao, T., *et al.* (2016) Multiple Polyploidization Events across Asteraceae with Two Nested Events in the Early History Revealed by Nuclear Phylogenomics. *Molecular Biology and Evolution,* 33**,** 2820-2835.

Huang, Q., Chen, C., Zhang, Z. & Xue, Q. (2023) Anti-Inflammatory Effects of Myristic Acid Mediated by the Nf-κb Pathway in Lipopolysaccharide-Induced Bv-2 Microglial Cells. *Molecular Omics,* 19**,** 726-734.

Hui, L., Li, Y., Huang, M.-K., Jiang, Y.-M. & Liu, T. (2024) Cxcl13: A Common Target for Immune-Mediated Inflammatory Diseases. *Clinical and Experimental Medicine,* 24**,** 244.

Hung, H.-C., Tsai, S.-F., Chou, H.-W., Tsai, M.-J., Hsu, P.-L., *et al.* (2023) Dietary Fatty Acids Differentially Affect Secretion of Pro-Inflammatory Cytokines in Human Thp-1 Monocytes. *Scientific reports,* 13**,** 5511.

Ikram, N. K. & Simonsen, H. T. (2017) A Review of Biotechnological Artemisinin Production in Plants. *Frontiers in Plant Science,* 8**,** 1966.

Inaba, J., Kim, B. M., Shimura, H. & Masuta, C. (2011) Virus-Induced Necrosis Is a Consequence of Direct Protein-Protein Interaction between a Viral Rna-Silencing Suppressor and a Host Catalase. *Plant Physiology,* 156**,** 2026-2036.

Itkin, M., Heinig, U., Tzfadia, O., Bhide, A., Shinde, B., *et al.* (2013) Biosynthesis of Antinutritional Alkaloids in Solanaceous Crops Is Mediated by Clustered Genes. *Science,* 341**,** 175-179.

Jacoby, R. P., Koprivova, A. & Kopriva, S. (2021) Pinpointing Secondary Metabolites That Shape the Composition and Function of the Plant Microbiome. *Journal of Experimental Botany,* 72**,** 57-69.

Jamtsho, T., Yeshi, K., Perry, M. J., Loukas, A. & Wangchuk, P. (2024) Approaches, Strategies and Procedures for Identifying Anti-Inflammatory Drug Lead Molecules from Natural Products. *Pharmaceuticals,* 17**,** 283.

Jan, N. & John, R. (2017) Calendula Officinalis-an Important Medicinal Plant with Potential Biological Properties.

Jan, R., Asaf, S., Numan, M., Lubna & Kim, K.-M. (2021) Plant Secondary Metabolite Biosynthesis and Transcriptional Regulation in Response to Biotic and Abiotic Stress Conditions. *Agronomy,* 11**,** 968.

Jänes, J. & Beltrao, P. (2024) Deep Learning for Protein Structure Prediction and Design—Progress and Applications. *Molecular Systems Biology,* 20**,** 162-169.

Jang, D.-I., Lee, A.-H., Shin, H.-Y., Song, H.-R., Park, J.-H., *et al.* (2021) The Role of Tumor Necrosis Factor Alpha (Tnf-α) in Autoimmune Disease and Current Tnf-α Inhibitors in Therapeutics. *International Journal of Molecular Sciences,* 22**,** 2719.

Jasoria, Y., Agrawal, M., Kumar, S., Chaudhary, H., Sahu, K. K., *et al.* (2024) In-Vivo Evaluation of Neuroprotective Effect of Chinese Plant Calendula Officinalis Linn. Flower Extract against Aluminium Chloride-Induced Alzheimer's in Wistar Rats. *Pharmacological Research-Modern Chinese Medicine,* 12**,** 100458.

Ji, Y., Xia, X., Xu, X. & Zhu, N. (2020) Three New Triterpenoids with Their Bioactives from the Roots of Rosa Cymosa. *Natural Product Research,* 34**,** 2931-2937.

Jiang, C.-J., Shimono, M., Maeda, S., Inoue, H., Mori, M., *et al.* (2009) Suppression of the Rice Fatty-Acid Desaturase Gene Osssi2 Enhances Resistance to Blast and Leaf Blight Diseases in Rice. *Molecular Plant-Microbe Interactions,* 22**,** 820-829.

Jiao, F., Tan, Z., Yu, Z., Zhou, B., Meng, L., *et al.* (2022) The Phytochemical and Pharmacological Profile of Taraxasterol. *Frontiers in Pharmacology,* 13**,** 927365.

Johnston, E. J., Tallis, J., Cunningham-Oakes, E., Moses, T., Moore, S. J., *et al.* (2023) Yeast Lacking the Sterol C-5 Desaturase Erg3 Are Tolerant to the Anti-Inflammatory Triterpenoid Saponin Escin. *Scientific reports,* 13**,** 13617.

Jones, H. D., Doherty, A. & Wu, H. X. (2005) Review of Methodologies and a Protocol for the Agrobacterium-Mediated Transformation of Wheat. *Plant Methods,* 1.

Jumper, J., Evans, R., Pritzel, A., Green, T., Figurnov, M., *et al.* (2021) Highly Accurate Protein Structure Prediction with Alphafold. *Nature,* 596**,** 583-589.

Jupin, I. (2013) A Protocol for Vigs in Arabidopsis Thaliana Using a One-Step Tymv-Derived Vector. *Virus-induced gene silencing: Methods and Protocols*, 197-210.

Kaas, Q. & Craik, D. J. (2013) Nmr of Plant Proteins. *Progress in Nuclear Magnetic Resonance Spectroscopy,* 71, 1-34.

Kabera, J. N., Semana, E., Mussa, A. R. & He, X. (2014) Plant Secondary Metabolites: Biosynthesis, Classification, Function and Pharmacological Properties. *J. Pharm. Pharmacol,* 2, 377-392.

Kallam, K., Moreno-Gimenez, E., Mateos-Fernandez, R., Tansley, C., Gianoglio, S., *et al.* (2023a) Tunable Control of Insect Pheromone Biosynthesis in <I>Nicotiana Benthamiana</I>. *Plant Biotechnology Journal,* 21, 1440-1453.

Kallam, K., Moreno-Giménez, E., Mateos-Fernández, R., Tansley, C., Gianoglio, S., *et al.* (2023b) Tunable Control of Insect Pheromone Biosynthesis in Nicotiana Benthamiana. *Plant Biotechnology Journal,* 21, 1440-1453.

Kalyaanamoorthy, S., Bui Quang, M., Wong, T. K. F., Von Haeseler, A. & Jermiin, L. S. (2017) Modelfinder: Fast Model Selection for Accurate Phylogenetic Estimates. *Nature Methods,* 14, 587-+.

Karakas, F. P., Turker, A. U., Karakas, A., Mshvildadze, V., Pichette, A., *et al.* (2017) In Vitro Cytotoxic, Antibacterial, Anti-Inflammatory and Antioxidant Activities and Phenolic Content in Wild-Grown Flowers of Common Daisy—a Medicinal Plant. *Journal of herbal medicine,* 8, 31-39.

Kautsar, S. A., Suarez Duran, H. G., Blin, K., Osbourn, A. & Medema, M. H. (2017) Plantismash: Automated Identification, Annotation and Expression Analysis of Plant Biosynthetic Gene Clusters. *Nucleic Acids Research,* 45, W55-W63.

Ke, D., Caiyin, Q., Zhao, F., Liu, T. & Lu, W. (2018) Heterologous Biosynthesis of Triterpenoid Ambrein in Engineered Escherichia Coli. *Biotechnology Letters,* 40, 399-404.

Kelley, L. A., Mezulis, S., Yates, C. M., Wass, M. N. & Sternberg, M. J. E. (2015) The Phyre2 Web Portal for Protein Modeling, Prediction and Analysis. *Nature Protocols,* 10, 845-858.

Khan, A. L., Hussain, J., Hamayun, M., Gilani, S. A., Ahmad, S., *et al.* (2010) Secondary Metabolites from Inula Britannica L. And Their Biological Activities. *Molecules,* 15, 1562-1577.

Khan, F., Pandey, P., Verma, M. & Upadhyay, T. K. (2024) Terpenoid-Mediated Targeting of Stat3 Signaling in Cancer: An Overview of Preclinical Studies. *Biomolecules,* 14, 200.

Khan, M. S. A. & Ahmad, I. (2019) Herbal Medicine: Current Trends and Future Prospects. *New Look to Phytomedicine.* Elsevier.

Khanra, R., Dewanjee, S., Dua, T. K. & Bhattacharjee, N. (2017) Taraxerol, a Pentacyclic Triterpene from Abroma Augusta Leaf, Attenuates Acute Inflammation Via Inhibition of Nf-κb Signaling. *Biomedicine & Pharmacotherapy,* 88, 918-923.

Kharissova, O. V., Kharisov, B. I., Oliva González, C. M., Méndez, Y. P. & López, I. (2019) Greener Synthesis of Chemical Compounds and Materials. *Royal Society open science,* 6, 191378.

Khouchlaa, A., El Baaboua, A., El Moudden, H., Lakhdar, F., Bakrim, S., *et al.* (2023) Traditional Uses, Bioactive Compounds, and Pharmacological Investigations of Calendula Arvensis L.: A Comprehensive Review. *Advances in Pharmacological and Pharmaceutical Sciences,* 2023, 2482544.

Kim, O. T., Kim, S. H., Ohyama, K., Muranaka, T., Choi, Y. E., *et al.* (2010) Upregulation of Phytosterol and Triterpene Biosynthesis in Centella Asiatica Hairy Roots Overexpressed Ginseng Farnesyl Diphosphate Synthase. *Plant Cell Reports,* 29, 403-411.

Kim, S.-H., Hong, J.-H., Yang, W.-K., Geum, J.-H., Kim, H.-R., *et al.* (2020) Herbal Combinational Medication of Glycyrrhiza Glabra, Agastache Rugosa Containing Glycyrrhizic Acid, Tilianin Inhibits Neutrophilic Lung Inflammation by Affecting

Cxcl2, Interleukin-17/Stat3 Signal Pathways in a Murine Model of Copd. *Nutrients,* 12**,** 926.

Kim, Y.-K., Kim, Y. B., Uddin, M. R., Lee, S., Kim, S.-U*., et al.* (2014) Enhanced Triterpene Accumulation in Panax Ginseng Hairy Roots Overexpressing Mevalonate-5-Pyrophosphate Decarboxylase and Farnesyl Pyrophosphate Synthase. *Acs Synthetic Biology,* 3**,** 773-779.

Kindler, S., Schuster, M., Seebauer, C., Rutkowski, R., Hauschild, A*., et al.* (2016) Triterpenes for Well-Balanced Scar Formation in Superficial Wounds. *Molecules,* 21**,** 1129.

Kirby, J. & Keasling, J. D. (2009) Biosynthesis of Plant Isoprenoids: Perspectives for Microbial Engineering. *Annual Review of Plant Biology,* 60**,** 335-355.

Klemke, R. L., Jiang, X., Choi, S. & Kelber, J. A. (2013) Proteomic and Biochemical Methods to Study the Cytoskeletome. *Adhesion protein protocols***,** 203-218.

Kliebenstein, D. J. & Osbourn, A. (2012) Making New Molecules–Evolution of Pathways for Novel Metabolites in Plants. *Current Opinion in Plant Biology,* 15**,** 415-423.

Klimyuk, V., Pogue, G., Herz, S., Butler, J. & Haydon, H. (2012) Production of Recombinant Antigens and Antibodies in Nicotiana Benthamiana Using 'Magnifection'technology: Gmp-Compliant Facilities for Small-and Large-Scale Manufacturing. *Plant viral vectors***,** 127-154.

Klusch, N., Dreimann, M., Senkler, J., Rugen, N., Kühlbrandt, W*., et al.* (2023) Cryo-Em Structure of the Respiratory I+ Iii2 Supercomplex from Arabidopsis Thaliana at 2 Å Resolution. *Nature plants,* 9**,** 142-156.

Koiwai, A., Suzuki, F., Matsuzaki, T. & Kawashima, N. (1983) The Fatty Acid Composition of Seeds and Leaves of Nicotiana Species. *Phytochemistry,* 22**,** 1409-1412.

Köllner, T. G., Lenk, C., Zhao, N., Seidl-Adams, I., Gershenzon, J*., et al.* (2010) Herbivore-Induced Sabath Methyltransferases of Maize That Methylate Anthranilic Acid Using S-Adenosyl-L-Methionine. *Plant Physiology,* 153**,** 1795-1807.

Komari, T. (1990) Transformation of Cultured-Cells of Chenopodium-Quinoa by Binary Vectors That Carry a Fragment of DNA from the Virulence Region of Ptibo542. *Plant Cell Reports,* 9**,** 303-306.

Kong, X., Zhang, Y., Wang, Z., Bao, S., Feng, Y*., et al.* (2023) Two-Step Model of Paleohexaploidy, Ancestral Genome Reshuffling and Plasticity of Heat Shock Response in Asteraceae. *Horticulture Research,* 10**,** uhad073.

König, A., Sadova, N., Dornmayr, M., Schwarzinger, B., Neuhauser, C*., et al.* (2023) Combined Acid Hydrolysis and Fermentation Improves Bioactivity of Citrus Flavonoids in Vitro and in Vivo. *Communications biology,* 6**,** 1083.

Kontra, L., Csorba, T., Tavazza, M., Lucioli, A., Tavazza, R*., et al.* (2016) Distinct Effects of P19 Rna Silencing Suppressor on Small Rna Mediated Pathways in Plants. *PLoS Pathogens,* 12**,** e1005935.

Korbecki, J. & Bajdak-Rusinek, K. (2019) The Effect of Palmitic Acid on Inflammatory Response in Macrophages: An Overview of Molecular Mechanisms. *Inflammation Research,* 68**,** 915-932.

Kriplani, P., Guarve, K. & Baghael, U. S. (2017) Arnica Montana L.–a Plant of Healing. *Journal of Pharmacy and Pharmacology,* 69**,** 925-945.

Kumagai, M. H., Donson, J., Della-Cioppa, G., Harvey, D., Hanley, K*., et al.* (1995) Cytoplasmic Inhibition of Carotenoid Biosynthesis with Virus-Derived Rna. *Proceedings of the National Academy of Sciences,* 92**,** 1679-1683.

Kumar, A., Srivastava, P., Srivastava, G., Sandeep, Kumar, N*., et al.* (2021) Bahd Acetyltransferase Contributes to Wound-Induced Biosynthesis of Oleo-Gum Resin Triterpenes in Boswellia. *The Plant Journal,* 107**,** 1403-1419.

Kumar, B., Vijayakumar, M., Govindarajan, R. & Pushpangadan, P. (2007) Ethnopharmacological Approaches to Wound Healing—Exploring Medicinal Plants of India. *Journal of Ethnopharmacology,* 114**,** 103-113.

Kumar, K. J. & Vijayan, V. (2014) An Overview of Liquid Chromatography-Mass Spectroscopy Instrumentation. *Pharmaceutical methods,* 5**,** 47.

Kumari, S., Nazir, F., Maheshwari, C., Kaur, H., Gupta, R.*, et al.* (2024) Plant Hormones and Secondary Metabolites under Environmental Stresses: Enlightening Defense Molecules. *Plant Physiology and Biochemistry,* 206**,** 108238.

Lacomme, C. & Chapman, S. (2008) Use of Potato Virus X (Pvx)–Based Vectors for Gene Expression and Virus-Induced Gene Silencing (Vigs). *Current protocols in microbiology,* 8**,** 16I. 1.1-16I. 1.13.

Lakatos, L., Szittya, G., Silhavy, D. & Burgyán, J. (2004) Molecular Mechanism of Rna Silencing Suppression Mediated by P19 Protein of Tombusviruses. *The EMBO journal,* 23**,** 876-884.

Lakshman, H., Yeasmin, T. & Gabriel, K. (2014) Herbs of Asteraceae and Their Ethano Medicinal Uses in Dermatological Problems. *Journal of Bio-Science,* 22**,** 127-129.

Lallemand, T., Leduc, M., Landès, C., Rizzon, C. & Lerat, E. (2020) An Overview of Duplicated Gene Detection Methods: Why the Duplication Mechanism Has to Be Accounted for in Their Choice. *Genes,* 11**,** 1046.

Lampugnani, M. G. (1999) Cell Migration into a Wounded Area in Vitro. *Adhesion protein protocols***,** 177-182.

Land, H. & Humble, M. S. (2018a) Yasara: A Tool to Obtain Structural Guidance in Biocatalytic Investigations. *Protein engineering: methods and protocols***,** 43-67.

Land, H. & Humble, M. S. (2018b) Yasara: A Tool to Obtain Structural Guidance in Biocatalytic Investigations. *Methods in molecular biology (Clifton, N.J.),* 1685**,** 43-67.

Lange, T., Hedden, P. & Graebe, J. E. (1994) Expression Cloning of a Gibberellin 20-Oxidase, a Multifunctional Enzyme Involved in Gibberellin Biosynthesis. *Proceedings of the National Academy of Sciences,* 91**,** 8552-8556.

Lau, W. & Sattely, E. S. (2015) Six Enzymes from Mayapple That Complete the Biosynthetic Pathway to the Etoposide Aglycone. *Science,* 349**,** 1224-1228.

Lazo, G. R., Stein, P. A. & Ludwig, R. A. (1991) A DNA Transformation–Competent Arabidopsis Genomic Library in Agrobacterium. *Bio/technology,* 9**,** 963-967.

Lee, A.-R., Kwon, M., Kang, M.-K., Kim, J., Kim, S.-U.*, et al.* (2019) Increased Sesqui-and Triterpene Production by Co-Expression of Hmg-Coa Reductase and Biotin Carboxyl Carrier Protein in Tobacco (Nicotiana Benthamiana). *Metabolic Engineering,* 52**,** 20-28.

Lee, J., Shin, M. S., Kim, M. O., Jang, S., Oh, S. W.*, et al.* (2016) Apple Ethanol Extract Promotes Proliferation of Human Adult Stem Cells, Which Involves the Regenerative Potential of Stem Cells. *Nutrition Research,* 36**,** 925-936.

Leite, A. C., Bueno, F. C., Oliveira, C. G., Fernandes, J. B., Vieira, P. C.*, et al.* (2005) Limonoids from Cipadessa Fruticosa and Cedrela Fissilis and Their Insecticidal Activity. *Journal of the Brazilian Chemical Society,* 16**,** 1391-1395.

Li, C., Cui, Z., Deng, S., Chen, P., Li, X.*, et al.* (2022a) The Potential of Plant Extracts in Cell Therapy. *Stem Cell Research & Therapy,* 13**,** 472.

Li, C., Wood, J. C., Vu, A. H., Hamilton, J. P., Rodriguez Lopez, C. E.*, et al.* (2023a) Single-Cell Multi-Omics in the Medicinal Plant Catharanthus Roseus. *Nature Chemical Biology,* 19**,** 1031-1041.

Li, C., Zha, W., Li, W., Wang, J. & You, A. (2023b) Advances in the Biosynthesis of Terpenoids and Their Ecological Functions in Plant Resistance. *International Journal of Molecular Sciences,* 24**,** 11561.

Li, W., Zeng, H., Xu, M., Huang, C., Tao, L.*, et al.* (2021a) Oleanolic Acid Improves Obesity-Related Inflammation and Insulin Resistance by Regulating Macrophages Activation. *Frontiers in Pharmacology,* 12**,** 697483.

Li, X., Shan, Y., Wang, S., Wang, J. & Heng, X. (2024a) Triptolide Induces Apoptosis of Glioma Cells by Inhibiting Nf-κb Activation during Oxidative Stress. *Scientific reports,* 14**,** 29740.

Li, Y., Grotewold, E. & Dudareva, N. (2024b) Enough Is Enough: Feedback Control of Specialized Metabolism. *Trends in Plant Science,* 29**,** 514-523.
Li, Y., Leveau, A., Zhao, Q., Feng, Q., Lu, H.*, et al.* (2021b) Subtelomeric Assembly of a Multi-Gene Pathway for Antimicrobial Defense Compounds in Cereals. *Nature Communications,* 12**,** 2563.
Li, Y. J., Tang, D., Liu, Z. R., Chen, J. J., Cheng, B. P.*, et al.* (2022b) An Improved Procedure for <I>Agrobacterium</I>-Mediated Transformation of 'Carrizo' Citrange. *Plants-Basel,* 11.
Liang, C.-C., Park, A. Y. & Guan, J.-L. (2007) In Vitro Scratch Assay: A Convenient and Inexpensive Method for Analysis of Cell Migration in Vitro. *Nature Protocols,* 2**,** 329-333.
Liang, M., Zhang, F., Xu, J., Wang, X., Wu, R.*, et al.* (2022) A Conserved Mechanism Affecting Hydride Shifting and Deprotonation in the Synthesis of Hopane Triterpenes as Compositions of Wax in Oat. *Proceedings of the National Academy of Sciences,* 119**,** e2118709119.
Liao, P., Chen, X., Wang, M., Bach, T. J. & Chye, M. L. (2018) Improved Fruit α-Tocopherol, Carotenoid, Squalene and Phytosterol Contents through Manipulation of Brassica Juncea 3-Hydroxy-3-Methylglutaryl-Coa Synthase 1 in Transgenic Tomato. *Plant Biotechnology Journal,* 16**,** 784-796.
Lin, M., Yang, S., Huang, J. & Zhou, L. (2021) Insecticidal Triterpenes in Meliaceae: Plant Species, Molecules and Activities: Part I (Aphanamixis-Chukrasia). *International Journal of Molecular Sciences,* 22**,** 13262.
Linde, K., Barrett, B., Bauer, R., Melchart, D. & Woelkart, K. (2006) Echinacea for Preventing and Treating the Common Cold. *Cochrane Database of Systematic Reviews*.
Liscombe, D. K. & O'connor, S. E. (2011) A Virus-Induced Gene Silencing Approach to Understanding Alkaloid Metabolism in <I>Catharanthus Roseus</I>. *Phytochemistry,* 72**,** 1969-1977.
Liu, H. & Naismith, J. H. (2008) An Efficient One-Step Site-Directed Deletion, Insertion, Single and Multiple-Site Plasmid Mutagenesis Protocol. *BMC Biotechnology,* 8.
Liu, J., Yin, X., Kou, C., Thimmappa, R., Hua, X.*, et al.* (2024a) Classification, Biosynthesis and Biological Function of Triterpene Esters in Plants. *Plant Communications*.
Liu, Q., Khakimov, B., Cárdenas, P. D., Cozzi, F., Olsen, C. E.*, et al.* (2019a) The Cytochrome P450 Cyp72a552 Is Key to Production of Hederagenin-Based Saponins That Mediate Plant Defense against Herbivores. *New Phytologist,* 222**,** 1599-1609.
Liu, Q., Manzano, D., Tanić, N., Pesic, M., Bankovic, J.*, et al.* (2014) Elucidation and in Planta Reconstitution of the Parthenolide Biosynthetic Pathway. *Metabolic Engineering,* 23**,** 145-153.
Liu, R., Carballo-Arce, A.-F., Singh, R., Saleem, A., Rocha, M.*, et al.* (2019b) A Selective Ion Hplc-Apci-Ms Method for the Quantification of Pentacyclic Triterpenes in an Anxiolytic Botanical Dietary Supplement for the Animal Health Market. *Natural Product Communications,* 14**,** 1934578X1901400104.
Liu, X., Yin, S., Chen, Y., Wu, Y., Zheng, W.*, et al.* (2018) Lps-Induced Proinflammatory Cytokine Expression in Human Airway Epithelial Cells and Macrophages Via Nf-κb, Stat3 or Ap-1 Activation. *Molecular medicine reports,* 17**,** 5484-5491.
Liu, Y., Schiff, M., Marathe, R. & Dinesh-Kumar, S. (2002) Tobacco Rar1, Eds1 and Npr1/Nim1 Like Genes Are Required for N-Mediated Resistance to Tobacco Mosaic Virus. *The Plant Journal,* 30**,** 415-429.
Liu, Y., Xiong, W., Wang, C.-W., Shi, J.-P., Shi, Z.-Q.*, et al.* (2021) Resveratrol Promotes Skin Wound Healing by Regulating the Mir-212/Casp8 Axis. *Laboratory Investigation,* 101**,** 1363-1370.
Liu, Y., Zhao, X., Gan, F., Chen, X., Deng, K.*, et al.* (2024b) Complete Biosynthesis of Qs-21 in Engineered Yeast. *Nature,* 629**,** 937-944.

Liu, Z., Cheema, J., Vigouroux, M., Hill, L., Reed, J., *et al.* (2020) Formation and Diversification of a Paradigm Biosynthetic Gene Cluster in Plants. *Nature Communications,* 11**,** 5354.
Livak, K. J. & Schmittgen, T. D. (2001) Analysis of Relative Gene Expression Data Using Real-Time Quantitative Pcr and the 2^{-ΔΔ<I>C</I>}_T Method. *Methods,* 25**,** 402-408.
Lomenick, B., Olsen, R. W. & Huang, J. (2011) Identification of Direct Protein Targets of Small Molecules. *ACS chemical biology,* 6**,** 34-46.
Lomonossoff, G. P. & D'aoust, M.-A. (2016) Plant-Produced Biopharmaceuticals: A Case of Technical Developments Driving Clinical Deployment. *Science,* 353**,** 1237-1240.
Lourenço, A., Marques, A. V. & Gominho, J. (2021) The Identification of New Triterpenoids in Eucalyptus Globulus Wood. *Molecules,* 26**,** 3495.
Love, M. I., Huber, W. & Anders, S. (2014) Moderated Estimation of Fold Change and Dispersion for Rna-Seq Data with Deseq2. *Genome Biology,* 15.
Lu, R., Zhang, Y.-G. & Sun, J. (2017) Stat3 Activation in Infection and Infection-Associated Cancer. *Molecular and Cellular Endocrinology,* 451**,** 80-87.
Lund, R. J., Chen, Z., Scheinin, J. & Lahesmaa, R. (2004) Early Target Genes of Il-12 and Stat4 Signaling in Th Cells. *The Journal of Immunology,* 172**,** 6775-6782.
Luo, K.-R., Huang, N.-C., Chang, Y.-H., Jan, Y.-W. & Yu, T.-S. (2024) Arabidopsis Cyclophilins Direct Intracellular Transport of Mobile Mrna Via Organelle Hitchhiking. *Nature plants,* 10**,** 161-171.
Lv, Y., Mi, P., Babon, J. J., Fan, G., Qi, J., *et al.* (2024) Small Molecule Drug Discovery Targeting the Jak-Stat Pathway. *Pharmacological Research***,** 107217.
Ma, Y.-C. & Kim, H.-Y. (1997) Determination of Steroids by Liquid Chromatography/Mass Spectrometry. *Journal of the American Society for Mass Spectrometry,* 8**,** 1010-1020.
Macht, D. I. (1955) Calendula or Marigold in Medical History and in Shakespeare. *Bulletin of the history of medicine,* 29**,** 491-502.
Macioszek, V. K., Jęcz, T., Ciereszko, I. & Kononowicz, A. K. (2023) Jasmonic Acid as a Mediator in Plant Response to Necrotrophic Fungi. *Cells,* 12**,** 1027.
Mahmoudi, Z., Soleimani, M., Khamisipour, G. & Azizsoltani, A. (2013) Effects of Foeniculum Vulgare Ethanol Extract on Osteogenesis in Human Mecenchymal Stem Cells. *Avicenna Journal of Phytomedicine,* 3**,** 135.
Malabadi, R., Kolkar, K., Acharya, M., Nityasree, B. & Chalannavar, R. (2022) Wound Healing: Role of Traditional Herbal Medicine Treatment. *International Journal of Innovation Scientific Research and Review,* 4**,** 2856-2874.
Maldonado, M., Fan, Z., Abe, K. & Letts, J. (2023) Plant-Specific Features of Respiratory Supercomplex I+ Iii2 from Vigna Radiata. *Nature plants,* 9**,** 157-168.
Malhotra, K. & Franke, J. (2022a) Cytochrome P450 Monooxygenase-Mediated Tailoring of Triterpenoids and Steroids in Plants. *Beilstein Journal of Organic Chemistry,* 18**,** 1289-1310.
Malhotra, K. & Franke, J. (2022b) Cytochrome P450 Monooxygenase-Mediated Tailoring of Triterpenoids and Steroids in Plants. *Beilstein Journal of Organic Chemistry,* 18**,** 1289-1310.
Mandel, J. R., Dikow, R. B., Siniscalchi, C. M., Thapa, R., Watson, L. E., *et al.* (2019) A Fully Resolved Backbone Phylogeny Reveals Numerous Dispersals and Explosive Diversifications Throughout the History of Asteraceae. *Proceedings of the National Academy of Sciences,* 116**,** 14083-14088.
Mardini, M., Kazancev, M., Ivoilova, E., Utkina, V., Vlasova, A., *et al.* (2024) Advancing Virus-Induced Gene Silencing in Sunflower: Key Factors of Vigs Spreading and a Novel Simple Protocol. *Plant Methods,* 20.
Martin, F. N., Abad, Z. G., Balci, Y. & Ivors, K. (2012) Identification and Detection of Phytophthora: Reviewing Our Progress, Identifying Our Needs. *Plant Disease,* 96**,** 1080-1103.

Matsushima, K., Yang, D. & Oppenheim, J. J. (2022) Interleukin-8: An Evolving Chemokine. *Cytokine,* 153**,** 155828.
Mcdaniel, D. K., Eden, K., Ringel, V. M. & Allen, I. C. (2016) Emerging Roles for Noncanonical Nf-κb Signaling in the Modulation of Inflammatory Bowel Disease Pathobiology. *Inflammatory bowel diseases,* 22**,** 2265-2279.
Medhe, S. (2018) Ionization Techniques in Mass Spectrometry: A Review. *Mass Spectrom Purif Tech,* 4**,** 1000126.
Megha, K., Joseph, X., Akhil, V. & Mohanan, P. (2021) Cascade of Immune Mechanism and Consequences of Inflammatory Disorders. *Phytomedicine,* 91**,** 153712.
Mehta, M., Branford, O. & Rolfe, K. (2016) The Evidence for Natural Therapeutics as Potential Anti-Scarring Agents in Burn-Related Scarring. *Burns & trauma,* 4.
Miettinen, K., Dong, L., Navrot, N., Schneider, T., Burlat, V.*, et al.* (2014) The Seco-Iridoid Pathway from Catharanthus Roseus. *Nature Communications,* 5**,** 3606.
Miettinen, K., Inigo, S., Kreft, L., Pollier, J., De Bo, C.*, et al.* (2018) The Triforc Database: A Comprehensive up-to-Date Resource of Plant Triterpene Biosynthesis. *Nucleic Acids Research,* 46**,** D586-D594.
Miettinen, K., Pollier, J., Buyst, D., Arendt, P., Csuk, R.*, et al.* (2017a) The Ancient Cyp716 Family Is a Major Contributor to the Diversification of Eudicot Triterpenoid Biosynthesis. *Nature Communications,* 8**,** 14153.
Miettinen, K., Pollier, J., Buyst, D., Arendt, P., Csuk, R.*, et al.* (2017b) The Ancient Cyp716 Family Is a Major Contributor to the Diversification of Eudicot Triterpenoid Biosynthesis. *Nature Communications,* 8.
Minerdi, D., Savoi, S. & Sabbatini, P. (2023) Role of Cytochrome P450 Enzyme in Plant Microorganisms' Communication: A Focus on Grapevine. *International Journal of Molecular Sciences,* 24**,** 4695.
Mipeshwaree Devi, A., Khedashwori Devi, K., Premi Devi, P., Lakshmipriyari Devi, M. & Das, S. (2023) Metabolic Engineering of Plant Secondary Metabolites: Prospects and Its Technological Challenges. *Frontiers in Plant Science,* 14**,** 1171154.
Misra, R. C., Sharma, S., Sandeep, Garg, A., Chanotiya, C. S.*, et al.* (2017) Two Cyp716a Subfamily Cytochrome P450 Monooxygenases of Sweet Basil Play Similar but Nonredundant Roles in Ursane- and Oleanane-Type Pentacyclic Triterpene Biosynthesis. *New Phytologist,* 214**,** 706-720.
Moghadam, S. E., Ebrahimi, S. N., Salehi, P., Moridi Farimani, M., Hamburger, M.*, et al.* (2017) Wound Healing Potential of Chlorogenic Acid and Myricetin-3-O-β-Rhamnoside Isolated from Parrotia Persica. *Molecules,* 22**,** 1501.
Moghe, G. D. & Last, R. L. (2015) Something Old, Something New: Conserved Enzymes and the Evolution of Novelty in Plant Specialized Metabolism. *Plant Physiology,* 169**,** 1512-1523.
Moglia, A., Acquadro, A., Eljounaidi, K., Milani, A. M., Cagliero, C.*, et al.* (2016) Genome-Wide Identification of Bahd Acyltransferases and <I>in Vivo</I> Characterization of Hqt-Like Enzymes Involved in Caffeoylquinic Acid Synthesis in Globe Artichoke. *Frontiers in Plant Science,* 7.
Mohamed, H. E., Asker, M. E., Kotb, N. S. & El Habab, A. M. (2020) Human Platelet Lysate Efficiency, Stability, and Optimal Heparin Concentration Required in Culture of Mammalian Cells. *Blood research,* 55**,** 35.
Molnár, A., Csorba, T., Lakatos, L., Várallyay, É., Lacomme, C.*, et al.* (2005) Plant Virus-Derived Small Interfering Rnas Originate Predominantly from Highly Structured Single-Stranded Viral Rnas. *Journal of Virology,* 79**,** 7812-7818.
Monika, P., Chandraprabha, M. N., Rangarajan, A., Waiker, P. V. & Chidambara Murthy, K. N. (2022) Challenges in Healing Wound: Role of Complementary and Alternative Medicine. *Frontiers in nutrition,* 8**,** 791899.
Monte, I. (2023) Jasmonates and Salicylic Acid: Evolution of Defense Hormones in Land Plants. *Current Opinion in Plant Biology,* 76**,** 102470.

Morcillo, M., Sales, E., Corredoira, E., Martínez, M. T., Segura, J., *et al.* (2022) Effect of Methyl Jasmonate in Gene Expression, and in Hormonal and Phenolic Profiles of Holm Oak Embryogenic Lines before and after Infection with Phytophthora Cinnamomi. *Frontiers in Plant Science,* 13**,** 824781.

Mosa, R. A., Nhleko, M. L., Dladla, T. V. & Opoku, A. R. (2014) Antibacterial Activity of Two Triterpenes from Stem Bark of Protorhus Longifolia. *J. Med. Plant. Res,* 8**,** 686-70.

Mugford, S. T., Louveau, T., Melton, R., Qi, X., Bakht, S., *et al.* (2013) Modularity of Plant Metabolic Gene Clusters: A Trio of Linked Genes That Are Collectively Required for Acylation of Triterpenes in Oat. *The Plant Cell,* 25**,** 1078-1092.

Muley, B., Khadabadi, S. & Banarase, N. (2009) Phytochemical Constituents and Pharmacological Activities of Calendula Officinalis Linn (Asteraceae): A Review. *Tropical journal of pharmaceutical research,* 8.

Müller, C. & Riederer, M. (2005) Plant Surface Properties in Chemical Ecology. *Journal of Chemical Ecology,* 31**,** 2621-2651.

Nakano, Y. (2017) Effect of Acetosyringone on Agrobacterium-Mediated Transformation of Eustoma Grandiflorum Leaf Disks. *Japan Agricultural Research Quarterly: JARQ,* 51**,** 351-355.

Neukirch, H., D'ambrosio, M., Sosa, S., Altinier, G., Della Loggia, R., *et al.* (2005) Improved Anti-Inflammatory Activity of Three New Terpenoids Derived, by Systematic Chemical Modifications, from the Abundant Triterpenes of the Flowery Plant Calendula Officinalis. *Chemistry & Biodiversity,* 2**,** 657-671.

Neves, G. P. D., Nakamura, M. J., Ramos, M. F. D. S., Siani, A. C. & Mazzei, J. L. (2020) Development of a Gas Chromatography Method for Quantification of Triterpenes in the Commercial Oleoresins from Protium Species. *Rodriguésia,* 71**,** e00702019.

Nicolaus, C., Junghanns, S., Hartmann, A., Murillo, R., Ganzera, M., *et al.* (2017) In Vitro Studies to Evaluate the Wound Healing Properties of Calendula Officinalis Extracts. *Journal of Ethnopharmacology,* 196**,** 94-103.

Nicolaus, C., Sievers-Engler, A., Murillo, R., D'ambrosio, M., Lämmerhofer, M., *et al.* (2016) Mastering Analytical Challenges for the Characterization of Pentacyclic Triterpene Mono-and Diesters of Calendula Officinalis Flowers by Non-Aqueous C30 Hplc and Hyphenation with Apci-Qtof-Ms. *Journal of Pharmaceutical and Biomedical Analysis,* 118**,** 195-205.

Ninomiya, K., Motai, C., Nishida, E., Kitagawa, N., Yoshihara, K., *et al.* (2016) Acylated Oleanane-Type Triterpene Saponins from the Flowers of Bellis Perennis Show Anti-Proliferative Activities against Human Digestive Tract Carcinoma Cell Lines. *Journal of natural medicines,* 70**,** 435-451.

Niżyński, B., Alsoufi, A. S. M., Pączkowski, C., Długosz, M. & Szakiel, A. (2015) The Content of Free and Esterified Triterpenoids of the Native Marigold (Calendula Officinalis) Plant and Its Modifications in in Vitro Cultures. *Phytochemistry Letters,* 11**,** 410-417.

Nora, S., Castro, S., Loureiro, J., Gonçalves, A. C., Oliveira, H., *et al.* (2013) Flow Cytometric and Karyological Analyses of Calendula Species from Iberian Peninsula. *Plant Systematics and Evolution,* 299**,** 853-864.

Nothias, L.-F., Petras, D., Schmid, R., Dührkop, K., Rainer, J., *et al.* (2020) Feature-Based Molecular Networking in the Gnps Analysis Environment. *Nature Methods,* 17**,** 905-908.

Nützmann, H. W., Huang, A. & Osbourn, A. (2016) Plant Metabolic Clusters–from Genetics to Genomics. *New Phytologist,* 211**,** 771-789.

Nwanochie, E. & Uversky, V. N. (2019) Structure Determination by Single-Particle Cryo-Electron Microscopy: Only the Sky (and Intrinsic Disorder) Is the Limit. *International Journal of Molecular Sciences,* 20**,** 4186.

O'connor, S. (2009) Methods for Molecular Identification of Biosynthetic Enzymes in Plants. *Plant-derived natural products: Synthesis, function, and application***,** 165-179.

Olennikov, D. N. & Kashchenko, N. I. (2013) New Isorhamnetin Glycosides and Other Phenolic Compounds from <I>Calendula Officinalis</I>. *Chemistry of Natural Compounds,* 49**,** 833-840.

Olennikov, D. N. & Kashchenko, N. I. (2022) Marigold Metabolites: Diversity and Separation Methods of Calendula Genus Phytochemicals from 1891 to 2022. *Molecules,* 27**,** 8626.

Oleszek, W. & Stochmal, A. (2010) 25 High Performance Liquid Chromatography of Triterpenes (Including Saponins).

Ono, E. & Murata, J. (2023) Exploring the Evolvability of Plant Specialized Metabolism: Uniqueness out of Uniformity and Uniqueness Behind Uniformity. *Plant and Cell Physiology,* 64**,** 1449-1465.

Opatíková, M., Semchonok, D. A., Kopečný, D., Ilík, P., Pospíšil, P*., et al.* (2023) Cryo-Em Structure of a Plant Photosystem Ii Supercomplex with Light-Harvesting Protein Lhcb8 and α-Tocopherol. *Nature plants,* 9**,** 1359-1369.

Paddon, C. J. & Keasling, J. D. (2014) Semi-Synthetic Artemisinin: A Model for the Use of Synthetic Biology in Pharmaceutical Development. *Nature Reviews Microbiology,* 12**,** 355-367.

Pagare, S., Bhatia, M., Tripathi, N., Pagare, S. & Bansal, Y. (2015) Secondary Metabolites of Plants and Their Role: Overview. *Current trends in biotechnology and pharmacy,* 9**,** 293-304.

Palmer, L., Chuang, L., Siegmund, M., Kunert, M., Yamamoto, K*., et al.* (2022) In Vivo Characterization of Key Iridoid Biosynthesis Pathway Genes in Catnip (<I>Nepeta Cataria</I>). *Planta,* 256.

Panero, J. L. & Crozier, B. S. (2016) Macroevolutionary Dynamics in the Early Diversification of Asteraceae. *Molecular Phylogenetics and Evolution,* 99**,** 116-132.

Pang, Z., Chen, J., Wang, T., Gao, C., Li, Z*., et al.* (2021) Linking Plant Secondary Metabolites and Plant Microbiomes: A Review. *Frontiers in Plant Science,* 12**,** 621276.

Papadopoulou, N., Devos, Y., Álvarez-Alfageme, F., Lanzoni, A. & Waigmann, E. (2020) Risk Assessment Considerations for Genetically Modified Rnai Plants: Efsa's Activities and Perspective. *Frontiers in Plant Science,* 11**,** 445.

Park, B. & Lee, J. Recognition of Lipopolysaccharide Pattern by Tlr4 Complexes. 2013. *Exp Mol Med, Vols,* 45**,** 12.

Park, J. H., Tran, L. H. & Jung, S. (2017) Perturbations in the Photosynthetic Pigment Status Result in Photooxidation-Induced Crosstalk between Carotenoid and Porphyrin Biosynthetic Pathways. *Frontiers in Plant Science,* 8.

Patron, N., Orzaez, D., Marillonnet, S., Warzecha, H., Matthewman, C*., et al.* (2015) Standards for Plant Synthetic Biology: A Common Syntax for Exchange of DNA Parts. *New Phytologist,* 208**,** 13-19.

Pauwels, L., Inzé, D. & Goossens, A. (2009) Jasmonate-Inducible Gene: What Does It Mean? *Trends in Plant Science,* 14**,** 87-91.

Petti, C., Wendt, T., Meade, C. & Mullins, E. (2009) Evidence of Genotype Dependency within Agrobacterium Tumefaciens in Relation to the Integration of Vector Backbone Sequence in Transgenic Phytophthora Infestans-Tolerant Potato. *Journal of Bioscience and Bioengineering,* 107**,** 301-306.

Pflieger, S., Blanchet, S., Camborde, L., Drugeon, G., Rousseau, A*., et al.* (2008) Efficient Virus-Induced Gene Silencing in Arabidopsis Using a 'One-Step' Tymv-Derived Vector. *Plant Journal,* 56**,** 678-690.

Piao, T., Ma, Z., Li, X. & Liu, J. (2015) Taraxasterol Inhibits Il-1β-Induced Inflammatory Response in Human Osteoarthritic Chondrocytes. *European Journal of Pharmacology,* 756**,** 38-42.

Pichersky, E. & Lewinsohn, E. (2011) Convergent Evolution in Plant Specialized Metabolism. *Annual Review of Plant Biology,* 62**,** 549-566.
Pin, P. A. & Nilsson, O. (2012) The Multifaceted Roles of Flowering Locus T in Plant Development. *Plant Cell and Environment,* 35**,** 1742-1755.
Plume, O. (2015) Hybridization, Genome Duplication, and Chemical Diversification in the Evolution of Calendula L.(Compositae).
Poirier, B. C., Buchanan, D. A., Rudell, D. R. & Mattheis, J. P. (2018) Differential Partitioning of Triterpenes and Triterpene Esters in Apple Peel. *Journal of Agricultural and Food Chemistry,* 66**,** 1800-1806.
Polturak, G., Liu, Z. & Osbourn, A. (2022) New and Emerging Concepts in the Evolution and Function of Plant Biosynthetic Gene Clusters. *Current Opinion in Green and Sustainable Chemistry,* 33**,** 100568.
Polturak, G. & Osbourn, A. (2021) The Emerging Role of Biosynthetic Gene Clusters in Plant Defense and Plant Interactions. *PLoS Pathogens,* 17**,** e1009698.
Preethi, K. C., Kuttan, G. & Kuttan, R. (2009) Anti-Inflammatory Activity of Flower Extract of Calendula Officinalis Linn. And Its Possible Mechanism of Action.
Prinz, W. A., Toulmay, A. & Balla, T. (2020) The Functional Universe of Membrane Contact Sites. *Nature Reviews Molecular Cell Biology,* 21**,** 7-24.
Prosser, G. A., Larrouy-Maumus, G. & De Carvalho, L. P. S. (2014) Metabolomic Strategies for the Identification of New Enzyme Functions and Metabolic Pathways. *EMBO reports,* 15**,** 657-669.
Pucker, B. & Iorizzo, M. (2023) Apiaceae Fns I Originated from F3h through Tandem Gene Duplication. *Plos One,* 18**,** e0280155.
Qamar, F., Ashrafi, K., Singh, A., Dash, P. K. & Abdin, M. (2024a) Artemisinin Production Strategies for Industrial Scale: Current Progress and Future Directions. *Industrial Crops and Products,* 218**,** 118937.
Qamar, F., Mishra, A., Ashrafi, K., Saifi, M., Dash, P. K.*, et al.* (2024b) Increased Artemisinin Production in Artemisia Annua L. By Co-Overexpression of Six Key Biosynthetic Enzymes. *International Journal of Biological Macromolecules,* 281**,** 136291.
Rahimi, S., Kim, J., Mijakovic, I., Jung, K.-H., Choi, G.*, et al.* (2019) Triterpenoid-Biosynthetic Udp-Glycosyltransferases from Plants. *Biotechnology Advances,* 37**,** 107394.
Rao, K. S. & Rohini, V. (1999) Agrobacterium-Mediated Transformation of Sunflower (Helianthus Annuusl.): A Simple Protocol. *Annals of Botany,* 83**,** 347-354.
Rao, T. R., Harshitha, S. & Lahari, K. L. (2023) Gas Chromatography-Mass Spectroscopy: An Overview. *Eur J Biomed Pharm Sci,* 10**,** 83-89.
Reddy, D. B. & Reddanna, P. (2009) Chebulagic Acid (Ca) Attenuates Lps-Induced Inflammation by Suppressing Nf-κb and Mapk Activation in Raw 264.7 Macrophages. *Biochemical and Biophysical Research Communications,* 381**,** 112-117.
Reddy, V. A., Leong, S. H., Jang, I.-C. & Rajani, S. (2022) Metabolic Engineering of Nicotiana Benthamiana to Produce Cannabinoid Precursors and Their Analogues. *Metabolites,* 12**,** 1181.
Reed, J. (2016) *Transient Expression for Engineering Triterpenoid Diversity in Plants.* University of East Anglia.
Reed, J., Orme, A., El-Demerdash, A., Owen, C., Martin, L. B.*, et al.* (2023) Elucidation of the Pathway for Biosynthesis of Saponin Adjuvants from the Soapbark Tree. *Science,* 379**,** 1252-1264.
Reed, J. & Osbourn, A. (2018) Engineering Terpenoid Production through Transient Expression in Nicotiana Benthamiana. *Plant Cell Reports,* 37**,** 1431-1441.
Reed, J., Stephenson, M. J., Miettinen, K., Brouwer, B., Leveau, A.*, et al.* (2017a) A Translational Synthetic Biology Platform for Rapid Access to Gram-Scale Quantities of Novel Drug-Like Molecules. *Metabolic Engineering,* 42**,** 185-193.

Reed, J., Stephenson, M. J., Miettinen, K., Brouwer, B., Leveau, A., *et al.* (2017b) A Translational Synthetic Biology Platform for Rapid Access to Gram-Scale Quantities of Novel Drug-Like Molecules. *Metabolic Engineering,* 42**,** 185-193.

Ren, H., Shi, C. & Zhao, H. (2020) Computational Tools for Discovering and Engineering Natural Product Biosynthetic Pathways. *Iscience,* 23.

Reynolds, K. B., Taylor, M. C., Zhou, X.-R., Vanhercke, T., Wood, C. C., *et al.* (2015) Metabolic Engineering of Medium-Chain Fatty Acid Biosynthesis in Nicotiana Benthamiana Plant Leaf Lipids. *Frontiers in Plant Science,* 6**,** 164.

Reznicek, G. & Zitterl-Eglseer, K. (2003) Quantitative Determination of the Faradiol Esters in Marigold Flowers and Extracts. *Scientia Pharmaceutica,* 71**,** 121-128.

Rhourri-Frih, B., Chaimbault, P., Claude, B., Lamy, C., André, P., *et al.* (2009) Analysis of Pentacyclic Triterpenes by Lc–Ms. A Comparative Study between Apci and Appi. *Journal of Mass Spectrometry,* 44**,** 71-80.

Riaz, T., Akram, M., Laila, U., Khalil, M. T., Zainab, R., *et al.* (2023) Milk Thistle: A Review of Its Phytochemistry, Pharmacology and Conventional Uses. *International Archives of Integrated Medicine,* 10.

Rice, A., Glick, L., Abadi, S., Einhorn, M., Kopelman, N. M., *et al.* (2015) The Chromosome Counts Database (Ccdb)–a Community Resource of Plant Chromosome Numbers. *New Phytologist,* 206**,** 19-26.

Rolnik, A. & Olas, B. (2021) The Plants of the Asteraceae Family as Agents in the Protection of Human Health. *International Journal of Molecular Sciences,* 22**,** 3009.

Romero-Estrada, A., Maldonado-Magaña, A., González-Christen, J., Bahena, S. M., Garduño-Ramírez, M. L., *et al.* (2016) Anti-Inflammatory and Antioxidative Effects of Six Pentacyclic Triterpenes Isolated from the Mexican Copal Resin of Bursera Copallifera. *BMC Complementary and Alternative Medicine,* 16**,** 1-10.

Romsuk, J., Yasumoto, S., Fukushima, E. O., Miura, K., Muranaka, T., *et al.* (2022) High-Yield Bioactive Triterpenoid Production by Heterologous Expression in Nicotiana Benthamiana Using the Tsukuba System. *Frontiers in Plant Science,* 13**,** 991909.

Rotenberg, D., Thompson, T. S., German, T. L. & Willis, D. K. (2006) Methods for Effective Real-Time Rt-Pcr Analysis of Virus-Induced Gene Silencing. *Journal of Virological Methods,* 138**,** 49-59.

Rozas, P., Kessi-Pérez, E. I. & Martínez, C. (2022) Genetically Modified Organisms: Adapting Regulatory Frameworks for Evolving Genome Editing Technologies. *Biological Research,* 55.

Rufino-Palomares, E. E., Perez-Jimenez, A., J. Reyes-Zurita, F., Garcia-Salguero, L., Mokhtari, K., *et al.* (2015) Anti-Cancer and Anti-Angiogenic Properties of Various Natural Pentacyclic Tri-Terpenoids and Some of Their Chemical Derivatives. *Current Organic Chemistry,* 19**,** 919-947.

Saha, S., Walia, S., Kumar, J., Dhingra, S. & Parmar, B. S. (2010) Screening for Feeding Deterrent and Insect Growth Regulatory Activity of Triterpenic Saponins from Diploknema Butyracea and Sapindus Mukorossi. *Journal of Agricultural and Food Chemistry,* 58**,** 434-440.

Salam, U., Ullah, S., Tang, Z.-H., Elateeq, A. A., Khan, Y., *et al.* (2023) Plant Metabolomics: An Overview of the Role of Primary and Secondary Metabolites against Different Environmental Stress Factors. *Life,* 13**,** 706.

Salem, M. A., Perez De Souza, L., Serag, A., Fernie, A. R., Farag, M. A., *et al.* (2020) Metabolomics in the Context of Plant Natural Products Research: From Sample Preparation to Metabolite Analysis. *Metabolites,* 10**,** 37.

Samatadze, T. E., Yurkevich, O. Y., Khazieva, F. M., Basalaeva, I. V., Savchenko, O. M., *et al.* (2023) Genome Studies in Four Species of Calendula L.(Asteraceae) Using Satellite Dnas as Chromosome Markers. *Plants,* 12**,** 4056.

Samuel, D. S. & Priyadarshoni, S. P. (2019) Echinacea Purpurea-a Potent Medicinal Herb. *Drug Invention Today,* 11.

Sanap, A., Chandravanshi, B., Shah, T., Tillu, G., Dhanushkodi, A.*, et al.* (2017) Herbal Pre-Conditioning Induces Proliferation and Delays Senescence in Wharton's Jelly Mesenchymal Stem Cells. *Biomedicine & Pharmacotherapy,* 93**,** 772-778.

Sapkota, B. & Kunwar, P. (2024) A Review on Traditional Uses, Phytochemistry and Pharmacological Activities of Calendula Officinalis Linn. *Natural Product Communications,* 19**,** 1934578X241259021.

Sawai, S. & Saito, K. (2011) Triterpenoid Biosynthesis and Engineering in Plants. *Frontiers in Plant Science,* 2**,** 25.

Scherlach, K. & Hertweck, C. (2021) Mining and Unearthing Hidden Biosynthetic Potential. *Nature Communications,* 12**,** 3864.

Schoch, C. L., Ciufo, S., Domrachev, M., Hotton, C. L., Kannan, S.*, et al.* (2020) Ncbi Taxonomy: A Comprehensive Update on Curation, Resources and Tools. *Database,* 2020**,** baaa062.

Schultz, G. S., Chin, G. A., Moldawer, L. & Diegelmann, R. F. (2011) Principles of Wound Healing. *Mechanisms of vascular disease: A reference book for vascular specialists [Internet]*.

Schulz-Bohm, K., Gerards, S., Hundscheid, M., Melenhorst, J., De Boer, W.*, et al.* (2018) Calling from Distance: Attraction of Soil Bacteria by Plant Root Volatiles. *The ISME Journal,* 12**,** 1252-1262.

Scofield, S. R., Huang, L., Brandt, A. S. & Gill, B. S. (2005) Development of a Virus-Induced Gene-Silencing System for Hexaploid Wheat and Its Use in Functional Analysis of the <I>Lr21</I>-Mediated Leaf Rust Resistance Pathway. *Plant Physiology,* 138**,** 2165-2173.

Segura, M. J., Meyer, M. M. & Matsuda, S. P. (2000) Arabidopsis T Haliana Lup1 Converts Oxidosqualene to Multiple Triterpene Alcohols and a Triterpene Diol. *Organic letters,* 2**,** 2257-2259.

Sen, C. K. (2021) Human Wound and Its Burden: Updated 2020 Compendium of Estimates. *Advances in wound care,* 10**,** 281-292.

Senguttuvan, J., Paulsamy, S. & Karthika, K. (2014) Phytochemical Analysis and Evaluation of Leaf and Root Parts of the Medicinal Herb, Hypochaeris Radicata L. For in Vitro Antioxidant Activities. *Asian Pacific journal of tropical biomedicine,* 4**,** S359-S367.

Senthil-Kumar, M., Hema, R., Anand, A., Kang, L., Udayakumar, M.*, et al.* (2007) A Systematic Study to Determine the Extent of Gene Silencing in <I>Nicotiana Benthamiana</I> and Other Solanaceae Species When Heterologous Gene Sequences Are Used for Virus-Induced Gene Silencing. *New Phytologist,* 176**,** 782-791.

Senthil-Kumar, M. & Mysore, K. S. (2014) Tobacco Rattle Virus-Based Virus-Induced Gene Silencing in <I>Nicotiana Benthamiana</I>. *Nature Protocols,* 9**,** 1549-1562.

Senthil-Kumar, M., Hema, R., Anand, A., Kang, L., Udayakumar, M.*, et al.* (2007) A Systematic Study to Determine the Extent of Gene Silencing in Nicotiana Benthamiana and Other Solanaceae Species When Heterologous Gene Sequences Are Used for Virus-Induced Gene Silencing. *New Phytologist,* 176**,** 782-791.

Septembre-Malaterre, A., Lalarizo Rakoto, M., Marodon, C., Bedoui, Y., Nakab, J.*, et al.* (2020) Artemisia Annua, a Traditional Plant Brought to Light. *International Journal of Molecular Sciences,* 21**,** 4986.

Shah, A. & Amini-Nik, S. (2017) The Role of Phytochemicals in the Inflammatory Phase of Wound Healing. *International Journal of Molecular Sciences,* 18**,** 1068.

Sharma, S. & Kumari, K. (2021) An Overview on Calendula Officinalis Linn.:(Pot Marigold). *Journal of Advanced Scientific Research,* 12**,** 13-18.

Sherpa, K., Jaishee, N., Naskar, C. & Thapa, S. (2017) An Ethnobotanical Survey of Medicinal Plants of Darjeeling District, West Bengal, India. *Bio Science Research Bulletin,* 33**,** 50-57.

Sheu-Gruttadauria, J. & Macrae, I. J. (2017) Structural Foundations of Rna Silencing by Argonaute. *Journal of Molecular Biology,* 429**,** 2619-2639.

Shih, Y.-T., Wang, M.-C., Peng, H.-H., Chen, T.-F., Chen, L., *et al.* (2012) Modulation of Chemotactic and Pro-Inflammatory Activities of Endothelial Progenitor Cells by Hepatocellular Carcinoma. *Cellular Signalling,* 24**,** 779-793.

Shin, J.-J., Suk, K. & Lee, W.-H. (2024) Lncrna Bre-As1 Regulates the Jak2/Stat3-Mediated Inflammatory Activation Via the Mir-30b-5p/Soc3 Axis in Thp-1 Cells. *Scientific reports,* 14**,** 25726.

Shomali, A., Das, S., Arif, N., Sarraf, M., Zahra, N., *et al.* (2022) Diverse Physiological Roles of Flavonoids in Plant Environmental Stress Responses and Tolerance. *Plants,* 11**,** 3158.

Silvestro, D., Andersen, T. G., Schaller, H. & Jensen, P. E. (2013) Plant Sterol Metabolism. Δ7-Sterol-C5-Desaturase (Ste1/Dwarf7), Δ5, 7-Sterol-Δ7-Reductase (Dwarf5) and Δ24-Sterol-Δ24-Reductase (Diminuto/Dwarf1) Show Multiple Subcellular Localizations in Arabidopsis Thaliana (Heynh) L. *Plos One,* 8**,** e56429.

Simmonds, M. S., Stevenson, P. C., Porter, E. A. & Veitch, N. C. (2001) Insect Antifeedant Activity of Three New Tetranortriterpenoids from Trichilia P Allida. *Journal of Natural Products,* 64**,** 1117-1120.

Singh, A., Pandey, S., Srivastava, R. P., Devkota, H. P., Singh, L., *et al.* (2022a) Helianthus Annuus L.: Traditional Uses, Phytochemistry, and Pharmacological Activities. *Medicinal Plants of the Asteraceae Family: Traditional Uses, Phytochemistry and Pharmacological Activities.* Springer.

Singh, K. S., Van Der Hooft, J. J., Van Wees, S. C. & Medema, M. H. (2022b) Integrative Omics Approaches for Biosynthetic Pathway Discovery in Plants. *Natural Product Reports,* 39**,** 1876-1896.

Sinno, H. & Prakash, S. (2013) Complements and the Wound Healing Cascade: An Updated Review. *Plastic surgery international,* 2013**,** 146764.

Smith, A. G., Miles, V. N., Holmes, D. T., Chen, X. & Lei, W. (2021) Clinical Trials, Potential Mechanisms, and Adverse Effects of Arnica as an Adjunct Medication for Pain Management. *Medicines,* 8**,** 58.

Smułek, W. & Kaczorek, E. (2022) Factors Influencing the Bioavailability of Organic Molecules to Bacterial Cells—a Mini-Review. *Molecules,* 27**,** 6579.

Sonawane, P. D., Pollier, J., Panda, S., Szymanski, J., Massalha, H., *et al.* (2017) Plant Cholesterol Biosynthetic Pathway Overlaps with Phytosterol Metabolism. *Nature plants,* 3.

Spivak, A. Y., Khalitova, R. R., Nedopekina, D. A. & Gubaidullin, R. R. (2020) Antimicrobial Properties of Amine-and Guanidine-Functionalized Derivatives of Betulinic, Ursolic and Oleanolic Acids: Synthesis and Structure/Activity Evaluation. *Steroids,* 154**,** 108530.

Steel, R. J., O'connell, M. A. & Searcey, M. (2018) Perfluoroarene-Based Peptide Macrocycles That Inhibit the Nrf2/Keap1 Interaction. *Bioorganic & medicinal chemistry letters,* 28**,** 2728-2731.

Steenwyk, J. L., Buida, T. J., Iii, Li, Y., Shen, X.-X. & Rokas, A. (2020) Clipkit: A Multiple Sequence Alignment Trimming Software for Accurate Phylogenomic Inference. *PLoS Biology,* 18.

Stephenson, M. J., Reed, J., Brouwer, B. & Osbourn, A. (2018) Transient Expression in Nicotiana Benthamiana Leaves for Triterpene Production at a Preparative Scale. *Journal of visualized experiments: JoVE***,** 58169.

Stobiecki, M. (2000) Application of Mass Spectrometry for Identification and Structural Studies of Flavonoid Glycosides. *Phytochemistry,* 54**,** 237-256.

Stroh, P. A., Walker, K. J., Humphrey, T. A., Pescott, O. L. & Burkmar, R. J. (2023) *Plant Atlas 2020: Mapping Changes in the Distribution of the British and Irish Flora*, Princeton University Press.

Su, Y., Wang, J., Gao, W., Wang, R., Yang, W., *et al.* (2023) Dynamic Metabolites: A Bridge between Plants and Microbes. *Science of the Total Environment***,** 165612.

Suh, Y. K., Robinson, A., Zanghi, N., Kratz, A., Gustetic, A., *et al.* (2022) Introducing Wound Healing Assays in the Undergraduate Biology Laboratory Using Ibidi Plates. *Journal of Microbiology & Biology Education,* 23**,** e00061-22.

Suhandono, S. & Chahyadi, A. (2014) Optimization of Genetic Transformation of Artemisia Annua L. Using Agrobacterium for Artemisinin Production. *Pharmacognosy Magazine,* 10**,** S176.

Sun, G. Y., Ju, Y. Q., Zhang, C. P., Li, L. L., Jiang, X. Q., *et al.* (2024a) Styrax Japonicus Functional Genomics: An Efficient Virus Induced Gene Silencing (Vigs) System. *Horticultural Plant Journal,* 10**,** 252-258.

Sun, K., Luo, J., Guo, J., Yao, X., Jing, X., *et al.* (2020) The Pi3k/Akt/Mtor Signaling Pathway in Osteoarthritis: A Narrative Review. *Osteoarthritis and cartilage,* 28**,** 400-409.

Sun, S.-C. (2011) Non-Canonical Nf-κb Signaling Pathway. *Cell Research,* 21**,** 71-85.

Sun, S.-C. (2017) The Non-Canonical Nf-κb Pathway in Immunity and Inflammation. *Nature reviews immunology,* 17**,** 545-558.

Sun, W. & Shi, J. (2021) Identification and Bioinformatic Analysis of the Asat Gene Family in Oryza Staiva. *Rice Genomics and Genetics,* 12.

Sun, W., Wan, S., Liu, C., Wang, R., Zhang, H., *et al.* (2024b) Establishing Cell Suitability for High-Level Production of Licorice Triterpenoids in Yeast. *Acta Pharmaceutica Sinica B*.

Swamidatta, S. H. & Lichman, B. R. (2024) Beyond Co-Expression: Pathway Discovery for Plant Pharmaceuticals. *Current Opinion in Biotechnology,* 88**,** 103147.

Szász, C., Pap, D., Szebeni, B., Bokrossy, P., Őrfi, L., *et al.* (2023) Optimization of Sirius Red-Based Microplate Assay to Investigate Collagen Production in Vitro. *International Journal of Molecular Sciences,* 24**,** 17435.

Szlasa, W., Ślusarczyk, S., Nawrot-Hadzik, I., Abel, R., Zalesińska, A., *et al.* (2023) Betulin and Its Derivatives Reduce Inflammation and Cox-2 Activity in Macrophages. *Inflammation,* 46**,** 573-583.

Tabana, Y., Babu, D., Fahlman, R., Siraki, A. G. & Barakat, K. (2023) Target Identification of Small Molecules: An Overview of the Current Applications in Drug Discovery. *BMC Biotechnology,* 23**,** 44.

Tan, Y., Bukys, A., Molnar, A. & Hudson, A. (2020) Rapid, High Efficiency Virus-Mediated Mutant Complementation and Gene Silencing in <I>Antirrhinum</I>. *Plant Methods,* 16.

Tanaka, Y., Nakamura, N. & Togami, J. (2008) Altering Flower Color in Transgenic Plants by Rnai-Mediated Engineering of Flavonoid Biosynthetic Pathway. *RNAi: Design and Application***,** 245-257.

Tao, H., Lauterbach, L., Bian, G., Chen, R., Hou, A., *et al.* (2022) Discovery of Non-Squalene Triterpenes. *Nature,* 606**,** 414-419.

Tate, J. A., Ni, Z., Scheen, A.-C., Koh, J., Gilbert, C. A., *et al.* (2006) Evolution and Expression of Homeologous Loci in Tragopogon Miscellus (Asteraceae), a Recent and Reciprocally Formed Allopolyploid. *Genetics,* 173**,** 1599-1611.

Teng, Q. (2005) Protein Structure Determination from Nmr Data. *Structural biology: practical NMR applications***,** 211-243.

Thimmappa, R., Geisler, K., Louveau, T., O'maille, P. & Osbourn, A. (2014) Triterpene Biosynthesis in Plants. *Annual Review of Plant Biology,* 65**,** 225-257.

Tian, J., Li, X., Zhao, L., Shen, P., Wang, Z., *et al.* (2020) Glycyrrhizic Acid Promotes Neural Repair by Directly Driving Functional Remyelination. *Food & function,* 11**,** 992-1005.

Tian, X., Ruan, J.-X., Huang, J.-Q., Yang, C.-Q., Fang, X., *et al.* (2018) Characterization of Gossypol Biosynthetic Pathway. *Proceedings of the National Academy of Sciences,* 115**,** E5410-E5418.

Tian, Y., Fang, Y., Zhang, K. X., Zhai, Z. Y., Yang, Y. J., *et al.* (2024) Applications of Virus-Induced Gene Silencing in Cotton. *Plants-Basel,* 13.

Tiedge, K., Destremps, J., Solano-Sanchez, J., Arce-Rodriguez, M. L. & Zerbe, P. (2022) Foxtail Mosaic Virus-Induced Gene Silencing (Vigs) in Switchgrass (Panicum Virgatum L.). *Plant Methods,* 18**,** 71.

Timoneda, A., Feng, T., Sheehan, H., Walker-Hale, N., Pucker, B.*, et al.* (2019) The Evolution of Betalain Biosynthesis in Caryophyllales. *New Phytologist,* 224**,** 71-85.

Todd, A. E., Orengo, C. A. & Thornton, J. M. (2002) Sequence and Structural Differences between Enzyme and Nonenzyme Homologs. *Structure,* 10**,** 1435-1451.

Tom, I. M., Ibrahim, M. M., Umoru, A. M., Umar, J. B., Bukar, M. A.*, et al.* (2019) Infection of Wounds by Potential Bacterial Pathogens and Their Resistogram. *Open Access Library Journal,* 6**,** 1-13.

Trares, K., Ackermann, J. & Koch, I. (2022) The Canonical and Non-Canonical Nf-κb Pathways and Their Crosstalk: A Comparative Study Based on Petri Nets. *BioSystems,* 211**,** 104564.

Treimer, J. F. & Zenk, M. H. (1979) Purification and Properties of Strictosidine Synthase, the Key Enzyme in Indole Alkaloid Formation. *European Journal of Biochemistry,* 101**,** 225-233.

Trendafilova, A., Ivanova, V., Todorova, M., Staleva, P. & Aneva, I. (2021) Terpenoids in Four Inula Species from Bulgaria. *Journal of the Serbian Chemical Society,* 86**,** 1229-1240.

Trifinopoulos, J., Lam-Tung, N., Von Haeseler, A. & Minh, B. Q. (2016) W-Iq-Tree: A Fast Online Phylogenetic Tool for Maximum Likelihood Analysis. *Nucleic Acids Research,* 44**,** W232-W235.

Ukiya, M., Akihisa, T., Yasukawa, K., Kasahara, Y., Kimura, Y.*, et al.* (2001) Constituents of Compositae Plants. 2. Triterpene Diols, Triols, and Their 3-O-Fatty Acid Esters from Edible Chrysanthemum Flower Extract and Their Anti-Inflammatory Effects. *Journal of Agricultural and Food Chemistry,* 49**,** 3187-3197.

Ukiya, M., Akihisa, T., Yasukawa, K., Tokuda, H., Suzuki, T.*, et al.* (2006) Anti-Inflammatory, Anti-Tumor-Promoting, and Cytotoxic Activities of Constituents of Marigold (Calendula Officinalis) Flowers. *Journal of Natural Products,* 69**,** 1692-1696.

Underwood, W., Gilley, M., Misar, C. G., Gulya, T. J., Seiler, G. J.*, et al.* (2022) Multiple Species of Asteraceae Plants Are Susceptible to Root Infection by the Necrotrophic Fungal Pathogen Sclerotinia Sclerotiorum. *Plant Disease,* 106**,** 1366-1373.

Urban, P., Jobert, A., Laine, R. & Pompon, D. (2001) Cytochrome P450 (Cyp) Mutants and Substrate-Specificity Alterations: Segment-Directed Mutagenesis Applied to Human Cyp1a1. *Biochemical Society Transactions,* 29**,** 128-135.

Van De Peer, Y., Ashman, T.-L., Soltis, P. S. & Soltis, D. E. (2021) Polyploidy: An Evolutionary and Ecological Force in Stressful Times. *The Plant Cell,* 33**,** 11-26.

Van De Peer, Y. & Meyer, A. (2005) Large-Scale Gene and Ancient Genome Duplications. *The Evolution of the Genome.* Elsevier.

Van Herpen, T. W., Cankar, K., Nogueira, M., Bosch, D., Bouwmeester, H. J.*, et al.* (2010) Nicotiana Benthamiana as a Production Platform for Artemisinin Precursors. *Plos One,* 5**,** e14222.

Vaou, N., Stavropoulou, E., Voidarou, C., Tsakris, Z., Rozos, G.*, et al.* (2022) Interactions between Medical Plant-Derived Bioactive Compounds: Focus on Antimicrobial Combination Effects. *Antibiotics,* 11**,** 1014.

Verma, P. K., Raina, R., Agarwal, S. & Kaur, H. (2018) Phytochemical Ingredients and Pharmacological Potential of Calendula Officinalis Linn. *Pharmaceutical and Biomedical Research,* 4**,** 1-17.

Villalva, M., Silvan, J. M., Alarcón-Cavero, T., Villanueva-Bermejo, D., Jaime, L.*, et al.* (2022) Antioxidant, Anti-Inflammatory, and Antibacterial Properties of an Achillea Millefolium L. Extract and Its Fractions Obtained by Supercritical Anti-Solvent Fractionation against Helicobacter Pylori. *Antioxidants,* 11**,** 1849.

Vitales, D., Fernández, P., Garnatje, T. & Garcia, S. (2019) Progress in the Study of Genome Size Evolution in Asteraceae: Analysis of the Last Update. *Database,* 2019**,** baz098.

Vo, N. N. Q., Nomura, Y., Muranaka, T. & Fukushima, E. O. (2019) Structure–Activity Relationships of Pentacyclic Triterpenoids as Inhibitors of Cyclooxygenase and Lipoxygenase Enzymes. *Journal of Natural Products,* 82**,** 3311-3320.

Vranová, E., Coman, D. & Gruissem, W. (2013) Network Analysis of the Mva and Mep Pathways for Isoprenoid Synthesis. *Annual Review of Plant Biology,* 64**,** 665-700.

Walker, K. & Croteau, R. (2000) Taxol Biosynthesis: Molecular Cloning of a Benzoyl-Coa: Taxane 2α-O-Benzoyltransferase Cdna from Taxus and Functional Expression in Escherichia Coli. *Proceedings of the National Academy of Sciences,* 97**,** 13591-13596.

Wang, C., Liwei, M., Park, J.-B., Jeong, S.-H., Wei, G.*, et al.* (2018) Microbial Platform for Terpenoid Production: Escherichia Coli and Yeast. *Frontiers in Microbiology,* 9**,** 2460.

Wang, C., Yuan, Y., Pan, H., Hsu, A. C.-Y., Chen, J.*, et al.* (2020) Protective Effect of Ocotillol, the Derivate of Ocotillol-Type Saponins in Panax Genus, against Acetic Acid-Induced Gastric Ulcer in Rats Based on Untargeted Metabolomics. *International Journal of Molecular Sciences,* 21**,** 2577.

Wang, H., Wang, Q., Liu, Y., Liao, X., Chu, H.*, et al.* (2021a) Pcpd: Plant Cytochrome P450 Database and Web-Based Tools for Structural Construction and Ligand Docking. *Synthetic and Systems Biotechnology,* 6**,** 102-109.

Wang, H., Wang, Q., Liu, Y., Liao, X., Chu, H.*, et al.* (2021b) Pcpd: Plant Cytochrome P450 Database and Web-Based Tools for Structural Construction and Ligand Docking. *Synthetic and Systems Biotechnology,* 6**,** 102-109.

Wang, R., Yang, X. X., Wang, N., Liu, X. D., Nelson, R. S.*, et al.* (2016) An Efficient Virus-Induced Gene Silencing Vector for Maize Functional Genomics Research. *Plant Journal,* 86**,** 102-115.

Wang, X., Pereira, J. H., Tsutakawa, S., Fang, X., Adams, P. D.*, et al.* (2021c) Efficient Production of Oxidized Terpenoids Via Engineering Fusion Proteins of Terpene Synthase and Cytochrome P450. *Metabolic Engineering,* 64**,** 41-51.

Wang, Y., Mostafa, S., Zeng, W. & Jin, B. (2021d) Function and Mechanism of Jasmonic Acid in Plant Responses to Abiotic and Biotic Stresses. *International Journal of Molecular Sciences,* 22**,** 8568.

Wang, Y., Yu, H., Xu, Y., Wu, M., Zhang, J.*, et al.* (2023) Expression of a Mycoparasite Protease in Plant Petals Suppresses the Petal-Mediated Infection by Necrotrophic Pathogens. *Cell Reports,* 42.

Wani, K. I., Choudhary, S., Zehra, A., Naeem, M., Weathers, P.*, et al.* (2021) Enhancing Artemisinin Content in and Delivery from Artemisia Annua: A Review of Alternative, Classical, and Transgenic Approaches. *Planta,* 254**,** 1-15.

Wankhede, N. L., Kale, M. B., Bawankule, A. K., Aglawe, M. M., Taksande, B. G.*, et al.* (2023) Overview on the Polyphenol Avenanthramide in Oats (Avena Sativa Linn.) as Regulators of Pi3k Signaling in the Management of Neurodegenerative Diseases. *Nutrients,* 15**,** 3751.

Warren, C. R. (2013) Use of Chemical Ionization for Gc–Ms Metabolite Profiling. *Metabolomics,* 9**,** 110-120.

Waters, E. R. (2003) Molecular Adaptation and the Origin of Land Plants. *Molecular Phylogenetics and Evolution,* 29**,** 456-463.

Wawrosch, C. & Zotchev, S. B. (2021) Production of Bioactive Plant Secondary Metabolites through in Vitro Technologies—Status and Outlook. *Applied Microbiology and Biotechnology,* 105**,** 6649-6668.

Webster, J. & Vucic, D. (2020) The Balance of Tnf Mediated Pathways Regulates Inflammatory Cell Death Signaling in Healthy and Diseased Tissues. Front Cell Dev Biol. 2020; 8: 365.

Wendisch, V. F., Brito, L. F., Lopez, M. G., Hennig, G., Pfeifenschneider, J., *et al.* (2016) The Flexible Feedstock Concept in Industrial Biotechnology: Metabolic Engineering of Escherichia Coli, Corynebacterium Glutamicum, Pseudomonas, Bacillus and Yeast Strains for Access to Alternative Carbon Sources. *Journal of Biotechnology,* 234**,** 139-157.

Whan Han, J., Gon Lee, B., Kee Kim, Y., Woo Yoon, J., Kyoung Jin, H., *et al.* (2001) Ergolide, Sesquiterpene Lactone from Inula Britannica, Inhibits Inducible Nitric Oxide Synthase and Cyclo-Oxygenase-2 Expression in Raw 264.7 Macrophages through the Inactivation of Nf-κb. *British Journal of Pharmacology,* 133**,** 503-512.

Wiłckomirski, B. (1987) Intracellular Localization of Metabolism of Lupeol and Its Palmitate in Calendula Officinalis Flowers. *Phytochemistry,* 26**,** 1635-1637.

Wilderman, P. R., Gay, S. C., Jang, H. H., Zhang, Q., Stout, C. D., *et al.* (2012) Investigation by Site-Directed Mutagenesis of the Role of Cytochrome P450 2b4 Non-Active-Site Residues in Protein–Ligand Interactions Based on Crystal Structures of the Ligand-Bound Enzyme. *The FEBS journal,* 279**,** 1607-1620.

Wilkomirski, B. & Kasprzyk, Z. (1979) Free and Ester-Bound Triterpene Alcohols and Sterols in Cellular Subfractions of Calendula Officinalis Flowers. *Phytochemistry,* 18**,** 253-255.

Wink, M. (2003) Evolution of Secondary Metabolites from an Ecological and Molecular Phylogenetic Perspective. *Phytochemistry,* 64**,** 3-19.

Wu, C., Jia, L. & Goggin, F. (2011) The Reliability of Virus-Induced Gene Silencing Experiments Using Tobacco Rattle Virus in Tomato Is Influenced by the Size of the Vector Control. *Molecular Plant Pathology,* 12**,** 299-305.

Wu, S., Jiang, Z., Kempinski, C., Eric Nybo, S., Husodo, S., *et al.* (2012) Engineering Triterpene Metabolism in Tobacco. *Planta,* 236**,** 867-877.

Xavier, T. F., Kannan, M. & Auxilia, A. (2015) Traditional Medicinal Plants Used in the Treatment of Different Skin Diseases. *International Journal of Current Microbiology and Applied Sciences,* 4**,** 1043-1053.

Xiao, K.-M., Wang, J.-M., Zhou, L.-Y., Guo, L., Tan, D.-C., *et al.* (2020) Cytotoxic Triterpenes from Trametes Orientalis. *Natural Product Communications,* 15**,** 1934578X20921621.

Xie, M., Yan, Z., Ren, X., Li, X. & Qin, B. (2017) Codonopilate a, a Triterpenyl Ester as Main Autotoxin in Cultivated Soil of Codonopsis Pilosula (Franch.) Nannf. *Journal of Agricultural and Food Chemistry,* 65**,** 2032-2038.

Xin, X.-F., Kvitko, B. & He, S. Y. (2018) Pseudomonas Syringae: What It Takes to Be a Pathogen. *Nature Reviews Microbiology,* 16**,** 316-328.

Xiong, R., Pajak, A., Wang, A., Yoshikawa, N., Marsolais, F., *et al.* (2019) Agrobacterium-Mediated Inoculation of Asymptomatic Apple Latent Spherical Virus as Gene Silencing Vector in Pea (Pisum Sativum L.). *Legume Science,* 1**,** e14.

Xu, D., Wang, Z., Zhuang, W., Wang, T. & Xie, Y. (2023a) Family Characteristics, Phylogenetic Reconstruction, and Potential Applications of the Plant Bahd Acyltransferase Family. *Frontiers in Plant Science,* 14**,** 1218914.

Xu, Z., Ullah, N., Duan, Y., Hou, Z., Liu, A., *et al.* (2023b) Plant Secondary Metabolites and Their Effects on Environmental Adaptation Based on Functional Genomics. Frontiers Media SA.

Yadav, V. R., Prasad, S., Sung, B., Kannappan, R. & Aggarwal, B. B. (2010) Targeting Inflammatory Pathways by Triterpenoids for Prevention and Treatment of Cancer. *Toxins,* 2**,** 2428-2466.

Yamamoto, K., Grzech, D., Koudounas, K., Stander, E. A., Caputi, L., *et al.* (2021) Improved Virus-Induced Gene Silencing Allows Discovery of a Serpentine Synthase Gene in Catharanthus Roseus. *Plant Physiology,* 187**,** 846-857.

Yan, H., Zhang, Z., Magnard, J.-L., Boachon, B., Baudino, S., *et al.* (2020) Virus-Induced Gene Silencing in Rose Flowers. *Virus-Induced Gene Silencing in Plants: Methods and Protocols***,** 223-232.

Yan, H. J., Shi, S. C., Ma, N., Cao, X. Q., Zhang, H., *et al.* (2018) Graft-Accelerated Virus-Induced Gene Silencing Facilitates Functional Genomics in Rose Flowers. *Journal of Integrative Plant Biology,* 60**,** 34-44.

Yang, B., Feng, X. & Li, C. (2020) Microbial Cell Factory for Efficiently Synthesizing Plant Natural Products Via Optimizing the Location and Adaptation of Pathway on Genome Scale. *Frontiers in Bioengineering and Biotechnology,* 8**,** 969.

Yang, E.-J., Lee, W., Ku, S.-K., Song, K.-S. & Bae, J.-S. (2012) Anti-Inflammatory Activities of Oleanolic Acid on Hmgb1 Activated Huvecs. *Food and Chemical Toxicology,* 50**,** 1288-1294.

Yang, H., Kim, H. W., Kim, Y. C. & Sung, S. H. (2017) Cytotoxic Activities of Naturally Occurring Oleanane-, Ursane-, and Lupane-Type Triterpenes on Hepg2 and Ags Cells. *Pharmacognosy Magazine,* 13**,** 118.

Yang, L., Ding, W., Xu, Y., Wu, D., Li, S., *et al.* (2016) New Insights into the Antibacterial Activity of Hydroxycoumarins against Ralstonia Solanacearum. *Molecules,* 21**,** 468.

Yang, L., Wen, K.-S., Ruan, X., Zhao, Y.-X., Wei, F., *et al.* (2018) Response of Plant Secondary Metabolites to Environmental Factors. *Molecules,* 23**,** 762.

Yang, Y., Yang, X., Guo, X., Hu, X., Dong, D., *et al.* (2022) Exogenously Applied Methyl Jasmonate Induces Early Defense Related Genes in Response to Phytophthora Infestans Infection in Potato Plants. *Horticultural Plant Journal,* 8**,** 511-526.

Yasukawa, K., Akihisa, T., Oinuma, H., Kasahara, Y., Kimura, Y., *et al.* (1996) Inhibitory Effect of Di-and Trihydroxy Triterpenes from the Flowers of Compositae on 12-O-Tetradecanoylphorbol-13-Acetate-Induced Inflammation in Mice. *Biological and Pharmaceutical Bulletin,* 19**,** 1329-1331.

Ye, J., Coulouris, G., Zaretskaya, I., Cutcutache, I., Rozen, S., *et al.* (2012) Primer-Blast: A Tool to Design Target-Specific Primers for Polymerase Chain Reaction. *BMC Bioinformatics,* 13**,** 1-11.

Yesilirmak, F. & Sayers, Z. (2009) Heterelogous Expression of Plant Genes. *International journal of plant genomics,* 2009**,** 296482.

Yi, G.-E., Robin, A. H. K., Yang, K., Park, J.-I., Hwang, B. H., *et al.* (2016) Exogenous Methyl Jasmonate and Salicylic Acid Induce Subspecies-Specific Patterns of Glucosinolate Accumulation and Gene Expression in Brassica Oleracea L. *Molecules,* 21**,** 1417.

Yinjun, L., Jie, J. & Yungui, W. (2005) Triptolide Inhibits Transcription Factor Nf-Kappab and Induces Apoptosis of Multiple Myeloma Cells. *Leukemia Research,* 29**,** 99-105.

Younis, A., Siddique, M. I., Kim, C.-K. & Lim, K.-B. (2014) Rna Interference (Rnai) Induced Gene Silencing: A Promising Approach of Hi-Tech Plant Breeding. *International journal of biological sciences,* 10**,** 1150.

Yu, C., Hou, K., Zhang, H., Liang, X., Chen, C., *et al.* (2023) Integrated Mass Spectrometry Imaging and Single-Cell Transcriptome Atlas Strategies Provide Novel Insights into Taxoid Biosynthesis and Transport in Taxus Mairei Stems. *The Plant Journal,* 115**,** 1243-1260.

Yu, H., Lin, L., Zhang, Z., Zhang, H. & Hu, H. (2020) Targeting Nf-κb Pathway for the Therapy of Diseases: Mechanism and Clinical Study. *Signal transduction and targeted therapy,* 5**,** 209.

Yu, Z., Chen, W., Wang, Y., Zhang, P., Shi, N., *et al.* (2022) Mobile Flowering Locus T Rna–Biological Relevance and Biotechnological Potential. *Frontiers in Plant Science,* 12**,** 792192.

Zadeh, J. B., Kor, N. M. & Kor, Z. M. (2014) Chamomile (Matricaria Recutita) as a Valuable Medicinal Plant. *International journal of Advanced Biological and Biomedical Research,* 2**,** 823-829.

Zagoskina, N. V., Zubova, M. Y., Nechaeva, T. L., Kazantseva, V. V., Goncharuk, E. A., *et al.* (2023) Polyphenols in Plants: Structure, Biosynthesis, Abiotic Stress Regulation, and Practical Applications. *International Journal of Molecular Sciences,* 24**,** 13874.

Zhan, J. & Meyers, B. C. (2023) Plant Small Rnas: Their Biogenesis, Regulatory Roles, and Functions. *Annual Review of Plant Biology,* 74**,** 21-51.
Zhan, X., Qiu, T., Zhang, H., Hou, K., Liang, X.*, et al.* (2023) Mass Spectrometry Imaging and Single-Cell Transcriptional Profiling Reveal the Tissue-Specific Regulation of Bioactive Ingredient Biosynthesis in Taxus Leaves. *Plant Communications,* 4.
Zhang, A.-H., Tan, S.-Q., Zhao, Y., Lei, F.-J. & Zhang, L.-X. (2015a) Effects of Total Ginsenosides on the Feeding Behavior and Two Enzymes Activities of Mythimna Separata (Walker) Larvae. *Evidence-Based Complementary and Alternative Medicine,* 2015**,** 451828.
Zhang, C., Wu, Z. J., Li, Y. & Wu, J. G. (2015b) Biogenesis, Function, and Applications of Virus-Derived Small Rnas in Plants. *Frontiers in Microbiology,* 6.
Zhang, D., Zhang, Z., Unver, T. & Zhang, B. (2021) Crispr/Cas: A Powerful Tool for Gene Function Study and Crop Improvement. *Journal of Advanced Research,* 29**,** 207-221.
Zhang, F., Wang, Y., Yue, J., Zhang, R., Hu, Y.-E.*, et al.* (2023a) Discovering a Uniform Functional Trade-Off of the Cbc-Type 2, 3-Oxidosqualene Cyclases and Deciphering Its Chemical Logic. *Science Advances,* 9**,** eadh1418.
Zhang, J., Chen, B., Gan, C., Sun, H., Zhang, J.*, et al.* (2023b) A Comprehensive Review of Small Interfering Rnas (Sirnas): Mechanism, Therapeutic Targets, and Delivery Strategies for Cancer Therapy. *International journal of nanomedicine***,** 7605-7635.
Zhang, M., Dang, M., Li, Y., Wei, P., Zhao, C.*, et al.* (2024) Natural Products Derived from Herbs as Promising Source for Diarrhea Predominant-Irritable Bowel Syndrome Via Gut Microbiota–Serotonin Pathway. *Journal of Pharmacy and Pharmacology,* 76**,** 75-85.
Zhang, P.-C., Zheng, C.-F., Wu, C.-S., Sheng, Y.-X. & Zhang, J.-L. (2010) Mass Spectral Fragmentation Analysis of Triterpene Saponins from Ardisia Crenata Sims by Electrospray Ionization Fourier Transform Ion Cyclotron Resonance Mass Spectrometry. *Journal of Asian Natural Products Research,* 12**,** 64-69.
Zhang, Q.-W., Lin, L.-G. & Ye, W.-C. (2018) Techniques for Extraction and Isolation of Natural Products: A Comprehensive Review. *Chinese medicine,* 13**,** 1-26.
Zhang, T. & Elomaa, P. (2024) Development and Evolution of the Asteraceae Capitulum. *New Phytologist,* 242**,** 33-48.
Zhang, T., Huo, T., Ding, A., Hao, R., Wang, J.*, et al.* (2019) Genome-Wide Identification, Characterization, Expression and Enzyme Activity Analysis of Coniferyl Alcohol Acetyltransferase Genes Involved in Eugenol Biosynthesis in Prunus Mume. *Plos One,* 14**,** e0223974.
Zhang, W. & Liu, H. T. (2002) Mapk Signal Pathways in the Regulation of Cell Proliferation in Mammalian Cells. *Cell Research,* 12**,** 9-18.
Zhang, Y., Chen, M., Siemiatkowska, B., Toleco, M. R., Jing, Y.*, et al.* (2020) A Highly Efficient Agrobacterium-Mediated Method for Transient Gene Expression and Functional Studies in Multiple Plant Species. *Plant Communications,* 1.
Zhao, H., Jia, Y., Cao, Y. & Wang, Y. (2020a) Improving T-DNA Transfer to Tamarix Hispida by Adding Chemical Compounds during Agrobacterium Tumefaciens Culture. *Frontiers in Plant Science,* 11**,** 501358.
Zhao, H., Wu, L., Yan, G., Chen, Y., Zhou, M.*, et al.* (2021) Inflammation and Tumor Progression: Signaling Pathways and Targeted Intervention. *Signal transduction and targeted therapy,* 6**,** 263.
Zhao, J., Jiang, H., Wang, G., Wang, Z., Dong, J.*, et al.* (2020b) Virus-Induced Gene Silencing in Diploid and Tetraploid Potato Species. *Virus-Induced Gene Silencing in Plants: Methods and Protocols***,** 39-50.
Zhou, Y., Grininger, M. & Alper, H. (2022) Pathway and Protein Engineering for Biosynthesis. *Synthetic and Systems Biotechnology,* 7**,** 1044.
Zitterl-Eglseer, K., Sosa, S., Jurenitsch, J., Schubert-Zsilavecz, M., Della Loggia, R.*, et al.* (1997) Anti-Oedematous Activities of the Main Triterpendiol Esters of Marigold (Calendula Officinalis L.). *Journal of Ethnopharmacology,* 57**,** 139-144.

Zulfiqar, S., Farooq, M. A., Zhao, T. T., Wang, P. P., Tabusam, J.*, et al.* (2023) Virus-Induced Gene Silencing (Vigs): A Powerful Tool for Crop Improvement and Its Advancement Towards Epigenetics. *International Journal of Molecular Sciences,* 24.

Zulkefli, N., Che Zahari, C. N. M., Sayuti, N. H., Kamarudin, A. A., Saad, N.*, et al.* (2023) Flavonoids as Potential Wound-Healing Molecules: Emphasis on Pathways Perspective. *International Journal of Molecular Sciences,* 24**,** 4607.

Supplemental Information

Supplementary Tables

Table S2.1 Plasmids used in this thesis.

Level 0 parts			
Name	**Description**	**Bacterial Selection**	**Origin**
pICH51277	PROM+5UTR: Short CaMV35 promoter + TMV omega 5'UTR	Spectinomycin	Engler *et al.*, 2014)
pEPQD0CM0030	TAA stop codon	Chloramphenicol	(Dudley *et al.*, 2021)
pUAP41414	3UTR+TERM: CaMV35S 3'UTR and terminator	Chloramphenicol	Patron lab (unpublished)
pEPQD1CB0104	CDS: P19 suppressor of silencing (Tomato Bushy Stunt Virus)	Spectinomycin	Dudley *et al.*, 2021)
pL0-AstHMGR	CDS: AstHMGR (*Avena strigosa* truncated 3-hydroxy, 3-methyglutary-coenzyme A reductase)	Spectinomycin	A gift from A. Osbourn. (Reed *et al.*, 2017)
pEPMS1CB0001	CDS: CoTXSS (pot marigold taraxasterol synthase)	Chloramphenicol	Patron lab (unpublished)
pEPMS0CM0038	CDS: CoCYP716A392 (pot marigold taraxasterol C16 hydroxylase)	Chloramphenicol	This project
pEPMS0CM0039	CDS: CoCYP716A393 (pot marigold taraxasterol C16 hydroxylase)	Chloramphenicol	This project
pEPMS0CM0040	CDS: CoCYP3 (pot marigold predicted taraxasterol C16 hydroxylase)	Chloramphenicol	This project
pEPMS0CM0041	CDS: CoCYP4 (pot marigold predicted taraxasterol C16 hydroxylase)	Chloramphenicol	This project
pEPMS0CM0042	CDS: CoCYP5 (pot marigold b-amyrin C28 hydroxylase)	Chloramphenicol	This project
pEPDG1CB0024	CDS: CoACT1 (pot marigold faradiol C3 fatty acid acyl acyltransferase)	Chloramphenicol	This project
pEPDG1CB0025	CDS: CoACT2 (pot marigold faradiol C3 fatty acid acyl acyltransferase)	Chloramphenicol	This project
pEPDG1CB0026	CDS: CoACT3 (pot marigold taraxasterol C3 fatty acid acyl acyltransferase)	Chloramphenicol	This project
pEPDG1CB0027	CDS: CaTXSS (field marigold taraxasterol synthase)	Chloramphenicol	This project
pEPDG1CB0028	CDS: CaCYP716A392 (field marigold taraxasterol C16 hydroxylase)	Chloramphenicol	This project

VIGS Plasmids			
pTRV2:GG_SP/CM	VIGS acceptor plasmid	Spectinomycin	Addgene #105349 (Stuttmann lab)
pTRV1	VIGS Helper plasmid	Kanamaycin	(Liu *et al.*, 2002)
MoClo Acceptors			
pICH47732	Level 1 Position 1 acceptor (forward)	Carbenicillin	(Engler *et al.*, 2014)
pICH47742	Level 1 Position 2 acceptor (forward)	Carbenicillin	Engler *et al.*, 2014)
Level 1 Plasmids			
Name	**Description**	**Selection**	**Origin**
pEPDG1CB0004	35Sshort_TMV_CaTXSS_35S	Carbenicillin	This project
pEPMS1CB0018	35Sshort_TMV_CYP716A392_35S	Carbenicillin	This project
pEPMS1CB0019	35Sshort_TMV_CYP716A393_35S	Carbenicillin	This project
pEPMS1CB0020	35Sshort_TMV_CYP716A429_35S	Carbenicillin	This project
pEPMS1CB0021	35Sshort_TMV_CYP716A430_35S	Carbenicillin	This project
pEPMS1CB0022	35Sshort_TMV_CYP716A431_35S	Carbenicillin	This project
pEPDG1CB0005	35Sshort_TMV_CYP716A392a_35S	Carbenicillin	This project
pEPDG1CB0001	35Sshort_TMV_CoACT1_35S	Carbenicillin	This project
pEPDG1CB0002	35Sshort_TMV_CoACT2_35S	Carbenicillin	This project
pEPDG1CB0003	35Sshort_TMV_CoACT3_35S	Carbenicillin	This project
pEPCTαKN001	35S:LucF:35S	Kanamycin	(Kallam *et al.*, 2023a)
pEPCTSP0169	pTRV2 CoPDS_CoTXSS	Spectinomycin	This project
pEPCTSP0172	pTRV2 CoPDS_CoCAS	Spectinomycin	This project
pEPCTSP0174	pTRV2 CoPDS_CoTXSS_FT	Spectinomycin	This project
pEPCTSP0176	pTRV2 CoPDS_GFP_short	Spectinomycin	This project
pEPCTSP0177	pTRV2 CoPDS_GFP_short_FT	Spectinomycin	This project
pEPQDKN0760	pTRV2-NbPDS-msgRNA-tFT	Spectinomycin	Dudley *et al.*, 2021)
Mutated Level 1 Plasmids			
Name	**Description**	**Selection**	**Origin**
pEPDG1CB0007	35Sshort_TMV_CYP716A392 (A285G)_35S	Carbenicillin	This project
pEPDG1CB0009	35Sshort_TMV_CYP716A392 (A357L)_35S	Carbenicillin	This project
pEPDG1CB0010	35Sshort_TMV_CYP716A392 (H424R)_35S	Carbenicillin	This project
pEPDG1CB0018	35Sshort_TMV_CYP716A392 (A285V)_35S	Carbenicillin	This project
pEPDG1CB0012	35Sshort_TMV_CYP716A393 (A285G)_35S	Carbenicillin	This project

pEPDG1CB0014	35Sshort_TMV_CYP716A393 (A357L)_35S	Carbenicillin	This project
pEPDG1CB0015	35Sshort_TMV_CYP716A393 (H424R)_35S	Carbenicillin	This project
pEPDG1CB0021	35Sshort_TMV_ CYP716A393 (A285V)_35S	Carbenicillin	This project

Table S2.2 Primers for site-directed mutagenesis.

Target gene	Mutation	Forward Primer (5' - 3')	Reverse Primer (5' - 3')
CYP716 A392	A285G	AGATTCTTGGTTTGTTG ATCGGTGGGCATGAC	AACAAACCAAGAATCTTGCCCG AAATGTCGTG
CYP716 A392	A356L	ACCGCTTCAAGGTGCTT TTAGAGAAGCCC	CTTGAAGCGGTGGGACTAATCT AAGAACTTCAC
CYP716 A392	H423R	CCCGAGAATGTGTCCC GGAAAAGAGTACG	CACATTCTCGGGCCTCCTCCAAA TGGCAC
CYP716 A392	A284V	AGATTCTTGTGTTGTTG ATCGGTGGGCATGAC	CAACAACACAAGAATCTTGCCC GAAATGTCGTG
CYP716 A393	A285G	AGATTCTTGTGTTGTTG ATCGGTGGGCATGAC	CAACAACACAAGAATCTTGCCC GAAATGTCGTG
CYP716 A393	A356L	ACCGCTTCAAGGTGCTT TTCGAGAAGCC	CTTGAAGCGGTGGGACTAATCT AAGAACTTCAC
CYP716 A393	H423R	CCCGAGAATGTGTCCA GGAAAAGAGTATGCC	CACATTCTCGGGCCTCCTCCAAA TGGCAC
CYP716 A393	A284V	AGATACTTGTGTTGCTG ATTGGTGGGCATGAC	AGCAACACAAGTATCTTGCCAG AAATGTCGTGTTC

Table S2.3 Primers for gene expression analysis by RT-qPCR.

Target gene	Forward Primer (5' - 3')	Reverse Primer (5' - 3')	Amplicon length (bp)	Spans Intron/Exon junction?	Primer efficiency (%)
SAND.2	TCTTTCAGTTGGA ACCCTGCA	CTGCAATATAGC ACCAGCAGC	93	Yes	100,65
TXSS.2	GGTGACTTGCTC ATGCGAAC	TTACCGCCATTGT CACAGCT	121	Yes	97.91
CYP716 A392	TGGCCCATAATC GGGGAAAG	CACACATCACTG CAGCATCC	145	No	114
CYP716 A393	TTAGCGACGAAG ATGGCGAG	CACCAATCAGCA ACGCAAGT	72	No	104,9
CoACT1	CGTTTCAAGAGT ACGAGGCG	TTTTGCGGCCGA GTAAAACT	105	No	97.31
CoACT2	GTAAAGCCTTCA CCCGTTGG	GTGCCCCACATTC ATTCGTT	84	No	100.84

CoACT3	TTTCTGACCAAAAAGCGGGC	GACGAAGAACCCCGTGACTT	132	No	112.85
CoPDS	GGGAAGTGGAAGTGGTTCCT	AGTGGCACTGCTATGAGGTT	74	Yes	96.94
CoCAS	GGAGACTTCCCACAACAGGA	AACAAGGTGGCTGAAGGACT	133	No	97.3

Table S2.4 Primers for amplification of fragments for VIGS.

Target gene	**Forward Primer (5' - 3')**	**Reverse Primer (5' - 3')**	**Amplicon length (bp)**
GCTT_*TXSS*_GGTG	TGTGGTCTCTGCTTCTCTTGTAACTCAAGC	ACAGGTCTCTACTAGGACATTCACAGCATC	328
GCTT_*TXSS*_TAGT	TGTGGTCTCTGCTTCTCTTGTAACTCAAGC	ACAGGTCTCTCACCGGACATTCACAGCATC	328
GCTT_*CAS*_ GGTG	TGTGGTCTCTGCTTCCTGAGATGTGGC	ACAGGTCTCTCACCATGGGCTCCAC	312
TATG_*PDS*_GCTT	TGTGGTCTCTTATGGAAGCAAGAGACG	ACAGGTCTCTAAGCTTTCTCAGGCC	319
TAGT_*FT*_GGTG	TGTGGTCTCTTAGTCTATAAATATAAGAGAtCC	ACAGGTCTCTCACCTTGGCCATAAGTAACC	126
GCTT_*GFP*_GGTG	TGTGGTCTCTGCTTTGACCACCTTCAGCTACGG	ACAGGTCTCTCACCTGCCGTTCTTCTGCTTGTCG	328
GCTT_*GFP*_GGTG	TGTGGTCTCTGCTTTGACCACCTTCAGCTACGG	ACAGGTCTCTACTATGCCGTTCTTCTGCTTGTCG	328
MVP	ATGGAAGACAAGTCATTGG	TTAAGACGAGTTTTTCTTATTAGG	759

Table S2.5 Sequencing primer.

Name	Sequence
213or	GAACCCTGTGGTTGGCATGCACATAC

Table S3.1 Peak area under compound peak identified using GC-MS.

Species	**Sterols**						
	α-Tocopherol	Campesterol	Stigmasterol	Stigmast-5-ene	Isofucosterol	β-Sitosterol	
pot marigold	18548111	3439744	12544751	9953765	9953765		
field marigold	20706196		8852685				
C.suffruticossa tomentosa	626217						
C. suffruticossa algarbiensis	9108998		3254197				
common daisy	466504			5042947		245183	

mouse-ear hawkweed	1679792		827750	6480573		833348	
common cat's ear	5661432		5387975	20556662	7416208	744021	
chamomile	1378287	10401866	17358577	15421727			
common sunflower	6711952	4006978	28489021	12091524			
yarrow	1018173	323112	1638074	7552429		333473	
milk thistle	10019062		16064081	30943712			
British yellowhead	11142699		6375912	6847571			
sword-leaved inula	10467134	1293296	6353317	5766113			
rush skeleton weed	1353636			1240215	2486041	1453324	
hemp agrimony		5957625					
Species	**Triterpene monols**					**Triterpene diols**	
	β-amyrin	α-amyrin	Lupeol	Ψ-Taraxasterol	Taraxasterol	Maniladiol	Faradiol
pot marigold	34746282	19822757	16262842	67571777	10487701	4183034	5398035
field marigold	25927022	26555846		47998022			
C.suffruticossa tomentosa	8103068	2473654		8511938			
C. suffruticossa algarbiensis	17113092	15602922		40233738			
common daisy	158152	463835	473209				
mouse-ear hawkweed	4105298	5908239	1746090				
common cat's ear	5217999	18114068	4303792				
chamomile	30993773	4032353	3836455	60630724	82655589		
common sunflower	50806442					9479651	traces
yarrow	9475410	1719418	2585537	7070901	31144822		
milk thistle	64151931	98375001					
British yellowhead	6337843	12097192	13751626	4236611	2562477		traces
sword-leaved inula	5294189	905325	13123731	4117580	3271319		867541
rush skeleton weed	2486041	2915400	98119313	1098113	6839292		765999
hemp agrimony	6776982	5957625	8759639	7349355	98119313		
Species	**Acylated triterpenes**						
	β-amyrin acetate	α-amyrin acetate	Ψ-Taraxasterol acetate	Taraxasterol acetate	Lupeol acetate		
pot marigold							
field marigold							
C.suffruticossa tomentosa							
C. suffruticossa algarbiensis							
common daisy							
mouse-ear hawkweed							
common cat's ear			6083194				
chamomile			50806442	9348102			
common sunflower							
yarrow			2304192	9029622			
milk thistle	489514650	686427006	848068144		21688072		
British yellowhead							
sword-leaved inula							
rush skeleton weed			1566805	3008391			
hemp agrimony							
Species	**Triterpene monol fatty acid esters**						
	Lupeol myristate	β-amyrin palmitate	α-amyrin palmitate	Lupeol palmitate	Ψ-Taraxasterol /Taraxasterol palmitate	Ψ-Taraxasterol /Taraxasterol stearate	

pot marigold	3433756				10589205		
field marigold							
C.suffruticossa tomentosa							
C. suffruticossa algarbiensis							
common daisy			595045				
mouse-ear hawkweed		1360036	1313387				
common cat's ear		2333873	4086910				
chamomile		16749074			13316807		
common sunflower		65818759			8580079		
yarrow		2085291	1668178		2881240		
milk thistle	27674908	292408718	515013920		388116177	19968376	
British yellowhead					11786456		
sword-leaved inula					9333236		
rush skeleton weed					1299854		
hemp agrimony	160043317	76862282	82223568				
Species	**Triterpene diol fatty acid esters**						
pot marigold	Faradiol/arnidiol laurate	Faradiol/arnidiol myristate	Faradiol/arnidiol palmitate	Maniladiol myristate	Maniladiol palmitate	Maniladiol stearate	
field marigold	39386454	103444009					
C.suffruticossa tomentosa		8613635	46895507				
C. suffruticossa algarbiensis		8549882					
common daisy		6405108	30631386				
mouse-ear hawkweed							
common cat's ear				1180621			
chamomile							
common sunflower							
yarrow	3085467		87300367	82785600	215148936	57161614	
milk thistle							
British yellowhead							
sword-leaved inula		25886386	68802569	5962336	15788396		
rush skeleton weed	3688437	35355942					
hemp agrimony							

Table S3.2 Major compounds found in each fraction of pot marigold extract. The NIST probability match the scores (%) found in Figure S3.1

Fraction 1	Fraction 2	Fraction 3	Fraction 4	Fraction 5	Fraction 6	Fraction 7
Compound	Compound	Compound	Compound	Faradiol laurate	Faradiol myristate	Myristic acid
Myristic acid	Myristic acid	Palmitic acid	Sigmasterol		Faradiol palmitate	
Palmitic acid	Palmitic acid	Stearic acid	Sigmast-5-ene			
Stearic acid	Stearic acid		β-amyrin			
Arachidic acid	Arachidic acid		Isofucosterol			
	α-Linolenic acid		α-amyrin			
			Lupeol			
			ψ-taraxasterol			

			Taraxasterol			

Table S3.3 Compounds identified using characteristic and molecular ions.
The breakdown of compound mass (Da) is detailed in the table.

Compound	Characteristic ion	scaffold (mass)	fatty acid (mass)	acetate (mass)	TMS (mass)	Loss of hydrogen	molecular ion
ψ-taraxasterol/taraxasterol/lupeol-based compounds							
ψ-taraxasterol	189	426			73		499
ψ-taraxasterol acetate	189	426		43	73		469
taraxasterol acetate	189	426		43	73		469
lupeol acetate	189	426		43	73		469
lupeol palmitate	189	426	239				665
taraxasterol palmitate	189	426	239				665
taraxasterol stearate	189	426	267				693
faradiol	189	442			146	1	587
calenduladiol	189	442			146	1	587
faradiol laurate	189	442	183		73	1	697
faradiol myristate	189	442	211		73	1	725
faradiol palmitate	189	442	239		73	1	753
α-amyrin/β-amyrin-based compounds							
α-amyrin acetate	218	426		43	73		469
β-amyrin acetate	218	426		43	73		469
α-amyrin palmitate	218	426	239				665
β-amyrin palmitate	218	426	239				665
β-amyrin stearate	218	426	267				693
maniladiol	216	442			146	1	587
maniladiol myristate	216	442	211		73	1	725
maniladiol palmitate	216	442	239		73	1	753
maniladiol stearate	216	442	267		73	1	781

Table S3.4 Table of statistics. Stars denote significance threshold. *=p<0.0332,**=p<0.0021, ***=p<0.0002, ****=p<0.0001.

Chapter 3						
Table 3.2 Effect of the Asteraceae on THP-1 and HL-60 cell viability.						
HL60						
Dunnett's multiple comparisons test	Mean Diff.	95.00% CI of diff.	Below threshold?	Summary	Adjusted P Value	
DMSO vs. Cells	-61.23	-112.5 to -9.981	Yes	*	0.0106	
DMSO vs. Staurosporine	93.41	37.62 to 149.2	Yes	***	0.0001	
DMSO vs. Calendula officinalis (Pot Marigold)	-60	-115.8 to -4.211	Yes	*	0.0281	
DMSO vs. Calendula officinalis (Snow Princess)	49.04	-6.755 to 104.8	No	ns	0.117	
DMSO vs. Achillea millefolium	70.15	14.36 to 125.9	Yes	**	0.0062	
DMSO vs. Helianthus annuus Ray	51.45	-4.339 to 107.2	No	ns	0.0873	
DMSO vs. Pilosella officinarum	34.32	-14.00 to 82.63	No	ns	0.3192	
DMSO vs. Silybum marianum	-20.14	-68.46 to 28.18	No	ns	0.9024	
DMSO vs. Hypochaeris radicata	-33.89	-82.21 to 14.42	No	ns	0.334	
DMSO vs. Veronia altissima	92.99	37.19 to 148.8	Yes	***	0.0001	
DMSO vs. Bellis perennis	95.57	44.32 to 146.8	Yes	****	<0.0001	
DMSO vs. Chondrilla juncea	-19.89	-71.14 to 31.36	No	ns	0.9375	
DMSO vs. Matricaria chamomilla	62.25	13.93 to 110.6	Yes	**	0.0047	
DMSO vs. Inula britannica	84.17	32.92 to 135.4	Yes	***	0.0002	
DMSO vs. Inula ensifolia	-6.116	-57.37 to 45.13	No	ns	>0.9999	
THP1						
DMSO vs. Cells	-75.49	-139.4 to -11.60	Yes	*	0.0114	
DMSO vs. Staurosporine	91.24	24.24 to 158.2	Yes	**	0.0022	
DMSO vs. Calendula officinalis (Pot Marigold)	-67.72	-139.1 to 3.702	No	ns	0.0732	
DMSO vs. Calendula officinalis (Snow Princess)	44.78	-26.65 to 116.2	No	ns	0.4795	
DMSO vs. Achillea millefolium	80.13	8.707 to 151.6	Yes	*	0.019	

DMSO vs. Heliant hus annuus Ray	-26.61	-98.03 to 44.82	No	ns	0.9539	
DMSO vs. Pilosell a officinarum	-1.602	-73.03 to 69.82	No	ns	>0.9999	
DMSO vs. Silybu m marianum	-13.84	-77.73 to 50.04	No	ns	0.9997	
DMSO vs. Hypoc haeris radicata	-57.05	-120.9 to 6.836	No	ns	0.1074	
DMSO vs. Veroni a altissima	76.66	9.660 to 143.7	Yes	*	0.0157	
DMSO vs. Bellis perennis	-10.77	-74.66 to 53.11	No	ns	>0.9999	
DMSO vs. Chondr illa juncea	-47.85	-111.7 to 16.04	No	ns	0.261	
DMSO vs. Matric aria chamomilla	4.437	-59.45 to 68.32	No	ns	>0.9999	
DMSO vs. Inula b ritannica	20.95	-42.93 to 84.83	No	ns	0.9826	
DMSO vs. Inula e nsifolia	-55.31	-119.2 to 8.575	No	ns	0.1287	
Figure 3.5 Effect of Asteraceae crude extracts (50 µg/mL) on THP-1 cell viability.						
Dunnett's multiple c omparisons test	Mean D iff.	95.00% CI of diff.	Below thres hold?	Summary	Adjusted P Value	
DMSO vs. Cells	8.602	-13.25 to 30.45	No	ns	0.8802	
DMSO vs. Stauros porine	96.47	74.62 to 118.3	Yes	****	<0.0001	
DMSO vs. CO	10.34	-11.52 to 32.19	No	ns	0.7344	
DMSO vs. AM	-4.64	-26.49 to 17.21	No	ns	0.9987	
DMSO vs. HA	4.802	-17.05 to 26.66	No	ns	0.9982	
DMSO vs. PO	16.85	-5.000 to 38.71	No	ns	0.203	
DMSO vs. SM	9.512	-12.34 to 31.36	No	ns	0.8091	
DMSO vs. HR	12.11	-9.739 to 33.97	No	ns	0.5615	
DMSO vs. BP	19.75	-2.100 to 41.61	No	ns	0.093	
DMSO vs. CJ	25.84	3.989 to 47.69	Yes	*	0.0139	

DMSO vs. MC	17.03	-4.823 to 38.88	No	ns	0.1942	
DMSO vs. PB	3.102	-18.75 to 24.95	No	ns	>0.9999	
DMSO vs. IE	19.94	-1.917 to 41.79	No	ns	0.0883	
Figure 3.6 Effect of BAY 11-7082 (10 μM) on TNF-α (A) and IL-6 secretion (B) from LPS-stimulated THP-1 cells.						
	TNF	IL6				
Column D	BAY	BAY				
vs.	vs.	vs.				
Column C	LPS + DMSO	LPS + DMSO				
Unpaired t test						
P value	0.0002	<0.0001				
P value summary	***	****				
Significantly different (P < 0.05)?	Yes	Yes				
Difference between means (D - C) ± SEM	-89.58 ± 6.733	-80.36 ± 3.085				
95% confidence interval	-108.3 to -70.88	-88.92 to -71.79				
R squared (eta squared)	0.9779	0.9941				
Figure 3.7 The effects of crude extracts of Asteraceae floral tissues on TNF-α and IL-6 secretion from LPS-stimulated THP-1 cells.						
TNF						
Dunnett's multiple comparisons test	Mean Diff.	95.00% CI of diff.	Below threshold?	Summary	Adjusted P Value	
LPS + DMSO vs. CO	45.84	-5.436 to 97.11	No	ns	0.0951	
LPS + DMSO vs. HA	13.32	-37.96 to 64.59	No	ns	0.9814	
LPS + DMSO vs. PO	8.989	-42.28 to 60.26	No	ns	0.9989	
LPS + DMSO vs. SM	18.06	-33.21 to 69.33	No	ns	0.8986	
LPS + DMSO vs. HR	15.4	-35.88 to 66.67	No	ns	0.9556	
LPS + DMSO vs. BP	60.57	9.297 to 111.8	Yes	*	0.0154	

LPS + DMSO vs. CJ	28.57	-22.71 to 79.84	No	ns	0.5105	
LPS + DMSO vs. MC	56.83	5.554 to 108.1	Yes	*	0.025	
LPS + DMSO vs. PB	88.23	36.95 to 139.5	Yes	***	0.0004	
LPS + DMSO vs. IE	46.03	-5.240 to 97.31	No	ns	0.093	
IL6						
Dunnett's multiple comparisons test	Mean Diff.	95.00% CI of diff.	Below threshold?	Summary	Adjusted P Value	
LPS + DMSO vs. CO	55.71	3.893 to 107.5	Yes	*	0.0312	
LPS + DMSO vs. HA	27.86	-23.95 to 79.68	No	ns	0.5478	
LPS + DMSO vs. PO	-153.7	-205.5 to -101.9	Yes	****	<0.0001	
LPS + DMSO vs. SM	2.344	-49.47 to 54.16	No	ns	>0.9999	
LPS + DMSO vs. HR	28.2	-23.62 to 80.01	No	ns	0.5348	
LPS + DMSO vs. BP	-212.9	-270.8 to -154.9	Yes	****	<0.0001	
LPS + DMSO vs. CJ	42.67	-9.148 to 94.48	No	ns	0.1416	
LPS + DMSO vs. MC	-334.6	-392.5 to -276.6	Yes	****	<0.0001	
LPS + DMSO vs. PB	94.34	42.53 to 146.2	Yes	***	0.0002	
LPS + DMSO vs. IE	13.1	-38.71 to 64.92	No	ns	0.9841	
Figure 3.9 Effect of pot marigold extracts on THP-1 cell viability.						
Dunnett's multiple comparisons test	Mean Diff.	95.00% CI of diff.	Below threshold?	Summary	Adjusted P Value	
DMSO vs. Basal	-34.76	-59.86 to -9.669	Yes	**	0.0047	
DMSO vs. Staurosporine	96.47	71.38 to 121.6	Yes	****	<0.0001	
DMSO vs. S1	5.894	-19.20 to 30.99	No	ns	0.9799	
DMSO vs. S2	3.214	-21.88 to 28.31	No	ns	0.9996	
DMSO vs. S3	5.29	-19.80 to 30.38	No	ns	0.9893	
DMSO vs. S4	1.658	-23.44 to 26.75	No	ns	>0.9999	
DMSO vs. S5	-1.337	-26.43 to 23.76	No	ns	>0.9999	

DMSO vs. S6	5.754	-19.34 to 30.85	No	ns	0.9825	
Figure 3.10 Effect of crude extracts from pot marigold flowers from six developmental stages on TNF-α and IL-6 secretion from LPS-stimulated THP-1 cells.						
TNF						
Tukey's multiple comparisons test	Mean Diff.	95.00% CI of diff.	Below threshold?	Summary	Adjusted P Value	
LPS + DMSO vs. BAY	82.33	28.83 to 135.8	Yes	**	0.0014	
LPS + DMSO vs. S1	17.46	-36.04 to 70.97	No	ns	0.9403	
LPS + DMSO vs. S2	8.676	-44.83 to 62.18	No	ns	0.9989	
LPS + DMSO vs. S3	24.86	-28.65 to 78.37	No	ns	0.7395	
LPS + DMSO vs. S4	15.57	-37.94 to 69.08	No	ns	0.9665	
LPS + DMSO vs. S5	26.98	-26.53 to 80.49	No	ns	0.6608	
LPS + DMSO vs. S6	43.79	-9.713 to 97.30	No	ns	0.1539	
BAY vs. S1	-64.87	-118.4 to -11.36	Yes	*	0.0122	
BAY vs. S2	-73.66	-127.2 to -20.15	Yes	**	0.004	
BAY vs. S3	-57.48	-111.0 to -3.969	Yes	*	0.0307	
BAY vs. S4	-66.76	-120.3 to -13.26	Yes	**	0.0096	
BAY vs. S5	-55.35	-108.9 to -1.845	Yes	*	0.0399	
BAY vs. S6	-38.54	-92.05 to 14.97	No	ns	0.2649	
S1 vs. S2	-8.787	-62.29 to 44.72	No	ns	0.9988	
S1 vs. S3	7.394	-46.11 to 60.90	No	ns	0.9996	
S1 vs. S4	-1.893	-55.40 to 51.62	No	ns	>0.9999	
S1 vs. S5	9.518	-43.99 to 63.03	No	ns	0.9981	
S1 vs. S6	26.33	-27.18 to 79.84	No	ns	0.6854	
S2 vs. S3	16.18	-37.33 to 69.69	No	ns	0.9592	

S2 vs. S4	6.894	-46.61 to 60.40	No	ns	0.9998	
S2 vs. S5	18.31	-35.20 to 71.81	No	ns	0.9252	
S2 vs. S6	35.12	-18.39 to 88.63	No	ns	0.3636	
S3 vs. S4	-9.287	-62.79 to 44.22	No	ns	0.9984	
S3 vs. S5	2.125	-51.38 to 55.63	No	ns	>0.9999	
S3 vs. S6	18.94	-34.57 to 72.45	No	ns	0.9125	
S4 vs. S5	11.41	-42.10 to 64.92	No	ns	0.9942	
S4 vs. S6	28.22	-25.28 to 81.73	No	ns	0.6132	
S5 vs. S6	16.81	-36.70 to 70.32	No	ns	0.9505	
IL-6						
Tukey's multiple comparisons test	Mean Diff.	95.00% CI of diff.	Below threshold?	Summary	Adjusted P Value	
LPS + DMSO vs. BAY	100	74.04 to 126.0	Yes	****	<0.0001	
LPS + DMSO vs. S1	61.49	35.53 to 87.45	Yes	****	<0.0001	
LPS + DMSO vs. S2	51.18	25.22 to 77.14	Yes	****	<0.0001	
LPS + DMSO vs. S3	40.24	14.28 to 66.20	Yes	**	0.0013	
LPS + DMSO vs. S4	51.35	25.39 to 77.32	Yes	****	<0.0001	
LPS + DMSO vs. S5	49.48	23.52 to 75.44	Yes	***	0.0001	
LPS + DMSO vs. S6	62.2	36.24 to 88.16	Yes	****	<0.0001	
BAY vs. S1	-38.51	-64.47 to -12.55	Yes	**	0.002	
BAY vs. S2	-48.82	-74.78 to -22.86	Yes	***	0.0002	
BAY vs. S3	-59.76	-85.72 to -33.80	Yes	****	<0.0001	
BAY vs. S4	-48.65	-74.61 to -22.68	Yes	***	0.0002	
BAY vs. S5	-50.52	-76.48 to -24.56	Yes	***	0.0001	
BAY vs. S6	-37.8	-63.76 to -11.84	Yes	**	0.0024	
S1 vs. S2	-10.31	-36.27 to 15.65	No	ns	0.8555	

S1 vs. S3	-21.25	-47.21 to 4.710	No	ns	0.1538	
S1 vs. S4	-10.14	-36.10 to 15.82	No	ns	0.8655	
S1 vs. S5	-12.01	-37.97 to 13.95	No	ns	0.7429	
S1 vs. S6	0.7082	-25.25 to 26.67	No	ns	>0.9999	
S2 vs. S3	-10.94	-36.90 to 15.02	No	ns	0.8174	
S2 vs. S4	0.1758	-25.78 to 26.14	No	ns	>0.9999	
S2 vs. S5	-1.701	-27.66 to 24.26	No	ns	>0.9999	
S2 vs. S6	11.02	-14.94 to 36.98	No	ns	0.812	
S3 vs. S4	11.11	-14.85 to 37.07	No	ns	0.8059	
S3 vs. S5	9.236	-16.72 to 35.20	No	ns	0.9104	
S3 vs. S6	21.96	-4.002 to 47.92	No	ns	0.131	
S4 vs. S5	-1.877	-27.84 to 24.08	No	ns	>0.9999	
S4 vs. S6	10.85	-15.12 to 36.81	No	ns	0.8233	
S5 vs. S6	12.72	-13.24 to 38.68	No	ns	0.6895	
Figure 3.11 Effect of pot marigold extract on THP-1 cell viability and IL-6 secretion.						
Cell viability						
Dunnett's multiple comparisons test	Mean Diff.	95.00% CI of diff.	Below threshold?	Summary	Adjusted P Value	
DMSO vs. Cells	-8.574	-54.53 to 37.38	No	ns	0.9727	
DMSO vs. 10 µg/mL	16.55	-29.41 to 62.50	No	ns	0.747	
DMSO vs. *25* µg/mL	20.82	-25.14 to 66.77	No	ns	0.5726	
DMSO vs. *50* µg/mL	21.3	-24.66 to 67.26	No	ns	0.5531	

DMSO vs. 100 µg/mL	23.58	-22.37 to 69.54	No	ns	0.4651	
IL-6 secretion						
Dunnett's multiple comparisons test	Mean Diff.	95.00% CI of diff.	Below threshold?	Summary	Adjusted P Value	
LPS +DMSO vs. 10 µg/mL	30.1	13.72 to 46.48	Yes	**	0.0012	
LPS +DMSO vs. *25* µg/mL	43.91	27.53 to 60.28	Yes	****	<0.0001	
LPS +DMSO vs. *50* µg/mL	60.56	44.19 to 76.94	Yes	****	<0.0001	
LPS +DMSO vs. 100 µg/mL	82.24	65.86 to 98.62	Yes	****	<0.0001	
Figure 3.14 The effects of pot marigold fractions on cell viability and release of IL-6 in LPS-activated THP-1 cells.						
Cell viability						
Dunnett's multiple comparisons test	Mean Diff.	95.00% CI of diff.	Below threshold?	Summary	Adjusted P Value	
DMSO vs. Cells	-5.003	-30.95 to 20.94	No	ns	0.9938	
DMSO vs. Staurosporine	86.85	60.91 to 112.8	Yes	****	<0.0001	
DMSO vs. Ψ-taraxasterol	1.627	-24.32 to 27.57	No	ns	>0.9999	
DMSO vs. Taraxasterol	0.6899	-25.25 to 26.63	No	ns	>0.9999	
DMSO vs. Faradiol	8.455	-17.49 to 34.40	No	ns	0.8986	
DMSO vs. Arnidiol	-3.263	-29.21 to 22.68	No	ns	0.9996	
DMSO vs. Faradiol myristate	-13.3	-39.24 to 12.65	No	ns	0.557	
DMSO vs. Faradiol palmitate	-11.52	-37.46 to 14.43	No	ns	0.6941	
IL-6 secretion						
Dunnett's multiple comparisons test	Mean Diff.	95.00% CI of diff.	Below threshold?	Summary	Adjusted P Value	
LPS +DMSO vs. BAY	99.06	64.70 to 133.4	Yes	****	<0.0001	
LPS +DMSO vs. Fraction 1	36.73	2.359 to 71.09	Yes	*	0.0332	
LPS +DMSO vs. Fraction 2	17.79	-16.57 to 52.16	No	ns	0.5469	
LPS +DMSO vs. Fraction 3	27.44	-6.930 to 61.80	No	ns	0.1544	

LPS +DMSO vs. Fraction 4	26.07	-8.296 to 60.44	No	ns	0.1895	
LPS +DMSO vs. Fraction 5	33.74	-0.6221 to 68.11	No	ns	0.0556	
LPS +DMSO vs. Fraction 6	48.25	13.89 to 82.62	Yes	**	0.0041	
LPS +DMSO vs. Fraction 7	45.63	11.26 to 80.00	Yes	**	0.0067	
Figure 3.17 Effect of pure compounds on cell viability and IL-6 secretion from LPS-stimulated THP-1 cells.						
Cell viability						
Dunnett's multiple comparisons test	Mean Diff.	95.00% CI of diff.	Below threshold?	Summary	Adjusted P Value	
DMSO vs. Cells	-5.003	-30.95 to 20.94	No	ns	0.9938	
DMSO vs. Staurosporine	86.85	60.91 to 112.8	Yes	****	<0.0001	
DMSO vs. Ψ-taraxasterol	1.627	-24.32 to 27.57	No	ns	>0.9999	
DMSO vs. Taraxasterol	0.6899	-25.25 to 26.63	No	ns	>0.9999	
DMSO vs. Faradiol	8.455	-17.49 to 34.40	No	ns	0.8986	
DMSO vs. Arnidiol	-3.263	-29.21 to 22.68	No	ns	0.9996	
DMSO vs. Faradiol myristate	-13.3	-39.24 to 12.65	No	ns	0.557	
DMSO vs. Faradiol palmitate	-11.52	-37.46 to 14.43	No	ns	0.6941	
IL-6 secretion						
Dunnett's multiple comparisons test	Mean Diff.	95.00% CI of diff.	Below threshold?	Summary	Adjusted P Value	
LPS +DMSO vs. Basal	99.34	53.48 to 145.2	Yes	****	<0.0001	
LPS +DMSO vs. BAY	98.89	53.03 to 144.7	Yes	****	<0.0001	
LPS +DMSO vs. ψ-taraxasterol	24.03	-21.83 to 69.89	No	ns	0.5779	
LPS +DMSO vs. Taraxasterol	-111.1	-157.0 to -65.25	Yes	****	<0.0001	
LPS +DMSO vs. Faradiol	54.73	8.874 to 100.6	Yes	*	0.0132	
LPS +DMSO vs. Arnidiol	56.2	10.34 to 102.1	Yes	*	0.0104	
LPS +DMSO vs. Faradiol myristate	33.24	-12.61 to 79.10	No	ns	0.2453	

LPS +DMSO vs. Faradiol palmitate	41.01	-4.850 to 86.87	No	ns	0.0967	
Figure 3.18 The effects of pot marigold fractions on THP-1 cell viability and IL-6 secretion.						
Cell viability						
Dunnett's multiple comparisons test	Mean Diff.	95.00% CI of diff.	Below threshold?	Summary	Adjusted P Value	
DMSO vs. Cells	-15.68	-37.29 to 5.937	No	ns	0.2178	
DMSO vs. 1 µM	-2.426	-24.04 to 19.19	No	ns	0.9992	
DMSO vs. 2.5 µM	-1.483	-23.10 to 20.13	No	ns	>0.9999	
DMSO vs. 5 µM	3.898	-17.72 to 25.51	No	ns	0.9902	
DMSO vs. 10 µM	2.985	-18.63 to 24.60	No	ns	0.9976	
DMSO vs. 20 µM	20.8	-2.547 to 44.15	No	ns	0.0926	
IL-6 secretion						
Dunnett's multiple comparisons test	Mean Diff.	95.00% CI of diff.	Below threshold?	Summary	Adjusted P Value	
LPS +DMSO vs. Basal	98.33	86.11 to 110.5	Yes	****	<0.0001	
LPS +DMSO vs. 1 µM	5.687	-6.535 to 17.91	No	ns	0.5892	
LPS +DMSO vs. 2.5 µM	11.75	-0.4759 to 23.97	No	ns	0.0616	
LPS +DMSO vs. 5 µM	24.36	12.13 to 36.58	Yes	***	0.0002	
LPS +DMSO vs. 10 µM	62.63	50.41 to 74.85	Yes	****	<0.0001	
LPS +DMSO vs. 20 µM	74.16	61.94 to 86.38	Yes	****	<0.0001	
Figure 3.19 The effects of selected compounds on THP-1 cell viability and IL-6 secretion.						
Cell viability						
Dunnett's multiple comparisons test	Mean Diff.	95.00% CI of diff.	Below threshold?	Summary	Adjusted P Value	
DMSO vs. Basal	-5.003	-24.65 to 14.65	No	ns	0.9566	
DMSO vs. Staurosporine	86.85	67.20 to 106.5	Yes	****	<0.0001	

DMSO vs. Faradiol	8.455	-11.20 to 28.11	No	ns	0.6916	
DMSO vs. Lupeol	-0.008304	-19.66 to 19.64	No	ns	>0.9999	
DMSO vs. Betulin	3.996	-15.66 to 23.65	No	ns	0.986	
DMSO vs. Oleanolic acid	-6.632	-26.28 to 13.02	No	ns	0.8583	
DMSO vs. Betulinic acid	-2.713	-22.36 to 16.94	No	ns	0.9985	
IL-6 secretion						
Dunnett's multiple comparisons test	Mean Diff.	95.00% CI of diff.	Below threshold?	Summary	Adjusted P Value	
LPS +DMSO vs. Faradiol	66.84	22.31 to 111.4	Yes	**	0.0026	
LPS +DMSO vs. Lupeol	31.74	-12.79 to 76.27	No	ns	0.219	
LPS +DMSO vs. Betulin	-23.14	-67.67 to 21.39	No	ns	0.487	
LPS +DMSO vs. Oleanolic acid	-22.69	-67.22 to 21.84	No	ns	0.5047	
LPS +DMSO vs. Betulinic acid	4.53	-40.00 to 49.06	No	ns	0.9986	
Figure 3.20 Effect of faradiol and faradiol palmitate (20 µM) on NF-κB and STAT3 signalling pathways in LPS-induced THP-1 cells.						
pSTAT3/STAT3						
Dunnett's multiple comparisons test	Mean Diff.	95.00% CI of diff.	Below threshold?	Summary	Adjusted P Value	
LPS + DMSO vs. Basal	0.7864	0.4376 to 1.135	Yes	***	0.0001	
LPS + DMSO vs. LPS	-0.6672	-1.016 to -0.3185	Yes	***	0.0005	
LPS + DMSO vs. BAY	0.6342	0.2855 to 0.9830	Yes	***	0.0008	
LPS + DMSO vs. Faradiol	0.4291	0.08038 to 0.7779	Yes	*	0.0153	
LPS + DMSO vs. Faradiol palmitate	0.07919	-0.2696 to 0.4280	No	ns	0.9415	
pNFKb/NFKb						
Dunnett's multiple comparisons test	Mean Diff.	95.00% CI of diff.	Below threshold?	Summary	Adjusted P Value	
LPS + DMSO vs. Basal	0.2758	-0.6574 to 1.209	No	ns	0.8491	
LPS + DMSO vs. LPS	-0.04836	-0.9816 to 0.8849	No	ns	>0.9999	

LPS + DMSO vs. BAY	0.2911	-0.6421 to 1.224	No	ns	0.8226	
LPS + DMSO vs. Faradiol	-0.3154	-1.249 to 0.6179	No	ns	0.7776	
LPS + DMSO vs. Faradiol palmitate	-0.5358	-1.856 to 0.7840	No	ns	0.6501	
Figure 3.21 The effects of (A) pot marigold extract and (B) selected compounds on HaCaT cell proliferation.						
Pot marigold extract						
Dunnett's multiple comparisons test	Mean Diff.	95.00% CI of diff.	Below threshold?	Summary	Adjusted P Value	
DMSO vs. Cells	-17.4	-55.23 to 20.43	No	ns	0.5465	
DMSO vs. 50 µg/mL	-25.11	-65.97 to 15.75	No	ns	0.3088	
DMSO vs. 25 µg/mL	-8.165	-45.99 to 29.66	No	ns	0.9351	
DMSO vs. 12.5 µg/mL	12.61	-25.22 to 50.44	No	ns	0.7728	
Pure compounds						
Dunnett's multiple comparisons test	Mean Diff.	95.00% CI of diff.	Below threshold?	Summary	Adjusted P Value	
DMSO vs. Cells	-17.4	-28.76 to -6.031	Yes	**	0.0018	
DMSO vs. ψ-taraxasterol	1.114	-10.25 to 12.48	No	ns	0.9996	
DMSO vs. taraxastrol	0.7688	-10.60 to 12.13	No	ns	>0.9999	
DMSO vs. faradiol	-2.654	-14.02 to 8.711	No	ns	0.9662	
DMSO vs. arnidiol 50 µM	12.06	0.6991 to 23.43	Yes	*	0.0348	
DMSO vs. faradiol myristate	9.689	-1.676 to 21.05	No	ns	0.1142	
Figure 3.22 Effect of hEGF on wound closure in HaCaT cells.						
Column B	hEGF					
vs.	vs.					
Column A	Untreated cells					
Unpaired t test						

P value	0.0033					
P value summary	**					
Significantly diff erent (P < 0.05)?	Yes					
Difference betwe en means (B - A) ± SEM	19.10 ± 4.055					
95% confidence i nterval	9.179 to 29.02					
R squared (eta sq uared)	0.7871					
Figure 3.23 Effect of pot marigold extracts and triterpenes on wound closure in HaCaT cell monolayer after 24h.						
Pot marigold						
Dunnett's multiple c omparisons test	Mean D iff.	95.00% CI of diff.	Below thres hold?	Summary	Adjusted P Value	
DMSO vs. Untreat ed cells	2.904	-6.022 to 11. 83	No	ns	0.8351	
DMSO vs. hEGF	-44.12	-53.05 to - 35.19	Yes	****	<0.0001	
DMSO vs. 50 µg/ mL	-0.2835	-9.210 to 8.6 43	No	ns	>0.9999	
DMSO vs. 25 µg/ mL	-9.809	-18.74 to - 0.8822	Yes	*	0.0286	
DMSO vs. 12.5 µ g/mL	-3.495	-12.42 to 5.4 31	No	ns	0.7219	
Pure compounds						
Dunnett's multiple c omparisons test	Mean D iff.	95.00% CI of diff.	Below thres hold?	Summary	Adjusted P Value	
DMSO vs. ψ-tar axasterol 20µM	-4.325	-10.18 to 1.5 28	No	ns	0.1928	
DMSO vs. taraxas terol 20 µM	-2.463	-8.316 to 3.3 90	No	ns	0.6672	
DMSO vs. faradio l 20 µM	-4.373	-10.23 to 1.4 80	No	ns	0.1855	
DMSO vs. arnidio l 20 µM	11.35	5.025 to 17. 67	Yes	***	0.0005	
DMSO vs. faradio l myristate 20 µM	1.55	-4.303 to 7.4 03	No	ns	0.9166	
Chapter 4						
Figure 4.3 Differential expression of pot marigold candidate *CoCYPs* genes in leaf, disc and ray floret tissues						

CYP1						
Tukey's multiple comparisons test	Mean Diff.	95.00% CI of diff.	Below threshold?	Summary	Adjusted P Value	
Leaf vs. Disc	-890.2	-8719 to 6939	No	ns	0.9463	
Leaf vs. Ray	-21922	-29751 to -14093	Yes	****	<0.0001	
Disc vs. Ray	-21032	-28860 to -13203	Yes	****	<0.0001	
CYP2						
Tukey's multiple comparisons test	Mean Diff.	95.00% CI of diff.	Below threshold?	Summary	Adjusted P Value	
Leaf vs. Disc	-617.3	-1662 to 427.1	No	ns	0.2753	
Leaf vs. Ray	-1687	-2732 to -642.7	Yes	**	0.0038	
Disc vs. Ray	-1070	-2114 to -25.34	Yes	*	0.045	
CYP3						
Tukey's multiple comparisons test	Mean Diff.	95.00% CI of diff.	Below threshold?	Summary	Adjusted P Value	
Leaf vs. Disc	-32.4	-133.1 to 68.26	No	ns	0.6545	
Leaf vs. Ray	-66.97	-167.6 to 33.70	No	ns	0.2063	
Disc vs. Ray	-34.56	-135.2 to 66.10	No	ns	0.6193	
CYP4						
Tukey's multiple comparisons test	Mean Diff.	95.00% CI of diff.	Below threshold?	Summary	Adjusted P Value	
Leaf vs. Disc	-299.1	-841.3 to 243.2	No	ns	0.3188	
Leaf vs. Ray	-343.8	-886.0 to 198.5	No	ns	0.2334	
Disc vs. Ray	-44.68	-586.9 to 497.5	No	ns	0.9713	
CYP5						
Tukey's multiple comparisons test	Mean Diff.	95.00% CI of diff.	Below threshold?	Summary	Adjusted P Value	
Leaf vs. Disc	9928	6768 to 13087	Yes	****	<0.0001	
Leaf vs. Ray	10024	6864 to 13184	Yes	****	<0.0001	

Disc vs. Ray	96.13	-3064 to 3256	No	ns	0.996	

Figure 4.12 GC-MS analysis and quantification of triterpenes in *N. benthamiana* leaves expressing mutants of CoCYP716A392 and CoCYP716A393

Sample	Code	P.adjusted for beta-amyrin to psi-taraxasterol ratio	P.adjusted for total content of beta-amyrin and psi-taraxasterol		Key	CoTXSS
CoTXSS-CoTXSS + CoCYP716A392	A-B	0.0054	0.0034		A	CoTXSS + CoCYP716 A392
CoTXSS-CoTXSS + CoCYP716A392 (A285G)	A-C	0.0054	0.0066		B	CoTXSS + CoCYP716 A392 (A285G)
CoTXSS-CoTXSS + CoCYP716A392 (A285V)	A-D	0.0077	0.0034		C	CoTXSS + CoCYP716 A392 (A285V)
CoTXSS-CoTXSS + CoCYP716A392 (A357L)	A-E	0.085	0.0034		D	CoTXSS + CoCYP716 A392 (A357L)
CoTXSS-CoTXSS + CoCYP716A392 (H424R)	A-F	0.0054	0.0034		E	CoTXSS + CoCYP716 A392 (H424R)
CoTXSS-CoTXSS + CoCYP716A392 (A285V)	A-G	0.0054	0.0034		F	CoTXSS + CoCYP716 A393
CoTXSS-CoTXSS + CoCYP716A393 (A285G)	A-H	0.0054	0.0034		G	CoTXSS + CoCYP716 A393 (A285G)
CoTXSS-CoTXSS + CoCYP716A393 (A285V)	A-I	0.0054	0.0034		H	CoTXSS + CoCYP716 A393 (A285V)
CoTXSS-CoTXSS + CoCYP716A393 (A357L)	A-J	0.0054	0.0916		I	CoTXSS + CoCYP716 A393 (A357L)
CoTXSS-CoTXSS + CoCYP716A393 (H424R)	A-K	0.0054	0.0916		J	CoTXSS + CoCYP716 A393 (H424R)
CoTXSS + CoCYP716A392-CoTXSS + CoCYP716A392 (A285G)	B-C	1	0.0034		K	
CoTXSS + CoCYP716A392-CoTXSS + CoCYP716A392 (A285V)	B-D	0.0077	0.5674			

CoTXSS + CoCYP716A392-CoTXSS + CoCYP716A392 (A357L)	B-E	0.0386	0.3073			
CoTXSS + CoCYP716A392-CoTXSS + CoCYP716A392 (H424R)	B-F	0.5128	0.7255			
CoTXSS + CoCYP716A392-CoTXSS + CoCYP716A392 (H424R)	B-G	0.5996	0.6476			
CoTXSS + CoCYP716A392-CoTXSS + CoCYP716A393 (A285G)	B-H	0.2753	0.0034			
CoTXSS + CoCYP716A392-CoTXSS + CoCYP716A393 (A285V)	B-I	0.0054	0.6476			
CoTXSS + CoCYP716A392-CoTXSS + CoCYP716A393 (A357L)	B-J	0.3474	0.0034			
CoTXSS + CoCYP716A392-CoTXSS + CoCYP716A393 (H424R)	B-K	0.085	0.0034			
CoTXSS + CoCYP716A392 (A285G)-CoTXSS + CoCYP716A392 (A285V)	C-D	0.0077	0.0034			
CoTXSS + CoCYP716A392 (A285G)-CoTXSS + CoCYP716A392 (A357L)	C-E	0.0054	0.0034			
CoTXSS + CoCYP716A392 (A285G)-CoTXSS + CoCYP716A392 (H424R)	C-F	0.085	0.0034			
CoTXSS + CoCYP716A392 (A285G)-CoTXSS + CoCYP716A393	C-G	0.5996	0.0034			
CoTXSS + CoCYP716A392 (A285G)-CoTXSS + CoCYP716A393 (A285G)	C-H	0.4248	0.0916			
CoTXSS + CoCYP716A392 (A285G)-CoTXSS + CoCYP716A393 (A285V)	C-I	0.0054	0.0034			

CoTXSS + CoCYP716A392 (A285G)-CoTXSS + CoCYP716A393 (A357L)	C-J	0.0238	0.0034			
CoTXSS + CoCYP716A392 (A285G)-CoTXSS + CoCYP716A393 (H424R)	C-K	0.0054	0.0034			
CoTXSS + CoCYP716A392 (A285V)-CoTXSS + CoCYP716A392 (A357L)	D-E	0.0382	0.471			
CoTXSS + CoCYP716A392 (A285V)-CoTXSS + CoCYP716A392 (H424R)	D-F	0.0077	0.6476			
CoTXSS + CoCYP716A392 (A285V)-CoTXSS + CoCYP716A393	D-G	0.0077	0.7255			
CoTXSS + CoCYP716A392 (A285V)-CoTXSS + CoCYP716A393 (A285G)	D-H	0.0077	0.0034			
CoTXSS + CoCYP716A392 (A285V)-CoTXSS + CoCYP716A393 (A285V)	D-I	0.1113	0.3869			
CoTXSS + CoCYP716A392 (A285V)-CoTXSS + CoCYP716A393 (A357L)	D-J	0.0077	0.0034			
CoTXSS + CoCYP716A392 (A285V)-CoTXSS + CoCYP716A393 (H424R)	D-K	0.0077	0.0034			
CoTXSS + CoCYP716A392 (A357L)-CoTXSS + CoCYP716A392 (H424R)	E-F	0.0149	0.1815			
CoTXSS + CoCYP716A392 (A357L)-CoTXSS + CoCYP716A393	E-G	0.0054	0.3073			
CoTXSS + CoCYP716A392 (A357L)-CoTXSS + CoCYP716A393 (A285G)	E-H	0.0054	0.0034			
CoTXSS + CoCYP716A392 (A357L)-CoTXSS + CoCYP716A393 (A285V)	E-I	0.085	0.241			

CoTXSS + CoCYP716A392 (A357L)-CoTXSS + CoCYP716A393 (A357L)	E-J	0.0054	0.0034			
CoTXSS + CoCYP716A392 (A357L)-CoTXSS + CoCYP716A393 (H424R)	E-K	0.1113	0.0034			
CoTXSS + CoCYP716A392 (H424R)-CoTXSS + CoCYP716A393	F-G	0.1113	1			
CoTXSS + CoCYP716A392 (H424R)-CoTXSS + CoCYP716A393 (A285G)	F-H	0.085	0.0034			
CoTXSS + CoCYP716A392 (H424R)-CoTXSS + CoCYP716A393 (A285V)	F-I	0.0054	0.8333			
CoTXSS + CoCYP716A392 (H424R)-CoTXSS + CoCYP716A393 (A357L)	F-J	0.4248	0.0034			
CoTXSS + CoCYP716A392 (H424R)-CoTXSS + CoCYP716A393 (H424R)	F-K	0.1113	0.0034			
CoTXSS + CoCYP716A393-CoTXSS + CoCYP716A393 (A285G)	G-H	0.2753	0.0034			
CoTXSS + CoCYP716A393-CoTXSS + CoCYP716A393 (A285V)	G-I	0.0054	0.471			
CoTXSS + CoCYP716A393-CoTXSS + CoCYP716A393 (A357L)	G-J	0.0238	0.0034			
CoTXSS + CoCYP716A393-CoTXSS + CoCYP716A393 (H424R)	G-K	0.0054	0.0034			
CoTXSS + CoCYP716A393 (A285G)-CoTXSS + CoCYP716A393 (A285V)	H-I	0.0054	0.0034			
CoTXSS + CoCYP716A393 (A285G)-CoTXSS + CoCYP716A393 (A357L)	H-J	0.0238	0.0034			

CoTXSS + CoCYP716A393 (A285G)-CoTXSS + CoCYP716A393 (H424R)	H-K	0.0054	0.0034			
CoTXSS + CoCYP716A393 (A285V)-CoTXSS + CoCYP716A393 (A357L)	I-J	0.0054	0.0034			
CoTXSS + CoCYP716A393 (A285V)-CoTXSS + CoCYP716A393 (H424R)	I-K	0.0054	0.0034			
CoTXSS + CoCYP716A393 (A357L)-CoTXSS + CoCYP716A393 (H424R)	J-K	0.0077	0.7255			
Visual representation for beta-amyrin to psi-taraxasterol ratio	CoTXSS	CoTXSS+CoCYP716A392	CoTXSS+CoCYP716A392 (A285G)	CoTXSS+CoCYP716A392 (A285V)	CoTXSS+CoCYP716A392 (A357L)	CoTXSS+CoCYP716A392 (H424R)
	A	B	C	D	E	F
	"a"	"bcd"	"b"	"e"	"afg"	"bcd"
		CoTXSS+CoCYP716A393	CoTXSS+CoCYP716A393 (A285G)	CoTXSS+CoCYP716A393 (A285V)	CoTXSS+CoCYP716A393 (A357L)	CoTXSS+CoCYP716A393 (H424R)
		G	H	I	J	K
		"b"	"b"	"ef"	"c"	"dg"
Visual representation for total content of beta-amyrin and psi-taraxasterol	CoTXSS	CoTXSS+CoCYP716A392	CoTXSS+CoCYP716A392 (A285G)	CoTXSS+CoCYP716A392 (A285V)	CoTXSS+CoCYP716A392 (A357L)	CoTXSS+CoCYP716A392 (H424R)
	A	B	C	D	E	F
	"a"	"b"	"c"	"b"	"b"	"b"
		CoTXSS+CoCYP716A393	CoTXSS+CoCYP716A393 (A285G)	CoTXSS+CoCYP716A393 (A285V)	CoTXSS+CoCYP716A393 (A357L)	CoTXSS+CoCYP716A393 (H424R)
		G	H	I	J	K
		"b"	"c"	"b"	"a"	"a"
Figure 4.14 Differential expression of pot marigold candidate *CoACT* genes in leaf, disc and ray floret tissues.						

ACT1						
Tukey's multiple comparisons test	Mean Diff.	95.00% CI of diff.	Below threshold?	Summary	Adjusted P Value	
Leaf vs. Disc	-12.04	-63.15 to 39.07	No	ns	0.7928	
Leaf vs. Ray	-41.14	-92.25 to 9.966	No	ns	0.1159	
Disc vs. Ray	-29.1	-80.21 to 22.01	No	ns	0.2985	
ACT2						
Tukey's multiple comparisons test	Mean Diff.	95.00% CI of diff.	Below threshold?	Summary	Adjusted P Value	
Leaf vs. Disc	-944.9	-1645 to -245.1	Yes	*	0.0111	
Leaf vs. Ray	-3381	-4081 to -2681	Yes	****	<0.0001	
Disc vs. Ray	-2436	-3136 to -1736	Yes	****	<0.0001	
ACT3						
Tukey's multiple comparisons test	Mean Diff.	95.00% CI of diff.	Below threshold?	Summary	Adjusted P Value	
Leaf vs. Disc	-3.484	-86.92 to 79.96	No	ns	0.9925	
Leaf vs. Ray	-58.54	-142.0 to 24.90	No	ns	0.1782	
Disc vs. Ray	-55.06	-138.5 to 28.38	No	ns	0.2108	
ACT4						
Tukey's multiple comparisons test	Mean Diff.	95.00% CI of diff.	Below threshold?	Summary	Adjusted P Value	
Leaf vs. Disc	132.1	-156.7 to 420.9	No	ns	0.4418	
Leaf vs. Ray	113.1	-175.7 to 401.9	No	ns	0.5416	
Disc vs. Ray	-19.02	-307.8 to 269.8	No	ns	0.9816	
ACT5						
Tukey's multiple comparisons test	Mean Diff.	95.00% CI of diff.	Below threshold?	Summary	Adjusted P Value	
Leaf vs. Disc	-20.32	-45.11 to 4.475	No	ns	0.109	

Leaf vs. Ray	-4.048	-28.84 to 20.75	No	ns	0.8931	
Disc vs. Ray	16.27	-8.523 to 41.07	No	ns	0.2138	
ACT6						
Tukey's multiple comparisons test	Mean Diff.	95.00% CI of diff.	Below threshold?	Summary	Adjusted P Value	
Leaf vs. Disc	4.697	-64.99 to 74.38	No	ns	0.9807	
Leaf vs. Ray	-56.74	-126.4 to 12.95	No	ns	0.1115	
Disc vs. Ray	-61.43	-131.1 to 8.252	No	ns	0.0836	
ACT7						
Tukey's multiple comparisons test	Mean Diff.	95.00% CI of diff.	Below threshold?	Summary	Adjusted P Value	
Leaf vs. Disc	-40.9	-184.0 to 102.2	No	ns	0.7134	
Leaf vs. Ray	-0.86	-143.9 to 142.2	No	ns	0.9998	
Disc vs. Ray	40.04	-103.0 to 183.1	No	ns	0.7232	
Figure 4.17 Proposed biosynthetic pathway and relative gene expression analysis of faradiol palmate pathway genes through flower development.						
TXSS						
Dunnett's multiple comparisons test	Mean Diff.	95.00% CI of diff.	Below threshold?	Summary	Adjusted P Value	
S1 vs. S2	0.8949	0.8142 to 0.9756	Yes	****	<0.0001	
S1 vs. S3	0.9628	0.8821 to 1.044	Yes	****	<0.0001	
S1 vs. S4	0.9869	0.9062 to 1.068	Yes	****	<0.0001	
S1 vs. S5	0.9939	0.9132 to 1.075	Yes	****	<0.0001	
S1 vs. S6	0.9897	0.9090 to 1.070	Yes	****	<0.0001	
CYP1						
Dunnett's multiple comparisons test	Mean Diff.	95.00% CI of diff.	Below threshold?	Summary	Adjusted P Value	
S1 vs. S2	0.1298	-3.350 to 3.610	No	ns	>0.9999	

S1 vs. S3	-3.065	-6.545 to 0.4153	No	ns	0.0911	
S1 vs. S4	-0.9923	-4.472 to 2.488	No	ns	0.8714	
S1 vs. S5	0.3364	-3.144 to 3.816	No	ns	0.9985	
S1 vs. S6	1.05	-2.430 to 4.530	No	ns	0.8465	
CYP2						
Dunnett's multiple comparisons test	Mean Diff.	95.00% CI of diff.	Below threshold?	Summary	Adjusted P Value	
S1 vs. S2	-0.9207	-2.541 to 0.7000	No	ns	0.3772	
S1 vs. S3	-1.145	-2.766 to 0.4756	No	ns	0.2088	
S1 vs. S4	0.01662	-1.604 to 1.637	No	ns	>0.9999	
S1 vs. S5	0.9279	-0.6928 to 2.549	No	ns	0.3706	
S1 vs. S6	0.9833	-0.6375 to 2.604	No	ns	0.3225	
ACT1						
Dunnett's multiple comparisons test	Mean Diff.	95.00% CI of diff.	Below threshold?	Summary	Adjusted P Value	
S1 vs. S2	1.074	0.5727 to 1.576	Yes	***	0.0002	
S1 vs. S3	1.075	0.5734 to 1.577	Yes	***	0.0002	
S1 vs. S4	1.075	0.5734 to 1.577	Yes	***	0.0002	
S1 vs. S5	1.074	0.5721 to 1.576	Yes	***	0.0002	
S1 vs. S6	1.077	0.5749 to 1.578	Yes	***	0.0002	
ACT2						
Dunnett's multiple comparisons test	Mean Diff.	95.00% CI of diff.	Below threshold?	Summary	Adjusted P Value	
S1 vs. S2	0.8913	0.5930 to 1.190	Yes	****	<0.0001	
S1 vs. S3	0.9231	0.6248 to 1.221	Yes	****	<0.0001	
S1 vs. S4	0.8674	0.5690 to 1.166	Yes	****	<0.0001	
S1 vs. S5	0.8816	0.5833 to 1.180	Yes	****	<0.0001	
S1 vs. S6	1.013	0.7142 to 1.311	Yes	****	<0.0001	

ACT3						
Dunnett's multiple comparisons test	Mean Diff.	95.00% CI of diff.	Below threshold?	Summary	Adjusted P Value	
S1 vs. S2	-0.2198	-9.372 to 8.933	No	ns	>0.9999	
S1 vs. S3	-2.64	-11.79 to 6.512	No	ns	0.8666	
S1 vs. S4	-7.381	-16.53 to 1.771	No	ns	0.1308	
S1 vs. S5	-12.25	-21.40 to -3.096	Yes	**	0.0088	
S1 vs. S6	-3.676	-12.83 to 5.477	No	ns	0.6694	
Figure 4.18 Expression analysis of faradiol palmate pathway genes after MeJa treatment.						
TXSS						
Tukey's multiple comparisons test	Mean Diff.	95.00% CI of diff.	Below threshold?	Summary	Adjusted P Value	
T0 vs. T6	0.01284	-3.716 to 3.742	No	ns	>0.9999	
T0 vs. T24	0.4249	-3.304 to 4.154	No	ns	>0.9999	
T0 vs. T0	-0.0814	-3.810 to 3.648	No	ns	>0.9999	
T0 vs. T6	-2.806	-6.535 to 0.9227	No	ns	0.2379	
T0 vs. T24	0.2664	-3.463 to 3.995	No	ns	>0.9999	
T0 vs. T0	-0.3842	-4.113 to 3.345	No	ns	>0.9999	
T0 vs. T6	-1.511	-5.240 to 2.218	No	ns	0.876	
T0 vs. T24	0.1092	-3.620 to 3.838	No	ns	>0.9999	
T6 vs. T24	0.4121	-3.317 to 4.141	No	ns	>0.9999	
T6 vs. T0	-0.09424	-3.823 to 3.635	No	ns	>0.9999	
T6 vs. T6	-2.819	-6.548 to 0.9099	No	ns	0.2333	

T6 vs. T24	0.2536	-3.475 to 3.983	No	ns	>0.9999	
T6 vs. T0	-0.3971	-4.126 to 3.332	No	ns	>0.9999	
T6 vs. T6	-1.524	-5.253 to 2.205	No	ns	0.8711	
T6 vs. T24	0.0964	-3.633 to 3.825	No	ns	>0.9999	
T24 vs. T0	-0.5063	-4.235 to 3.223	No	ns	0.9999	
T24 vs. T6	-3.231	-6.960 to 0.4978	No	ns	0.1206	
T24 vs. T24	-0.1585	-3.887 to 3.571	No	ns	>0.9999	
T24 vs. T0	-0.8092	-4.538 to 2.920	No	ns	0.9967	
T24 vs. T6	-1.936	-5.665 to 1.793	No	ns	0.6705	
T24 vs. T24	-0.3157	-4.045 to 3.413	No	ns	>0.9999	
T0 vs. T6	-2.725	-6.454 to 1.004	No	ns	0.2681	
T0 vs. T24	0.3478	-3.381 to 4.077	No	ns	>0.9999	
T0 vs. T0	-0.3028	-4.032 to 3.426	No	ns	>0.9999	
T0 vs. T6	-1.43	-5.159 to 2.299	No	ns	0.9045	
T0 vs. T24	0.1906	-3.538 to 3.920	No	ns	>0.9999	
T6 vs. T24	3.073	-0.6563 to 6.802	No	ns	0.1569	
T6 vs. T0	2.422	-1.307 to 6.151	No	ns	0.4034	
T6 vs. T6	1.295	-2.434 to 5.024	No	ns	0.9421	
T6 vs. T24	2.916	-0.8135 to 6.645	No	ns	0.2014	
T24 vs. T0	-0.6507	-4.380 to 3.078	No	ns	0.9993	
T24 vs. T6	-1.778	-5.507 to 1.951	No	ns	0.7559	

T24 vs. T24	-0.1572	-3.886 to 3.572	No	ns	>0.9999	
T0 vs. T6	-1.127	-4.856 to 2.602	No	ns	0.9733	
T0 vs. T24	0.4935	-3.236 to 4.222	No	ns	>0.9999	
T6 vs. T24	1.62	-2.109 to 5.349	No	ns	0.8313	
CYP1						
Tukey's multiple comparisons test	Mean Diff.	95.00% CI of diff.	Below threshold?	Summary	Adjusted P Value	
LT0 vs. LT6	0.2772	-5.288 to 5.843	No	ns	>0.9999	
LT0 vs. LT24	0.4113	-5.154 to 5.977	No	ns	>0.9999	
LT0 vs. DT0	0	-5.566 to 5.566	No	ns	>0.9999	
LT0 vs. DT6	-5.669	-11.23 to -0.1035	Yes	*	0.044	
LT0 vs. DT24	0.2605	-5.305 to 5.826	No	ns	>0.9999	
LT0 vs. T0	0	-5.566 to 5.566	No	ns	>0.9999	
LT0 vs. T6	-0.2254	-5.791 to 5.340	No	ns	>0.9999	
LT0 vs. T24	0.7431	-4.823 to 6.309	No	ns	>0.9999	
LT6 vs. LT24	0.1341	-5.431 to 5.700	No	ns	>0.9999	
LT6 vs. DT0	-0.2772	-5.843 to 5.288	No	ns	>0.9999	
LT6 vs. DT6	-5.946	-11.51 to -0.3808	Yes	*	0.0311	
LT6 vs. DT24	-0.01669	-5.582 to 5.549	No	ns	>0.9999	
LT6 vs. T0	-0.2772	-5.843 to 5.288	No	ns	>0.9999	
LT6 vs. T6	-0.5027	-6.068 to 5.063	No	ns	>0.9999	
LT6 vs. T24	0.4658	-5.100 to 6.031	No	ns	>0.9999	
LT24 vs. DT0	-0.4113	-5.977 to 5.154	No	ns	>0.9999	

LT24 vs. DT6	-6.08	-11.65 to -0.5149	Yes	*	0.0262	
LT24 vs. DT24	-0.1508	-5.716 to 5.415	No	ns	>0.9999	
LT24 vs. T0	-0.4113	-5.977 to 5.154	No	ns	>0.9999	
LT24 vs. T6	-0.6368	-6.202 to 4.929	No	ns	>0.9999	
LT24 vs. T24	0.3317	-5.234 to 5.897	No	ns	>0.9999	
DT0 vs. DT6	-5.669	-11.23 to -0.1035	Yes	*	0.044	
DT0 vs. DT24	0.2605	-5.305 to 5.826	No	ns	>0.9999	
DT0 vs. T0	0	-5.566 to 5.566	No	ns	>0.9999	
DT0 vs. T6	-0.2254	-5.791 to 5.340	No	ns	>0.9999	
DT0 vs. T24	0.7431	-4.823 to 6.309	No	ns	>0.9999	
DT6 vs. DT24	5.93	0.3641 to 11.50	Yes	*	0.0318	
DT6 vs. T0	5.669	0.1035 to 11.23	Yes	*	0.044	
DT6 vs. T6	5.444	-0.1219 to 11.01	No	ns	0.058	
DT6 vs. T24	6.412	0.8466 to 11.98	Yes	*	0.0172	
DT24 vs. T0	-0.2605	-5.826 to 5.305	No	ns	>0.9999	
DT24 vs. T6	-0.486	-6.052 to 5.080	No	ns	>0.9999	
DT24 vs. T24	0.4825	-5.083 to 6.048	No	ns	>0.9999	
T0 vs. T6	-0.2254	-5.791 to 5.340	No	ns	>0.9999	
T0 vs. T24	0.7431	-4.823 to 6.309	No	ns	>0.9999	
T6 vs. T24	0.9685	-4.597 to 6.534	No	ns	0.9993	
CYP2						
Tukey's multiple comparisons test	Mean Diff.	95.00% CI of diff.	Below threshold?	Summary	Adjusted P Value	
T0 vs. T6	-0.01872	-6.343 to 6.305	No	ns	>0.9999	

T0 vs. T24	0.1641	-6.160 to 6.488	No	ns	>0.9999	
T0 vs. T0	0.1591	-6.165 to 6.483	No	ns	>0.9999	
T0 vs. T6	-3.277	-9.601 to 3.047	No	ns	0.6727	
T0 vs. T24	0.2629	-6.061 to 6.587	No	ns	>0.9999	
T0 vs. T0	-1.667E-09	-6.324 to 6.324	No	ns	>0.9999	
T0 vs. T6	-3.238	-9.562 to 3.086	No	ns	0.6855	
T0 vs. T24	-1.182	-7.506 to 5.142	No	ns	0.9988	
T6 vs. T24	0.1829	-6.141 to 6.507	No	ns	>0.9999	
T6 vs. T0	0.1778	-6.146 to 6.502	No	ns	>0.9999	
T6 vs. T6	-3.258	-9.582 to 3.066	No	ns	0.6789	
T6 vs. T24	0.2816	-6.042 to 6.606	No	ns	>0.9999	
T6 vs. T0	0.01872	-6.305 to 6.343	No	ns	>0.9999	
T6 vs. T6	-3.219	-9.543 to 3.105	No	ns	0.6916	
T6 vs. T24	-1.163	-7.487 to 5.161	No	ns	0.999	
T24 vs. T0	-0.005068	-6.329 to 6.319	No	ns	>0.9999	
T24 vs. T6	-3.441	-9.765 to 2.883	No	ns	0.6182	
T24 vs. T24	0.09876	-6.225 to 6.423	No	ns	>0.9999	
T24 vs. T0	-0.1641	-6.488 to 6.160	No	ns	>0.9999	
T24 vs. T6	-3.402	-9.726 to 2.922	No	ns	0.6313	
T24 vs. T24	-1.346	-7.670 to 4.978	No	ns	0.9971	
T0 vs. T6	-3.436	-9.760 to 2.888	No	ns	0.6199	

T0 vs. T24	0.1038	-6.220 to 6.428	No	ns	>0.9999	
T0 vs. T0	-0.1591	-6.483 to 6.165	No	ns	>0.9999	
T0 vs. T6	-3.397	-9.721 to 2.927	No	ns	0.633	
T0 vs. T24	-1.341	-7.665 to 4.983	No	ns	0.9972	
T6 vs. T24	3.539	-2.784 to 9.863	No	ns	0.5852	
T6 vs. T0	3.277	-3.047 to 9.601	No	ns	0.6727	
T6 vs. T6	0.03902	-6.285 to 6.363	No	ns	>0.9999	
T6 vs. T24	2.095	-4.229 to 8.419	No	ns	0.9552	
T24 vs. T0	-0.2629	-6.587 to 6.061	No	ns	>0.9999	
T24 vs. T6	-3.5	-9.824 to 2.824	No	ns	0.5983	
T24 vs. T24	-1.445	-7.769 to 4.879	No	ns	0.9954	
T0 vs. T6	-3.238	-9.562 to 3.086	No	ns	0.6855	
T0 vs. T24	-1.182	-7.506 to 5.142	No	ns	0.9988	
T6 vs. T24	2.056	-4.268 to 8.380	No	ns	0.9596	
ACT1						
Tukey's multiple comparisons test	Mean Diff.	95.00% CI of diff.	Below threshold?	Summary	Adjusted P Value	
T0 vs. T6	-2.875	-18.17 to 12.42	No	ns	0.9988	
T0 vs. T24	-0.02043	-15.31 to 15.27	No	ns	>0.9999	
T0 vs. T0	-3.333E-09	-15.29 to 15.29	No	ns	>0.9999	
T0 vs. T6	-9.724	-25.02 to 5.570	No	ns	0.4294	
T0 vs. T24	0.1762	-15.12 to 15.47	No	ns	>0.9999	

T0 vs. T0	0	-15.29 to 15.29	No	ns	>0.9999	
T0 vs. T6	-4.016	-19.31 to 11.28	No	ns	0.9886	
T0 vs. T24	-0.1807	-15.48 to 15.11	No	ns	>0.9999	
T6 vs. T24	2.854	-12.44 to 18.15	No	ns	0.9989	
T6 vs. T0	2.875	-12.42 to 18.17	No	ns	0.9988	
T6 vs. T6	-6.85	-22.14 to 8.445	No	ns	0.8087	
T6 vs. T24	3.051	-12.24 to 18.35	No	ns	0.9982	
T6 vs. T0	2.875	-12.42 to 18.17	No	ns	0.9988	
T6 vs. T6	-1.141	-16.44 to 14.15	No	ns	>0.9999	
T6 vs. T24	2.694	-12.60 to 17.99	No	ns	0.9992	
T24 vs. T0	0.02043	-15.27 to 15.31	No	ns	>0.9999	
T24 vs. T6	-9.704	-25.00 to 5.590	No	ns	0.432	
T24 vs. T24	0.1966	-15.10 to 15.49	No	ns	>0.9999	
T24 vs. T0	0.02043	-15.27 to 15.31	No	ns	>0.9999	
T24 vs. T6	-3.995	-19.29 to 11.30	No	ns	0.989	
T24 vs. T24	-0.1603	-15.45 to 15.13	No	ns	>0.9999	
T0 vs. T6	-9.724	-25.02 to 5.570	No	ns	0.4294	
T0 vs. T24	0.1762	-15.12 to 15.47	No	ns	>0.9999	
T0 vs. T0	3.333E-09	-15.29 to 15.29	No	ns	>0.9999	
T0 vs. T6	-4.016	-19.31 to 11.28	No	ns	0.9886	
T0 vs. T24	-0.1807	-15.48 to 15.11	No	ns	>0.9999	

T6 vs. T24	9.901	-5.394 to 25.20	No	ns	0.4075	
T6 vs. T0	9.724	-5.570 to 25.02	No	ns	0.4294	
T6 vs. T6	5.708	-9.586 to 21.00	No	ns	0.9163	
T6 vs. T24	9.544	-5.751 to 24.84	No	ns	0.4525	
T24 vs. T0	-0.1762	-15.47 to 15.12	No	ns	>0.9999	
T24 vs. T6	-4.192	-19.49 to 11.10	No	ns	0.9851	
T24 vs. T24	-0.3569	-15.65 to 14.94	No	ns	>0.9999	
T0 vs. T6	-4.016	-19.31 to 11.28	No	ns	0.9886	
T0 vs. T24	-0.1807	-15.48 to 15.11	No	ns	>0.9999	
T6 vs. T24	3.835	-11.46 to 19.13	No	ns	0.9915	
ACT2						
Tukey's multiple comparisons test	Mean Diff.	95.00% CI of diff.	Below threshold?	Summary	Adjusted P Value	
T0 vs. T6	-0.5116	-23.54 to 22.51	No	ns	>0.9999	
T0 vs. T24	-0.00969	-23.03 to 23.02	No	ns	>0.9999	
T0 vs. T0	3.333E-09	-23.02 to 23.02	No	ns	>0.9999	
T0 vs. T6	-27.38	-50.41 to -4.357	Yes	*	0.0132	
T0 vs. T24	0.398	-22.63 to 23.42	No	ns	>0.9999	
T0 vs. T0	0	-23.02 to 23.02	No	ns	>0.9999	
T0 vs. T6	0.5813	-22.44 to 23.61	No	ns	>0.9999	
T0 vs. T24	0.8396	-22.19 to 23.86	No	ns	>0.9999	
T6 vs. T24	0.5019	-22.52 to 23.53	No	ns	>0.9999	

T6 vs. T0	0.5116	-22.51 to 23.54	No	ns	>0.9999	
T6 vs. T6	-26.87	-49.89 to -3.845	Yes	*	0.0154	
T6 vs. T24	0.9096	-22.12 to 23.93	No	ns	>0.9999	
T6 vs. T0	0.5116	-22.51 to 23.54	No	ns	>0.9999	
T6 vs. T6	1.093	-21.93 to 24.12	No	ns	>0.9999	
T6 vs. T24	1.351	-21.67 to 24.38	No	ns	>0.9999	
T24 vs. T0	0.00969	-23.02 to 23.03	No	ns	>0.9999	
T24 vs. T6	-27.37	-50.40 to -4.347	Yes	*	0.0132	
T24 vs. T24	0.4077	-22.62 to 23.43	No	ns	>0.9999	
T24 vs. T0	0.00969	-23.02 to 23.03	No	ns	>0.9999	
T24 vs. T6	0.591	-22.43 to 23.62	No	ns	>0.9999	
T24 vs. T24	0.8493	-22.18 to 23.87	No	ns	>0.9999	
T0 vs. T6	-27.38	-50.41 to -4.357	Yes	*	0.0132	
T0 vs. T24	0.398	-22.63 to 23.42	No	ns	>0.9999	
T0 vs. T0	-3.333E-09	-23.02 to 23.02	No	ns	>0.9999	
T0 vs. T6	0.5813	-22.44 to 23.61	No	ns	>0.9999	
T0 vs. T24	0.8396	-22.19 to 23.86	No	ns	>0.9999	
T6 vs. T24	27.78	4.755 to 50.80	Yes	*	0.0116	
T6 vs. T0	27.38	4.357 to 50.41	Yes	*	0.0132	
T6 vs. T6	27.96	4.938 to 50.99	Yes	*	0.011	
T6 vs. T24	28.22	5.196 to 51.25	Yes	*	0.0101	
T24 vs. T0	-0.398	-23.42 to 22.63	No	ns	>0.9999	
T24 vs. T6	0.1833	-22.84 to 23.21	No	ns	>0.9999	

T24 vs. T24	0.4416	-22.58 to 23.47	No	ns	>0.9999	
T0 vs. T6	0.5813	-22.44 to 23.61	No	ns	>0.9999	
T0 vs. T24	0.8396	-22.19 to 23.86	No	ns	>0.9999	
T6 vs. T24	0.2583	-22.77 to 23.28	No	ns	>0.9999	
ACT3						
Tukey's multiple comparisons test	Mean Diff.	95.00% CI of diff.	Below threshold?	Summary	Adjusted P Value	
T0 vs. T6	-0.9796	-3.138 to 1.178	No	ns	0.798	
T0 vs. T24	0.0823	-2.076 to 2.240	No	ns	>0.9999	
T0 vs. T0	0	-2.158 to 2.158	No	ns	>0.9999	
T0 vs. T6	0.03525	-2.123 to 2.193	No	ns	>0.9999	
T0 vs. T24	0.5309	-1.627 to 2.689	No	ns	0.9925	
T0 vs. T0	0	-2.158 to 2.158	No	ns	>0.9999	
T0 vs. T6	-1.33	-3.488 to 0.8278	No	ns	0.4676	
T0 vs. T24	-0.1782	-2.336 to 1.980	No	ns	>0.9999	
T6 vs. T24	1.062	-1.096 to 3.220	No	ns	0.7258	
T6 vs. T0	0.9796	-1.178 to 3.138	No	ns	0.798	
T6 vs. T6	1.015	-1.143 to 3.173	No	ns	0.7681	
T6 vs. T24	1.511	-0.6475 to 3.669	No	ns	0.3152	
T6 vs. T0	0.9796	-1.178 to 3.138	No	ns	0.798	
T6 vs. T6	-0.3507	-2.509 to 1.807	No	ns	0.9996	
T6 vs. T24	0.8014	-1.357 to 2.959	No	ns	0.9184	

T24 vs. T0	-0.0823	-2.240 to 2.076	No	ns	>0.9999	
T24 vs. T6	-0.04705	-2.205 to 2.111	No	ns	>0.9999	
T24 vs. T24	0.4486	-1.709 to 2.607	No	ns	0.9976	
T24 vs. T0	-0.0823	-2.240 to 2.076	No	ns	>0.9999	
T24 vs. T6	-1.413	-3.571 to 0.7455	No	ns	0.394	
T24 vs. T24	-0.2605	-2.418 to 1.898	No	ns	>0.9999	
T0 vs. T6	0.03525	-2.123 to 2.193	No	ns	>0.9999	
T0 vs. T24	0.5309	-1.627 to 2.689	No	ns	0.9925	
T0 vs. T0	0	-2.158 to 2.158	No	ns	>0.9999	
T0 vs. T6	-1.33	-3.488 to 0.8278	No	ns	0.4676	
T0 vs. T24	-0.1782	-2.336 to 1.980	No	ns	>0.9999	
T6 vs. T24	0.4957	-1.662 to 2.654	No	ns	0.9952	
T6 vs. T0	-0.03525	-2.193 to 2.123	No	ns	>0.9999	
T6 vs. T6	-1.365	-3.523 to 0.7925	No	ns	0.4353	
T6 vs. T24	-0.2134	-2.371 to 1.945	No	ns	>0.9999	
T24 vs. T0	-0.5309	-2.689 to 1.627	No	ns	0.9925	
T24 vs. T6	-1.861	-4.019 to 0.2968	No	ns	0.1238	
T24 vs. T24	-0.7091	-2.867 to 1.449	No	ns	0.9571	
T0 vs. T6	-1.33	-3.488 to 0.8278	No	ns	0.4676	
T0 vs. T24	-0.1782	-2.336 to 1.980	No	ns	>0.9999	
T6 vs. T24	1.152	-1.006 to 3.310	No	ns	0.6398	

Chapter 5						
Figure 5.3 Quantification of luciferase expression in (A) N. benthamiana and (B) pot marigold.						
N. benthamiana						
Dunn's multiple co mparisons test	Mean r ank diff .		Significant?	Summary	Adjusted P Value	
Media only vs. G V3101	-39.08		Yes	****	<0.0001	
Media only vs. LB A4404	-62.04		Yes	****	<0.0001	
Media only vs. A GL1	-29.38		Yes	**	0.0012	
Pot marigold						
Dunn's multiple co mparisons test	Mean r ank diff .		Significant?	Summary	Adjusted P Value	
Media only vs. G V3101	-25.83		Yes	**	0.0052	
Media only vs. LB A4404	-43.58		Yes	****	<0.0001	
Media only vs. A GL1	-43.96		Yes	****	<0.0001	
Figure 5.12 Gene expression analysis of *CoPDS* in pot marigold plants infiltrated with VIGS vectors.						
PDS Leaf						
Column B	PDS_G FP					
vs.	vs.					
Column A	WT					
Unpaired t test						
P value	<0.000 1					
P value summary	****					
Significantly diff erent (P < 0.05)?	Yes					
Difference betwe en means (B - A) ± SEM	- 0.8124 ± 0.098 34					
95% confidence i nterval	- 1.023 to - 0.6015					
R squared (eta sq uared)	0.8298					

PDS Flower						
Column B	PDS_GFP					
vs.	vs.					
Column A	WT					
Unpaired t test						
P value	0.6115					
P value summary	ns					
Significantly different (P < 0.05)?	No					
Difference between means (B - A) ± SEM	0.2475 ± 0.4764					
95% confidence interval	-0.7743 to 1.269					
R squared (eta squared)	0.01891					
Figure 5.13 Gene expression analysis of *CoCAS* in plants infiltrated with VIGS vectors.						
CAS Leaf						
Column B	PDS_CAS					
vs.	vs.					
Column A	PDS_GFP					
Unpaired t test						
P value	0.004					
P value summary	**					
Significantly different (P < 0.05)?	Yes					
Difference between means (B - A) ± SEM	-1.375 ± 0.3995					
95% confidence interval	-2.232 to -0.5180					
R squared (eta squared)	0.4583					
CAS Flower						
Table Analyzed	F_CAS					
Column B	PDS_CAS					
vs.	vs.					

Column A	PDS_GFP					
Unpaired t test						
P value	0.3082					
P value summary	ns					
Significantly different (P < 0.05)?	No					
Difference between means (B - A) ± SEM	-0.3927 ± 0.3714					
95% confidence interval	-1.189 to 0.4038					
R squared (eta squared)	0.07396					
Figure 5.14 Gene expression analysis of *CoPDS* and *CoTXSS* in flowers of pot marigold infiltrated with VIGS vectors.						
PDS						
Column B	PDS_TXSS					
vs.	vs.					
Column A	PDS_GFP					
Unpaired t test						
P value	0.0514					
P value summary	ns					
Significantly different (P < 0.05)?	No					
Difference between means (B - A) ± SEM	0.6231 ± 0.2925					
95% confidence interval	0.004281 to 1.250					
R squared (eta squared)	0.2448					
Column E	PDS_TXSS_FT					
vs.	vs.					
Column D	PDS_GFP_FT					
Unpaired t test						
P value	0.9091					
P value summary	ns					

Significantly different (P < 0.05)?	No					
Difference between means (E - D) ± SEM	0.03736 ± 0.3213					
95% confidence interval	-0.6518 to 0.7265					
R squared (eta squared)	0.000967					
TXSS						
Column E	PDS_TXSS_FT					
vs.	vs.					
Column D	PDS_GFP_FT					
Unpaired t test						
P value	0.0353					
P value summary	*					
Significantly different (P < 0.05)?	Yes					
Difference between means (E - D) ± SEM	-0.9577 ± 0.4110					
95% confidence interval	-1.839 to -0.07625					
R squared (eta squared)	0.2795					
Column E	PDS_TXSS_FT					
vs.	vs.					
Column B	PDS_TXSS					
Unpaired t test						
P value	0.0262					
P value summary	*					
Significantly different (P < 0.05)?	Yes					
Difference between means (E - B) ± SEM	-0.6148 ± 0.2473					

95% confidence interval	-1.145 to -0.08441					
R squared (eta squared)	0.3063					
Column B	PDS_TXSS					
vs.	vs.					
Column A	PDS_GFP					
Unpaired t test						
P value	0.9877					
P value summary	ns					
Significantly different (P < 0.05)?	No					
Difference between means (B - A) ± SEM	-0.01187 ± 0.7570					
95% confidence interval	-1.661 to 1.637					
R squared (eta squared)	0.0000205					

Supplementary Figures

Figure S3.1 GC trace and mass spectra for compounds identified in the study. A. Compounds identified using commercially available standards. B. Compounds identified using the NIST database. C. Compounds identified using the internal database.

A. Compounds identified using commercially available standards.

Triterpene monols

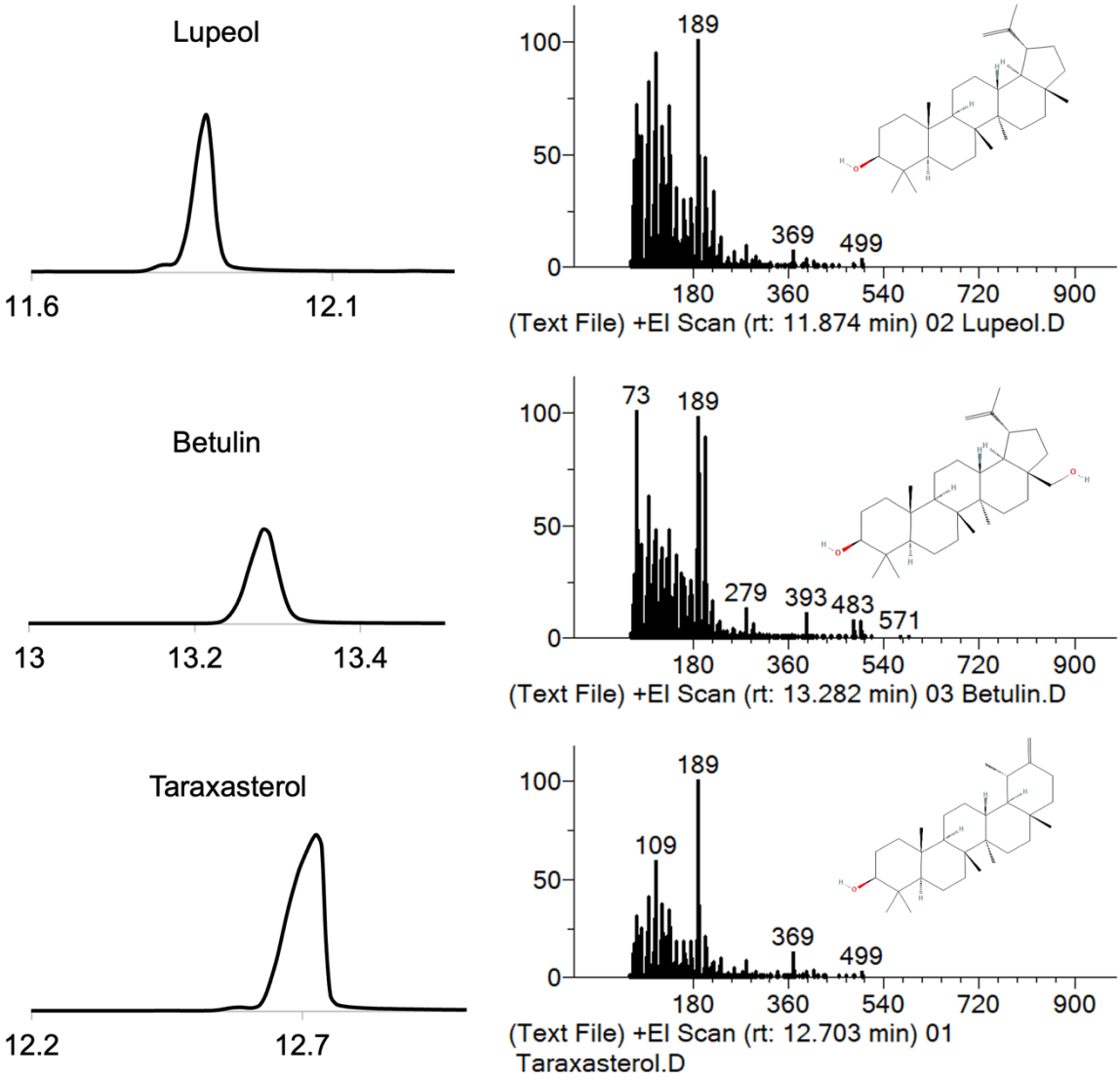

Triterpene diols

Triterpene acids

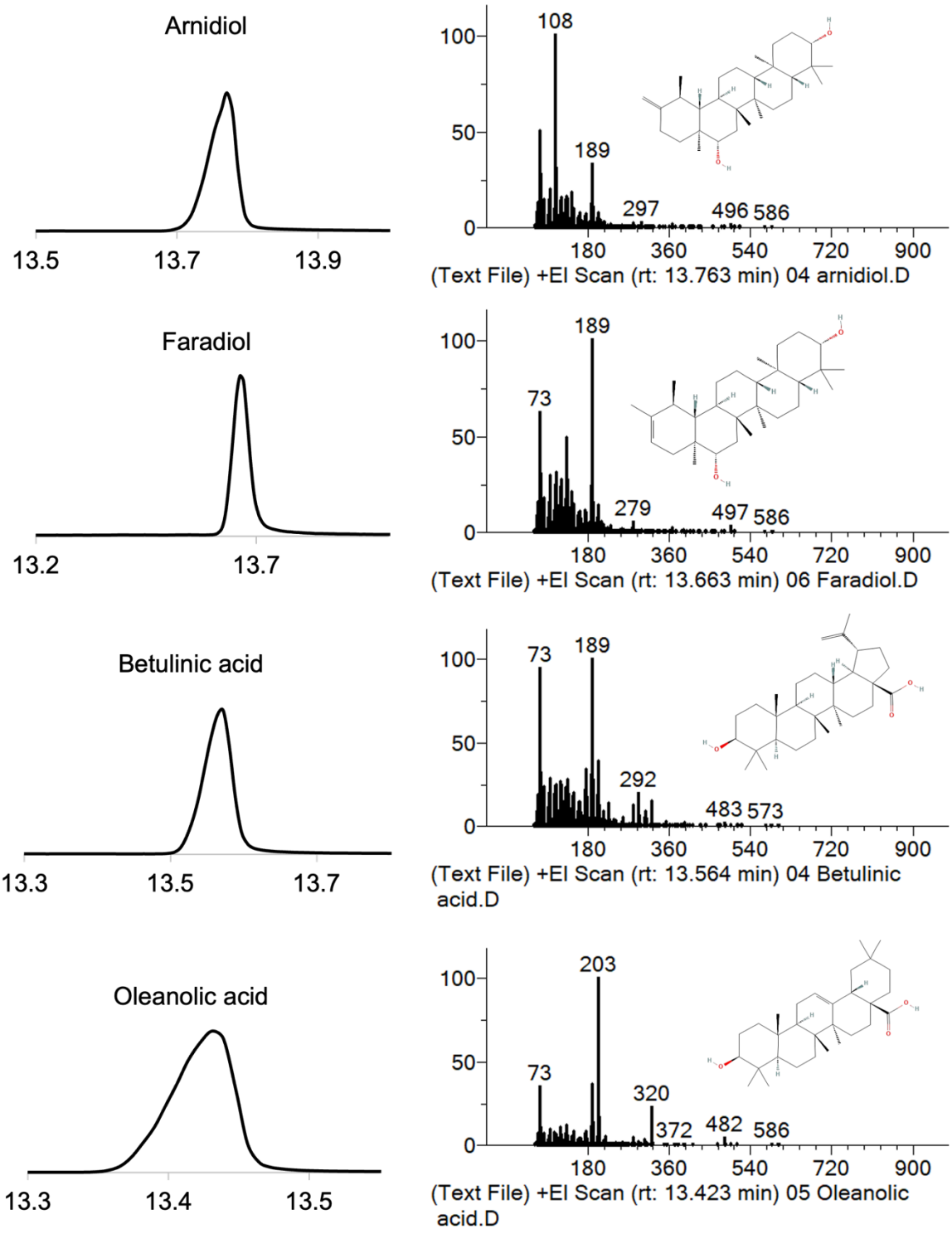

B. Compounds identified using the NIST database. The percentage match to NIST database is shown on the mass spectrum.

Fatty acids

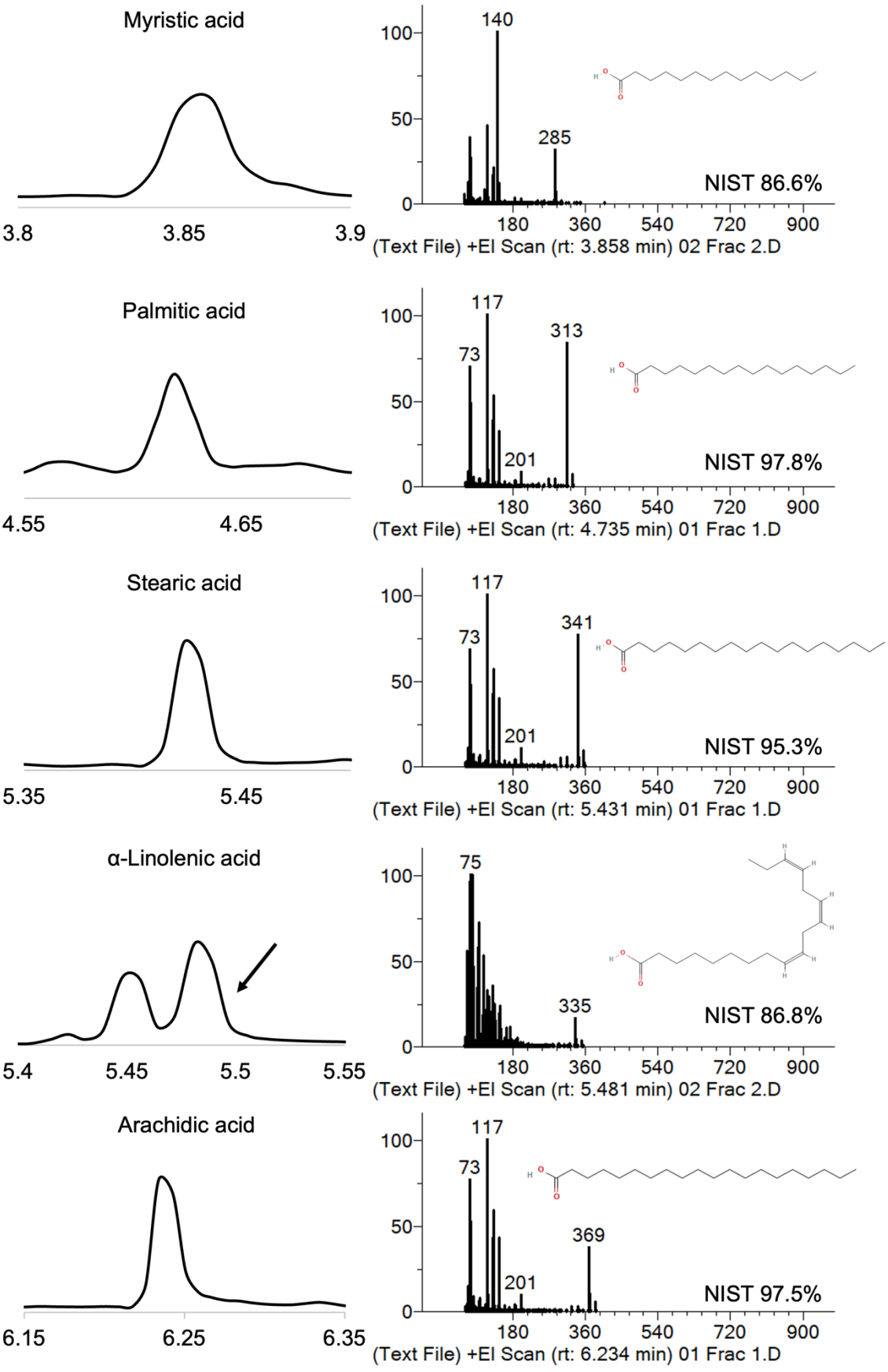
Myristic acid
3.8
3.85
3.9
140
285
NIST 86.6%
(Text File) +EI Scan (rt: 3.858 min) 02 Frac 2.D
Palmitic acid
4.55
4.65
117
73
313
201
NIST 97.8%
(Text File) +EI Scan (rt: 4.735 min) 01 Frac 1.D
Stearic acid
5.35
5.45
117
73
341
201
NIST 95.3%
(Text File) +EI Scan (rt: 5.431 min) 01 Frac 1.D
α-Linolenic acid
5.4
5.45
5.5
5.55
75
335
NIST 86.8%
(Text File) +EI Scan (rt: 5.481 min) 02 Frac 2.D
Arachidic acid
6.15
6.25
6.35
117
73
369
201
NIST 97.5%
(Text File) +EI Scan (rt: 6.234 min) 01 Frac 1.D

Sterols

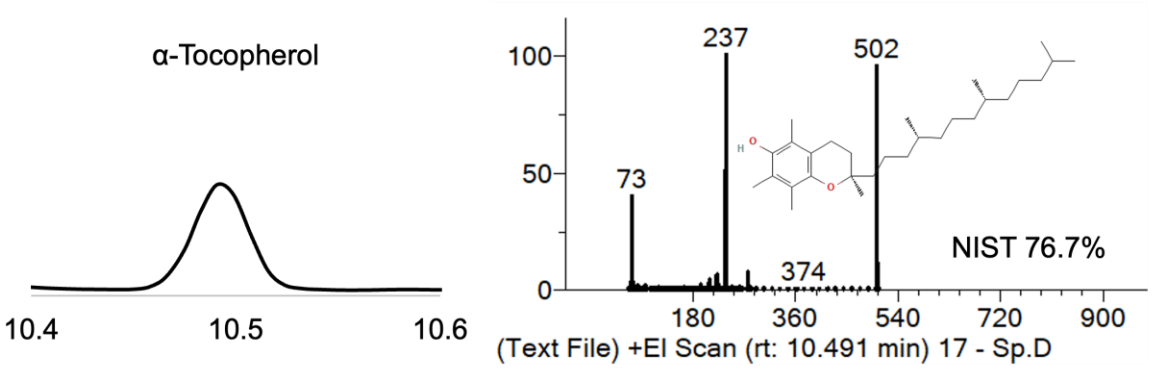
α-Tocopherol
10.4
10.5
10.6
237
502
73
374
NIST 76.7%
100
50
0
180
360
540
720
900
(Text File) +EI Scan (rt: 10.491 min) 17 - Sp.D

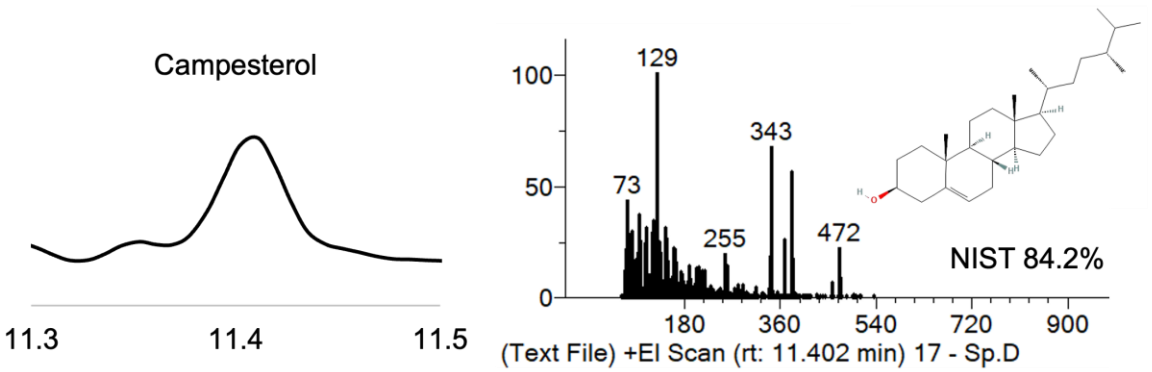
Campesterol
11.3
11.4
11.5
129
343
73
255
472
NIST 84.2%
100
50
0
180
360
540
720
900
(Text File) +EI Scan (rt: 11.402 min) 17 - Sp.D

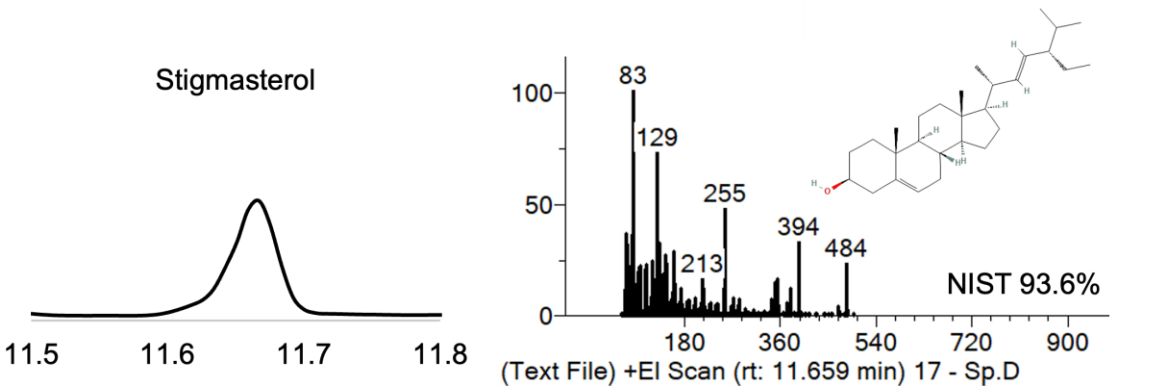
Stigmasterol
11.5
11.6
11.7
11.8
83
129
255
394
213
484
NIST 93.6%
100
50
0
180
360
540
720
900
(Text File) +EI Scan (rt: 11.659 min) 17 - Sp.D

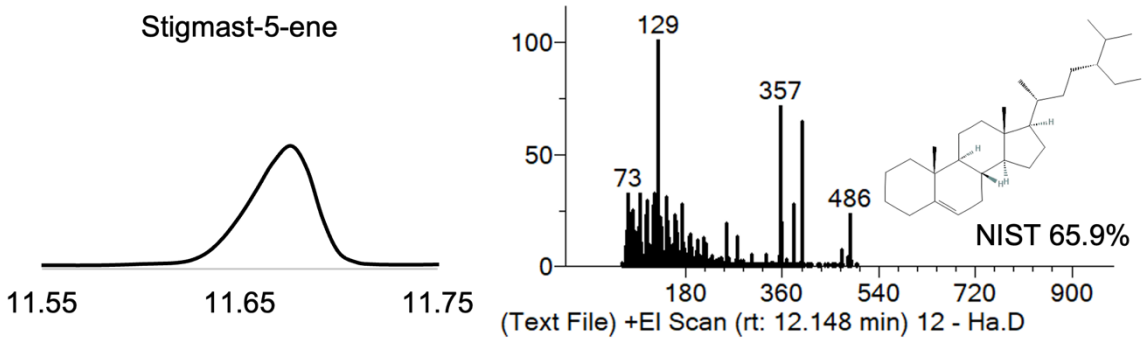

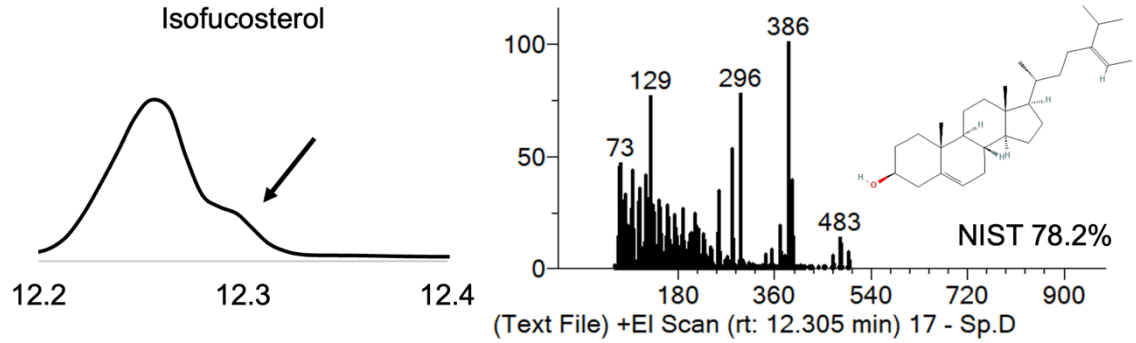

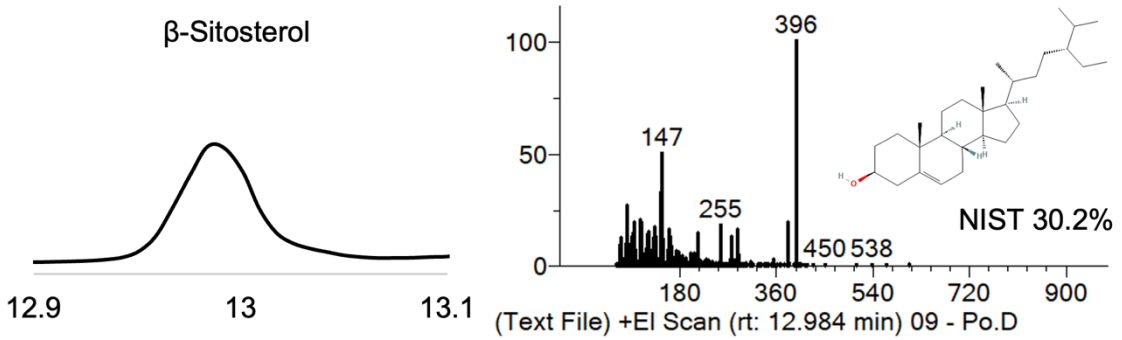

Triterpene monols

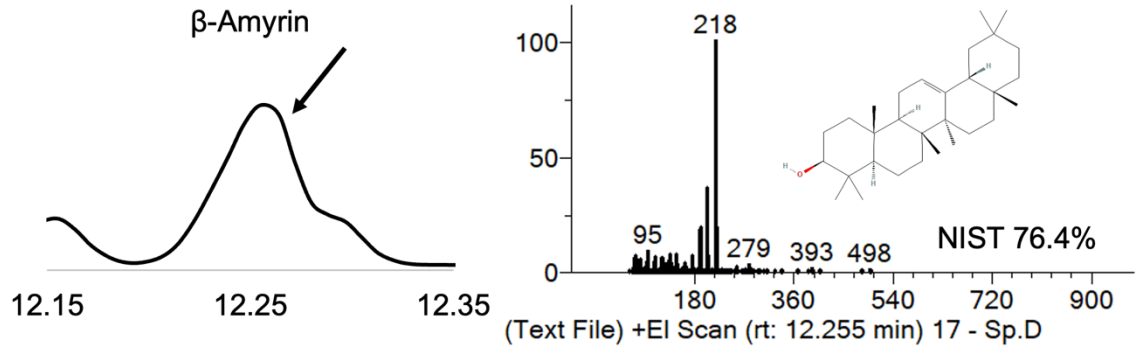

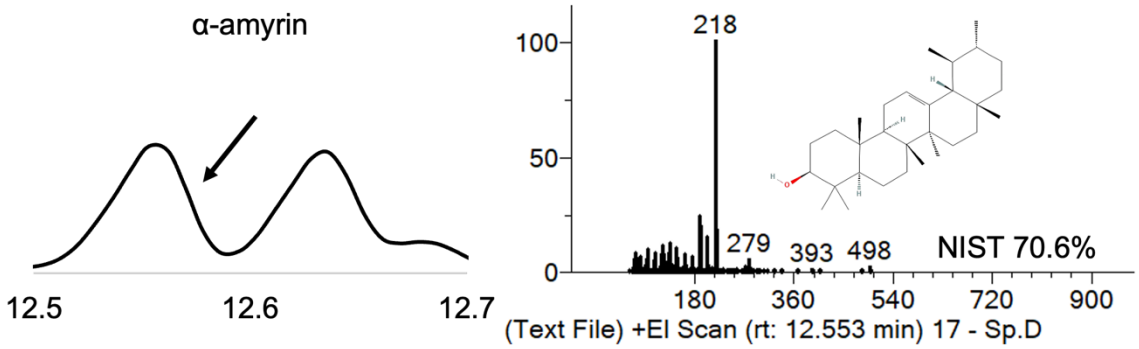

C. Compounds identified using the internal database.

Triterpene monols

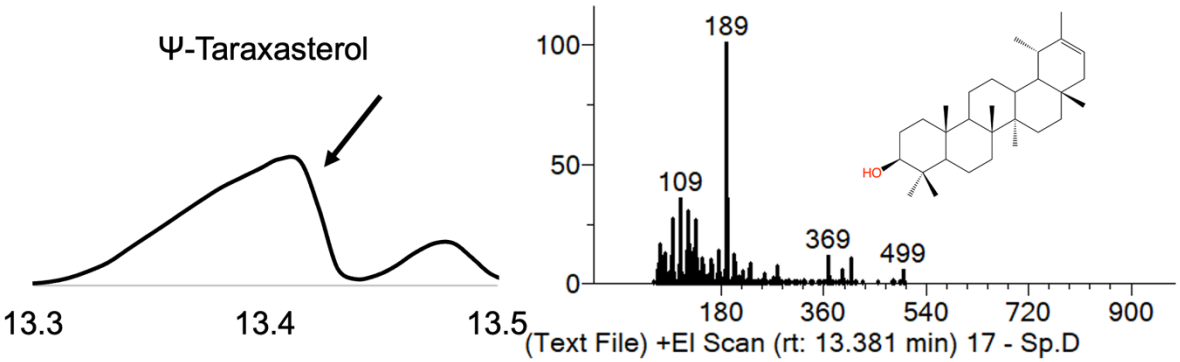

Triterpene diols

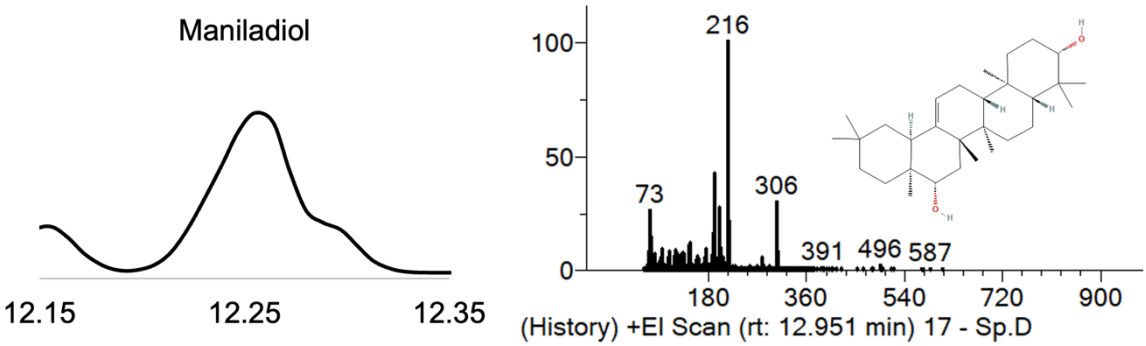

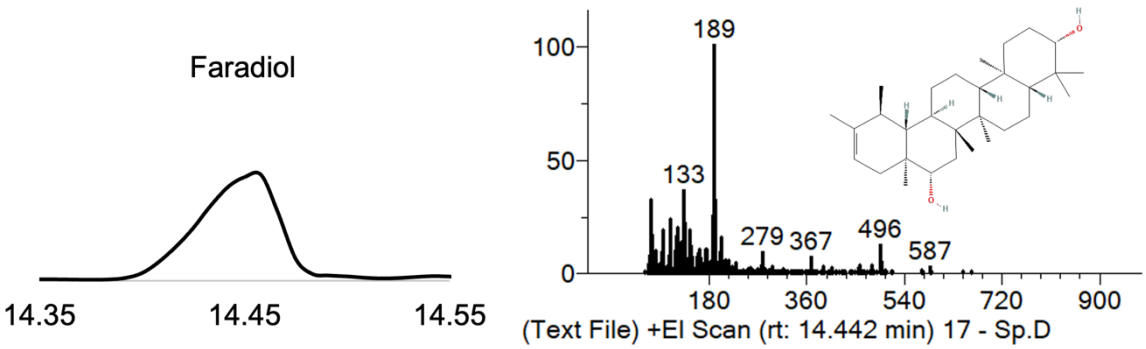

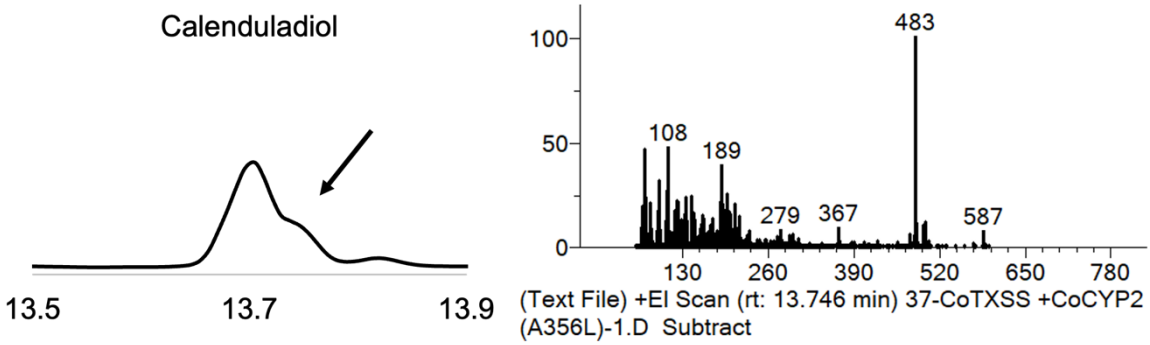

Triterpene acetates

β-Sitosterol acetate

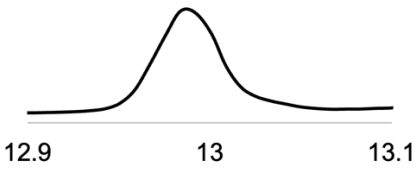

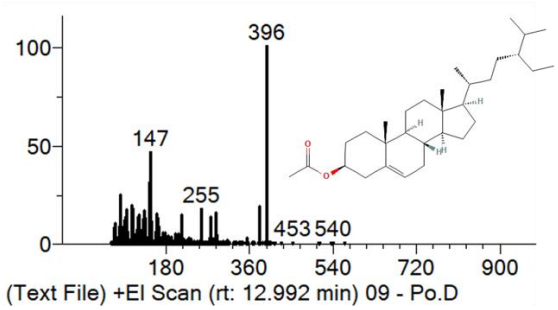

β-amyrin acetate

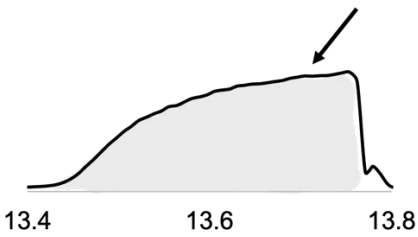

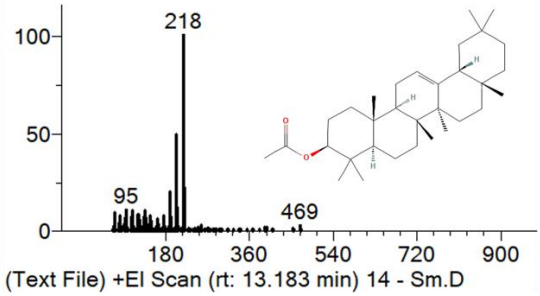

α-amyrin acetate

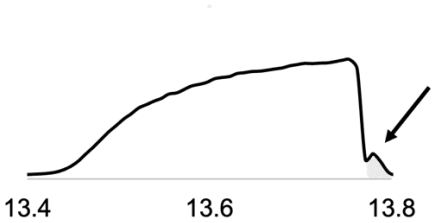

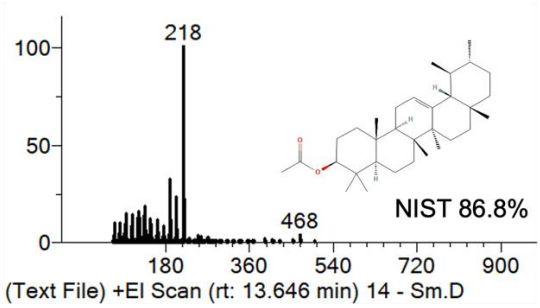

Ψ-Taraxasterol acetate

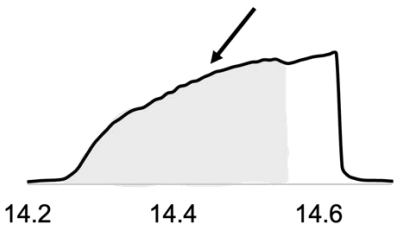

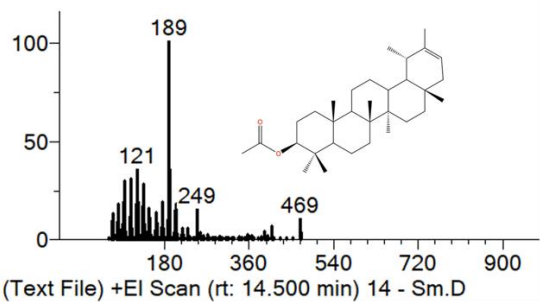

Taraxasterol acetate

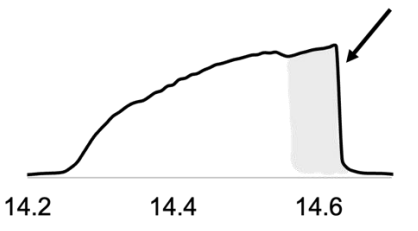

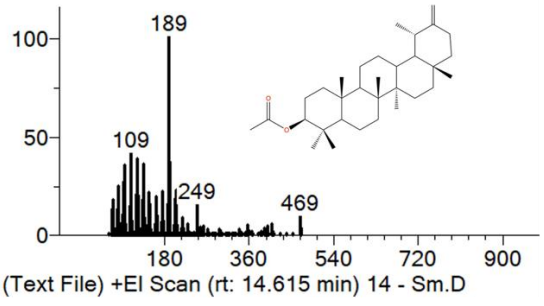

Lupeol acetate

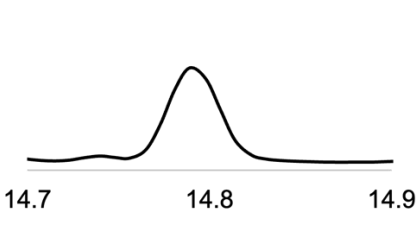

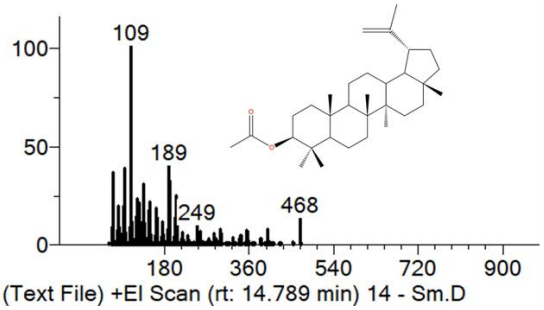

Triterpene monol fatty acid esters

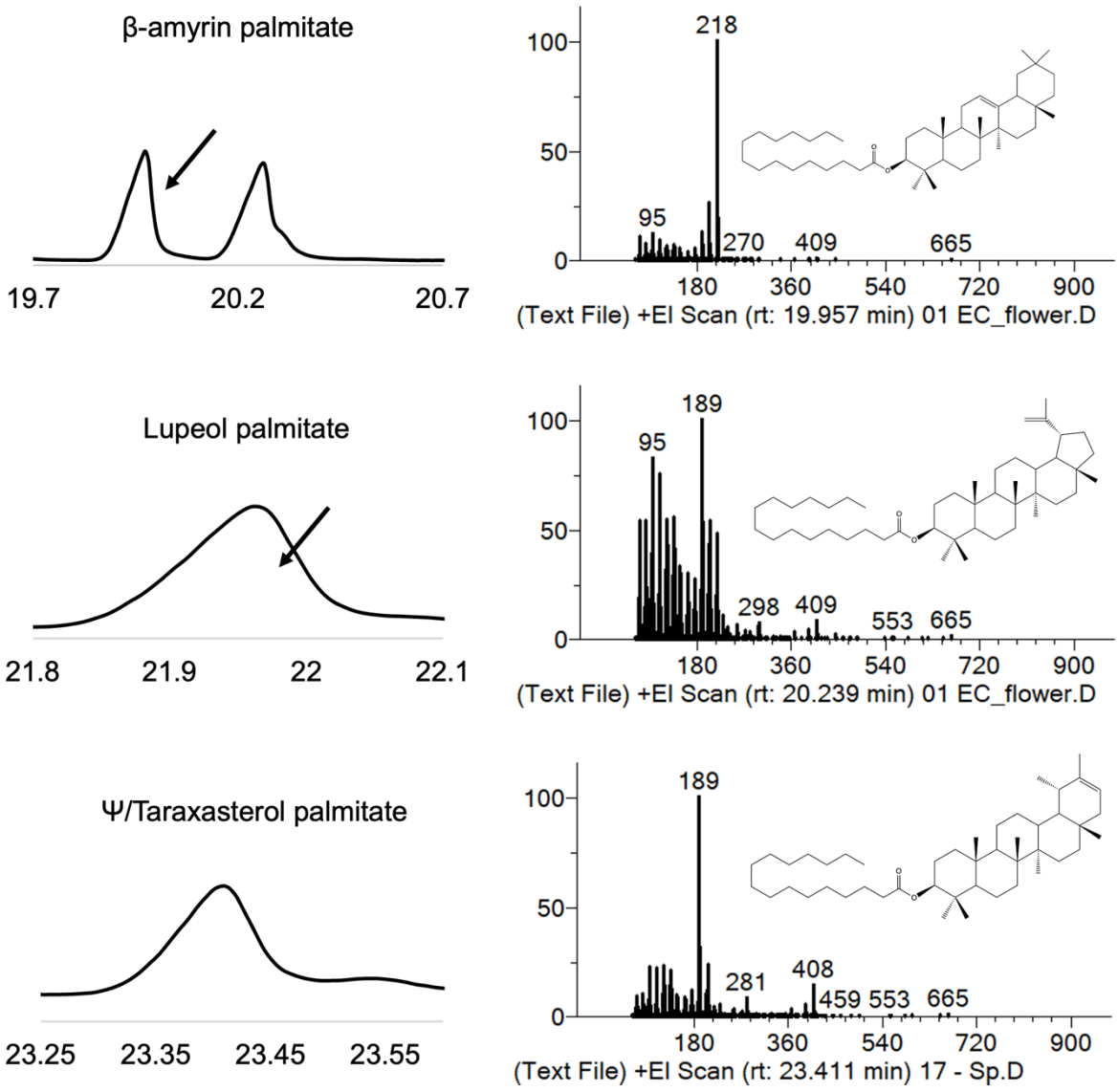

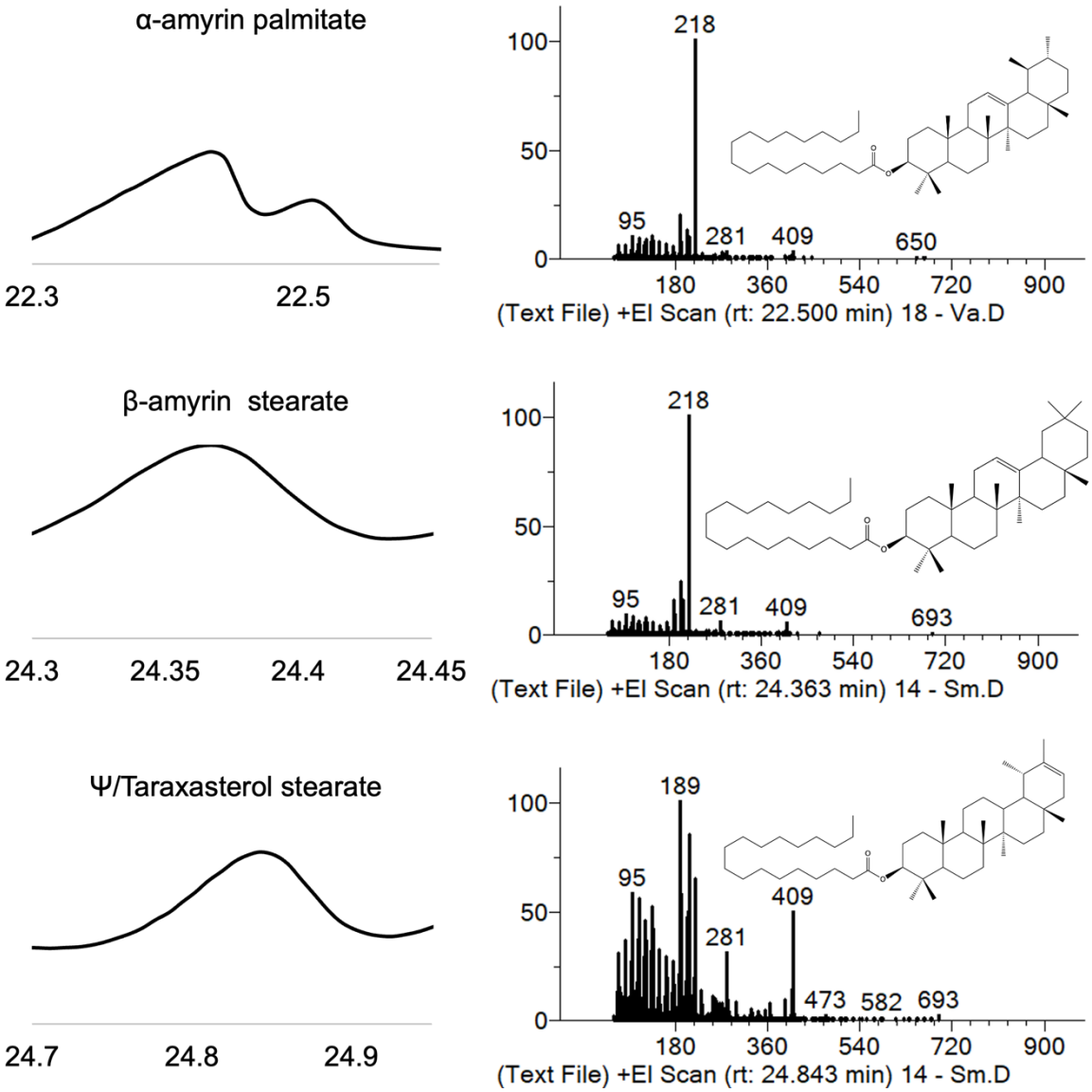

Triterpene diol fatty acid esters

Faradiol laurate

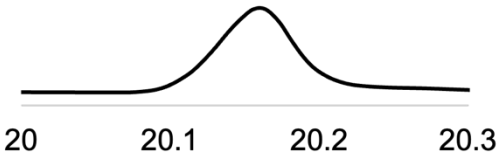

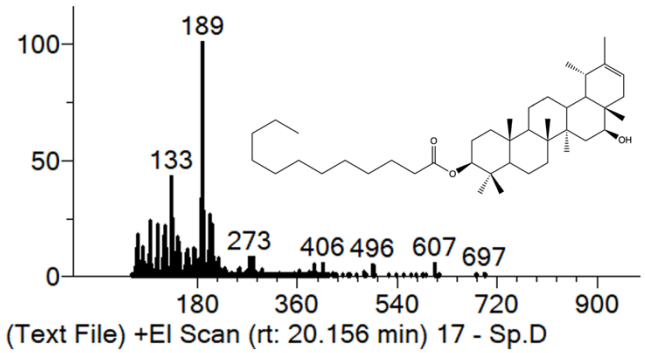

(Text File) +EI Scan (rt: 20.156 min) 17 - Sp.D

Faradiol myristate

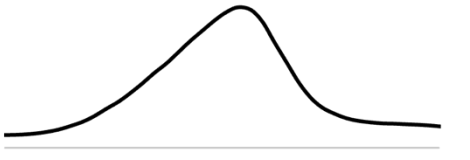

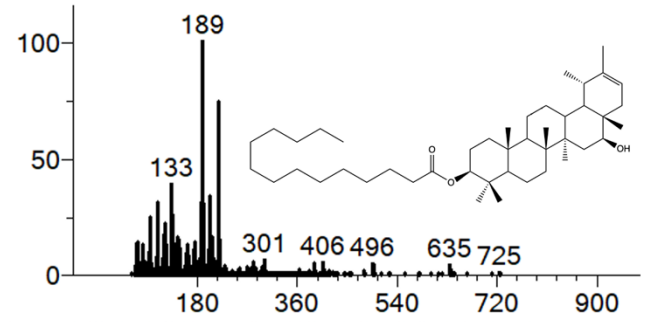

(Text File) +EI Scan (rt: 21.961 min) 17 - Sp.D

Faradiol palmitate

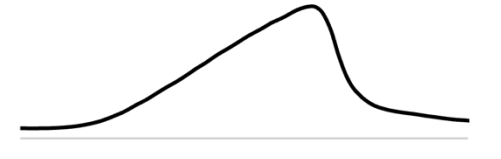

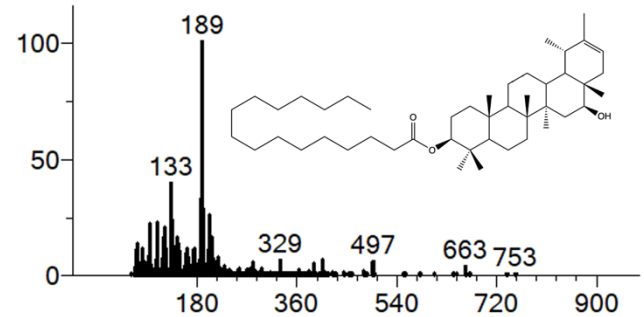

(Text File) +EI Scan (rt: 24.297 min) 17 - Sp.D

Maniladiol myristate

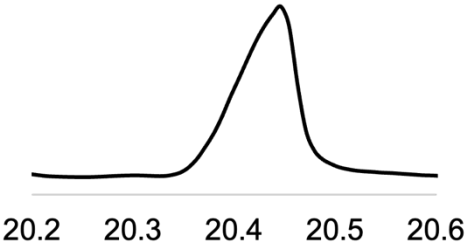

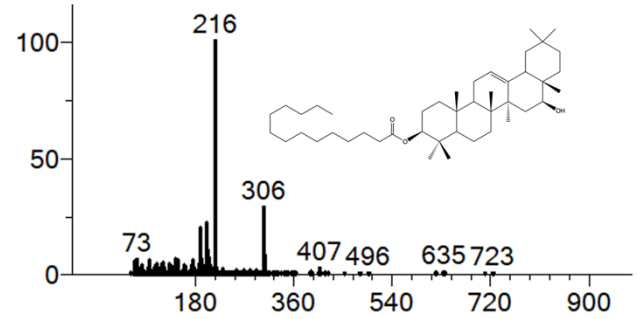

(Text File) +EI Scan (rt: 20.446 min) 12 - Ha.D

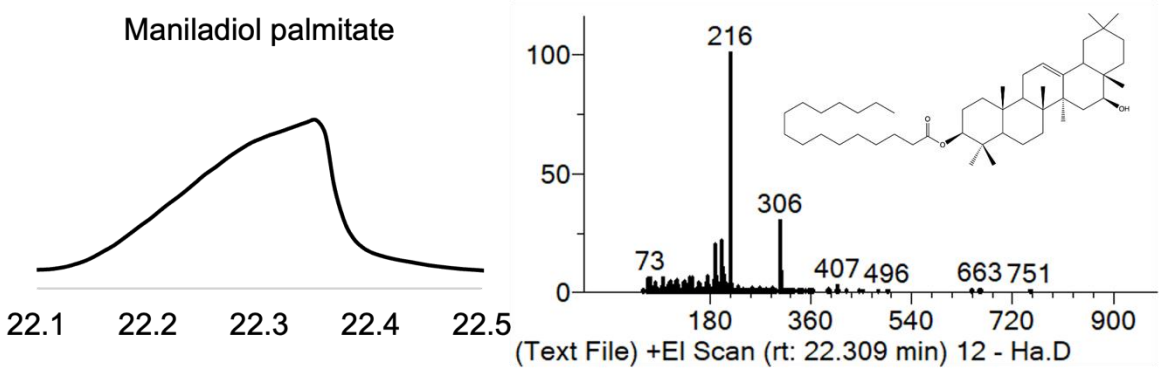
Maniladiol palmitate
22.1
22.2
22.3
22.4
22.5
216
306
73
407
496
663
751
100
50
0
180
360
540
720
900
(Text File) +EI Scan (rt: 22.309 min) 12 - Ha.D

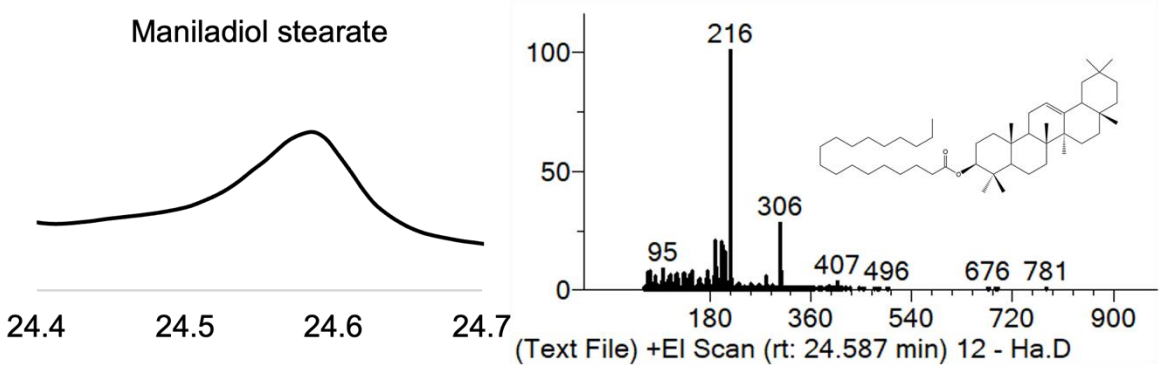
Maniladiol stearate
24.4
24.5
24.6
24.7
216
306
95
407
496
676
781
100
50
0
180
360
540
720
900
(Text File) +EI Scan (rt: 24.587 min) 12 - Ha.D